N° d'ordre 2014 ISAL 0103 Année 2014

Thèse

Nanoparticle-doped lubricants: potential of Inorganic Fullerene-like (IF-) molybdenum disulfide for automotive applications

Présentée devant

L'Institut National des Sciences Appliquées de Lyon

Ecole doctorale des Sciences pour l'Ingénieur de Lyon:
Mécanique, Energétique, Génie Civil, Acoustique (MEGA)
Spécialité : Mécanique

Pour obtenir

Le grade de docteur

Par

Pierre RABASO
Ingénieur INSA Lyon

Soutenue le 13 novembre 2014 devant la commission d'examen composée de :

Pr. Fabrice DASSENOY	LTDS – Ecole Centrale de Lyon	Directeur de thèse
Dr. Moussa DIABY	PSA Peugeot Citroën	Encadrant industriel
Pr. Rob DWYER-JOYCE	University of Sheffield	Rapporteur
Pr. Michel FILLON	Institut Pprime – Université de Poitiers	Président du jury
Pr. Christophe GEANTET	IRCELYON – CNRS	Membre invité
Pr. Mitjan KALIN	University of Ljubljana	Rapporteur
Pr. Fabrice VILLE	LaMCoS – INSA Lyon	Directeur de thèse

Laboratoires de recherche :

LaMCoS – INSA Lyon
LTDS – Ecole Centrale de Lyon

INSA Direction de la Recherche - Ecoles Doctorales – Quinquennal 2011-2015

SIGLE	ECOLE DOCTORALE	NOM ET COORDONNEES DU RESPONSABLE
CHIMIE	**CHIMIE DE LYON** **http://www.edchimie-lyon.fr** Sec : Renée EL MELHEM Bat Blaise Pascal 3e etage 04 72 43 80 46 Insa : R. GOURDON	M. Jean Marc LANCELIN Université de Lyon – Collège Doctoral Bât ESCPE 43 bd du 11 novembre 1918 69622 VILLEURBANNE Cedex Tél : 04.72.43 13 95 directeur@edchimie-lyon.fr
E.E.A.	**ELECTRONIQUE, ELECTROTECHNIQUE, AUTOMATIQUE** **http://edeea.ec-lyon.fr** Sec : M.C. HAVGOUDOUKIAN eea@ec-lyon.fr	M. Gérard SCORLETTI Ecole Centrale de Lyon 36 avenue Guy de Collongue 69134 ECULLY Tél : 04.72.18 60.97 Fax : 04 78 43 37 17 Gerard.scorletti@ec-lyon.fr
E2M2	**EVOLUTION, ECOSYSTEME, MICROBIOLOGIE, MODELISATION** **http://e2m2.universite-lyon.fr** Sec : Safia AIT CHALAL Bat Darwin - UCB Lyon 1 04.72.43.28.91 Insa : H. CHARLES	Mme Gudrun BORNETTE CNRS UMR 5023 LEHNA Université Claude Bernard Lyon 1 Bât Forel 43 bd du 11 novembre 1918 69622 VILLEURBANNE Cédex Tél : 06.07.53.89.13 e2m2@ univ-lyon1.fr
EDISS	**INTERDISCIPLINAIRE SCIENCES-SANTE** **http://www.ediss-lyon.fr** Sec : Safia AIT CHALAL Hôpital Louis Pradel - Bron 04 72 68 49 09 Insa : M. LAGARDE Safia.ait-chalal@univ-lyon1.fr	Mme Emmanuelle CANET-SOULAS INSERM U1060, CarMeN lab, Univ. Lyon 1 Bâtiment IMBL 11 avenue Jean Capelle INSA de Lyon 696621 Villeurbanne Tél : 04.72.68.49.09 Fax :04 72 68 49 16 Emmanuelle.canet@univ-lyon1.fr
INFOMATHS	**INFORMATIQUE ET MATHEMATIQUES** **http://infomaths.univ-lyon1.fr** Sec :Renée EL MELHEM Bat Blaise Pascal 3e etage infomaths@univ-lyon1.fr	Mme Sylvie CALABRETTO LIRIS – INSA de Lyon Bat Blaise Pascal 7 avenue Jean Capelle 69622 VILLEURBANNE Cedex Tél : 04.72. 43. 80. 46 Fax 04 72 43 16 87 Sylvie.calabretto@insa-lyon.fr
Matériaux	**MATERIAUX DE LYON** **http://ed34.universite-lyon.fr** Sec : M. LABOUNE PM : 71.70 –Fax : 87.12 Bat. Saint Exupéry Ed.materiaux@insa-lyon.fr	M. Jean-Yves BUFFIERE INSA de Lyon MATEIS Bâtiment Saint Exupéry 7 avenue Jean Capelle 69621 VILLEURBANNE Cedex Tél : 04.72.43 83 18 Fax 04 72 43 85 28 Jean-yves.buffiere@insa-lyon.fr
MEGA	**MECANIQUE, ENERGETIQUE, GENIE CIVIL, ACOUSTIQUE** **http://mega.universite-lyon.fr** Sec : M. LABOUNE PM : 71.70 –Fax : 87.12 Bat. Saint Exupéry mega@insa-lyon.fr	M. Philippe BOISSE INSA de Lyon Laboratoire LAMCOS Bâtiment Jacquard 25 bis avenue Jean Capelle 69621 VILLEURBANNE Cedex Tél :04.72 .43.71.70 Fax : 04 72 43 72 37 Philippe.boisse@insa-lyon.fr
ScSo	**ScSo*** **http://recherche.univ-lyon2.fr/scso/** Sec : Viviane POLSINELLI Brigitte DUBOIS Insa : J.Y. TOUSSAINT	Mme Isabelle VON BUELTZINGLOEWEN Université Lyon 2 86 rue Pasteur 69365 LYON Cedex 07 Tél : 04.78.77.23.86 Fax : 04.37.28.04.48 viviane.polsinelli@univ-lyon2.fr

*ScSo : Histoire, Géographie, Aménagement, Urbanisme, Archéologie, Science politique, Sociologie, Anthropologie

"And this I believe: that the free, exploring mind of the individual human is the most valuable thing in the world."

- John Steinbeck

Foreword

This work results from a collaboration between the laboratory of Contact and Structure Mechanics (LaMCoS) from INSA Lyon (France), the laboratory of Tribology and System Dynamics (LTDS) from Ecole Centrale de Lyon (France) and the car manufacturer PSA Peugeot Citroën.

The PhD took place in the doctoral school MEGA (Mechanics, Energetics, Civil Engineering, Acoustics), and was funded by the National Agency for Research and Technology (ANRT) through an Industrial Research Convention (CIFRE).

PhD supervisors	LaMCoS LTDS PSA Peugeot Citroën	*Fabrice VILLE* *Fabrice DASSENOY* *Moussa DIABY*
Reviewers	University of Sheffield (UK) University of Ljubljana (Slovenia)	*Rob DWYER-JOYCE* *Mitjan KALIN*
LaMCoS	Director Head of the SMC* team	*David DUREISSEIX* *Philippe VELEX*
LTDS	Director Head of the TPCDI** team	*Denis MAZUYER* *Thierry LE MOGNE*
INSA Lyon	Director Director of Research	*Eric MAURINCOMME* *Jean-François GERARD*
Ecole Centrale de Lyon	Director Director of Research	*Frank DEBOUCK* *Jean-Pierre BERTOGLIO*
MEGA doctoral school	Director	*Philippe BOISSE*
PSA Peugeot Citroën	Chairman of the Managing Board Director of Research & Development Scientific Director Head of the TLPA*** team	*Carlos TAVAREZ* *Gilles LE BORGNE* *Sylvain ALLANO* *Vanina SABATHIER*

** Contacts and Mechanical Systems*
*** Tribology, Physico-Chemistry and Interface Dynamics*
**** Tribology, Industrial liquids and Assemblies*

Acknowledgments

I am very grateful to the members of my jury for assessing my work on the day of my defense. Thank you Pr. Michel Fillon for presiding this jury, and Pr. Christophe Géantet for responding to my invitation. I would also like to give particular thanks to my reviewers, Pr. Rob Dwyer-Joyce and Pr. Mitjan Kalin, for reading this manuscript in great detail and for coming all the way to Lyon on November 13th.

Je retrouve désormais la langue de Molière pour remercier chaleureusement mes directeurs de thèse Pr. Fabrice Ville et Pr. Fabrice Dassenoy, ainsi que mon encadrant chez PSA Peugeot Citroën Dr. Moussa Diaby. Vous avez tous les trois su vous montrer disponibles et pédagogues, su m'orienter tout en préservant ma liberté, et su m'apprendre énormément tout en m'écoutant. Vous avez su créer une atmosphère de travail alliant à la perfection sérieux et bonne humeur, et su me considérer non comme un étudiant mais comme un véritable collègue. Quelle chance pour moi d'avoir pu travailler avec vous !

Merci également à Jérôme Cavoret, Vincent Baudin, Thierry Le Mogne, Béatrice Vacher et Michel Belin pour l'aide précieuse - que dis-je, inestimable - qu'ils m'ont apportée sur les différents dispositifs expérimentaux durant toute ma thèse. De l'usinage de pièces pour la HFRR à la calibration de la MTM en passant par le profilomètre optique, de l'XPS au TEM sans oublier la Nanovisu, ce travail n'aurait jamais vu le jour sans vous. Merci pour tout ce que m'avez appris, pour votre patience et pour votre gentillesse.

Je souhaite aussi remercier l'ensemble des personnes avec qui j'ai été amené à collaborer chez PSA Peugeot Citroën, durant cette thèse mais également lors de mon stage de fin d'études d'ingénieur. Votre accueil sur le site de Belchamp a été formidable, et j'ai beaucoup appris à vos côtés. Merci à Pavel Afanasiev de IRCELYON pour la synthèse de l'ensemble des nanoparticules étudiées lors de ces travaux, ainsi qu'à PCS Instruments pour les réponses à mes nombreuses questions et à Powertrib pour la réalisation des essais de fatigue présentés à la fin de ce manuscrit.

Merci à tous mes collègues du LaMCoS et du LTDS, présents et passés, qui ont rendu chaque journée agréable de par leur bonne humeur. Merci tout particulièrement à mes supers co-bureau, Arnaud (« p'tite pause ? »), Marion (« chocolat ? ») et Jérôme (« Djobi ? »), ainsi qu'à mes quasi-co-bureau Matthieu (« café ? ») et Nina (« sucre ? »). Un clin d'œil également aux doctorants des autres bureaux, étages, voire bâtiments avec qui j'ai eu le plaisir de partager davantage que le quotidien du laboratoire : Charlotte, Nico L., Vincent, Nico V., Jean-David et les « anciens » Florian et Rudy. Je voudrais aussi remercier Paula, Imène, Sophie, Catia et Modestino pour m'avoir toujours accueilli avec le sourire et fait une place dans leur bureau lorsque je venais au LTDS. Merci également aux services informatiques et aux secrétariats pour leur assistance, et notamment à Sophie – promis, cette fois j'arrête de venir te déranger ! Merci enfin à Yann, Jean-Philippe et Christophe de l'ECAM pour les conseils que vous avez pu m'apporter au cours de nos nombreuses discussions.

Un grand merci à l'ensemble des personnes présentes à ma soutenance de thèse, ce fut un réel plaisir de vous présenter mon travail et votre venue n'a fait que rendre cette journée encore plus mémorable. « Last but not least », un grand merci à ma famille et à mes amis qui ont été présents tout au long de ces trois années, notamment à mes colocataires Mag puis Stéphane (« p'tit mario ? ») et à mes parents qui m'ont toujours conseillé, soutenu et encouragé dans mes choix.

Abstract

The growing environmental concerns, along with the continuous increase in the price of fossil fuels, have highly motivated car manufacturers worldwide to improve the efficiency of their vehicles. The tribological properties of engine and gearbox lubricants have a significant impact on the global efficiency of vehicles, as they contribute to reducing friction in many contacts and allow the downsizing of various components by providing their surfaces with anti-wear protection. The recent breakthroughs in nanoparticle synthesis have opened new prospects in terms of lubricant additivation, with the discovery of the excellent friction and wear reducing properties of nanoparticles such as Inorganic Fullerene-like (IF-) molybdenum or tungsten disulfides.

The tribological potential of IF-MoS_2 for automobile applications was investigated in this work. The respective influences of nanoparticle size and structure were first of all studied, revealing that poorly crystalline nanoparticles were more efficient in maintaining low-friction tribofilms on steel substrates in severe boundary lubrication regimes regardless of size (for the range studied). All the nanoparticles tested however showed similar performances when proper oil recirculation was ensured, providing a continuous feeding of the contact in nanoparticles.

The IF-MoS_2 nanoparticles lost their lubricating abilities when added to fully-formulated lubricants. This behavior was attributed to the presence of dispersants in the oil, which dispersed the nanoparticles effectively but prevented them from forming tribofilms on the rubbing surfaces. The well-dispersed IF-MoS_2 were shown to enter the contact and exfoliate, but an excessive adsorption of the dispersants on the released MoS_2 platelets and/or the steel surfaces is thought to prevent tribofilm adhesion. A balance between nanoparticle dispersion and tribological performance was then found, by using very low concentrations of dispersants.

The behavior of nanoparticle-doped oils in various scenarios related to automobile applications was finally explored. The IF-MoS_2 provided significant friction and wear reduction at ambient temperature and in milder rolling/sliding test conditions, for smooth and rough surfaces. The risks related to the presence of nanoparticles in the oil in full-film lubrication regimes were partially lifted, with no significant influence on friction witnessed for all the test conditions considered. The ability of IF-MoS_2 nanoparticles to protect steel surfaces from surface-initiated Rolling Contact Fatigue was finally shown.

Keywords: *IF-MoS_2 nanoparticles, lubricant additives, boundary lubrication, friction, wear, dispersants, Rolling Contact Fatigue.*

Résumé

Les enjeux environnementaux actuels, ainsi que la hausse continue du prix du pétrole, ont incité les constructeurs automobiles du monde entier à améliorer le rendement de leurs véhicules. Les propriétés tribologiques des lubrifiants des moteurs et boîtes de vitesses ont une influence considérable sur le rendement global des véhicules. Ils réduisent en effet le frottement généré par un grand nombre de contacts, et permettent parfois la réduction de la taille de différents composants en leur conférant une meilleure résistance à l'usure. Les avancées récentes en termes de synthèse de nanoparticules ont ouvert de nouvelles perspectives en termes d'additivation de lubrifiants avec, par exemple, la découverte des excellentes propriétés tribologiques des nanoparticules inorganiques de type fullerène comme le disulfure de molybdène ou de tungstène.

L'objectif de ce manuscrit est d'évaluer le potentiel tribologique des nanoparticules IF-MoS_2 dans l'optique d'une application automobile. L'influence de la taille et de la structure des nanoparticules a d'abord été étudiée. Les nanoparticules peu cristallines se sont révélées être plus aptes à maintenir un tribofilm performant sur des surfaces en acier dans des conditions de lubrification limite, indépendamment de leur taille. Toutes les nanoparticules testées ont cependant atteint des performances équivalentes lorsqu'une recirculation de l'huile était imposée, permettant de maintenir une alimentation continue du contact en nanoparticules.

Une fois incorporées dans une formulation d'huile complète, les nanoparticules IF-MoS_2 perdent leurs propriétés tribologiques. Les dispersants contenus dans l'huile, bien que permettant une bonne dispersion des IF-MoS_2, semblent responsables de leur inefficacité en empêchant la formation de tribofilms sur les surfaces antagonistes. Une fois correctement dispersées, les nanoparticules pénètrent toujours le contact et se retrouvent bien exfoliées. Une adsorption excessive des dispersants sur les feuillets de MoS_2 ainsi libérés et/ou sur les surfaces en acier semble nuire à l'adhésion du tribofilm. Un équilibre entre dispersion des nanoparticules et performance tribologique a ensuite été trouvé, en utilisant de très faibles concentrations de dispersants.

Le comportement des huiles dopées en nanoparticules dans des conditions plus proches d'une application automobile a finalement été exploré. Les IF-MoS_2 ont permis une réduction significative du frottement et de l'usure à température ambiante et en roulement/glissement, à la fois pour des surfaces lisses et rugueuses. Les risques associés à la présence de nanoparticules dans l'huile dans les régimes de lubrification en film complet ont été partiellement levés. Aucun impact significatif n'a en effet été constaté sur le coefficient de frottement pour l'ensemble des conditions d'essais retenues. Le potentiel des nanoparticules IF-MoS_2 pour la protection des surfaces soumises à la fatigue de contact a enfin été démontré.

Mots clés: *nanoparticules IF-MoS_2, additifs, lubrification limite, frottement, usure, dispersants, fatigue de contact.*

Table of contents

List of Figures

List of Tables

Nomenclature

a	Major semi-axis of contact area	[m]
b	Minor semi-axis of contact area	[m]
h_c	Central film thickness	[m]
h_m	Minimum film thickness	[m]
w	Load	[N]
x	Rolling direction	[-]
y	Direction transverse to rolling	[-]
AW	Anti-Wear	
DLS	Dynamic Light Scattering	
E_i	Young modulus of material *i*	[Pa]
E^*	Equivalent Young Modulus $E^*=[(1-\nu_1^2)/E_1+(1-\nu_2^2)/E_2]^{-1}$	[Pa]
EDX	Energy-Dispersive X-ray spectroscopy	
EHL	Elasto-Hydrodynamic Lubrication	
EP	Extreme Pressure	
FIB	Focused Ion Beam	
FM	Friction Modifier	
HD	HydroDynamic	
HFRR	High-Frequency Reciprocating Rig	
HR-TEM	High-Resolution Transmission Electron Microscopy	
IF-MoS_2	Inorganic Fullerene-like Molybdenum disulfide	
IF-WS_2	Inorganic Fullerene-like Tungsten disulfide	
LC	Large Crystalline	
LpC	Large, poorly Crystalline	
MoDTC	Molybdenum Dithio-Carbamates	
MPR	Micro-Pitting Rig	
MTM	Mini-Traction Machine	
NTR	Nanovisu Test Rig	

P_h	Maximum hertzian pressure	[Pa]
PAO	PolyAlphaOlefin	
R_i	Radius of curvature in the *i* direction	[m]
Ra_i	Arithmetic average surface roughness of surface *i*	[m]
Rq_i	Root mean square surface roughness of surface *i*	[m]
RCF	Rolling Contact Fatigue	
SC	Small Crystalline	
SpC	Small, poorly Crystalline	
SRR	Slide-to-Roll Ratio [$SRR=U_s/U_r$]	
T	Temperature	[°C]
U_i	Velocity of *i*	[$m.s^{-1}$]
U_r	Rolling velocity [$U_r=(U_1+U_2)/2$]	
U_s	Sliding velocity [$U_s=\lvert U_2-U_1 \rvert$]	
V_i	Volume of *i*	[m^3]
XPS	X-ray Photoelectron Spectroscopy	
ZnDTP	Zinc Dialkyldithiophosphates	
η	Dynamic viscosity	[$Pa.s^{-1}$]
λ	Film thickness ratio	[-]
ν_i	Poisson's ratio of material *i*	[-]
ϱ_i	Volumetric mass density of material *i*	[$kg.m^{-3}$]
υ	Kinematic viscosity	[$m^2.s^{-1}$]
Φ_i	Diameter of *i*	[m]

Introduction

Driving to work on a rainy day, packing the trunk with goods for the family, getting away for the weekend or leaving on holiday with the kids: we often favor our car over other means of transportation to get from point A to point B easily, quickly and comfortably. According to INSEE (National Institute of Statistics and Economics), more than 82% of French households owned a car in 2008. These vehicles are mostly powered by fossil fuels, therefore contributing significantly to the global greenhouse gas emissions. The growing environmental concerns, along with the continuous increase in the price of petrol, have motivated car manufacturers worldwide to improve the efficiency of their vehicles while maintaining competitive performances. From hybrid fuel technologies to more aerodynamic car profiles, this race for efficiency has sometimes led to a complete structural remodeling of recent vehicles. Countless other improvements, often more discreet, are also continuously being developed to reduce vehicle consumption and gas emissions such as innovative tires, cleaner exhausts, or optimized combustion chambers. Many manufacturers have moreover adopted a downsizing policy for their engines and gearboxes, in order to reduce the weight of their vehicles. Reducing the size of contacting components is however likely to increase their friction and wear. Although adapted solutions can be found to protect specific surfaces or reduce friction locally (geometrical modifications, stronger materials or surface coatings for example), the oil properties will affect the tribological performance of all lubricated contacts.

This work results from a collaboration between LaMCoS, LTDS and PSA Peugeot Citroën, and investigates the potential of nanoparticle-doped lubricants for automobile applications. The very first Inorganic Fullerene-like (IF-) nanoparticles, such as those studied here, were synthesized less than twenty years ago. In recent years, their addition to base oils has been shown to provide exceptional benefits in terms of friction and wear reduction for severe mechanical contacts. Fullerene-like nanoparticles furthermore hold many advantages over current additives. They are consumed only when needed inside the most severe contacts and are theoretically chemically inert, providing interesting prospects in terms of additive durability. The particle structure of these phosphorus-free additives may also prevent them from entering the combustion chamber along with oil residues, participating in the reduction of polluting emissions. The lubrication mechanisms associated to the outstanding tribological performance of these nanoparticles have been studied extensively, but the ideal test conditions chosen to understand their behavior are not representative of their potential in complex, real-life mechanical systems.

The aim of this study was to address some of the many issues remaining before eventually incorporating Inorganic Fullerene-like nanoparticles in fully formulated lubricants. The two first chapters of this manuscript are devoted to providing the reader with sufficient information for a full understanding of the following sections. **Chapter One** describes the basics of automobile lubrication and proposes a state of the art concerning nanoparticle lubrication. The experimental techniques and methodologies used throughout this work are then exposed in **Chapter Two**. This includes general information about the different tribometers and test procedures, as well as the description of the various observation and characterization techniques used to analyze the test samples.

The incorporation of nanoparticles in future lubricant formulations can be seen as a three-step process, as schematized below. The first step, addressed in **Chapter Three**, is to determine which parameters will affect the efficiency of these additives. Nanoparticles of different sizes and structures were tested, so as to be able to differentiate the influences of these two properties on their tribological performance. Surface analyses and cross-sections provided further understanding of the test results, by revealing the structure, composition and evolution of the tribofilms formed on the surfaces.

The second step of the process is to be able to include the nanoparticles in the lubricant while guaranteeing their compatibility with the other oil additives, as well as a proper dispersion and a low sedimentation rate. This challenge, faced in **Chapter Four**, was made difficult by the initial finding that the nanoparticles lost all of their tribological properties when added to a fully-formulated lubricant. An investigation was then carried out to understand the cause of this performance loss, by combining surface analysis and observation techniques.

The final step in the development of nanoparticle-doped lubricants is to determine their potential in a complex environment such as a car. **Chapter Five** provides a glimpse of the behavior of such oils in various real-life scenarios, with tribological testing under various temperatures and contact conditions. The influence of surface roughness was also addressed, as well as the performance of the nanoparticles in applications subject to fatigue. The risks related to the presence of nanoparticles in the oil for specific contacts were finally investigated.

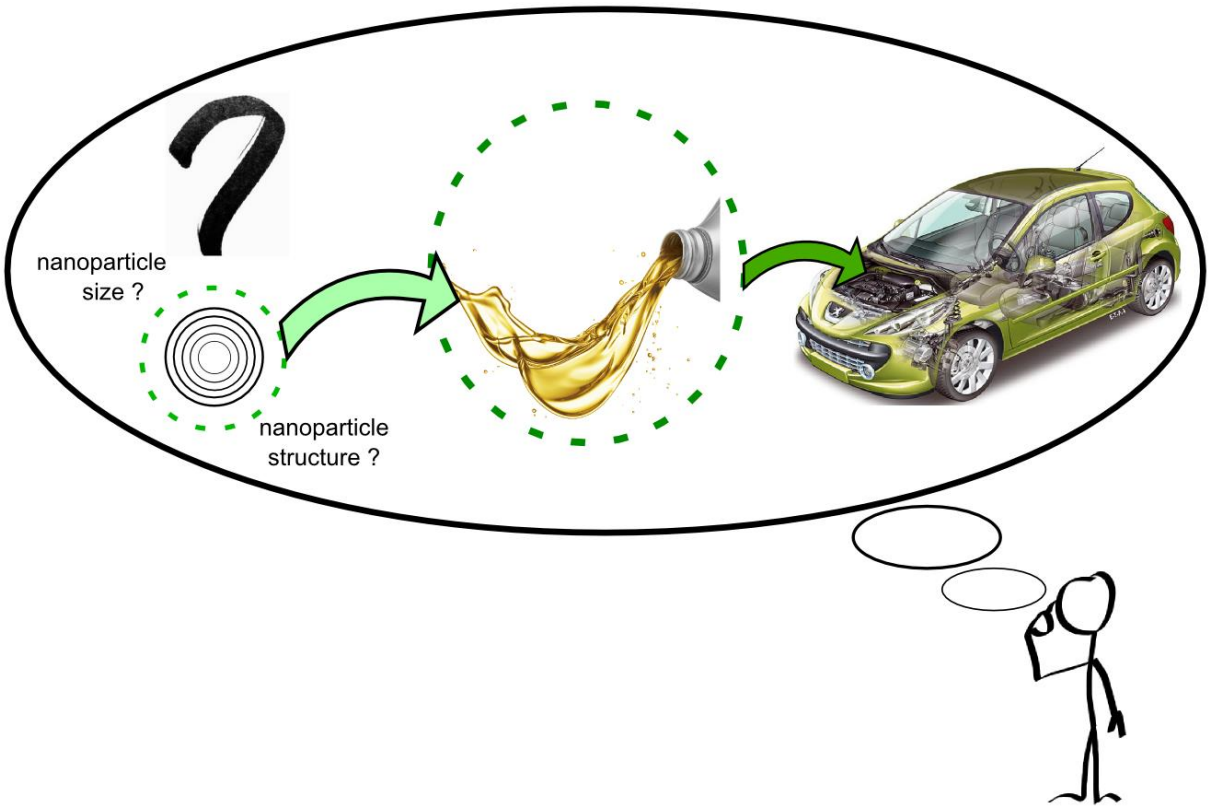

Chapter One

State of the Art

The first chapter of this work introduces the reader to automotive lubricants and to their recent doping with specific nanoparticles. The influence of engine and gearbox oils on the efficiency of vehicles is first described through environmental considerations and tribological aspects. The composition of modern, fully formulated oils is then detailed, along with the particular role of the chosen base oils and the different additives. A brief history of the relatively recent nanoparticle-doped lubricants is then proposed, in order to provide the reader with an overview of the existing solutions and their limitations.

1. 1. Automotive lubrication

1. 1. 1. Environmental issues and regulations

There has been a wide debate in recent years regarding the influence of human presence on the climate changes observed in the last decades. Whether or not parameters other than the exponential growth of industrial activities have contributed to the average temperature rise, the continuous increase in polluting emissions is undeniable. The Intergovernmental Panel on Climate Change (IPCC) recently provided a report in which the evolution of the anthropogenic emissions and their sources were synthesized (**Figure 1.1**). The results were unambiguous: the worldwide greenhouse gas (GHG) emissions increased from 28.7 to 49.0 CO_2-equivalent gigatonnes per year between 1970 and 2004. Although many human activities are responsible for these GHG (deforestation, decay, agriculture, waste, energy supply…), the use of fossil fuels alone represented more than half of the total emissions (56.6 %). These fuels are used to provide energy in many sectors, but transportation alone caused 13.1% of the global GHG emissions in 2004.

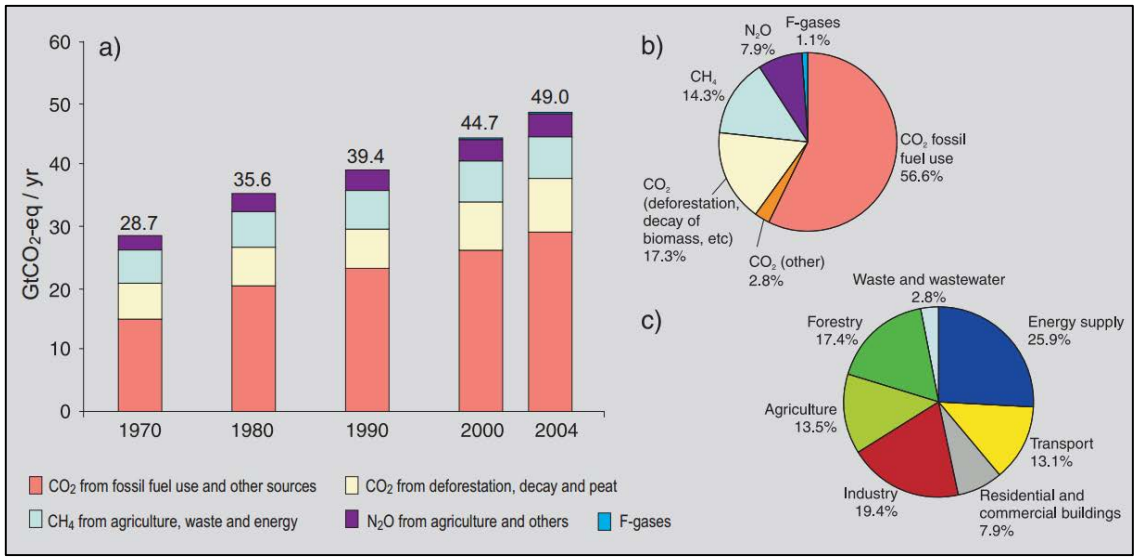

Figure 1.1. Evolution of polluting emissions and their sources (IPCC synthesis report, 2007)
(a) Global annual emissions of anthropogenic GHGs from 1970 to 2004
(b) Share of the different GHGs in the total emissions of 2004 (in terms of CO_2-eq.)
(c) Share of different sectors in total GHG emissions of 2004 (in terms of CO_2-eq.)

Following the United Nations Framework Convention on Climate Change (UNFCCC, also known as the "Earth Summit" and signed in 1992), many nations committed to undertaking strong measures to reduce their greenhouse gas emissions. In the European Union, emission standards were set to limit the exhaust emissions of new vehicles. These regulations currently concern nitrogen oxides (NO_x), hydrocarbons (HC), carbon monoxide (CO) and particulate matters (PM), and are adapted to the different vehicle types and motorizations. Lower limits have continuously been applied since the first standard (Euro 1) in 1992. The latest Euro 6 standard will be effective by the end of 2014. For the diesel engines of passenger cars, CO emission limits have been reduced from 2.72 to 0.5 g/km in those 22 years, and HC+No_x and PM emission limits have decreased from 0.97 to 0.17 g/km and 0.14 to 0.005 g/km respectively (see **Figure 1.2**). The nature and quantity of emissions due to a given vehicle depends on many factors, such as the type of fuel and lubricant used or the quality of the exhaust line. GHG emissions are however directly linked to the fuel consumption, as they originate from the combustion of the diesel or petrol.

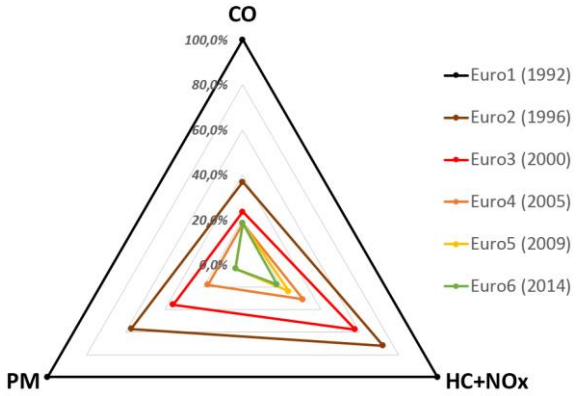

Figure 1.2. Relative evolution of CO, HC+NO_x and PM European emission limits from 1992 (Euro 1 standard) to 2014 (Euro 6 standard)

From a customer's perspective, reducing the fuel consumption of new vehicles has also become a real sales argument in recent years. Apart from the general concern for the environment, the decreasing amount of fossil fuels left on the planet causes a continuous increase in their price. Improving the efficiency of new vehicles has therefore become a priority for most car manufacturers, who have been analyzing and working on all potential sources of energy loss. The quality of the combustion taking place in the combustion chamber has for example been widely studied in order to optimize the quantity of fuel effectively used [1–3]. Many companies have also adopted the "Down-sizing" strategy, which consists in preserving – or even increasing – the power of their vehicles while decreasing the size (and therefore mass) of as many components of the engine and gearbox as possible. Reducing friction in mechanical contacts has furthermore become an important issue for car manufacturers, as attested by the many collaborations with tire manufacturers to develop resistant low-friction tires to mount on new vehicles. The main sources of mechanical energy loss however reside in engines and gearboxes, as shown on **Figure 1.3**. Many solutions exist to reduce friction in these contacts, such as using different materials, coatings, geometries or varying the surface finish. Although lubricant formulation has been widely

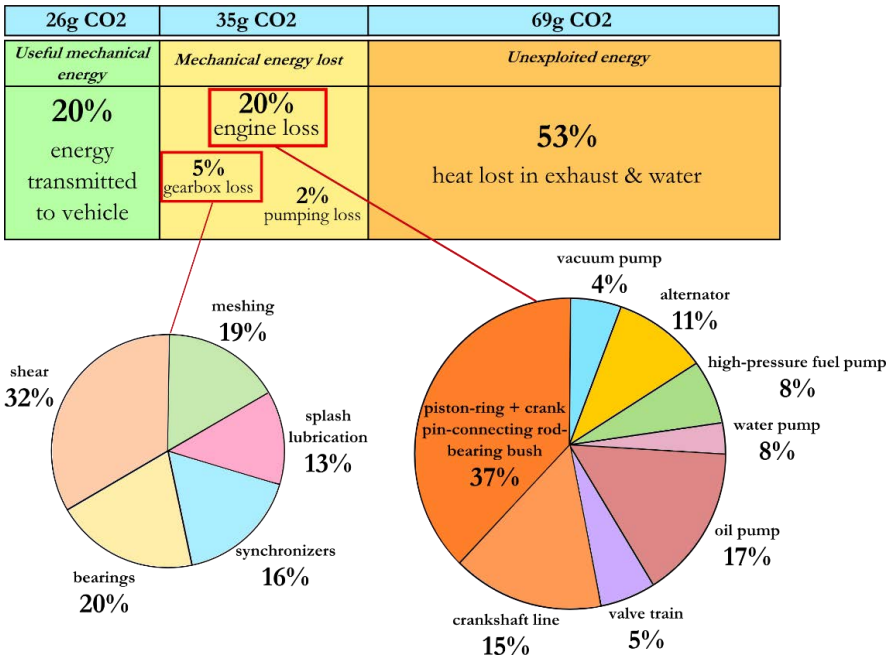

Figure 1.3. Estimation of the main sources of energy loss and corresponding CO_2 emissions for a typical Diesel 1.6L engine and gearbox (values extracted from internal PSA Peugeot Citroën data)

overlooked in the early years of automobile history, it has now been recognized as a key parameter in vehicle efficiency. The friction-reducing properties of the oil will indeed affect all the lubricated contacts of the system, albeit differently depending on the lubrication regime and film thicknesses involved.

1. 1. 2. From mechanical systems to tribological contacts: the different lubrication regimes

The choice of an engine or gearbox oil is made difficult by the variety of contacts to lubricate. The main components and associated contacts of common internal combustion engines are shown on **Figure 1.4** [4]. These contacts operate at varying temperatures, and have different geometries and operating conditions (surface velocities, contact pressures, amount of sliding…).

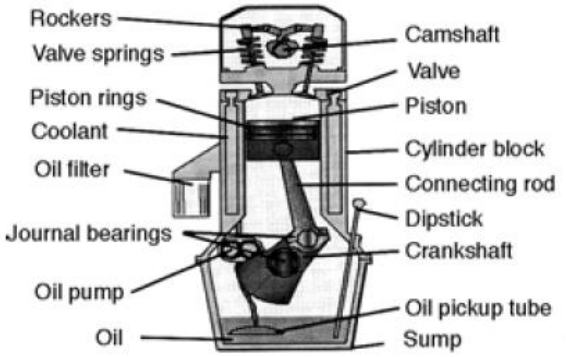

Figure 1.4. Main engine components in a reciprocating internal combustion engine [4]

Depending on the lubricant film thicknesses involved for each contact, they are said to operate in one or several lubrication regimes. These are best depicted by the Stribeck curve (**Figure 1.5**), which plots the friction coefficient as a function of a dimensionless number sometimes referred to as the Hersey number [5], which depends on the lubricant viscosity, the contact velocity and the contact pressure. Varying Hersey numbers affect the film thickness of the oil, which will have direct consequences on the friction generated inside the contact.

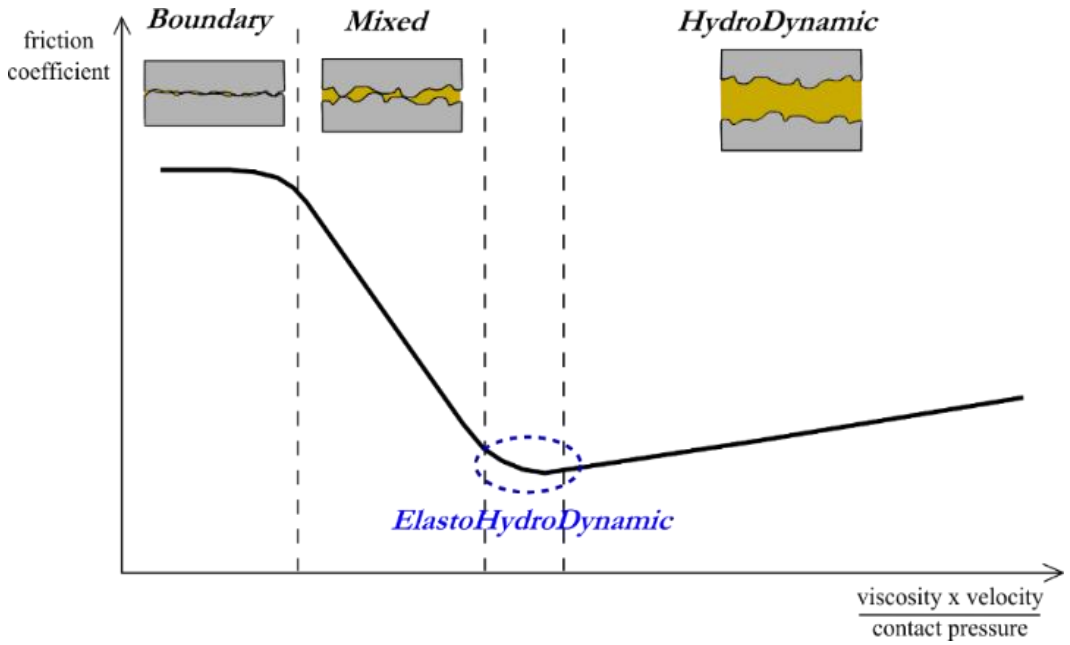

Figure 1.5. Typical Stribeck curve and the associated lubrication regimes

Three main lubrication regimes are generally considered:

- HydroDynamic (HD) lubrication. For high lubricant viscosities, high velocities and/or low contact pressures, the oil film is thick enough to fully separate the contacting surfaces and therefore supports all the load. There is no (adhesive) wear occurring on the surfaces, and the friction coefficients are generally very low as they only originate from the shearing of the fluid. In this lubrication regime, friction will therefore increase for more viscous fluids and thicker film thicknesses.

- Mixed lubrication. This lubrication regime constitutes the transition between the HydroDynamic and Boundary regimes, and is characterized by increasing friction for lower viscosities, lower velocities and/or higher contact pressures. As the film thickness drops below the height of the surface roughness, an increasing number of direct contacts occurs between both surfaces. The load is then supported by both the fluid and the surface asperities, and wear starts occurring.

- Boundary lubrication. For low lubricant viscosities, low velocities and/or high contact pressures, little to no lubricant separates the surfaces. This is the most severe lubrication regime, characterized by high friction and wear. The presence of the lubricant however remains vital, as the oil dissipates part of the heat generated by the surfaces and provides the contact with friction and wear-reducing additives.

For highly loaded contacts in the HydroDynamic regimes, the elastic deformation of the surfaces may become significant. The lubrication regime is then ElastoHydroDynamic (EHD), and is generally associated with non-conformal contacts and very thin film thicknesses. The full separation of the surfaces, along with the low amount of fluid subjected to shearing, results in the minimum friction point on the Stribeck curve (shown on **Figure 1.5**). This lubrication regime is therefore of great interest in terms of contact efficiency, and most bearings are designed to operate under the corresponding Hersey number. The term "*full-film lubrication*" is often used to designate both HD and EHD contacts.

A simple tool, called the film thickness ratio (or parameter), can be used to predict the lubrication regime of a given contact. It is defined by the ratio between the film thickness and the mean surface roughness, as follows:

$$\lambda = \frac{h}{\sqrt{\left(R_{q_1}{}^2 + R_{q_2}{}^2\right)}} \tag{1}$$

where λ is the film thickness ratio, h is the film thickness calculated for smooth surfaces and R_{qi} is the root mean square roughness of surface i.

The value of lambda gives an indication on the separation of the surfaces, and therefore on the severity of the contact. Different definitions of λ can be found in the literature depending on the application, with h for example chosen either as the minimum (h_m) or central (h_c) film thickness. When calculating the film thickness ratio using h_c, the following cases are generally considered [6]:

- **$\lambda \geq 3$**: the film thickness exceeds the surface roughness, full-film lubrication is ensured.

- **$1 \leq \lambda < 3$**: the film thickness is of the same order of magnitude as the surface roughness, resulting in mixed lubrication.
- **$\lambda < 1$**: the film thickness is smaller than the surface roughness, resulting in boundary lubrication.

All of the lubrication regimes presented above are met in automotive applications. Most conformal contacts, such as found in thrust or journal bearings, generally operate in the HD regime [5]. Boundary or mixed lubrication contacts are however common in the valve train, the piston-ring assembly and the transmission clutch [4]. Many contacts are furthermore prone to transitions between the different lubrication regimes, as illustrated on **Figure 1.6** in the case of gears [7].

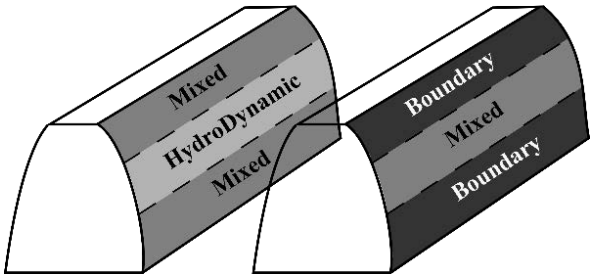

Figure 1.6. Transitions between the different lubrication regimes on gear teeth for mild (left) and more severe (right) operating conditions

The engine or gearbox lubricant chosen must therefore be able to minimize friction for the widest range of lambda values possible. The general trend among car manufacturers today is to choose low-viscosity oils, which is the only solution to reduce friction in the HydroDynamic regime for a given set of operating conditions. As a direct consequence, friction and wear tend to increase in all boundary/mixed lubricated contacts. In order to counteract this effect, new and more efficient additives are constantly being sought to protect the surfaces and provide low-friction interfaces in these severe contacts.

1. 1. 3. Composition of current lubricants

Three different natures of lubricants exist: liquid (vegetal/animal, mineral and synthetic), semi-solid (grease, paraffin, vaseline, wax…) and solid (lamellar, polymeric, soft metals, oxides…). The use of liquid lubricants is however more widespread (more than 95% of the market [8]). They are also the main source of lubrication in automotive engines and gearboxes, although additional solutions such as solid coatings are often used for additional benefits. Although the primary function of liquid lubricants is to separate the surfaces in order to reduce friction and wear, it also plays a predominant role in cooling the mechanical system by absorbing part of the heat generated in the contacts. Liquid lubricants finally contribute to the riddance of particle contaminants, by washing away any wear debris issued from the interface between two surfaces.

Current commercial liquid lubricants are mostly made of base oil, either natural or synthetic. The base oil alone however rarely meets all the requirements of the lubricant, and is therefore enriched with additives to comply with the specifications in terms of viscosity, friction, ageing, oxidation, foaming, etc.

The different base oils can be divided into three categories:

- **Vegetable oils.** These oils are extracted from plants, such as rapeseed. They are currently extensively studied for their biodegradable properties, and could be of interest for outdoor

applications presenting risks of polluting the environment (agricultural machinery for example). They are however not used for automotive applications because of their low stability in terms of oxidation for high-temperature applications.

- **Mineral oils.** Mineral oils are extracted from the petroleum fractions formed during the distillation of crude oils. The result is a mixture of many hydrocarbons with a small amount of oxygen, sulfur and nitrogen-based residues. Depending on the nature of the crude oil, the hydrocarbons contained in the base oil can be either mainly paraffinic, naphthenic or aromatic [9]. This will affect various properties of the oil such as their Viscosity Index (VI, measures the drop in viscosity when temperature rises from 40 to 100°C: low VIs indicates a very viscous oil at low temperatures and very fluid at high temperatures), their resistance to oxidation, their compatibility with elastomers, their solvent power and their pour point (**Table 1.1**). Most European refineries produce mainly paraffinic mineral oils, and the naphthenic-based mineral oils are slowly disappearing mostly because of their higher price, higher toxicity, lower availability and behavior at high temperatures [8]. The aromatic hydrocarbons in mineral oils are furthermore reduced to the maximum during the refining process, given their low performances (**Table 1.1**).

Type of oil / *Property*	Paraffinic	Naphthenic	Aromatic
Pour point	Bad (-9/-18°C)	Very low	Very low (-73/-20°C)
VI	High (≈ 100)	Low (0<VI<60)	Very low (<0)
Resistance to oxidation	Good	Not as good	Bad
Solvent power	Medium to low	Fairly high	Very high
Compatibility with elastomers	Good	Not as good	Bad

Table 1.1. Comparison of the properties for the different natures of mineral oils [9]

- **Synthetic oils.** Synthetic base oils were originally developed to handle the temporary lack of mineral oils on the market [10]. There are many different types of synthetic base oils: they can be produced from a number of components (olefins, aromatics, alcohols, acids, halogenated compounds…) and using a variety of techniques (polymerization, esterification, alkylation, fluorination…). In the automotive industry, the most commonly used synthetic oils are undoubtedly polyalphaolefins (PAOs). Their chemical structure resembles the best hydrocarbons found in mineral oils, making them ideal candidates for applications where the latter are usually used. All PAOs are given a number indicating their kinematic viscosity at 100°C in $mm^2.s^{-1}$ (PAO 4, PAO 8…). They do not contain any aromatic compounds nor impurities, and exhibit very good properties compared to those presented in **Table 1.1** for mineral oils. PAOs stand out by their very high VIs (from 120 up to 170 for the more viscous oils) and for the wide range of viscosities they can achieve (from PAO 2 to PAO 100). Their pour points are furthermore very low (between -60 and -70°C for the most common PAOs), and they are also very resistant to thermo-oxidation and neutral towards elastomers. Being very apolar, they have a very low solvent power. This is beneficial in terms of foaming, aeration and demulsification but is detrimental in terms of additive solubility. This last aspect can however be compensated by adding small quantities of ester in the oil (3 to 15%).

The American Petroleum Institute (API) currently classifies mineral and synthetic base oils into 5 groups, depending on their saturated hydrocarbon (HC) content, their sulfur content and their VI [11]. All mineral oils belong to the groups 1 - 3, while the synthetic base oils belong to

groups 4 - 5 (**Table 1.2**).

Group	Type	Saturated HC content (wt%)	Sulfur content (wt%)	VI
I	HC	< 90	> 0,03	80 ≤ VI ≤ 120
II	HC	≥ 90	≤ 0,03	80 ≤ VI ≤ 120
III	HC	≥ 90	≤ 0,03	≥ 120
IV	All hydrogenated polyalphaolefins (PAOs)			
V	Others (esters, PIB, DAB, PAG, alkylnaphthalens etc.)			

Table 1.2. API classification of base oils [11]

As of today, the use of synthetic and semi-synthetic (mixtures of synthetic and mineral) base oils has become nearly systematic in the automotive industry because of their better thermal stability and resistance to oxidation (among others).

In fully formulated lubricants, the properties of the base oil are enhanced by the presence of many additives in their composition. The nature of the base oil may however have an influence on additive performance, by affecting their solubility and/or their response [12]. A base oil with high solubility characteristics may indeed retain certain surface active additives in solution, preventing them from adsorbing or reacting chemically with the surfaces. An excessively poor solubility of the additives, on the other hand, may cause the additives to separate from the oil before fulfilling their role. Before refining, base oils often contain natural sulfur, nitrogen and phenolic inhibitors as well as undesirable materials. These natural inhibitors contribute to providing unrefined stocks with a good resistance to oxidation, but are removed because they interfere with additive performance. Surface protecting additives are furthermore known to be less efficient when the base oil possesses a strong aromaticity [13]. The performance of the additives will also depend on the viscosity of the base oil, as they will be more mobile – and thus more active – in a less viscous media.

The nature of the additives added in the lubricant formulation will therefore greatly depend on the base oil. Synthetic hydrocarbons, such as polyalphaolefins, often exhibit poor solubility characteristics but excellent additive response. Esters are however excellent solvents (when they don't react with the additives to form precipitates) and may vary in additive response. Optimal solubility and additive response can be sought by mixing these synthetic base oils with each other or with mineral oils.

The base oil generally constitutes between 75 and 95% in mass of a lubricant, the rest of the formulation consisting in additives of different natures [14]. The main types of additives are the following:

- **Boundary lubrication additives.** In the most severe lubrication regimes, when surface separation is near non-existent, these additives adsorb or react chemically with the surfaces to form protective films on the steel substrate. There are different types of boundary lubrication additives, fulfilling different functions. Friction reducers form low shear-strength films on the surfaces, ensuring a reduction of the friction taking place at the interface. Friction Modifiers (FM) have a very similar behavior, but their primary function is to avoid stick-slip (uneven friction) in components immerged in the oil [15]. In the transmission, for instance, FM ensure smooth gear shifting at low velocities while maintaining sufficient friction under regular conditions to prevent clutch slippage. Fully formulated lubricants generally contain under 2% in mass of friction reducers

and FM [14]. Molybdenum dithio-carbamates (MoDTC) are most often used in automobile applications, due to their capacity to form excellent friction-reducing MoS_2 films on steel surfaces.

Under the high temperatures generated by severe metal-metal contacts, Extreme Pressure (EP) additives release sulfur and/or chlorine, forming friction-reducing metal sulfide and/or chloride films on the substrate. More importantly, these films resist to very high loads and prevent surface adhesion and welding up to very high temperatures (800-850°C for sulfides and 600-650°C for chlorides [16]).

EP additives are a particular type of Anti-Wear (AW) additives, which define all the surface-protecting compounds. Other AW additives are very reactive chemically, less labile and more thermally stable. The most common AW additives for automotive engines are zinc dialkyldithiophosphates (ZnDTP), which are also good oxidation inhibitors. Anti-Wear additives are generally found in concentrations varying from 0.5 to 2 wt% in current lubricants [14].

Because of their action on the contacting surfaces, friction-reducing, Extreme-Pressure, Anti-Wear and other boundary lubrication additives often fulfill several roles at once.

- **Rust and corrosion inhibitors.** These additives are generally named "rust inhibitors" when aiming to reduce the humid corrosion of ferrous metals and "corrosion inhibitors" when fighting the acid or sulfur corrosion of non-ferrous metals such as copper alloys [16]. Rust inhibitors are polar compounds, and act by forming a waterproof film by adsorption on the surfaces. The polar, hydrophobic group of the compound attaches to the surface while the hydrocarbon chain of the compound is directed towards the lubricant. The surface has then changed from hydrophilic to hydrophobic and is said to have been "passivated". The most common rust inhibitors for engines are organometallic detergents such as calcium or magnesium sulfates, as well as barium-based detergents. Corrosion inhibitors may also act by surface passivation (formation of a protective film on the surface), or by deactivating corrosive contaminants in the lubricant (such as the sulfur liberated by some EP additives at moderate temperatures) through the formation of stable chemical compounds [12]. Low concentrations of rust and corrosion inhibitors are used in fully formulated oils, typically under 1 wt% [14].

- **Oxidation inhibitors.** For temperatures above 50-60°C, the presence of oxidation inhibitors in fully formulated lubricants becomes essential to slow down the oxidation of hydrocarbons and other constituents of the lubricant. The reaction of free radicals with oxygen eventually leads to the formation of new free radicals and hydroperoxides. The oxidation rate then increases as these free-radicals are formed faster than they are used. The polymerization of oxygen compounds can cause lubricant thickening and the formation of sludge and deposits [12]. The role of the oxidation inhibitors is to interfere with these mechanisms. This can be achieved by (a) deactivating the free radicals with radical inhibitors (phenolic compounds, aromatic amines, phenates…), (b) metal deactivation or surface passivation to reduce the catalytic action of metals (these additives then also act as corrosion inhibitors) or (c) the destruction of the hydroperoxides responsible for the propagation of the chain reaction of oxidation [16]. Zinc dithiophosphates (ZnDTC) are very effective in decomposing these hydroperoxides into stable compounds, and are therefore often used in engines both as AW additives and oxidation inhibitors. Typical concentrations of oxidation inhibitors in engine lubricants are below 1 wt% [14].
- **Detergents and dispersants.** The role of these additives is to ensure the cleanliness of

the lubricant and of the surfaces. Detergents, more active for hotter lubricant temperatures, prevent deposits from adhering to the surfaces. The primary function of dispersants is to maintain insoluble materials (soot, wear debris, external contaminants…) in suspension and non-agglomerated until they are removed by the oil filter. Although detergents also have a dispersing effect, dispersants are vital to preserve sedimentation and slow down sludge deposit under ambient temperatures and under cold start/stop conditions. The three main types of detergents are calcium- or magnesium-based alkylsulfonates (very detergent, moderately dispersant and also rust inhibitors), alkyl phenates (less detergent than sulfonates but also oxidation and wear inhibitors) and alkyl salicylates (also less detergent than sulfonates but anti-wear too) [15]. Barium-based detergents (alkylphosphonates and alkylthiophosphonates) have been used in the past for their combined detergent, anti-wear and anti-oxidation properties but are being abandoned due to their poor thermal stability and their toxicity.

The most widely used types of dispersants (alkenyl succinimides and succinate esters) consist of a polar, lipophobic group (sometimes referred to as the "head") which adsorbs on insoluble impurities (solid or liquid) and of a long, non-polar, lipophilic hydrocarbon chain (the "tail") which is oil-miscible. Dispersants more or less active can be used depending on the tendency of the oil to form sludge in a given environment, but strongly polar materials have proved detrimental in terms of anti-wear film formation [14]. Alkenyl succinimides, for instance, alter the AW and oxidation inhibiting properties of ZnDTP. One solution to this problem consists in treating the succinimides with boric acid in order to obtain borate succinimides, which interact less with ZnDTP [15].

Relatively high concentrations of detergents and dispersants are used in commercial lubricants. Detergent contents can vary from 3 to 8% in petrol engines and from 4 to 12% in diesel engines, while dispersants concentrations can reach up to 6 and 8% for these two fuels respectively [15].

- **VI improvers.** The viscosity of oils is very sensitive to changes in temperature: the viscosity of a high-quality mineral oil may decrease by a factor of 400 between -5°C (cold starting temperature) and 120°C (lubricant temperature reached in some parts of the engine) [14]. While high viscosities are generally desirable at high temperatures to ensure sufficient film thicknesses and therefore prevent wear, excessive viscosities at low temperatures will generate great power losses and can even prevent certain mechanical systems from operating. The viscosity of a typical SAE 40 viscosity grade oil is for example adapted to engine lubrication at 100°C (14.0 cSt) but is far too viscous to operate under very cold temperatures. An SAE 10W oil, compatible with extreme temperatures, will on the other hand not be viscous enough to protect the engine under an operating temperature of 100°C. The addition of VI improvers will result in so-called "multigrade" lubricants, with suitable viscosities for low temperatures and sufficient viscosities for engine lubrication under more common operating conditions (**Table 1.3**).

SAE viscosity grade	VI improver	Viscosity		VI
		cSt at 100°C	cP at -18°C	
40	No	14.0	15 000	100
10W	No	6.5	2 000	100
10W40	**Yes**	**14.0**	**2 350**	**145**

Table 1.3. Effect of VI improver (dynamic viscosity, here in cP, is used for low temperatures while the kinematic viscosity, here in cSt, is quoted for the high temperature part of the SAE classification) [12]

To achieve this, VI improvers consist in polymers that are increasingly oil-miscible at higher

temperatures. As a result, the polymer macromolecules are closed up at low temperatures and occupy a small volume fraction of the oil. For higher temperatures, the interactions between the VI improvers and the oil increase drastically, causing the polymer chains of the additive to unfold and the macromolecules to expand. The friction between the larger polymers results in a significant increase in the viscosity of the oil. Depending on the Viscosity Index needed, VI improvers can account for up to 15% of the lubricant formulation [15].

- **Emulsifiers and Demulsifiers.** Emulsifiers are used to stabilize oil-in-water or water-in-oil emulsions. These compounds exhibit a structure similar to dispersants, with a polar, hydrophilic group and a lipophilic hydrocarbon chain. The presence of water in lubricants is sometimes desired to improve cooling, due to its high specific heat and thermal conductivity [12]. For applications where water contamination of the lubricant is an issue (marine or industrial applications for example), demulsifiers are used to create unstable emulsions and therefore separate oil and water.

- **Foam decomposers.** Contact between the many surface active additives found in lubricants (dispersants, detergents, rust inhibitors…) and air may lead to foaming. This tendency can be greatly reduced by adding low concentrations (under 50 ppm) of foam decomposers to the oil formulation. These additives must be insoluble in the oil (such as high molar-mass silicones), have a lower surface tension than the oil and have high dispersing capacities (for storage). A poorly cohesive insoluble film will then form at the oil-air interface, removing the foam [15]. The presence of excessive amounts of foam decomposers in the lubricant may however have the opposite effect and favor foam formation.

- **Pour Point Depressants (PPDs).** Paraffinic hydrocarbons contained in mineral oils tend to crystallize in a lattice-like structure at relatively high temperatures (-6 to -18°C), called pour points, under which the lubricant loses its ability to flow. PPDs co-crystallize with the paraffin, modifying the growth of the structure and lowering the pour point of the lubricant. These additives, including polymethacrylates, alkylated naphthalene or phenol polymers and chlorinated polymers, are typically found in concentrations under 0.5 % [14]. They are useless for naphtenic and synthetic oils, as their pour point depends only on their viscosity and not on a crystallization process.

- **Others (tackiness agents, seal swell/anti-swell agents, dyes).** Various other types of additives can be found in lubricants, depending on the desired application. For open mechanisms (chainsaws, bare gears, motorbike chains…), tackiness agents provide oils with adhesive properties to prevent them from splashing. Lubricants can furthermore affect contacting elastomers, potentially inducing swelling, shrinking, hardening, softening or cracking of seals. Depending on the nature of the base oil used, seal swell or anti-swell agents may be used to reduce these effects. Finally, different dyes can be added to lubricant formulations for identification or marketing purposes. These dyes must not affect the other additives, and must be oil-miscible, stable, and effective under low concentrations.

The most common additives for the main categories presented above are listed in **Table 1.4**. Elaborating a lubricant formulation to meet given specifications consists in finding the balance between one or several base oils and the right additives. This is made even more complicated by the potential interactions between additives, as most are active chemicals and can lead to the

formation of new compounds. Some additives furthermore have several functions (AW and anti-oxidant properties of ZnDTP for example), while others may compete to achieve their role. Wear and rust inhibitors, for instance, both need to adsorb on metal surfaces to fulfill their function and one may therefore prevent the other from being fully active. The ratio between MoDTC and ZnDTP concentrations in the lubricant must also be carefully chosen to optimize both friction and wear reduction [17]. Boundary lubrication additives in general need a limited solubility in order to leave the bulk of the lubricant and interact with friction surfaces. The presence of excessive amounts of dispersants and/or detergents in the oil is therefore likely to hold these additives in solution and reduce their effectiveness.

BOUNDARY LUBRICATION (FM, EP, AW…)	**CORROSION INHIBITORS**	**OXIDATION INHIBITORS**	**DETERGENTS**	**VI IMPROVERS**
Metal dialkyl/ diaryl dithiophosphates	Zinc and other dithiophosphates	Zinc dithiophosphates	Metal sulfonates	Ethylene-propylene copolymers
Alkyl phosphates	Metal sulfonates	Metal dithiocarbamates	Overbased metal sulfonates	Polymethacrylates
Phosphorized fats and olefins	Overbased metal sulfonates	Hindered phenols	Metal phenate sulfides	Styrene isoprene/butadiene/ maleic ester copolymers
Phospho-sulfurized fats and olefins	Metal phenate sulfides	Phenol sulfides	Overbased metal phenate sulfides	Polyisobutylenes
Sulfurized olefins/paraffins/fats/ fat derivatives/ carboxylic acids	Overbased metal phenate sulfides	Metal phenol sulfides	Metal salicylates	**EMULSIFIERS**
Chlorinated fats/fat derivatives/ carboxylic acids	Fatty acids	Metal salicylates	Metal thiophosphonates	Soaps of fats and fatty acids
Fatty acids/other carboxylic acids and their metal salts	Acide phosphate esters	Aromatic amines	**DISPERSANTS**	Low-molecular weight Na and Ca sulfonates/ naphthenates
Esters of fatty acids	Chlorinated was	Phospho-sulfurized fats and olefins	Polyamine succinimides	**DEMULSIFIERS**
Oxidized paraffins and oils	Amines	Sulfurized olefins/fats/fat derivatives/ paraffins/ carboxylic acids	Hydroxy benzyl polamines	High-molecular weight Ca and Mg sulfonates
Organic molybdenum compounds/ molybdenum disulfide	2,4-Bis (alkyldithio)-1,3,4-thiadiazoles	Disalieylal-1,2-propane diamine	¨Polyamine succinamides	Alkylene oxide derivatives
Graphite	Alkyl succinic acids	2,4-Bis (alkyldithio)-1,3,4-thiadiazoles	Polyhydroxy succinic esters	Heavy metal soaps
Borate dispersions		Dilauryl selenide	Polyamine amide imidazolines	

Table 1.4. Most common additives in modern lubricants listed by category [12]

In recent years, the discovery of nanoparticle synthesis techniques has widened considerably the scope of possibilities in terms of lubricant additivation. Boundary lubrication additives, in particular, could greatly benefit from the different tribofilm-forming mechanism of nanoparticles additives. The molecular form of MoDTC and ZnDTP, for example, allows them to potentially adsorb on any steel surface they meet. Nanoparticles are on the other hand chemically inert, and deliver the active additives only when damaged by the contacting surfaces. This implies additive consumption exclusively inside high-friction contacts, where they are the most needed. This mechanism also implies that tribofilm adsorption does not (in theory) depend on the temperature of the lubricant, meaning they hold high potential under ambient or even cold temperatures. The limited liberation of chemical compounds (including sulfur) in the lubricant is also expected to

reduce polluting emissions for engine applications if piston-ring assemblies can prevent whole nanoparticles from reaching the combustion chamber.

A brief history of nanoparticle synthesis and of the successive discoveries regarding their tribological potential is proposed in the next section.

1. 2. A brief history of nanoparticle-doped lubricants

Different types of nanoparticles exist, varying in their composition, structure and size. The two main geometries are spherical and tubular nanoparticles (also called "nanotubes" or "nanofibers", **Figure 1.7**).

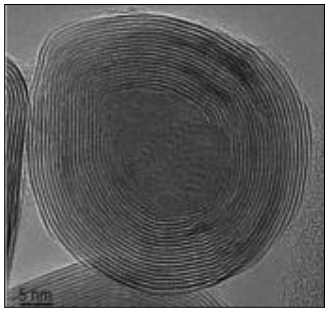

IF-MoS_2

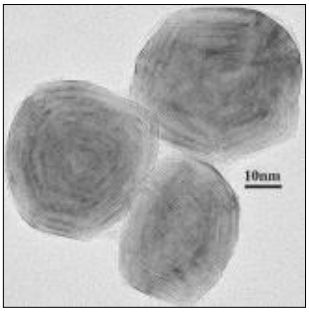

IF-WS_2

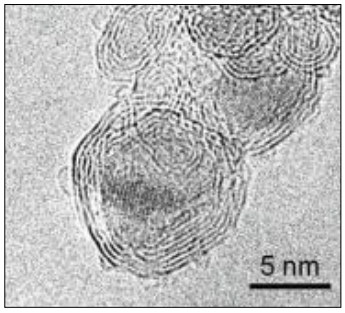

carbon onions

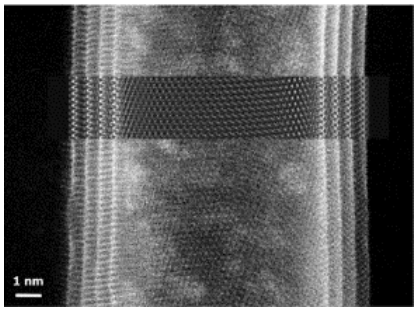

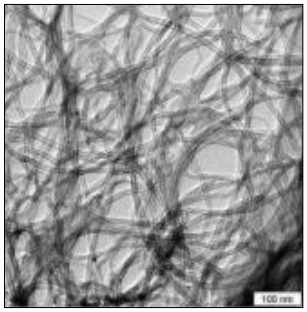

WS_2 and C nanotubes (nanofibers)

Figure 1.7. Examples of existing types of nanoparticles [10,23,51,56,64]

Nanoparticles of various chemical compositions have shown great tribological potential throughout the years for both geometries (spherical and tubular). The following paragraphs describe these various particles and their tribological potential, before focusing more specifically on the nanoparticles studied in this work and on the risks associated with the presence of particles in lubricants.

1. 2. 1. Different chemical natures

Many different nanoparticle compositions and shapes have been tested in the past. Tubular Mo-S-I nanoparticles have for example shown interesting tribological properties, as shown by L. Joly-Pottuz [18,19]. These nanofibers (shown on **Figure 1.8**) form an MoS_2 tribofilm similar to those formed using bulk, hexagonal MoS_2 when passing through the contact, providing important friction reduction in boundary lubrication regimes. They are however also effective under ambient temperatures and after a low number of cycles, and contain less sulfur.

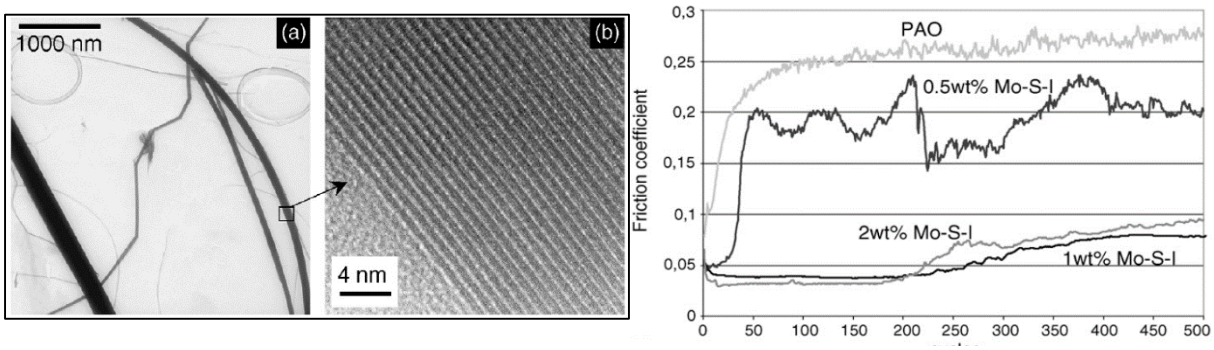

Figure 1.8. Visual aspect and structure of Mo-S-I nanofibers (left) and associated friction reduction (right)

Carbon-base nanotubes were also studied, such as those presented by Dassenoy et al in 2004 [20]. These nanotubes were only made of one external sheet (SWNTs – Single-Wall carbon NanoTubes), as opposed to MWNT (Multi-Wall carbon NanoTubes). Their tribological properties also proved very interesting, particularly for the mixed/boundary lubrication regimes. For tests carried out under the same operating conditions as for the Mo-S-I nanotubes described earlier, the SWNT did not reduce friction as much but revealed better anti-wear properties. Carbon MWNT were studied by Chauveau et al in 2012 [21] for ElastoHydroDynamic (EHD) lubrication regimes. Their addition to the base oil, even in low concentrations, created a local increase of the lubricant film thickness. *In-situ* contact observations obtained by interferometry showed that the contact could be compared to a "particle aggregate filter", with a decreasing number of aggregates passing through the contact for increasing sliding ratios.

Among the carbon-based nanoparticles, "carbon onions" have also shown great tribological promises, both in terms of friction and wear reduction. Joly-Pottuz et al exposed the efficiency of these particles (**Figure 1.9**) in 2008 [22,23], their performance being attributed to their spherical shape, their chemical inertness and their very small size. It is indeed possible to obtain carbon onions under 10 nm in diameter, which is smaller than any other type of spherical nanoparticle synthesized today.

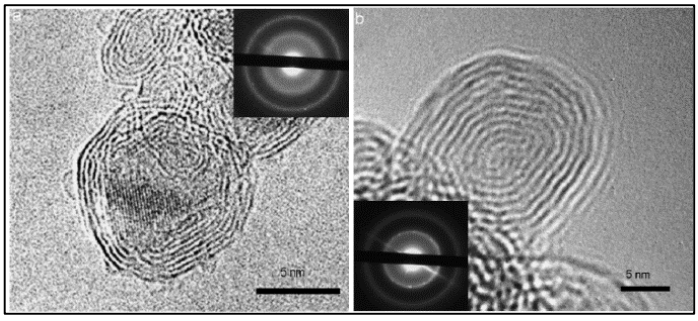

Figure 1.9. Examples of "carbon onions"

Nanoparticles based on other elements, such as copper or titanium, have also been studied. Wang et al, for example, evaluated the performances of CuO and TiO_2 nanoparticles [24]. These additives achieved maximal friction reductions of approximately 18% in the test conditions considered. Fe, Cu and Co nanoparticles were studied by Padgurskas et al [25], with maximal friction and wear reduction for the Cu particles.

For severe boundary lubrication regimes, the most efficient nanoparticles found in the literature however appear to be metal dichalcogenides (MX_2 compounds with M=Mo, W, Nb, Ta, Ti, Zr, Hf, Re… and X=S, Se, Te…), as they have the ability to form low-friction tribofilms on the contacting surfaces.

1. 2. 2. Metal dichalcogenides of different shapes and structures

Knowing the high lubricating properties of metal dichalcogenide coatings [26], different methods for the synthesis of nanoparticles of this nature were explored. A major breakthrough was achieved by Tenne et al in 1992 [27], with the very first synthesis of spherical nanoparticles with a fullerene (C_{60})-like structure (shown on **Figure 1.10**). This was first achieved for layered semiconductor tungsten disulphide (WS_2), before being extended to molybdenum disulphide (MoS_2) the following year [28]. These nanoparticles have a closed structure, and withhold many concentric layers.

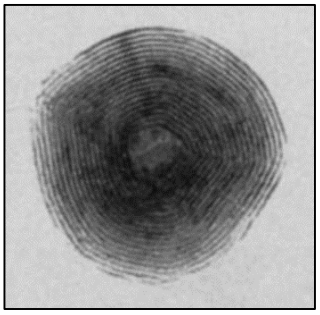

Figure 1.10. First fullerene-like nanoparticles synthesized in 1992

Other types of metal dichalcogenide particles were studied, such as the highly dispersed MoS_2 prepared by P. Afanasiev et al in 1999 using reactions between $(NH_4)_2MoS_4$ and N_2H_4 or $NH_2OH.H_2SO_4$ followed by thermal treatments under nitrogen [29]. In 2000, the same compounds were used to obtain $(NH_3OH)_{3.9}MoS_{4.8}$ [30], which produces highly dispersed MoS_2 nanotubes upon crystallization (**Figure 1.11**, left). Two years later, reactions using the $(NH_4)_2Mo_2S_{12}$ precursor produced MoS_x compounds ($5 < x < 6$). These MoS_5, $MoS_{5.6}$ and MoS_6 compounds have structures similar to MoS_3 but with more S-S bonds. A thermal decomposition of $MoS_{5.6}$ produces hollow MoS_2 nanospheres [31], as shown in **Figure 1.11** (right).

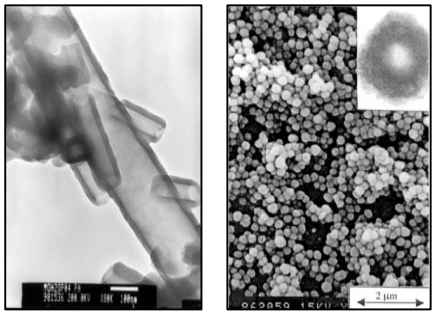

Figure 1.11. Hollow nanotubes and nanospheres synthesized in [30] and [31]

Alternative particle geometries, such as nanofibers, were also explored. Nath et al presented the formation of tubular nanoparticles combining molybdenum and tungsten, $Mo_{(1-x)}W_wS_2$, from solid solution precursors $(NH_4)_2MoS_4$ and $(NH_4)_2WS_4$ in 2002 [32]. These nanotubes consist of a variable number of external sheets and contain many structural defects (**Figure 1.12**).

Figure 1.12. Example of a nanotube synthesized by Nath et al ($Mo_{0.94}W_{0.06}S_2$)

The lubricating properties of MoS_2 MWNT was recently explored by Kalin et al [33,34] for very severe contact conditions, in the presence of both smooth and rough surfaces (**Figure 1.13**). Important friction reduction was observed for boundary and mixed lubrication regimes, before being reduced to nil for the least severe lubrication regimes. Surfaces analyses carried out after the tests revealed the formation of an MoS_2 tribofilm in the contact, which highly reduces friction when opposing asperities come in contact.

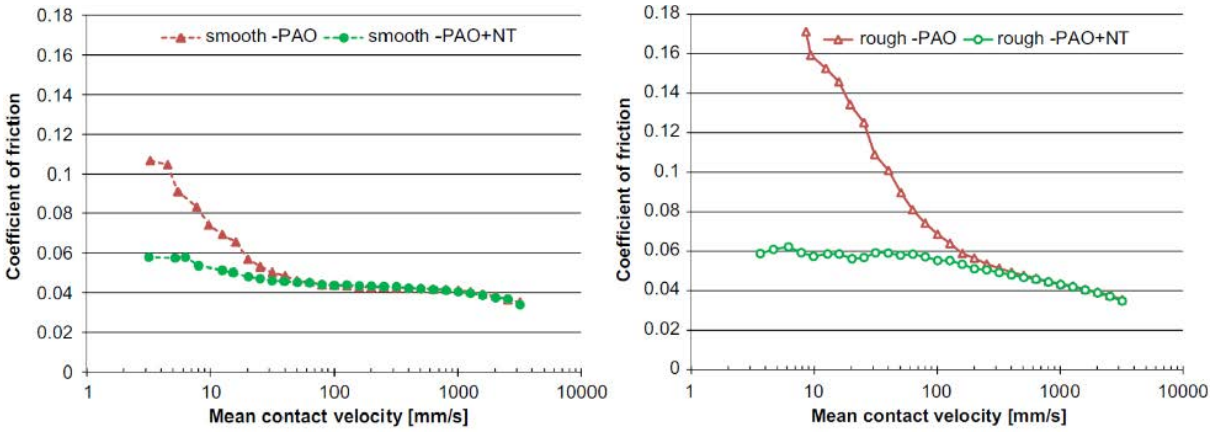

Figure 1.13. MoS_2 MWNT (left) and associated friction reduction for smooth (center) and rough (right) contact surfaces

Alongside the advances made in terms of nanoparticle synthesis by the end of the 1990s, Rapoport et al showed the tribological benefit of using metal dichalcogenides as Inorganic Fullerene-like (IF-) nanoparticles in 1999, by comparing the wear resulting from tests carried out with a base oil containing either IF-WS_2 nanoparticles, 2H-MoS_2 platelets or 2H-WS_2 platelets [35]. The spherical shape of the nanoparticles, as well as their chemical inertness, were then thought to be the main reasons for their good tribological properties (**Figure 1.14**).

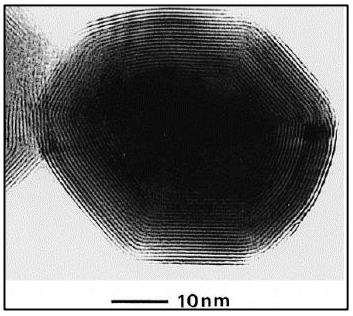

Figure 1.14. IF-WS_2 studied in [35]: closed nanoparticles with many concentric layers

The processes used for the synthesis of fullerene-like nanoparticles were greatly improved at the beginning of this new century. In 2000, Feldman et al proposed a method for a large-scale synthesis of IF-WS_2, capable of producing uniform nanoparticles with a controlled structure [36]. Their tribological potential also became increasingly obvious throughout the years, especially for the smaller particles. Margolin et al synthesized perfectly spherical TiS_2 nanoparticles in 2005 [37], with diameters comprised between 60 and 80 nm (**Figure 1.15**, left). Yang et al, on the other hand, used a new synthesis process in 2006 to form IF-WS_2 with temperatures not exceeding 650°C [38]. These particles have a mean diameter of 50 nm. These two types of nanoparticles (shown on **Figure 1.15**, right), added to a base oil, showed interesting friction reduction properties.

Among all the nanoparticles synthesized until today, two types stand out by their tribological potential in terms of friction and wear: spherical fullerene-like molybdenum and tungsten disulfide

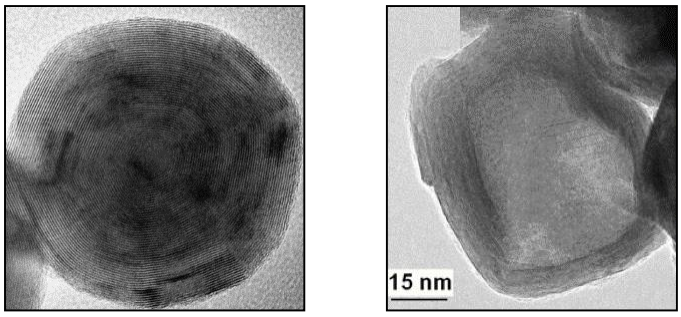

Figure 1.15. IF-TiS_2 synthesized by Margolin et al (left) and IF-WS_2 produced by Yang et al (right)

nanoparticles (IF-MoS_2 and IF-WS_2), which exhibit very similar behaviors. Rapoport et al showed, in 2001 and 2002 [39–41], that the incorporation of IF-WS_2 nanoparticles in porous matrices based on bronze, iron and an iron-nickel alloy reduced considerably friction and wear of the surfaces, even under high loads. The same authors then studied the contact between two porous media, lubricated by nanoparticle-doped oils and greases [42]. The benefits in terms of friction and wear were then more important (**Figure 1.16**) than those observed in the presence of classical additives (2H-WS_2).

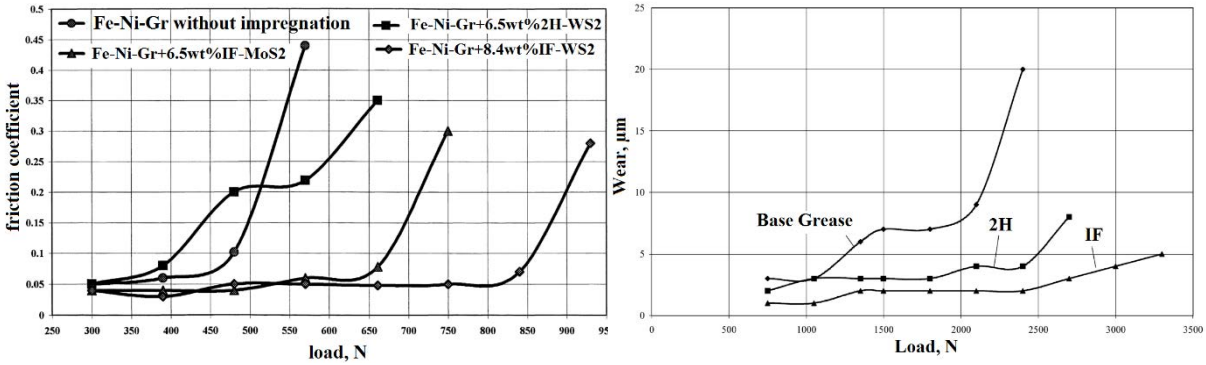

Figure 1.16. Friction and wear reductions observed for the contact between two porous materials in the case of "classical" (2H-WS_2) and nanoparticle (IF-WS_2) lubrication

In 2003, Rapoport et al showed that the potential of this type of nanoparticles becomes more important for increasingly severe lubrication regimes [43]. A pin-on-disc tribometer was used to create mixed lubrication conditions for a steel-steel contact lubricated by IF-WS_2-doped oil. This study gave the first hints as to the lubrication mechanism associated to fullerene-like nanoparticles: the final shape of the nanoparticles which suffered the lowest contact pressures was preserved, whereas the nanoparticles which bore the higher loads were damaged (**Figure 1.17**). From these observations, the authors suggested that this degradation could lead to the formation of a low-friction protective tribofilm on the opposing surfaces.

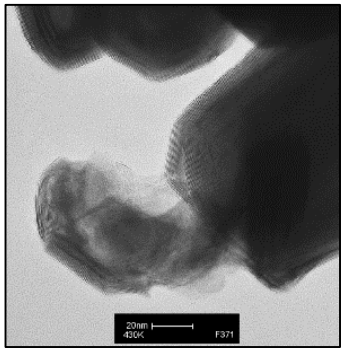

Figure 1.17. TEM observation of an IF-WS_2 nanoparticle after high-load tribological testing

Rapoport et al also studied the use of these particles in the case of friction between two ceramic materials, in 2005 [44,45]. Significant friction and wear reduction was also observed in this case, particularly for the higher loads. The nanoparticles were found to have no effect when the separation between the contact surfaces was smaller than the size of the IF-WS_2. Their behavior was however different in the case of pores and surface roughness (with sizes larger than the particle diameter), which allowed nanoparticle entry in the contact and in the valleys of the rough surfaces, protecting them from direct contact.

In 2005 also, Joly-Pottuz et al tried to find out more about the potential of IF-WS_2 nanoparticles in the case of boundary lubrication [46], particularly depending on their concentration in the base oil and the suffered contact pressures (**Figure 1.18**). In addition to the significant wear reduction obtained, this study showed that an optimal nanoparticle concentration exists, over which friction will not continue to decrease (1wt% for the conditions presented in the study). This article also revealed that the size of this type of nanoparticles was all the more reduced for severe contact conditions, which led the authors to believe that the exfoliation of these nanoparticles under mechanical solicitation is the main mechanism associated to this lubrication mode.

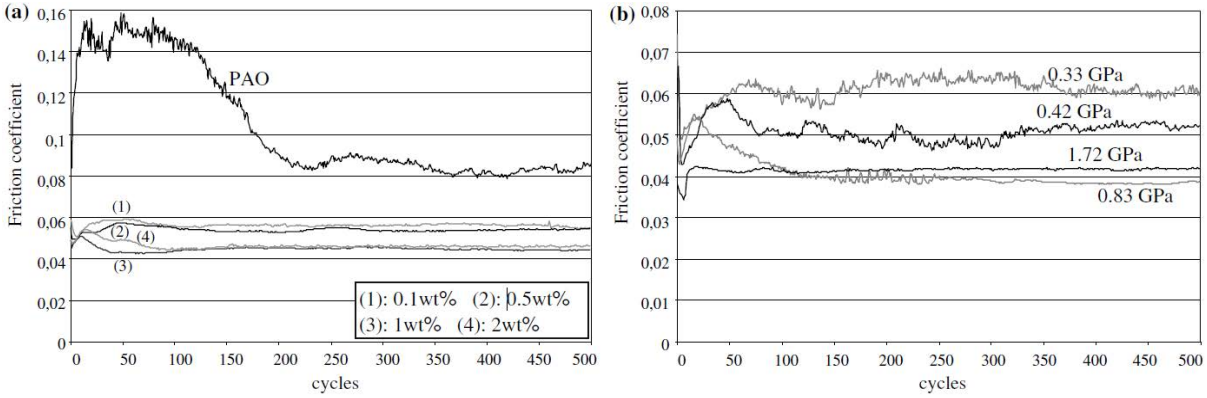

Figure 1.18. Friction reduction for different IF-WS_2 concentrations (left, 1.12 GPa) and contact pressures (right, 1wt%)

This exfoliation mechanism had incidentally been foreseen by Leshchinsky et al in 2004, during comparative compression tests carried out on IF-WS_2 nanoparticles and 2H-WS_2 platelets [47]. The IF-WS_2 remained intact (elastic deformation) for the lowest pressures (under 300 MPa) but were damaged when submitted to higher pressures (**Figure 1.19**). This phenomenon was also observed by Joly-Pottuz et al in 2006 [48], during hydrostatic and uni-axial compressions of IF-WS_2 nanoparticles. In the case of hydrostatic pressures, the IF-WS_2 withstand pressures up to 20 GPa

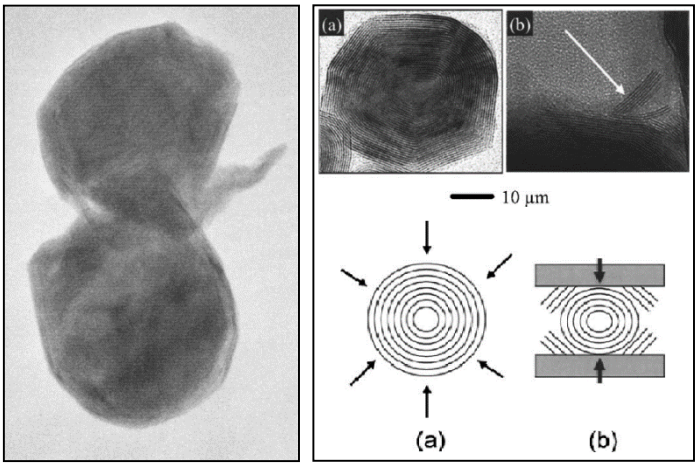

Figure 1.19. IF-WS_2 exfoliation as observed by Leshchinsky et al (left) and Joly-Pottuz et al (top right), and schematized behavior of fullerene-like nanoparticles under hydrostatic (a) and uni-axial (b) pressures

without damage, whereas a uni-axial compression of approximately 1 GPa is enough to partly exfoliate the nanoparticles (**Figure 1.19**).

In 2010, Tevet et al succeeded in estimating the mechanical resistance of WS_2 nanoparticles of different sizes and shapes by carrying out nano-compression tests using an AFM (Atomic Force Microscopy) tip mounted in a HR-SEM (High Resolution Scanning Electron Microscope). Although this mechanical property is difficult to estimate, the order of magnitude of the compressive strength of the different particles tested was between 1 and 2 GPa [49]. The next year, the same authors carried out rolling/sliding tests of individual IF-WS_2 nanoparticles in a HR-SEM [50]. These two studies underlined the co-existence of several operating modes for the nanoparticles: under moderate compression loads (under 1 GPa), the nanoparticles deform and roll/slide in the contact without suffering damage; whereas higher pressures induce nanoparticle exfoliation, creating platelets likely to form a tribofilm on the surfaces (**Figure 1.20**).

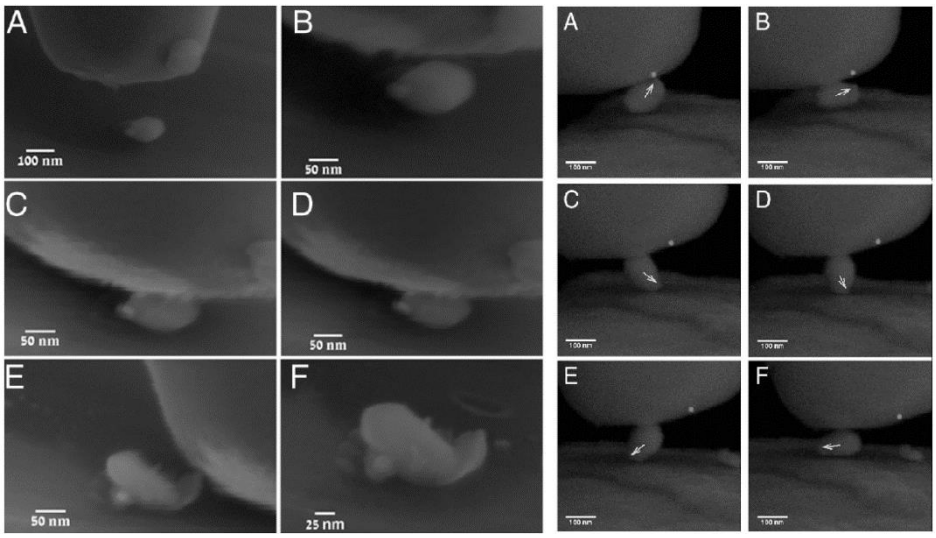

Figure 1.20. Exfoliation (left) and rolling/sliding (right) of an IF-WS_2 nanoparticle in a HR SEM

In order to prove that the nanoparticle exfoliation took place during sliding contacts, Joly-Pottuz et al imagined an *in-situ* analysis of the IF-WS_2 additives using Raman spectroscopy in 2007 [51]. The formation of 2H-WS_2 from IF-WS_2 nanoparticles was confirmed by comparing the spectra of 2H-WS_2 platelets to those of IF-WS_2 before the tribological test, and after 1 and 4 minutes of friction (**Figure 1.21**).

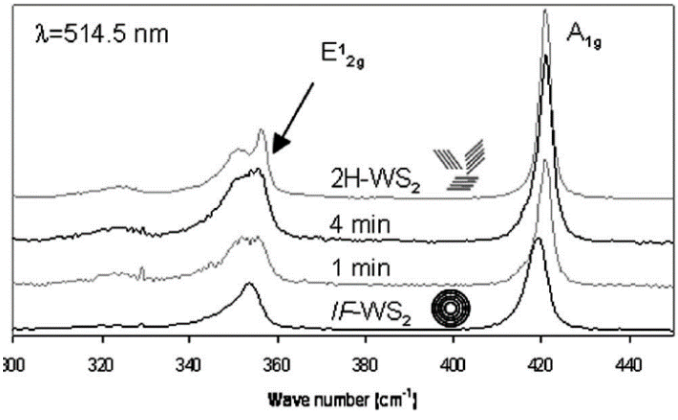

Figure 1.21. Progressive formation of 2H-WS_2 platelets from the exfoliation of IF-WS_2 nanoparticles observed using *in-situ* Raman analysis

Although these different studies have brought a better understanding of the behavior of individual nanoparticles when submitted to compression and shear stresses, the issue of ensuring

proper dispersions of the particles in the oil has not yet been resolved. Nanoparticles are therefore not likely to pass through tribological contacts individually, but rather in an agglomerated state. In recent years, Tenne et al studied the influence of IF-WS_2 agglomeration and sedimentation on friction and wear [52,53]. It was shown that agitating the oil before testing effectively reduced the size of the agglomerates, which improved their tribological results and made them more reproducible for long agitation times (**Figure 1.22**, left). Other tests were carried out while imposing mechanical oscillations to the contact, in order to favor the entrapment of the smaller agglomerates by the opposing surfaces. These contact excitations led to spectacular friction reduction (**Figure 1.22**, right).

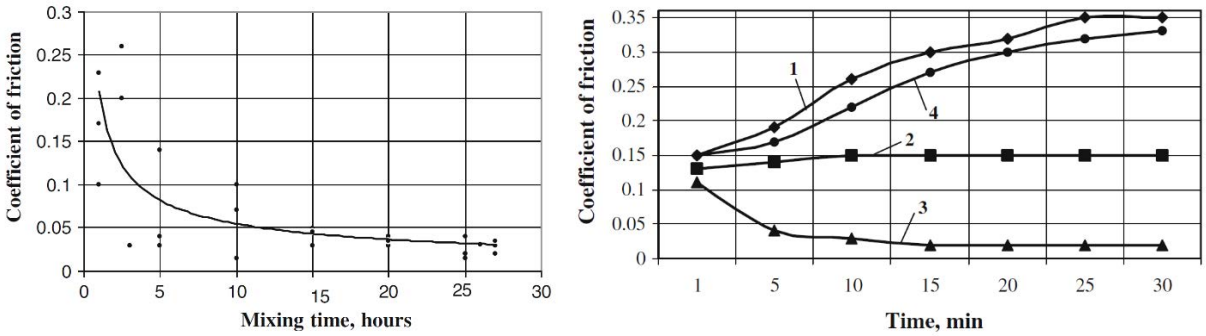

Figure 1.22. Influence of oil agitation before testing (left) and mechanical excitation of the contact (right) - 1. base oil with no excitation; 2. doped oil with no excitation; 3. doped oil with excitation and 4. base oil with excitation

Unsure of which of the IF-WS_2 or the IF-MoS_2 held more potential, Dassenoy et al published a comparative study in 2010 in which the tribological performances of $Mo_xW_{(1-x)}S_2$ nanoparticles of different stoichiometry were studied, ranging from IF-MoS_2 to IF-WS_2 and including IF-$Mo_{0,8}W_{0,2}S_2$, IF-$Mo_{0,5}W_{0,5}S_2$ and IF-$Mo_{0,2}W_{0,8}S_2$ [54]. All of these nanomaterials proved very effective in boundary lubrication regimes. For a given concentration, the IF-MoS_2 produced the lowest friction as well as smaller wear rates for various contact pressures (**Figure 1.23**). The synthesis of these different types of nanoparticles however affected their size, crystallinity and structure, which are likely to influence their tribological behavior. The IF-MoS_2 ranked third (out of five) in terms of nanoparticle size and quantity of defects in their structure, but were also the less crystalline of all the nanoparticles tested. This parameter, as well as their chemical nature, may also have affected their frictional performance.

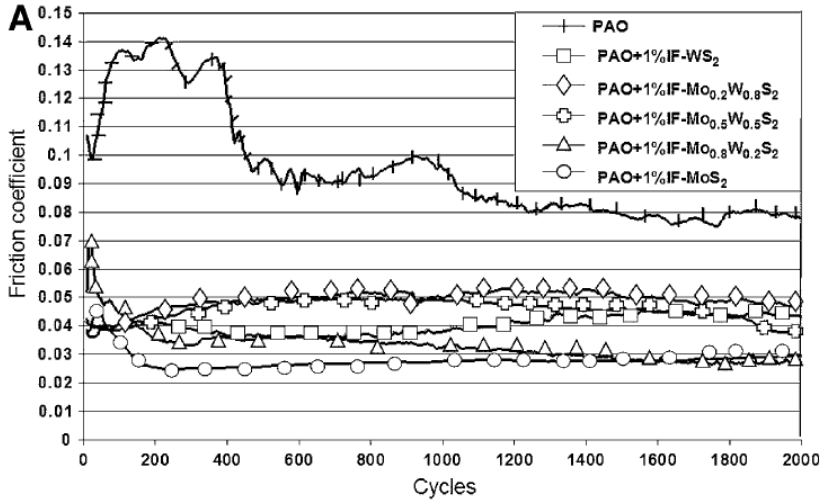

Figure 1.23. Friction coefficients for IF-$Mo_xW_{(1-x)}S_2$ nanoparticles of varying stoichiometry (contact pressure of 1.12 GPa)

Besides these many advances in terms of nanoparticle synthesis, their intrinsic properties were also studied. Schuffenhauer et al, for instance, examined the stability of different types of fullerene-like nanoparticles by carrying out thermal analyses of IF-NbS_2, IF-MoS_2 and IF-WS_2 under oxidant and inert atmospheres [55]. This study revealed that the stability of the fullerene-like nanoparticles was comparable to that of the bulk material regarding oxidation. The IF-MoS_2 and IF-WS_2 nanoparticles were also more stable than the IF-NbS_2, in addition to their greater tribological potential.

The recent evolution of imaging techniques helped providing a better understanding of the structure of the nanoparticles. Bar-Sadan et al [56] used a High-Resolution Transmission Electron Microscope (HR-TEM) to reveal the atomic structure of WS_2 nanotubes and confirm the validity of existing numerical models (**Figure 1.24**).

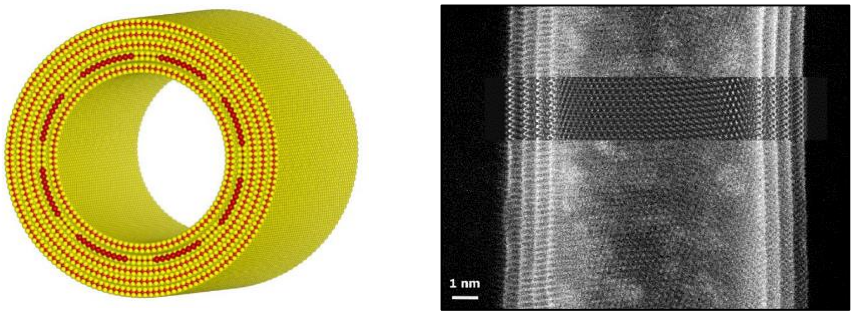

Figure 1.24. Numerical model (left) and HR-TEM observation (right) of a multi-wall WS_2 nanotube

Today, the synthesis of nanotubes and fullerene-like nanoparticles is well mastered, and it is possible to create nanoparticles of different compositions, sizes and structures. The latest advances in terms of nanoparticle synthesis concern the doping of nanoparticles with other chemical elements. Yadgarov et al, for example, have published a doping method for nanotubes and fullerene-like MS_2 nanoparticles (S=Mo or W) by replacing a small quantity (under 1%) of Mo or W atoms by Nb or Re atoms [57]. This type of doping makes it possible to alter the nanoparticle behavior, by modifying their electric, optical and magnetic properties. These changes may have consequences on their tribological potential, by affecting their tendency to agglomerate for example. More information regarding advances made in terms of nanoparticle synthesis may be found in reviews written by Reshef Tenne [58,59]

1. 2. 3. Focus on Inorganic Fullerene-like (IF-) MoS_2 nanoparticles

The tribological benefits of molybdenum-based additives have been known for a long time. In addition to their use in oils, particularly in MoDTC, they have been widely used as solid lubricants such as coatings, for instance. Wahl et al, for example, explored the behavior of MoS_2 coatings on steel substrates in 1998 [60]. This lubrication mode is extensively used for aerospace applications, where liquid lubricants cannot be used.

Alongside the advances made in the field of nanoparticle synthesis, Chhowalla et al tried, in 2000, to deposit IF-MoS_2 on steel substrates [61]. Their closed structure, ensuring chemical inertness, reduced their interactions with oxygen and made this coating more efficient in a humid environment. The excellent tribological behavior of metallic coatings impregnated with IF-MoS_2 nanoparticles was later confirmed by Rosentsveig et al [62].

The first incorporations of IF-MoS_2 nanoparticles in lubricants in order to reduce friction appeared at the beginning of the 21st century [63]. These new additives were added to a polyalphaolefin (PAO) and to a mineral base oil, and proved efficient in both cases. Different morphologies were found for the IF-MoS_2 collected on the wear scars after testing (spherical, flattened or exfoliated), suggesting that different mechanisms may occur to provide low friction. The authors evoked the possibility of nanoparticles rolling inside the contact, but also of sliding between flattened IF-MoS_2 or slipping between individual unwrapped MoS_2 sheets.

After witnessing the tribological benefits attributed to the use of IF-WS_2 nanoparticles, both the performances of the molybdenum and tungsten disulfide nanoparticles were later compared [64]. The IF-MoS_2 nanoparticles proved increasingly efficient for more severe contact conditions (**Figure 1.25**). IF-MoS_2 and IF-WS_2 had similar characteristics and very close performances, but the molybdenum-based nanoparticles once again proved slightly more effective in the test conditions used.

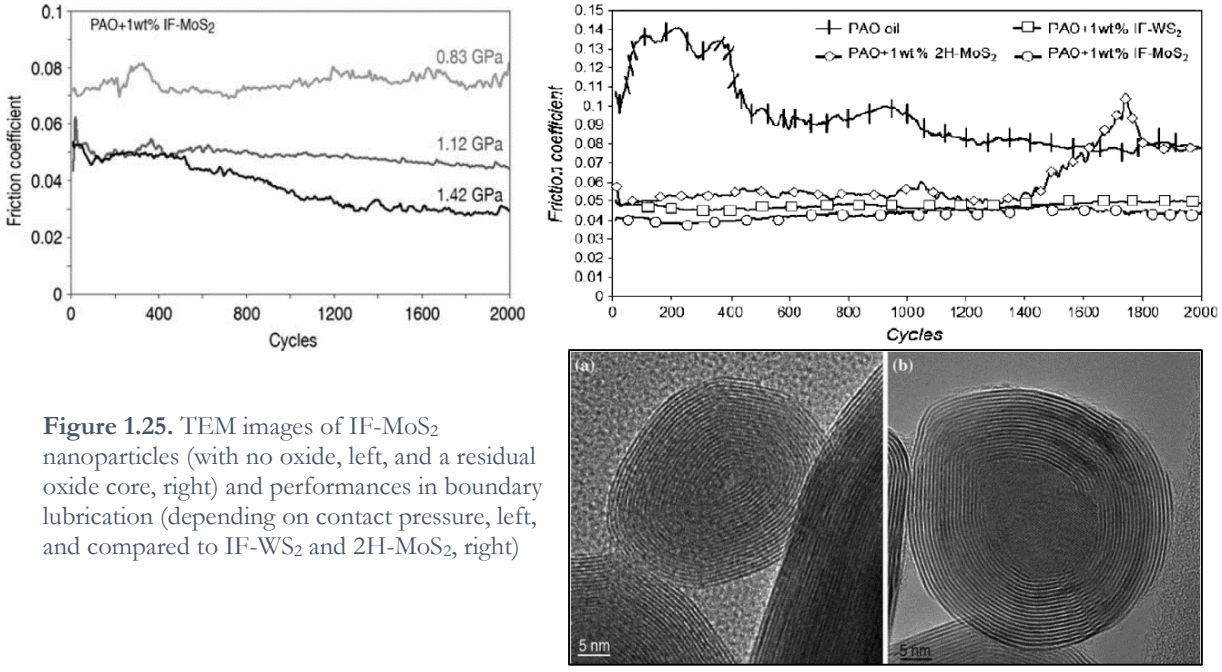

Figure 1.25. TEM images of IF-MoS_2 nanoparticles (with no oxide, left, and a residual oxide core, right) and performances in boundary lubrication (depending on contact pressure, left, and compared to IF-WS_2 and 2H-MoS_2, right)

The following year, in 2010, Lahouij et al studied the chemical interactions between platelets originating from the exfoliation of IF-MoS_2 and the contact surfaces [65]. To achieve this, an IF-MoS_2-doped oil was used to lubricate boundary lubrication contacts between different materials: steel, alumina and DLC. If important friction reduction was obtained in the case of steel surfaces, the use of the IF-MoS_2 nanoparticles did not affect friction significantly in the case of alumina or DLC. Surface analyses carried out on the wear scars revealed the presence of molybdenum and sulfur on the steel surfaces, but none was detected on the alumina and DLC surfaces. Focused Iron Beam (FIB) cross sections were then made to observe and further characterize the tribofilms formed on the steel surfaces. This study highlights the possible importance of the role played by iron oxide on the steel surface, as the adhesion of the MoS_2 tribofilm may originate from S - O, Mo - O and Fe - S bonding.

More recently, in 2012, Lahouij et al showed the influence of the structure of the IF-MoS_2 nanoparticles on their tribological behavior, by comparing the performances of poorly crystalline particles (containing more structural defects) with more crystalline particles [66]. Nanoparticles

containing more structural defects are likely to exfoliate more easily, creating more 2H-MoS_2 platelets when passing through the contact. These poorly crystalline nanoparticles achieved better friction and wear reduction than the more crystalline nanoparticles, in the case of a boundary lubrication steel-steel contact (**Figure 1.26**). Because of the synthesis processes used, these poorly crystalline nanoparticles were however also significantly smaller than the more crystalline ones, which makes it difficult to conclude on the separate influences of size and crystallinity of the nanoparticles.

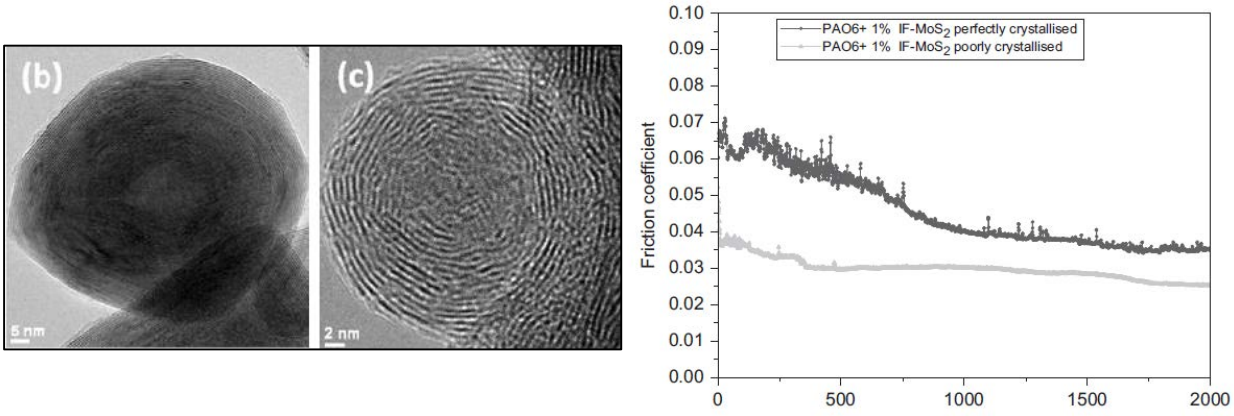

Figure 1.26. Crystalline (left) and poorly crystalline (center) IF-MoS2 and associated tribological performances (right)

In recent years, Rapoport et al have investigated doping IF-MoS_2 nanoparticles with rhenium atoms [67]. This technique consists replacing a small amount (under 1at.%) of Mo atoms by Re atoms, which modifies the electrical properties of the nanoparticles by decreasing their resistance. The authors suggest that this doping provides the nanoparticles with a negative charge, establishing mutual repulsion between all of them. This effect was verified by sedimentation tests, which revealed that Re-doped IF-MoS_2 were less agglomerated at the end of the test (**Figure 1.27**). For given test conditions (mixed lubrication), non-doped IF-MoS_2 nanoparticles produced an average friction coefficient of 0.04 whereas the doped IF-(Re)MoS_2 nanoparticles achieved a value of 0.015, along with negligible wear.

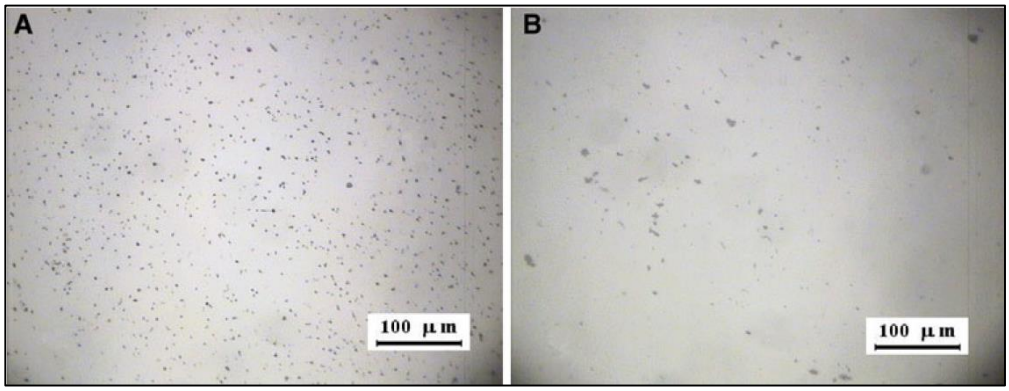

Figure 1.27. Sedimentation tests and resulting agglomeration state for rhenium doped IF-(Re)MoS_2 (left) and common IF-MoS_2 (right)

With the discovery of the tribological potential of IF-MoS_2 and the numerous applications considered, understanding precisely the mechanisms associated to nanoparticle lubrication became vital. If the formation of MoS_2 tribofilms on the contact surfaces attests of the exfoliation of the IF-MoS_2 in severe lubrication regimes, some authors suggest a possible rolling/sliding of the

nanoparticles inside of the contact for milder contact conditions, which would then act as "nano-scale ball bearings". In order to investigate this possibility, Lahouij et al succeeded in isolating individual IF-MoS_2 and carrying out compression and shear tests on them in a HR-TEM. The resulting *in-situ* observations, first of a kind, displayed the evidence for both the rolling and the sliding of the nanoparticle in the contact, depending on the load imposed. Occasional exfoliation of the nanoparticle when submitted to sliding was also clearly visible (**Figure 1.28**).

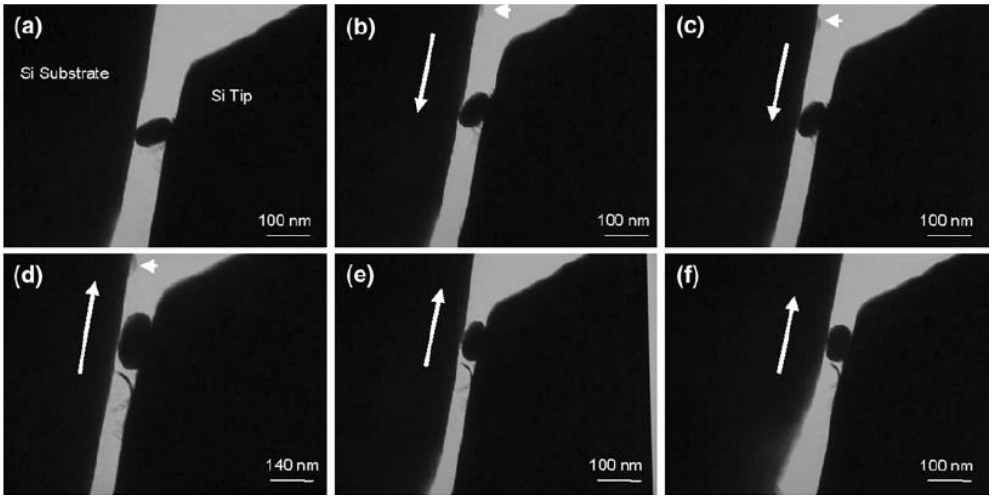

Figure 1.28. Rolling/sliding of an individual IF-MoS_2 and partial exfoliation during an *in-situ* HR TEM experiment

This experimental set-up was then used to study more specifically the exfoliation process of fullerene-like nanoparticles [68]. It was shown that the nanoparticles could deform plastically when submitted to pure compression (**Figure 1.29**), and that exfoliation only took place under the combined solicitations of compression and shear.

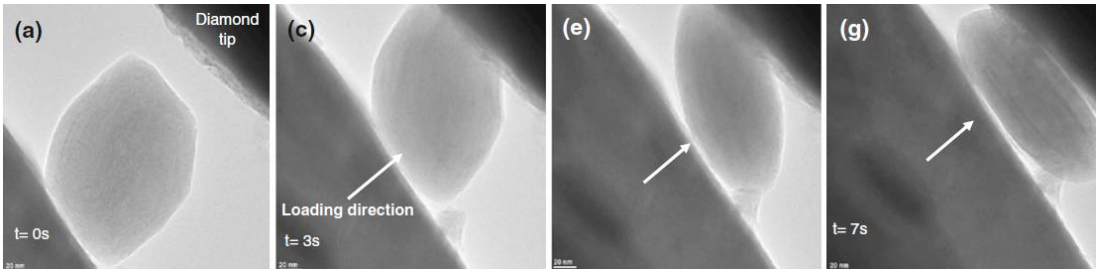

Figure 1.29. Compression of an individual IF-MoS_2 during *in-situ* HR-TEM experiments

The authors observed rolling/sliding of the nanoparticles for milder loads, confirming that this phenomenon may participate in reducing friction in the case of lightly loaded contacts. The nanoparticles rolled in the contact without exfoliating when exposed to an estimated pressure of 20 MPa, whereas sliding and exfoliation of the nanoparticle was observed for a pressure of 90 MPa. The adhesive forces between de nanoparticles and the walls may be the cause of this difference in behaviors despite the very low pressures applied.

1. 2. 4. Particle contamination of lubricants and associated risks

The presence of undesirable particles in lubricants usually accelerates the wear rates of gearbox and/or engine components. The hardest particles, such as combustion soot or wear debris for example, may indeed create indents on the contact surfaces. These defects are the source of local

pressure spikes, which often precipitates wear phenomena. Inorganic Fullerene-like nanoparticles are however easily deformable (see part ***1. 2. 3***), and are therefore not likely to affect the steel surfaces when passing through the contact.

The presence of particles in the oil, whatever their nature, may however cause other issues. While studying graphite dispersions in oil in 1981, Cusano and Sliney showed that particle accumulation could take place at the contact entry under rolling/sliding conditions [69]. This accumulation may starve the contact by reducing the oil flow passing through it, which in turn may increase wear drastically. Wan and Spikes then studied, in 1987, the behavior of various particles suspended in lubricants in rolling/sliding EHD contacts [70]. The general tendency was the same for all the particles tested (copper, glass, graphite and MoS_2 of different shapes and sizes): for pure rolling and sliding ratios up to approximately 0.7 (depending on the size and concentration of the particles tested), the particles passed through the contact. They were able to pass through contacts with film thicknesses up to a hundred times smaller than their diameter, due to the deformations of both the particles and the surfaces. The authors witnessed particle agglomeration at the contact entry for higher sliding ratios, creating progressive contact starvation until the agglomerated particles were forced into the contact, often damaging the surfaces. A simple bi-dimensional model was then created by the authors in order to determine which conditions would lead the particles to pass through the contact. This model took into account all the forces applied on a particle when it reaches the two opposing surfaces. An approximation of the friction coefficient needed between the particle and the surfaces for particle entrapment may then be found, depending on the particle size and the film thickness (**Figure 1.30**). Although this study remains fairly basic, as it does not take fluid effects and particle inertia into account, an estimation of the particles likely to agglomerate at the entry of a given contact may still be given.

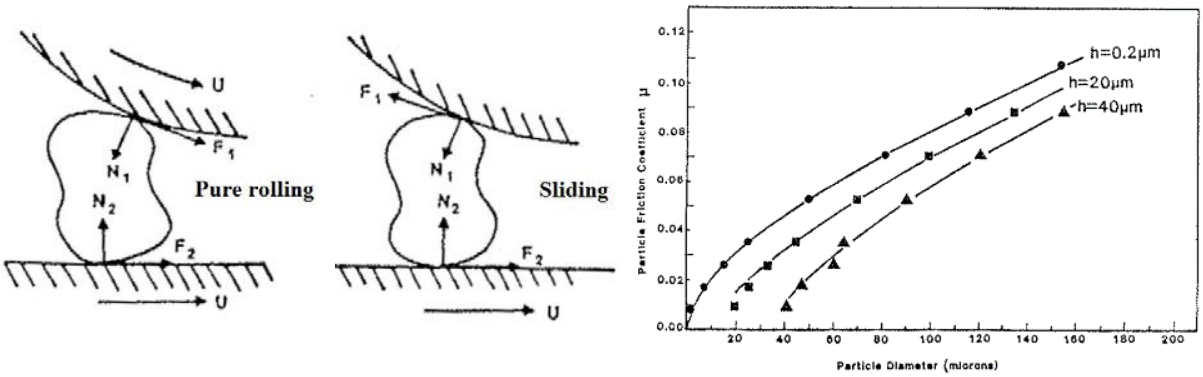

Figure 1.30. Force balance on a particle and estimation of the needed friction coefficient for particle entrapment

In 1996, Dwyer-Joyce and Heymer published a quantitative study on solid particle entrapment in EHD contacts [71]. The number of particles passing through the contact was estimated from the quantity of indents found on the surfaces. In the test conditions considered (pure rolling, particle sizes between 1 and 32 μm), the particle concentration in the contact was sometimes several times higher than the particle concentration in the oil. The larger particles were furthermore more prone to contact entrapment, and increasing speeds were found to reduce the number of particles passing through the contact (**Figure 1.31**).

As computers were not yet powerful enough for the development of efficient numerical simulations such as CFD (Computational Fluid Dynamics) models, most of the studies on particle contamination in lubricants in the late 1990s were experimental. In 1996 also, Cann et al [72] made

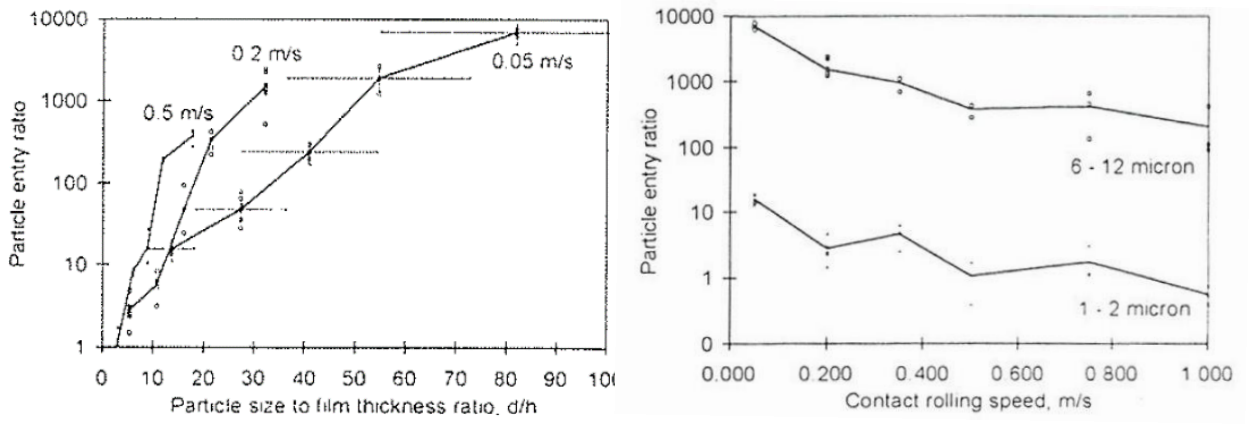

Figure 1.31. Number of particles entering the contact depending on their size and the rolling velocity

direct observations of particle entry and deformation in pure rolling EHD contacts (**Figure 1.32**). Optical interferometry was used with a silica layer/chromium disc, offering better visualization of the particles passing through the contact than the usual semi-reflective chromium coatings.

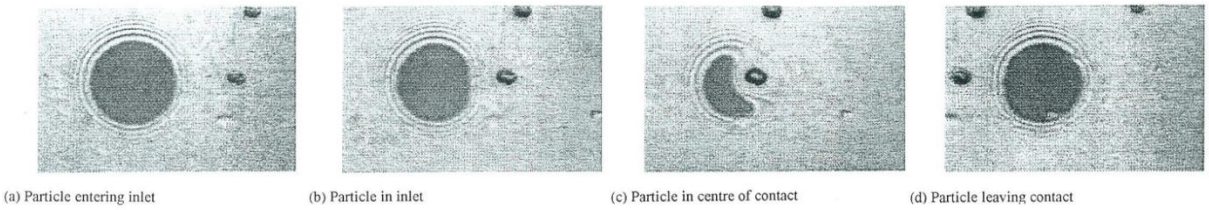

Figure 1.32. Particle passing through a pure rolling EHD contact

Alongside the development of these innovative experimental techniques, some authors have tried to simulate theoretically the behavior of particles entering a contact. In 1998, Nikas et al, for instance, proposed a more detailed approach than the one used by Spikes et al (**Figure 1.30**), taking into account not only the friction forces between the particle and the surfaces but also the fluid forces and the inertia of the particles [73]. The model predicts the trajectory of particles of a given size and nature arriving near a contact, for a given load, oil viscosity and rolling speed (**Figure 1.33**). This numerical approach makes it possible to predict which operating conditions are likely to cause particle agglomeration at the entry of the contact, inducing risks of oil starvation. Many conclusions arose from the practical case presented in this study. For example, the friction forces between the particles and the contacting surfaces were found to be significantly bigger than the fluid forces and the inertia of the particles (negligible mass), so they are responsible for the behavior

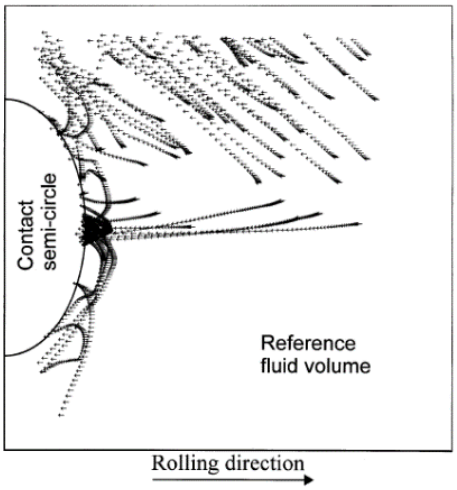

Figure 1.33. Prediction of the trajectory of a 20 μm particle when it is randomly placed before an EHD contact (h_c=0.3 μm)

of the particles once they come in contact with the surfaces.

With the advances in the field of computing, the same author presented a new, three-dimensional model in 2006 [74]. This model simulates particle entrapment in the case of elliptical rolling/sliding contacts, for conformal or convex surface geometries and dry or lubricated conditions (**Figure 1.34**). A parametric study using this model was published the following year [75], in which the conditions needed for particle entrapment were described for different particles and contact conditions.

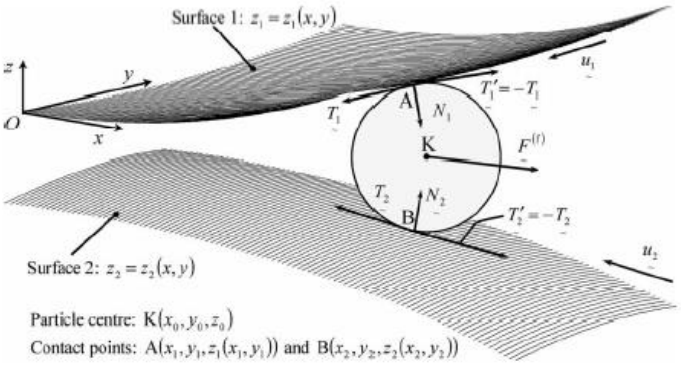

Figure 1.34. Tri-dimensional model for the simulation of particle entrapment

To illustrate the type of results that can be obtained using this numerical method, **Figure 1.35** shows the conditions for which a particle will enter the contact depending on load (top) and on the friction coefficients between the particle and the opposing surfaces (bottom), for a given contact configuration (in terms of speed, sliding ratio, oil viscosity…). The top graphs, for example, give the maximum particle diameter for them to be necessarily forced in through the contact when

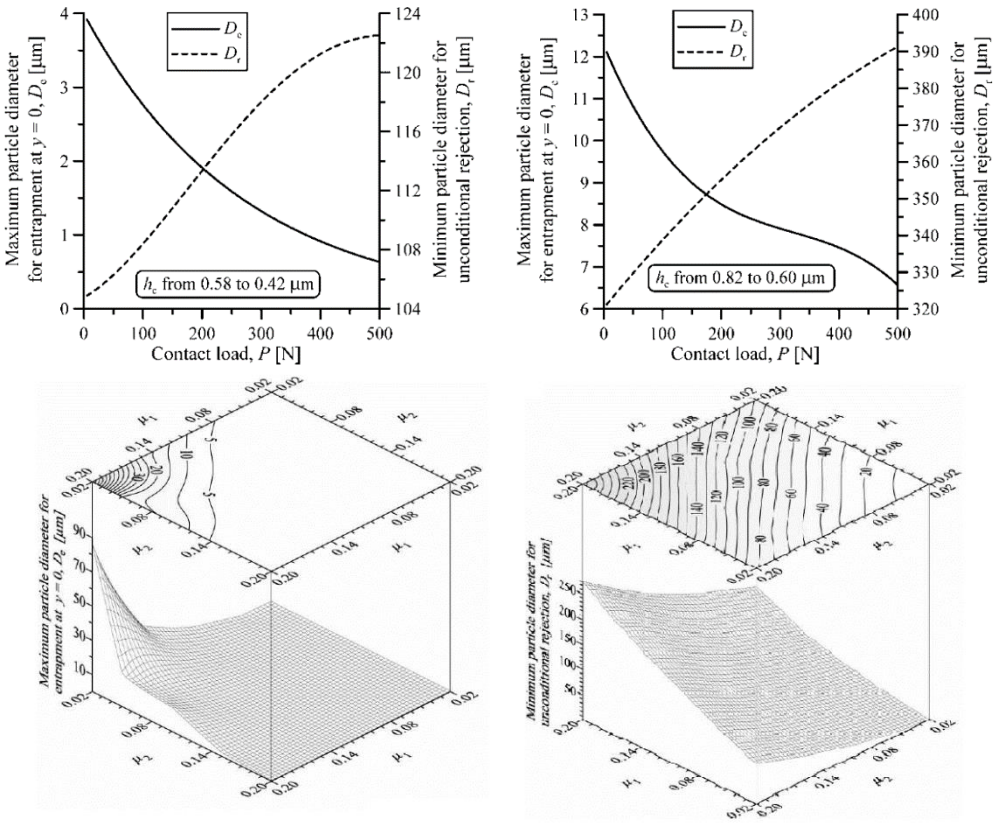

Figure 1.35. Conditions needed for particle entrapment in an EHD contact for given contact configurations (convex for the top-right graph, conformal elsewhere)

arriving at the centerline (solid line) and the minimum diameters over which the particles will be unconditionally rejected (dotted line) depending on the contact load, for a conformal (left) and convex (right) contact. For both cases, increasing loads (implying thinner film thicknesses) will increase the particle diameter for which they will be unconditionally rejected from the contact, and decrease the one under which they will necessarily pass through the contact.

The two bottom graphs on **Figure 1.35** show a surface representing the friction coefficients needed between the particles and each surface in order for the particles to either enter in or be rejected from the contact. These types of calculations may be of great interest in the case of contacts between two surfaces of different natures. A more detailed description of the phenomena occurring in the case of particle contamination of mechanical contacts, as well as the associated risks, may be found in the review published by Nikas in 2010 [76].

Even though these results are not directly applicable in the case of nanoparticle lubrication, they highlight the reality of the risks inherent to the use of solid additives in lubricants. For future use on common vehicles, the behavior of the nanoparticles should be fully understood, in particular in the surroundings of full-film contacts.

1. 3. Objectives and challenges of the present work

Although they are continuously being improved, most of the additives found in modern lubricants have been used for many decades. The development of disruptive lubricant technologies is essential to further increase the efficiency of future vehicles, as the oil properties will affect most contacts responsible for power losses in engines and gearboxes.

The discovery of novel nanoparticle synthesis techniques has opened new prospects for innovative oil formulations. The friction and wear reducing capacities of nanoparticle-doped lubricants has been vastly explored in recent years, and their large potential has become all the more obvious with the wider understanding of their operating mechanisms. As of today, Inorganic Fullerene-like nanoparticles are known to be increasingly effective for the more severe contact conditions, and to form low-shear strength tribofilms on rubbing metal surfaces through the exfoliation of their outer nano-layers. Most studies reported in the literature focus on the lubricating mechanisms related to these additives and are therefore often carried out in the simplest operating conditions possible, with small lubricant volumes (no problems related to nanoparticle dispersion), few cycles achieved (limiting the number of phenomena occurring in time), smooth surfaces (more control over the film thickness ratio and the evolution of the surfaces) and simple contact geometries.

The main objective of this study is to evaluate the potential of nanoparticle-doped lubricants in real-life applications such as automobile engines and/or gearboxes. Inorganic Fullerene-like molybdenum disulfide (IF-MoS_2) nanoparticles were chosen, as they appear to be among the most efficient in the literature. A number of issues are to be addressed, such as the dispersion of the nanoparticles, their incorporation in formulated oils, their durability (in time and for high cycle numbers) and their behavior when faced to rough surfaces and to the variety of lubrication regimes met in complex mechanical systems.

The present work was segmented into three sections to face these challenges. The first step was to determine which characteristics influence the performance of IF-MoS_2 nanoparticles in severe boundary lubrication regimes, taking into account high cycle numbers and splash lubrication (**Chapter Three**). The second step was to incorporate these additives in fully formulated lubricants, and to determine if and how interactions with other additives could affect their lubricating mechanism (**Chapter Four**). Real-life aspects were then considered, such as the behavior of nanoparticle-doped oils in different lubrication regimes (for varying temperatures, contact conditions and surface roughness) and when facing fatigue issues (**Chapter Five**).

Chapter Two

Experimental Techniques and Methodologies

This chapter presents the main experimental test rigs and characterization techniques used throughout this work. Focus is first made on four different tribometers, exploited to test the friction and wear reducing properties of the IF-MoS_2 nanoparticles. Together, these test rigs make it possible to explore a wide range of operating conditions and lubrication regimes, from simple configurations to more complex real-life applications. Complementary techniques were used to quantify the resulting wear on the specimens and to characterize, observe, and analyze the oil media, as well as the nanoparticles and the tribofilms formed on the worn surfaces.

2. 1. Overall methodology

The aim of the present work is to achieve a better understanding of nanoparticle-doped lubricants and their tribological properties; and to – hopefully – bring this recent technology one step closer to reducing friction and wear in mechanical systems such as engines and/or gearboxes.

Although the tribological testing of the lubricants is essential to evaluate the benefits resulting from the addition of nanoparticles in the oil, many other techniques are needed to fully understand the phenomena occurring during the lubrication of two contacting surfaces. The composition of the nanoparticle-doped lubricant, as well as its rheological properties, should for example be considered. This includes its viscosity, but also the nature of the nanoparticle additives (chemical composition, concentration, shape, structure…) and their agglomeration state. Experimental set-ups of different natures will then provide information on the friction and wear generated by the use of a given blend for different contact conditions, simulating their use in various real-life applications. Different lubrication regimes can for example be considered, by varying the load, the surface velocities, the temperature, the surface roughness… Further steps are then often needed to fulfill the understanding of the results obtained. *In-situ* visualizations of the contact and observations of the nanoparticles after testing can for instance provide information on the action of the IF-MoS_2 in the contact, and analyzing the wear scar will indicate the presence and nature of tribofilms on the contacting surfaces.

This chapter describes the main experimental techniques used throughout this work. A brief summary of the general methodology is also shown on **Figure 2.1**.

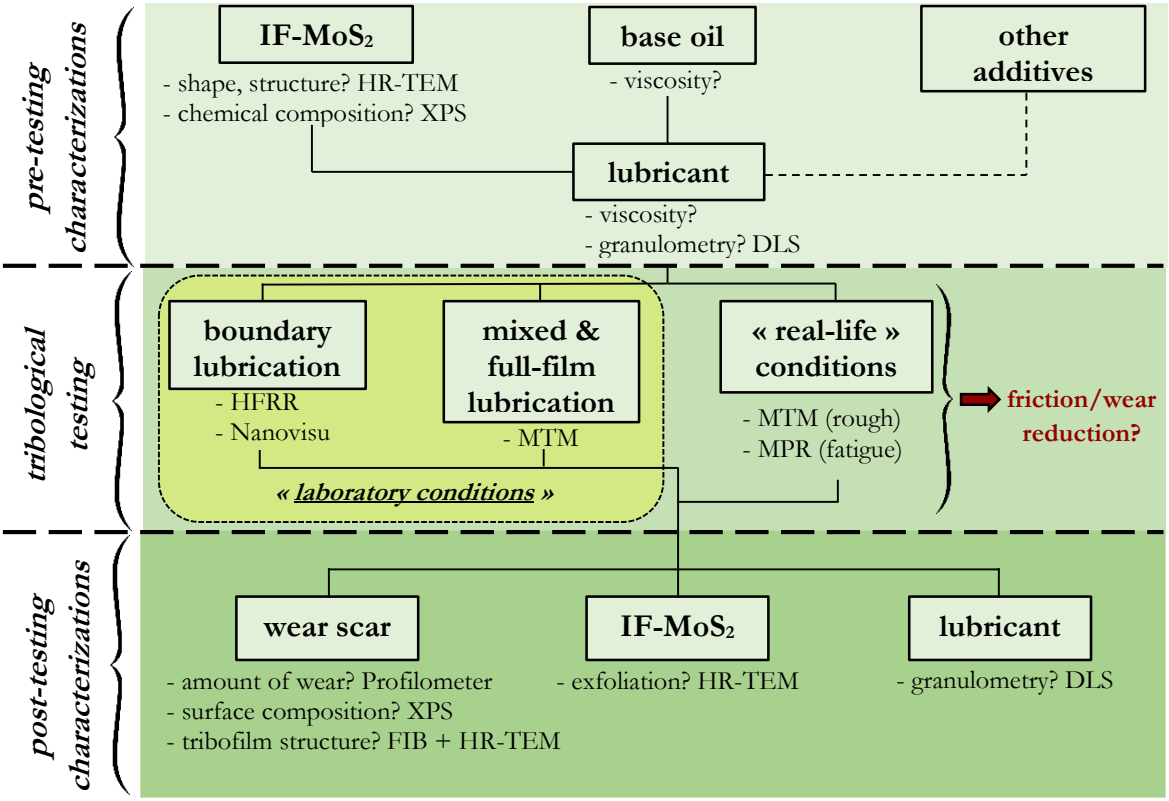

Figure 2.1. Overview of the methodology and main experimental techniques used

2. 2. Tribological Testing

Unless specified otherwise, the base oil used for the tribological tests was a blend of PAO 4 and PAO 40 provided by LUBRIZOL, with a viscosity of 9.3 cSt at 100°C and 54.0 cSt at 40°C.

2. 2. 1. High-Frequency Reciprocating Rig (HFRR)

A PCS Instruments HFRR (High Frequency Reciprocating Rig) was used to evaluate the friction and wear reducing properties of the nanoparticles in severe boundary lubrication conditions. The test consists in a pure-sliding reciprocating motion between a ball and a disc, as shown on **Figure 2.2**. The system provides friction and average film measurements, and the resulting wear on the specimens can be quantified using appropriate measurement techniques (refer to ***2. 3. 1***). The friction coefficient is deduced from the friction force generated between the ball and the disc during the test, which is measured by a piezoelectric force transducer placed against the heater block supporting the lower specimen holder. The film formation can be assessed qualitatively through the changes in electrical contact potential. This measurement was however not used in this work, as the surface separation was almost inexistent in the chosen test conditions and the electrical properties of MoS_2 nanoparticles and tribofilms are not well known.

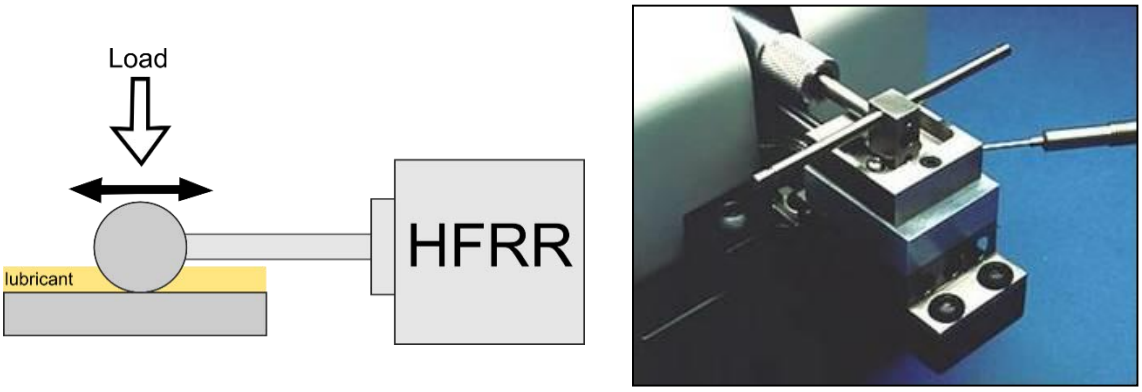

Figure 2.2. Schematic (left) and picture (right, *source PCS Instruments*) of the HFRR

The load is applied by suspending a given number (ranging from 1 to 10) of small weights (100g each) to the top specimen holder, resulting in loads ranging from 0.98 N to 9.81 N. The frequency and stroke of the reciprocating motion can be adjusted, from 10 Hz to 200 Hz on a length ranging from 20 µm to 2.0 mm. The bottom specimen holder also serves as a recipient for the 2 mL of lubricant needed for each test, which can be heated up to 150°C by the heater block placed beneath it. The specimens used are a 6.00 mm diameter ball (top specimen) and a flat disc (bottom specimen), both made of polished AISI 52100 (100Cr6, composition shown in **Table 2.1**) steel (Ra < 50 nm for the ball and Ra < 20 nm for the disc).

Element	C	Cr	Fe	Mn	P	S	Si
wt %	0.98 - 1.1	1.3 - 1.6	96.5 - 97.3	0.25 - 0.45	< 0.025	< 0.025	0.15 - 0.30

Table 2.1. Composition of the AISI 52100 (100Cr6) steel used for the HFRR and MTM tests

As the full friction reduction potential of IF-MoS_2 nanoparticles is only achieved for the most severe contact conditions, the maximal load of 9.81 N was used for all the HFRR tests. Under these conditions, the contact radius and maximum hertzian pressures are determined by the following equations (see **Appendix A** for details):

$$a = \sqrt[3]{\frac{3wR}{4E^*}} = \sqrt[3]{\frac{3\times 9.81\times 3\times 10^{-3}\times\left(1-0.3^2\right)}{2\times 2.11\times 10^{11}}} \approx 5.75\times 10^{-5} m \quad (2)$$

$$P_h = \frac{3w}{2\pi a^2} \approx \frac{3\times 9.81}{2\pi\left(5.75\times 10^{-5}\right)^2} \approx 1,42 GPa \quad (3)$$

Low surface velocities were also needed in order to maintain a severe boundary lubrication regime, implying small stroke lengths and low frequencies. The stroke length was set to 1 mm for all tests in order to preserve a high enough (stroke length) / (contact radius) ratio and avoid fretting conditions, while still making it possible to achieve a high number of cycles in a sufficiently short amount of time. The frequencies used were 10 Hz and 20 Hz respectively, implying average velocities of respectively 0.02 $m.s^{-1}$ and 0.04 $m.s^{-1}$.

This rig provides very repeatable test results (**Appendix C. 1**). The main test parameters, along with the corresponding technical solutions used to apply and/or measure them are given in **Table 2.2**.

	Parameter	Technical solution (operating range)
Applied	*Stroke length/Frequency*	electromagnetic vibrator (20 µm – 2.0 mm / 10 – 200 Hz)
	Normal load	hanging weights (0 - 1.0 kg)
	Temperature	two 24V, 15W cartridge heaters (ambient to 150°C)
Measured	*Stroke length/Frequency*	Linear Variable Differential Transformer (LVDT)
	Friction force	piezoelectric force transducer (Up to 10.0 N)
	Film variation	changes in electric contact potential
	Temperature	platinum RTD probe

Table 2.2. Test parameters on the PCS Instruments HFRR

Before each test, both specimens (ball and disc) as well as all the detachable rig parts (upper and lower specimen holder, screws, hex keys, tweezers) were thoroughly rinsed and cleaned in an ultrasonic bath. This operation was repeated using three different solvents: first ethyl acetate, then ethanol and finally heptane. All the blends were thoroughly mixed using a magnetic agitator before testing. The ultrasonic bath was deliberately not used for the mixing, so as to obtain dispersions representative of real-life test conditions.

2. 2. 2. Mini-Traction Machine (MTM)

A second PCS Instruments test rig, the Mini-Traction Machine (MTM), was used to evaluate the potential of the IF-MoS_2 nanoparticles in milder rolling/sliding conditions (**Figure 2.3**). A ball is loaded against a disc, both being mounted on rotating shafts driven independently to create the desired Slide-to-Roll Ratio (SRR). Various types of friction measurements can be made using this rig, such as traction curves (varying SRR for a given rolling speed), Stribeck curves (varying rolling velocity, load or temperature for a given SRR) or evolution of the friction coefficient in time (for a given set of operating conditions). A wide range of loads, velocities and temperatures can be defined to perform these tests (**Table 2.3**). The simple configuration of the rig allows for an excellent repeatability of the tests (**Appendix C. 2**).

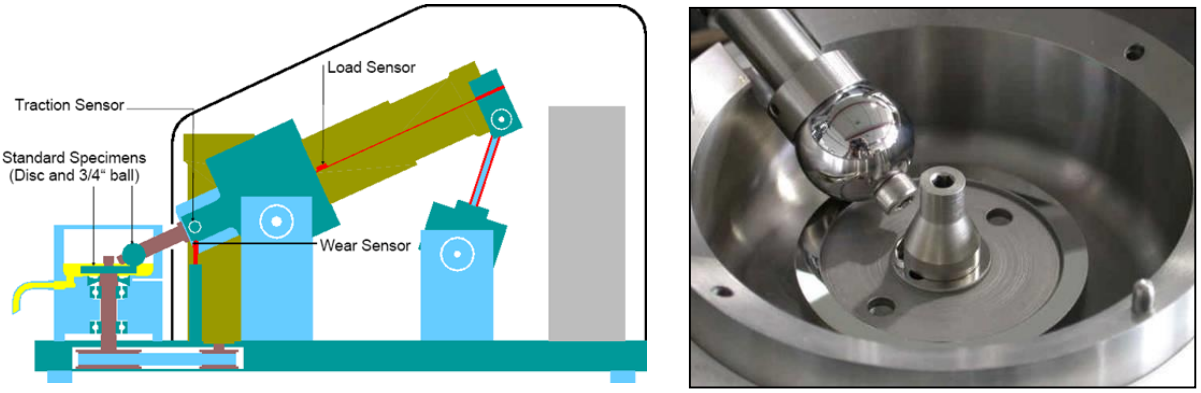

Figure 2.3. Schematic (left) and picture (right) of the MTM (*source: PCS Instruments)*

	Parameter	Technical solution (operating range and precision)
Applied	*Velocity/SRR*	direct current motor (-4 – 4 $m.s^{-1}$ / 0 – 100%)
	Normal load	imposed displacement (0 – 75 N)
	Temperature	electrical resistance (ambient to 150°C)
Measured	*Velocity/SRR*	tachymeter (+/- 2 $mm.s^{-1}$ below 100 $mm.s^{-1}$ +/- 2% above)
	Normal load	load sensor (+/- 1 N)
	Friction force	piezoelectric force transducer (+/- 0.2 N)
	Temperature	thermocouples (+/- 0.5°C)

Table 2.3. Test parameters on the PCS Instruments MTM

The standard specimens are made of super finished AISI 52100 (100Cr6, composition shown in **Table 2.1**) steel, and the discs can be either smooth (mirror finish, Ra < 0.01 µm) or rough (Ra > 0.1 µm). Two different ball diameters are available: ¾" (19.05 mm) and ½" (12.70 mm), so as to reach higher contact pressures for a given load (**Table 2.4**). The wide range of operating conditions available on the MTM makes it possible to carry out tests in all lubrication regimes, ranging from boundary to full-film EHL contacts.

Load	**6N**		**16N**		**45N**		**55N**		**75N**	
Ball diameter	*½"*	*¾"*	*½"*	*¾"*	*½"*	*¾"*	*½"*	*¾"*	*½"*	*¾"*
a (µm)	62.7	71.8	85.1	97.4	122.7	140.5	131.2	150.2	145.5	166.6
P_h (GPa)	0.73	0.56	1.01	0.77	1.43	1.09	1.53	1.16	1.69	1.29

Table 2.4. Contact radii and maximum hertzian pressures for the two MTM ball diameters under different loads

The original MTM set-up requires 35 mL of oil per test, but a mini-pot assembly was used to reduce the lubricant sample volume to 4 mL and facilitate the cleaning of the rig. All tests were carried out by following the same cleaning procedure as for the HFRR tests, with three successive rinses and ultrasonic baths of all specimens and detachable parts in ethyl acetate, ethanol and heptane. All the blends tested on the MTM were mixed using a magnetic agitator only.

2. 2. 3. Nanovisu Test Rig (NTR)

The Nanovisu Test Rig (NTR) is a tribometer designed and developed at LTDS. It was used in order to obtain real-time visualizations of the contact. This rig reproduces the pure sliding reciprocating conditions of the HFRR, but a sapphire flat is used instead of steel to be able to visualize the contact during the test (**Figure 2.4**). A microscope is focused on the ball surface, and the images are recorded by a CCD (Charge-Coupled Device) camera. The friction coefficient between the ball and the flat is also recorded, but is not representative of real-life contacts as one surface is made of sapphire.

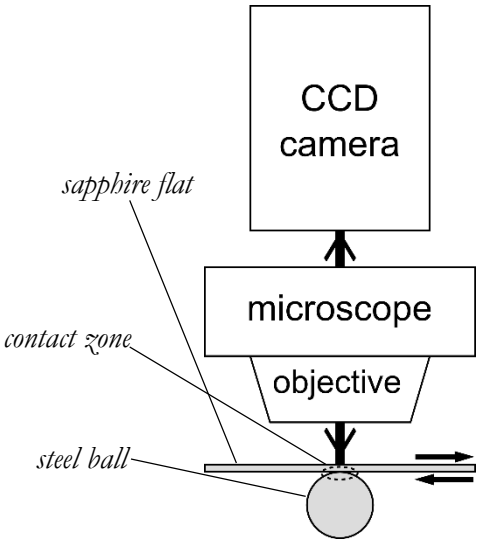

Figure 2.4. Schematic of the NTR

The mechanical properties of sapphire differ from steel, so the load must be adjusted to obtain a maximum hertzian pressure similar to the HFRR tests. Considering Young's modulus and Poisson's ratio of sapphire to be respectively E_{sapph}=460 GPa and ν_{szpph}=0.35, the equivalent Young's modulus of the contact is:

$$E^* = \left(\frac{1-\nu_{steel}^{\ 2}}{E_{steel}} + \frac{1-\nu_{sapph}^{\ 2}}{E_{sapph}} \right)^{-1} = \left(\frac{1-0,3^2}{211.10^9} + \frac{1-0,35^2}{460.10^9} \right)^{-1} = 161GPa \tag{4}$$

The load *w* may be extracted from equations (2) and (3) as follows:

$$P_h = \frac{3w}{2\pi \left(\sqrt[3]{\frac{3wR}{4E^*}} \right)^2} = \sqrt[3]{w} \frac{3}{2\pi \left(\frac{3R}{4E^*} \right)^{\frac{2}{3}}}$$

$$\therefore w = \frac{8\pi^3 P_h^{\ 3} \left(\frac{3R}{4E^*} \right)^2}{27} = \frac{\pi^3 P_h^{\ 3} R^2}{6E^{*2}} = \frac{\pi^3 \left(1.42 \times 10^9 \right)^3 \times 0.003^2}{6 \times \left(161.10^9 \right)^2} = 5.1N \tag{5}$$

In order to obtain a contact pressure similar to the HFRR tests, the load was set to 5 N. The resulting contact area was however somewhat smaller, with a contact radius of 41 μm (instead of the 57.5 μm determined previously). The stroke and frequency of the test can be set to match the

HFRR tests, but the vibrations induced on the rig are then too important to acquire steady images. Lower speeds were therefore preferred, and a stroke length of 2 mm with a frequency of 0.75 Hz (mean velocity of 3 $mm.s^{-1}$) was used. Given the nature of the test and the small number of cycles achieved, lubrication is ensured by depositing a single droplet of oil on the ball surface before the beginning of the test. This droplet was collected from a well-agitated flask just before the beginning of the test. All the detachable parts, as well as the ball and the sapphire disc were thoroughly cleaned using heptane before each test.

2. 2. 4. Micro-Pitting Rig (MPR)

The influence of nanoparticle-doped oils on the fatigue life of lubricated components was evaluated using another PCS Instruments test rig, the MPR (Micro-Pitting Rig). The set-up consists in loading a single roller with 3 discs, so as to achieve a large number of cycles on this specimen in short periods of time (**Figure 2.5**). The surface velocity of the discs is higher, ensuring faster crack propagation on the roller [77].

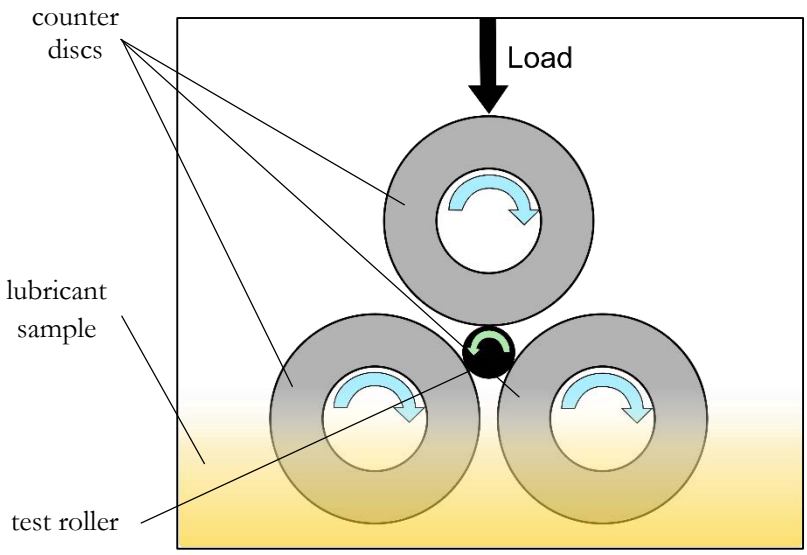

Figure 2.5. Schematic of the MPR

The tests were performed by Powertrib, using a method specifically developed to screen for the FZG C/9/90 pitting test (namely the "20h Powertrib MPR Pitting Test method"). It consists in a 20-hour test with three evenly spaced monitoring steps, during which the weight loss and wear track width of the roller are measured and the surfaces are examined using optical microscopy. The test may be interrupted before completion in the case of large pit formation, detected by measuring the vibration level in the rig with an accelerometer. This method was however slightly adapted for the purpose of the study, with an oil temperature of 80°C and an additional monitoring step added after 2.5 hours of testing. All tests showed very good repeatability (**Appendix C. 3**).

All samples (test roller and counter discs) were made of case hardened 16MnCr5 steel, with a Ra roughness comprised between 0.1 and 0.2 µm. The surface hardnesses were 680 HV (57.7 HRC) for the barrel and 750 HV (60.5 HRC) for the three counter discs.

2. 3. Characterization and Analysis

2. 3. 1. Sensofar Optical Profilometer

The topography of the wear scars presented in this work was obtained using an optical Sensofar PLu neox profilometer. The resulting measurements were analyzed using the MountainsMap Topography XT software, providing information on the depth, volume, length and width of the scars. The same methodology was applied for quantifying the wear on all HFRR lower specimens (see **Figure 2.6**). The choice of analyzing the flat surface instead of the ball was made so as to reveal any plastic deformation occurring during the test.

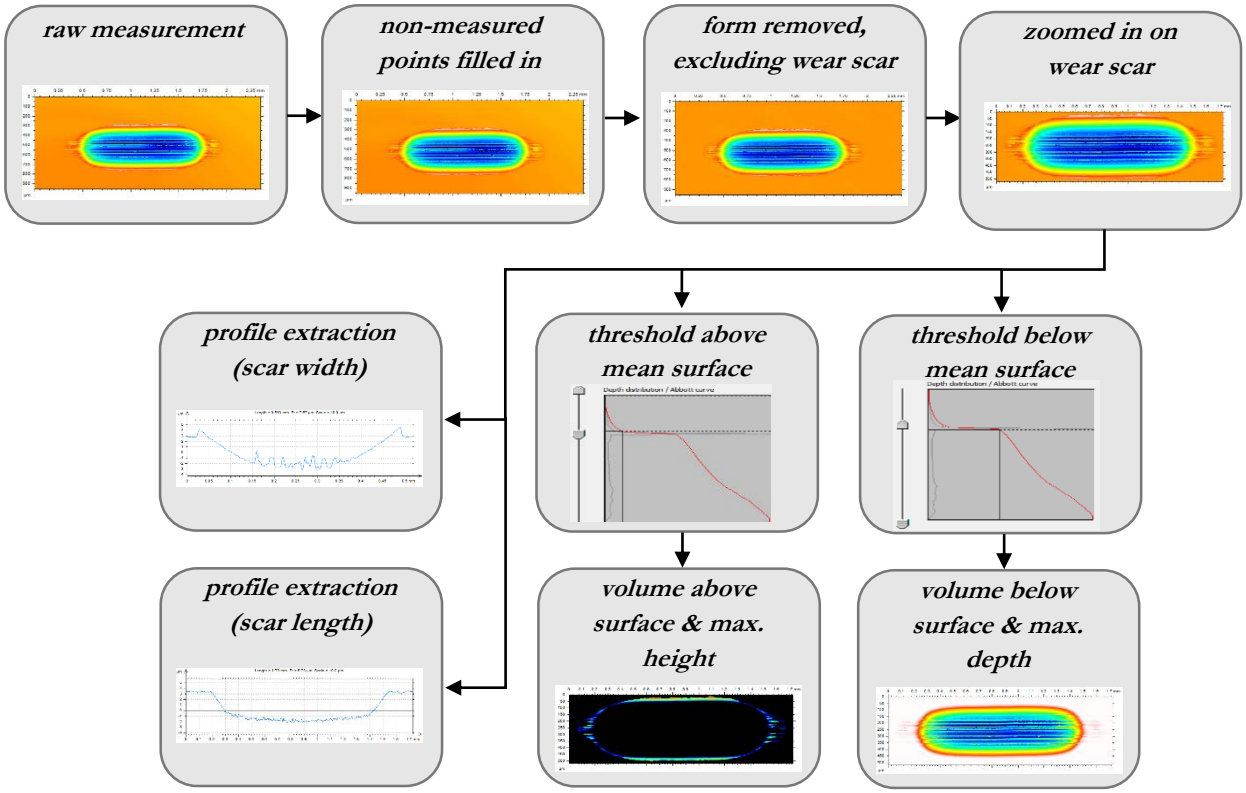

Figure 2.6. Methodology for the quantification of wear on lower HFRR specimens

The filling of non-measured points may be needed for acquisitions where local slopes are too steep to be measured optically. These points are then given a value based on interpolations of surrounding point measurements. The second step (form removal) is used to ensure that the resulting wear scar representation is perfectly horizontal, which is difficult to achieve during the acquisition. It is then possible to set thresholds above and under the mean surface (flat surface outside the contact zone) in order to quantify the volumes of plastically deformed matter and of the scar. The final criteria chosen to quantify the wear were the maximum depth of the scar, and the volume of steel lost during the test. This worn volume was obtained by subtracting the plastically deformed matter (total volume above the mean surface) to the volume of the scar (total volume below the mean surface).

2. 3. 2. Zetasizer Nano ZS Granulometer

The agglomeration state of the nanoparticles in the oil was evaluated by Dynamic Light Scattering (DLS). A Malvern Zetasizer ZS with NIBS (Non-Invasive Back Scattering, detection angle of 173°) was used, allowing for precise measurements of small nanoparticles over a wide range of particle concentrations.

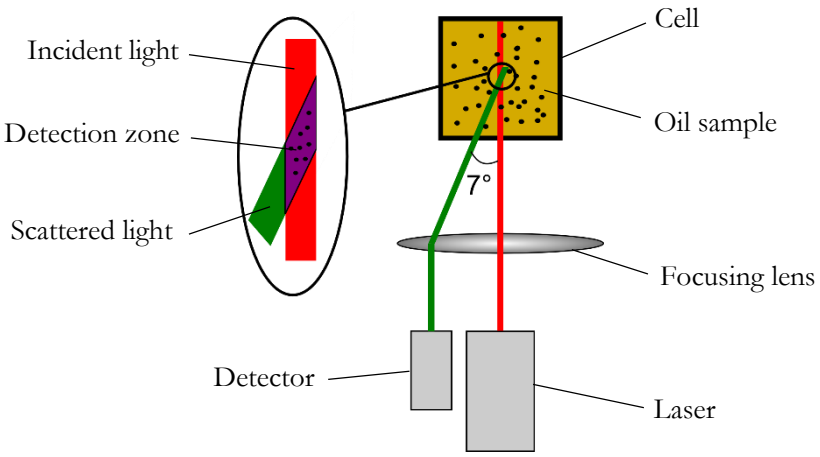

Figure 2.7. Schematic representation of granulometry measurement by DLS

All the particles in the oil are subjected to Brownian motion, and move randomly throughout the fluid with a velocity depending on their size. When hit by an incident light source, the detection of the backscattered light gives information on their velocity, and therefore on their size according to the Stokes-Einstein equation for spherical particles:

$$d = \frac{kT}{3\pi\eta D} \quad \text{with } \overline{x^2} = 2Dt \tag{6}$$

where ***d*** *is the particle diameter in nm;* ***k*** *is the Boltzmann constant 1.3806488×10^{-23} J.K^{-1};* ***T*** *is the absolute temperature in K;* $\boldsymbol{\eta}$ *is the dynamic viscosity in cP;* ***D*** *is the diffusion coefficient in cm^2.s^{-1};* ***t*** *is the time and* $\overline{x^2}$ *is the mean squared distance travelled by the particle in cm^2.s^{-1} during time* ***t.***

The only physical parameters that are needed for the measurements are then the dynamic viscosity and the refractive index of the solvent media at a given temperature. The placing of the detector at an angle of 173° results in a much larger analyzed volume then when placed at 90°, and makes it possible to measure much smaller particles (under 1 nm).

As the IF-MoS_2 concentration in the oil resulted in a totally opaque media, large dilutions (order of magnitude of 1/1000) were done in the base oil before placing the sample in the Zetasizer in order to obtain a transparent medium and therefore be able to quantify the back-scattered light.

2. 3. 3. Viscometer

The viscosities of the different oils used in this study were measured using a CANNON CAV-2100 viscometer. This instrument consists in vertical tubes, inside which the flow rate of the oil sample is measured by electronically timing the liquid meniscus as it moves between thermistor sensors. The bath temperatures of the tubes as well as the flow rate are measured with great precision (**Table 2.5**). A wide range of calibration tests were initially done on the instrument with

a number of oils of known viscosity in order to relate the flow rate to a given viscosity. The viscometer provides three measurements per sample, and the final value of the measured flow rate is the average of the two closest ones.

Measurement	Precision	Technical solution
Flow rate (0,5 cSt ≤ υ ≤ 5000 cSt)	± 0.001 second	Electronic timing
Temperature (20°C ≤ T ≤ 100°C)	± 0.01 °C	Thermistor sensor
Temperature (100°C < T ≤ 150°C)	± 0.03 °C	Thermistor sensor

Table 2.5. Range and precision of the measurements made by the CAV-2100 viscometer

All the measurements carried out in this thesis were carried out at 40 and 100°C, and the viscosity for any given temperature was then extrapolated when necessary, using the following relationship [78]:

$$\log(\log(\upsilon + 0.8)) = A + B\log(T) \tag{7}$$

where υ is the kinematic viscosity in cSt, T is the temperature in K and A and B are two constants to be determined for each oil.

2. 3. 4. X-Ray Photoelectron Spectroscopy (XPS)

X-Ray Photoelectron Spectroscopy (XPS) was used to analyze the chemical composition of the nanoparticle powders and of the extreme surface of the wear scars obtained after tribological testing. This technique provides information on the elements present in the sample, as well as on their chemical environment.

XPS measurements rely on the photoelectric effect, which is the emission of electrons by the atoms hit by incident photons. The measured kinetic energy of the emitted electrons depends on the energy of the incident X-ray (which is known, in the keV range) and of the binding energy needed to free them from their element:

$$E_B = h\nu - E_C \tag{8}$$

where E_B is the binding energy for a given element, $h\nu$ is the energy of the incident photon (h is the Planck constant and ν is the frequency of the photon) and E_C is the energy of the emitted photon.

The energy of incident photons will depend on the source used, generally Al K_α (1486.6 eV) or Mg K_α (1253.6 eV). The photons emitted by the photoelectric effect have low kinetic energies (< 1500 eV), which prevents them from exiting the sample if their source atom is further than 3-5 nm from the surface of the sample. This technique can therefore only provide extreme surface analyses, which is most convenient for tribofilm characterization. XPS analysis is furthermore possible on insulating materials, but the accumulation of positive charges at the surface will decrease the kinetic energy of the emitted electrons, resulting in a shifting of the acquired spectra. These positive charges can be neutralized by electrons in order to reduce this effect.

An Ulvac-PHI Versaprobe II system, with a high power monochromatized Al K_α X-ray source (hv=1486.68eV) was used. The X-ray beam was focused on the samples (tribofilms or nanoparticle powder) and areas of 100µm x 100µm were probed. A survey scan was first recorded in order to identify the chemical elements present in the probed area. Scans were then recorded at some

selected peaks in order to get complete information on the chemical composition (chemical bonding) of the sample. The resolution of the XPS was 0.2 eV, and the position of C1s peak (284.8 eV) was considered as the reference for charge correction. A flood gun was used for charge compensation. The XPS analyses were performed in several areas, in order to verify the repeatability of the results. The software MultiPack was used to analyze the XPS spectra obtained from the scans. Quantitative analyses of the peaks were performed using peak area sensitivity factors. An XPS handbook and online databases were used to attribute the binding energies to the different chemical species.

The chemical analyses of the tribofilms were performed after rinsing the samples with n-heptane and placing them in an ultrasonic bath of n-heptane for 10 minutes. The nanoparticle powders were deposited on a copper tape before placing them in the XPS for analysis.

2. 3. 5. High-Resolution Transmission Electron Microscopy (HR-TEM)

High-Resolution Transmission Electron Microscopy (HR-TEM) provided high quality images of the nanoparticles tested throughout this work. An electron beam (of known energy) is focused on the observed sample, and the energy loss of the transmitted beam corresponds to the absorption of part of the primary electrons in the sample. The resulting images are then of chemical nature, with the darker zones corresponding to either thicker parts of the sample or elements of higher atomic number. A JEOL 2010F operating with an accelerating voltage of 200 kV was used in this work. This TEM is equipped with an Energy-dispersive X-ray spectrometer (EDX), providing the elemental composition of the surfaces through the detection of the characteristic X-rays emitted by the sample while under the incident electron beam.

The observations of the nanoparticles were achieved by diluting the IF-MoS_2 in n-heptane and depositing a single drop of the resulting blend on a carbon-covered copper micro-grid. For the observation of nanoparticles having been submitted to tribological testing, the micro-grid was placed upside-down on the wear scar. A drop of heptane was then deposited on the micro-grid: when drying off, the nanoparticles remaining on the steel surface adhered onto the micro-grid.

Chapter Three

Synthesis of efficient IF-MoS_2: influence of nanoparticle size and structure

The first step in formulating an efficient nanoparticle-doped lubricant is to determine which properties the nanoparticle additives should possess in order to achieve maximum friction and wear reduction. Inorganic Fullerene-like (IF-) MoS_2 nanoparticles were selected as the main constituents of the oil, as they have shown great tribological potential in the past. The influence of their size and structure on their lubricating behavior however remains unknown, and will be studied in this chapter. Four different types of IF-MoS_2 nanoparticles were synthesized and tested, and the results made it possible to clearly differentiate the influences of nanoparticle size and crystallinity on their ability to form efficient friction-reducing tribofilms on steel surfaces.

3. 1. Introduction

The outstanding friction reducing abilities of Inorganic Fullerene-like (IF-) MoS_2 nanoparticles have been reported many times before [63–65], and the main lubrication mechanism associated with their tribological performances in severe boundary lubrication regimes is well known. After being entrapped by the contacting surfaces and forced through the contact, the combined stresses of compression and shear lead to nanoparticle exfoliation. The liberated hexagonal 2H-MoS_2 nanosheets then adhere to the steel surfaces, forming a low-friction tribofilm inside the contact [68]. From these observations, it has been shown that the tribological potential of the nanoparticles depends on their internal structure: poorly crystalline particles (i.e. containing many structural defects) will be less resistant and exfoliate faster, therefore facilitating tribofilm formation [66].

According to the literature, and considering this exfoliation mechanism taking place in the boundary lubrication regime, the general agreement today is that the synthesis of smaller fullerene-like nanoparticles will improve friction reduction by increasing the probability of the nanoparticles passing through the contact. Some studies have comforted this idea, such as the interesting results presented in [66] for small (20 – 50 nm) and poorly crystalline IF-MoS_2 nanoparticles. The larger and less efficient IF-MoS_2 nanoparticles tested in the same operating conditions were however also more crystalline, which makes it difficult to conclude on the influence of nanoparticle size alone. The benefits in reducing the size of IF-WS_2 aggregates has also been shown, either by an effective mixing of the oil before testing [53,79] or by grafting the appropriate dispersants on the nanoparticles [80].

The beneficial effect of reducing nanoparticle size however remains an assumption, as no study has yet compared the tribological performances of similar IF-MoS_2 varying only in size. In this chapter, the tribological behavior of four types of IF-MoS_2 nanoparticles of different sizes and degrees of crystallinity was explored, by comparing their friction and wear reduction capacities under severe boundary lubrication conditions. The results obtained during these tests made it possible to differentiate the influences of nanoparticle size and crystallinity. Oil recirculation was also shown to be of great importance for real-life conditions, with splash lubrication taking place in non-negligible volumes of lubricant. The relative importance of nanoparticle size and structure in these lubricating conditions are discussed in the light of these results.

3. 2. Nanoparticle synthesis and characterization

3. 2. 1. Different types of nanoparticles tested

All the nanoparticles presented in this thesis were synthesized at IRCELYON (CNRS, France). The synthesis is a two-step process. The first step is the preparation of nanoparticles of an amorphous MoS_x ($x > 3$) compound by chemical reaction of ammonium heptamolybdate and sulfur in ethylene glycol under reflux. The process was similar to the preparation described in [31], but the cellulose was replaced by an equivalent amount of starch in the reaction mixture. The reaction conditions were modified to obtain particles of different sizes, by changing the order of addition of the reactants, the duration and the temperature of the reaction. In order to obtain large particles, the reactants were added simultaneously before heating the mixture for 4 h at the boiling point of ethylene glycol. The smaller particles were obtained by adding the solution of ammonium heptamolybdate subsequently in four equal portions with an interval of five minutes, before heating

the reaction mixture for one hour only at 180 °C. After the reaction, the mixture was cooled down to room temperature and diluted by a twofold excess of ethanol. The amorphous compound was then extracted by centrifugation, washed and dried.

The second step consisted in treating the MoS_x powder in a quartz reactor under a flow with a mixture of hydrogen and H_2S. The thermal treatment step results in the formation of crystalline MoS_2, and eventually of the IF-MoS_2 nanoparticles. This second step may be carried out at different temperatures, lower temperatures leading to the formation of less crystallized nanoparticles, containing more structural defects. An overview of the characteristics of the four types of IF-MoS_2 synthesized is given in **Table 3.1**.

Designation	Average Diameter (nm)	Treatment temperature (°C)
LpC (**L**arge, **p**oorly **C**rystalline)	350	400
LC (**L**arge **C**rystalline)	350	700
SpC (**S**mall, **p**oorly **C**rystalline)	150	400
SC (**S**mall **C**rystalline)	150	700

Table 3.1. Main characteristics of the four types of IF-MoS_2 nanoparticles synthesized

The synthesis of these four types of IF-MoS_2 covers all the possible combinations between nanoparticles of two different sizes and two different structures, so as to be able to differentiate the influence of each parameter on their lubricating performances. The same reactants and similar processes were furthermore used for the synthesis of all the batches, theoretically leading to identical chemical compositions for all nanoparticles.

The visual aspect (shape and structure) as well as the chemical nature of the nanoparticles were verified experimentally, and the results are shown in the next section.

3. 2. 2. HR-TEM observations and chemical analysis

The four types of nanoparticles described in **Table 3.1** were observed using HR-TEM, and a narrow particle size distribution was noted (**Figure 3.1**).

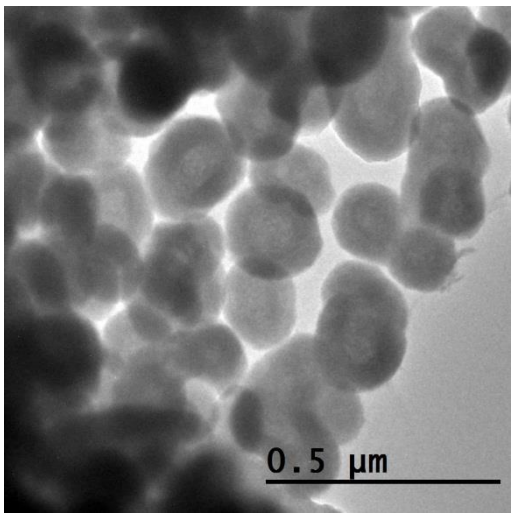

Figure 3.1. Typical size distribution of the nanoparticles (SC IF-MoS_2 shown here)

The rather large size (300-400 nm) of the LpC and LC particles was confirmed, and their good sphericity was revealed (**Figure 3.2**). The high-temperature (700 °C) thermal treatment carried out at the end of the synthesis process of the LC IF-MoS_2 improved the fullerene-like aspect of the structure, which is composed of long and concentric atomic layers. Some defects can however be observed in the nanoparticle structure, with some discontinuities between the layers. The lower temperature (400 °C) used for the thermal treatment of the LpC nanoparticle resulted in short MoS_2 layers (4-6 nm in length), stacked in a seemingly chaotic manner.

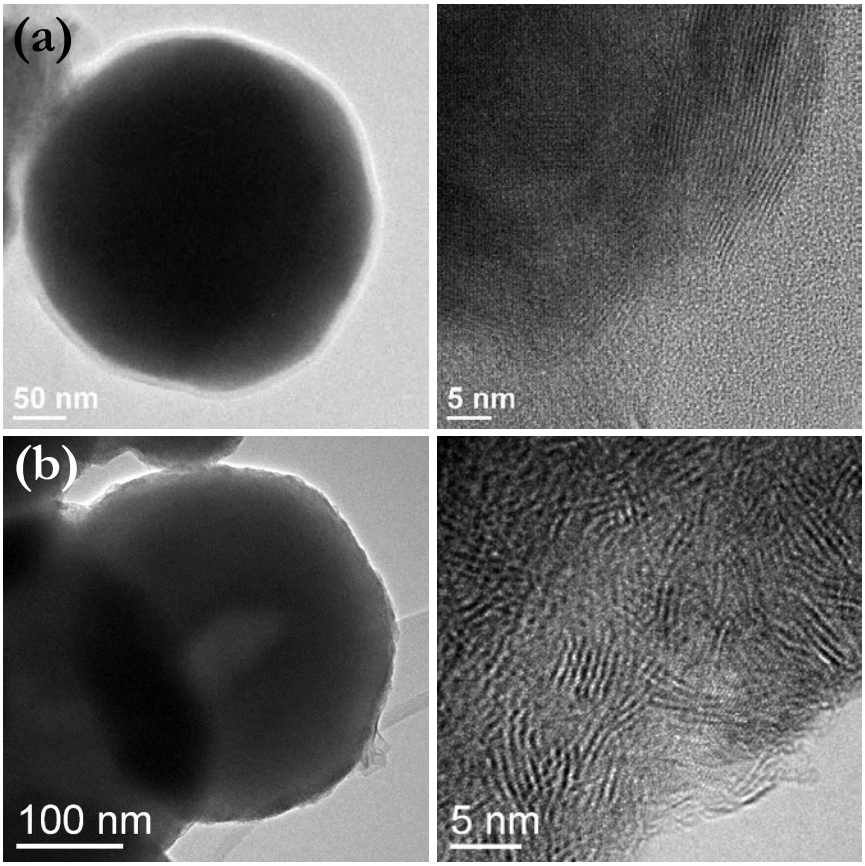

Figure 3.2. HR-TEM images of LC (a) and LpC (b) IF-MoS_2 nanoparticles

The differences between the smaller SC and SpC nanoparticles are similar to those witnessed between the previous LC and LpC nanoparticles, with long and concentric atomic layers clearly visible in the first case and short and randomly stacked atomic layers in the other (**Figure 3.3**).

Both types of particles treated at 400 °C have so many structural defects that they do not have a visual fullerene-like aspect. For the sake of simplicity, the term "IF-MoS_2" will however still include these LpC and SpC particles throughout this chapter, even though they are simply spherical and poorly crystalline MoS_2 nanoparticles.

The average diameter of the SC and SpC nanoparticles observed was approximately 150 nm, representing an average diameter reduction by 2.33 compared to the LC and LpC IF-MoS_2. Considering perfectly spherical nanoparticles, this would imply a reduction by 12.65 in terms of volume.

To put these notions into perspective, the order of magnitude of the number of both small and large nanoparticles contained in 1 mL of oil was determined with the following hypotheses:

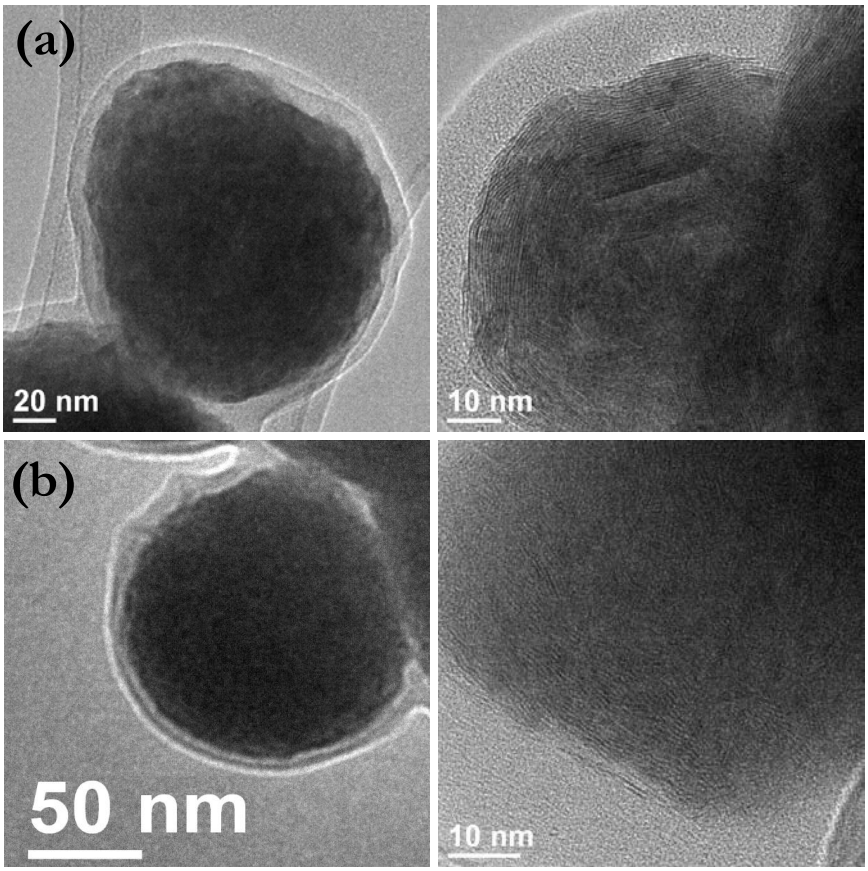

Figure 3.3. HR-TEM images of SC (a) and SpC (b) IF-MoS_2 nanoparticles

- the IF-MoS_2 are all perfectly spherical and of equal size (for a given sample);
- the mass concentration of IF-MoS_2 in the oil was 1%;
- all the IF-MoS_2 have the same density;
- the IF-MoS_2 are not agglomerated and their dispersion in the oil is optimal;
- $\Phi_{SC,SpC} = 150$ nm, $\Phi_{LC,LpC} = 350$ nm, $\varrho_{IF\text{-}MoS2} = 5000$ kg.m^{-3}, $\varrho_{oil} = 830$ kg.m^{-3}.

Under these conditions, 1 mL of base oil weights 0,83 g and therefore contains $8{,}3.10^{-3}$ g of IF-MoS_2 nanoparticles. The total volume of MoS_2 nanoparticles in the oil is then:

$$V_{MoS_2} = \frac{8.3\times10^{-6}}{5000} = 1.66\times10^{-9}\,\mathrm{m}^3 \qquad (9)$$

Depending on the nanoparticle size, this volume of MoS_2 results in the following quantity of IF-MoS_2:

$$N_{SC,SpC} = \frac{V_{MoS_2}}{V_{SC,SpC}} = \frac{V_{MoS_2}}{\frac{4}{3}\pi r_{SC,SpC}^{\ 3}}$$

$$N_{SC,SpC} = \frac{1.66\times10^{-9}}{\frac{4}{3}\pi\times(75\times10^{-9})^3}$$

$$N_{SC,SpC} \simeq 9.4\times10^{11}$$

$$N_{LC,LpC} = \frac{V_{MoS_2}}{V_{LC,L\,pC}} = \frac{V_{MoS_2}}{\frac{4}{3}\pi r_{LC,LpC}^{\ 3}}$$

$$N_{LC,LpC} = \frac{1.66\times10^{-9}}{\frac{4}{3}\pi\times(175\times10^{-9})^3}$$

$$N_{LC,LpC} \simeq 7.4\times10^{10}$$

Reducing the diameter of the IF-MoS_2 therefore increases their quantity in the oil by approximately 12.7 for a given mass concentration. This size reduction may therefore not only affect the properties of single nanoparticles, but also their agglomeration and their availability throughout the oil medium.

The chemical composition of the IF-MoS_2 was verified using X-Ray Photoelectron Spectroscopy, as described in paragraph ***2. 3. 4***. The molybdenum (Mo 3d) and sulfur (S 2p) energy peaks for the four types of nanoparticles are shown on **Figure 3.4** and **Figure 3.5**, respectively.

The main Mo $3d_{5/2}$ and S $2p_{3/2}$ peaks clearly have the same energies for all four types of IF-MoS_2, confirming that they are of identical nature (**Table 3.2**). The Mo $3d_{5/2}$ peaks are found at approximately 229.8 eV and the S $2p_{3/2}$ at 162.7 eV, which are typical energy peaks corresponding to molybdenum sulfide species.

	nanoparticle type			
	LC	**LpC**	**SC**	**SpC**
Mo $3d_{5/2}$	229.8 eV	229.8 eV	229.9 eV	229.8 eV
S $2p_{3/2}$	162.7 eV	162.6 eV	162.8 eV	162.7 eV
S 2s	227.0 eV	227.0 eV	227.1 eV	227.0 eV

Table 3.2. Measured energies for the main Mo and S peaks

The surface of the LC and SpC nanoparticles appeared to be somewhat oxidized, with Mo – O species found at 232.5 eV and 233.9 eV for the LC IF-MoS_2 and 234.4 eV for the SpC IF-MoS_2. This was confirmed with the observation of S – O species at 169.1 eV and 170.3 eV (LC IF-MoS_2), and 168.7 eV and 170.7 eV (SpC). Partial oxidation of the surface may have occurred due to air exposure before the XPS experiments. This did however not appear to be due to the nanoparticle synthesis process or to the many defects in the nanoparticles (structure not as well closed), as both the LC and SpC were found to be oxidized but not the LpC and SC nanoparticles.

Small energy contributions were finally found at 164.1 eV (SpC) and 163.8 eV (LpC), which were attributed to a small excess of sulfur in the poorly crystalline nanoparticles.

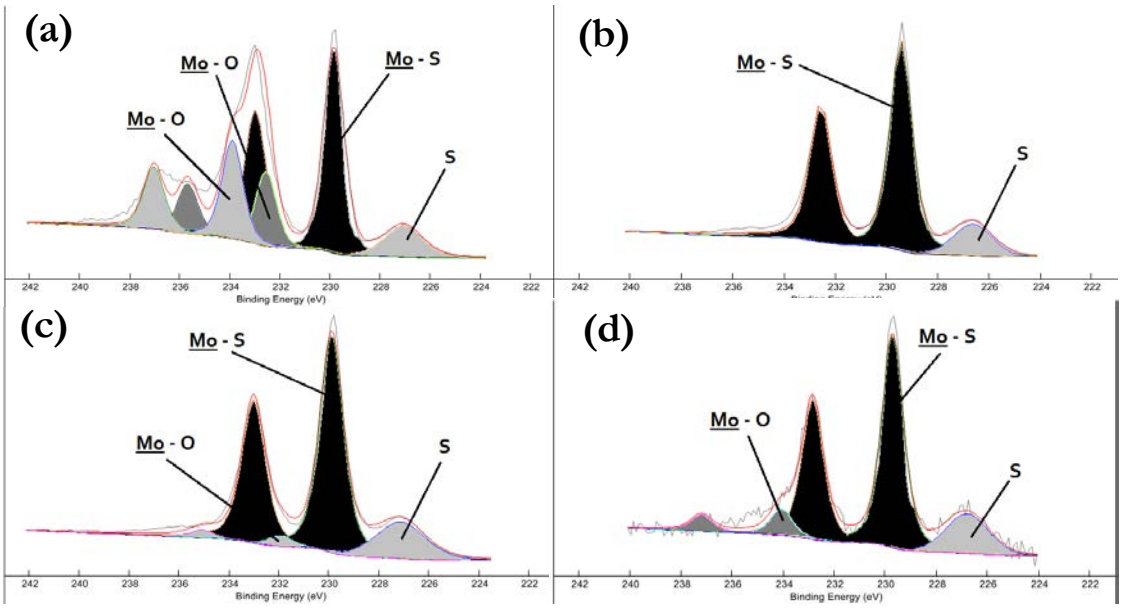

Figure 3.4. Molybdenum 3d spectra measured by XPS for the (a) LC, (b) LpC, (c) SC and (d) SpC IF-MoS_2

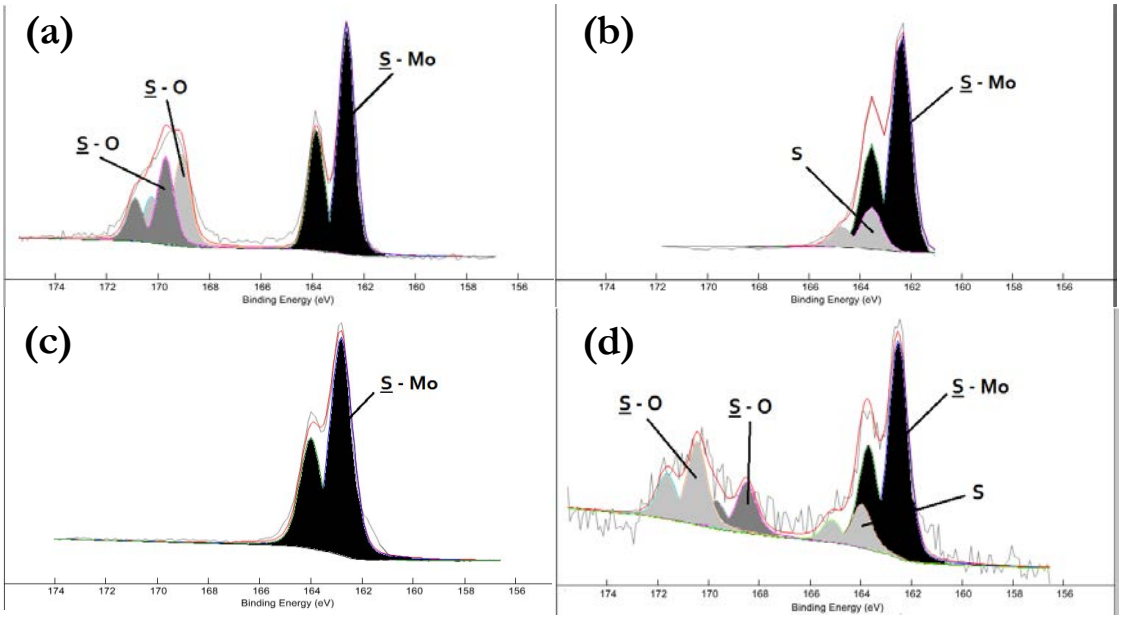

Figure 3.5. Sulfur 2p spectra measured by XPS for the (a) LC, (b) LpC, (c) SC and (d) SpC IF-MoS_2

3. 3. Tribological testing of the IF-MoS_2 nanoparticles

3. 3. 1. Influence of nanoparticle size and structure

The four types of IF-MoS_2 nanoparticles presented in the previous section were tested on the High-Frequency Reciprocating Rig (HFRR) described in ***2. 2. 1***. The test conditions summarized in **Table 3.3** lead to particularly severe boundary lubrication, with a high number of cycles achieved and splash lubrication taking place in a non-negligible volume of oil. This was chosen in order to assess the tribological potential of the IF-MoS_2 nanoparticles for conditions closer to real-life applications; as opposed to the many studies focusing on the lubrication mechanism associated to the IF-MoS_2 where the tests are often short (low number of cycles) and lubrication is ensured by a single droplet of oil deposited on the contact surfaces before testing [22,44,46,54,63–66].

Load (N)	**10**
Maximum hertzian pressure (GPa)	**1.4**
Stroke length (mm)	**1**
Frequency (Hz)	**10**
Number of cycles (-)	**144 000**
Oil capacity (mL)	**2**
IF-MoS_2 concentration (wt%)	**1**
Base oil	**PAO**
kinematic viscosity at 40°C (cSt)	**54.0**
kinematic viscosity at 100°C (cSt)	**9.3**
Material	**AISI 52100 (100Cr6)**
Ra (ball, nm)	**< 50**
Ra (flat, nm)	**< 20**
Temperature (°C)	**80**

Table 3.3. HFRR test conditions used hereafter

The addition of 1wt% of nanoparticles in the PAO base oil did not change its viscosity. Under these conditions, the average velocity of the ball is 0.02 $m.s^{-1}$. This value leads to a theoretical central film thickness h_c (see **Appendix B**) of 2.7 nm. The film thickness parameter (described in part ***1. 1. 2***) is then under 0.05, confirming the severity of the lubrication regime.

The evolution of the friction coefficient for the large (LpC and LC) IF-MoS_2 nanoparticles during the 4 hour HFRR test is shown on **Figure 3.6**.

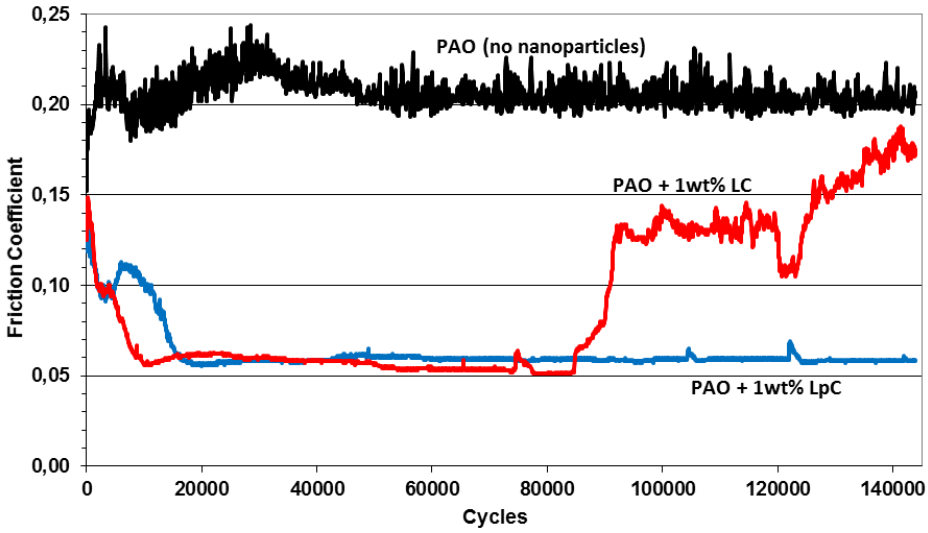

Figure 3.6. Friction coefficients of the LC and LpC nanoparticles during the HFRR test

Under these operating conditions, the reference test for the PAO oil produced a fairly constant friction coefficient of 0.2. Both types of large nanoparticles showed great friction reduction abilities, with a friction coefficient quickly dropping to 0.06. The LpC and LC nanoparticles showed similar behaviors at the beginning of the test, with the associated friction coefficient decreasing progressively before reaching minimum friction and stabilizing during approximately 75 000 cycles. The test results then differed, as the friction coefficient remained stable throughout the 144 000 cycles for the LpC IF-MoS_2-doped base oil, but started increasing continuously for the LC nanoparticle-doped PAO. The sudden raise in the coefficient of friction observed after approximately 85 000 cycles may be due to a progressive wearing out of the tribofilm formed on the friction surfaces, slowly increasing the coefficient of friction back to the value obtained for the base oil only.

The smaller SC and SpC IF-MoS_2 nanoparticles were tested with the same operating conditions, and the results are shown on **Figure 3.7**.

The tribological behavior of these smaller SC and SpC nanoparticles was strikingly similar to that of the LC and LpC nanoparticles tested before. Both types of IF-MoS_2 decreased the friction coefficient abruptly at the beginning of the test, which then stabilized between 0.06 and 0.07. While the small and poorly crystalline SpC nanoparticles maintained the friction coefficient stable throughout the 144 000 cycles of the test, the more crystalline IF-MoS_2 were once again effective only for a limited number of cycles, as the friction coefficient started increasing after 85 000 cycles until it reached the value obtained for the base oil alone.

The extreme friction reduction abilities of IF-MoS_2 nanoparticles in severe boundary lubrication regimes have been shown before, but for milder test conditions. The test results

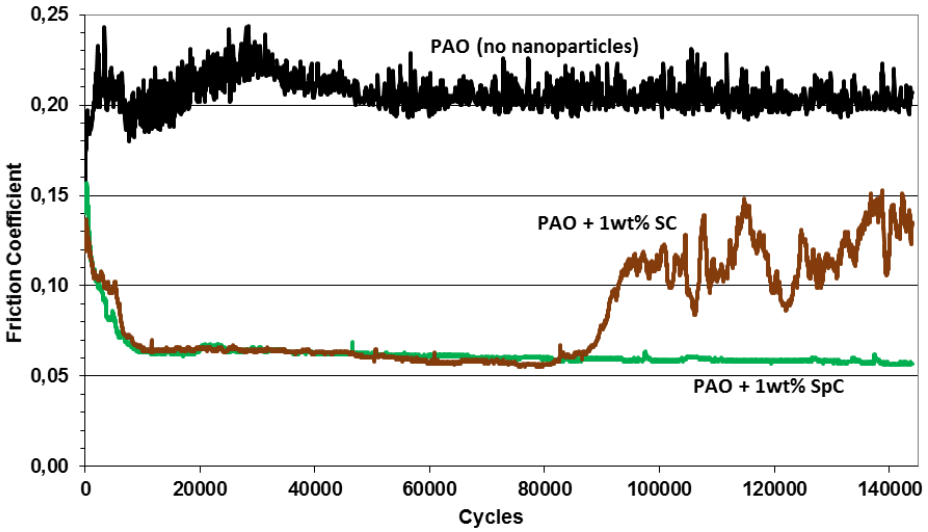

Figure 3.7. Friction coefficients of the SC and SpC nanoparticles during the HFRR test

depicted in **Figure 3.6** and **Figure 3.7** highlight the efficiency of IF-MoS_2 nanoparticles under conditions more likely to be encountered in real-life applications, with a high number of cycles achieved and splash lubrication taking place in a small volume of oil. All four nanoparticle types proved to be very effective additives, by reducing friction by approximately 70% compared to the base oil alone for a high number of cycles (75 000 cycles of maximum friction reduction for the least durable type of IF-MoS_2).

When comparing the tribological results for both sets of nanoparticles (large and small), it becomes clear that their crystallinity is the main parameter dictating their effectiveness, predominant over particle size (**Figure 3.8**). Both types of poorly crystalline nanoparticles (large and small) indeed produced a very low friction coefficient throughout the whole test, whereas both types of more crystalline IF-MoS_2 (large and small) were only effective until 85 000 cycles were reached. For these LC and SC nanoparticles, the friction coefficient then rose steadily throughout the test before reaching the value obtained for the base oil alone, behavior attributed to the progressive wearing out of the tribofilm.

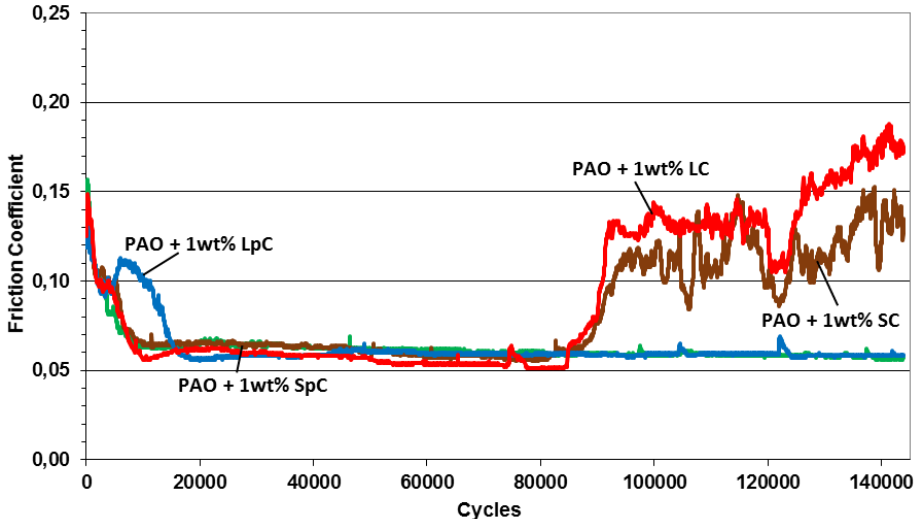

Figure 3.8. Compared friction coefficients for the four types of nanoparticles tested

As a complement to the friction coefficients recorded for the LC, LpC, SC and SpC nanoparticle types, the corresponding wear scars were measured (see section ***2. 3. 1***) and compared

using optical profilometry (**Figure 3.9**). The corresponding quantities (the maximum scar depth measured, the measured scar volume, the measured volume of deformed matter and the calculated worn volume) are reported in **Table 3.4**. For the sake of clarity, the criteria chosen to quantify the wear were also plotted on **Figure 3.10**.

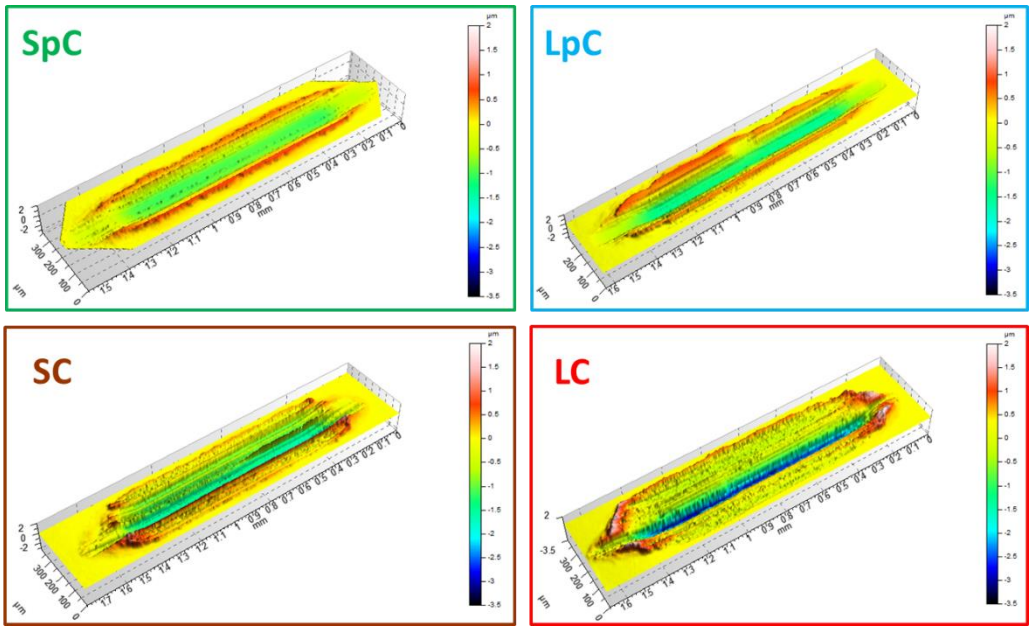

Figure 3.9. 3D measurements of the wear scars obtained for the four different types of IF-MoS_2 nanoparticles

Criteria / *Test*	***Max. depth (µm)***	*Scar volume (.10³ µm³)*	*Deformed volume (.10³ µm³)*	***Worn volume (.10³ µm³)***
PAO alone	**13.6**	3 037	25	**3 012**
LC IF-MoS₂	**3.3**	254	43	**211**
LpC IF-MoS₂	**1.6**	136	43	**93**
SC IF-MoS₂	**2.5**	263	30	**233**
SpC IF-MoS₂	**1.2**	106	27	**79**

Table 3.4. Depths and volumes of the wear scars obtained after tribological testing

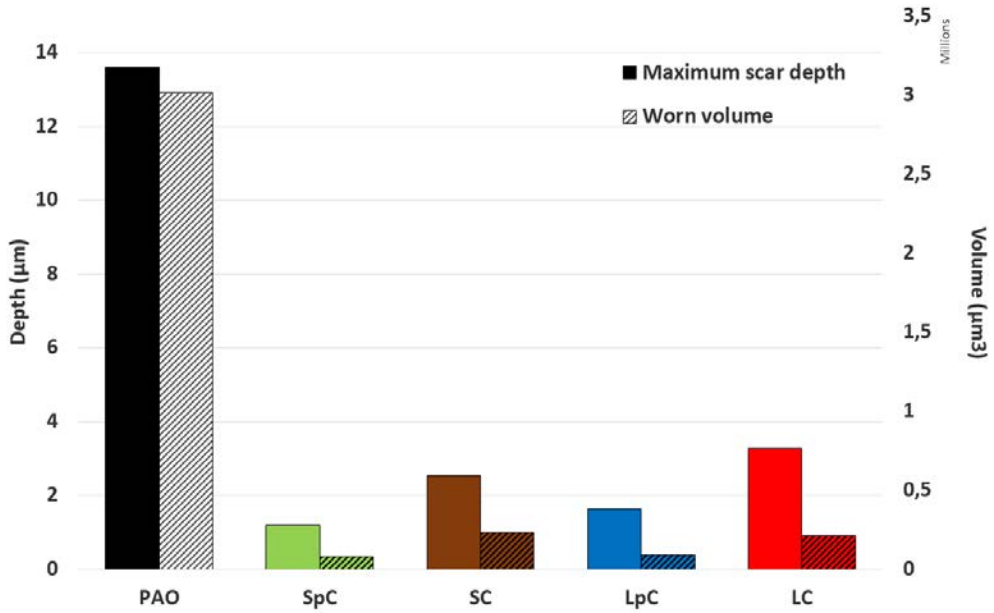

Figure 3.10. Maximum depths and wear volumes of the scars obtained for the different types of IF-MoS_2

In addition to their friction reduction properties, all the IF-MoS_2 nanoparticles reduced wear significantly during the tests. Compared to the PAO base oil alone, the more crystalline nanoparticles (large and small) reduced the maximum depth of the wear scar by 4.5 on average, and the worn volume by nearly 14. Both types of poorly crystalline particles were even more effective in reducing wear (maximum depth of the wear scar reduced by nearly 10 on average, and worn volume reduced by approximately 35), which is consistent with the friction results showed previously.

3. 3. 2. Effects of the oil flow on nanoparticle starvation of the contact

For the nanoparticle sizes and morphologies studied, the crystallinity was shown not have a significant influence on the minimum friction coefficient achieved, but it had a great impact on the durability of the additive during the test. Assuming that the nature of the formed friction-reducing tribofilms is identical for all the nanoparticles, two hypotheses first come to mind to explain this result:

(a) the LC and SC nanoparticles were consumed faster than the LpC and SpC during the test;

(b) after 85 000 cycles, the LC and SC stop entering the contact and/or agglomerate at the contact entry, causing oil starvation.

A full consumption of the nanoparticle additives could have occurred during the test, due to a lack of nanoparticles and/or because the oil flow favored the passage of some types of IF-MoS_2 through the contact. As discussed previously, the quantity of nanoparticles in the oil however depends on their size, as does their inertia and, consequently, their reaction to the oil flow. Once inside the contact, the poorly crystalline nanoparticles are more fragile, and more prone to exfoliation for given loads and shear stresses. Their consumption rate may therefore be higher than the more resistant crystalline IF-MoS_2.

Hypothesis (a) could therefore have been relevant if the nanoparticle size had an influence on their durability, and/or if the poorly crystalline nanoparticles had proved less durable. This hypothesis is however not acceptable in the case where large and small poorly crystalline IF-MoS_2 exhibited higher performances than the more crystalline nanoparticles of both sizes.

For the nanoparticles to stop entering the contact and/or to induce oil starvation, they must be drawn away by the oil flow and/or agglomerate at contact entry without being trapped by the surfaces. For a given nanoparticle shape and composition, these phenomena will depend solely on their size. Hypothesis (b) should therefore also be dismissed.

In order to explain the shorter effectiveness of the LC and SC additives, a schematic top view of the HFRR set-up is shown on **Figure 3.11**. The reciprocating motion of the ball (upper specimen) on the flat (lower specimen) is thought to progressively draw the nanoparticles away from the contact, causing it to be starved in nanoparticles as the test goes on. This will slow down tribofilm formation, until it wears off faster than it regenerates. Friction then starts rising as the tribofilm wears off.

Considering that all IF-MoS_2 have the same density, it seems safe to assume that nanoparticles of same size will behave similarly when subjected to the oil flow during the HFRR test. The durability of the poorly crystalline nanoparticles, compared to the more crystalline ones

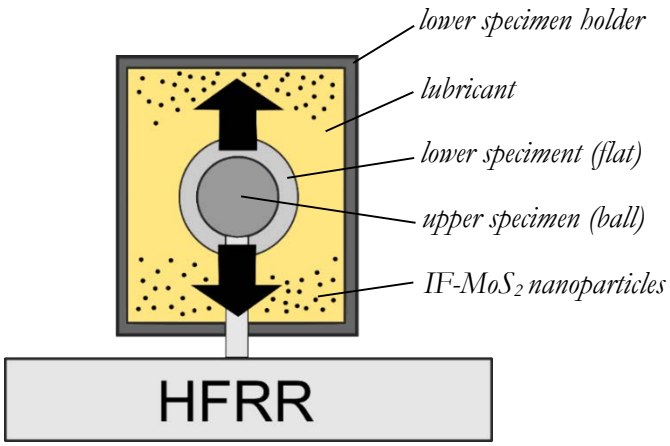

Figure 3.11. Top view of the HFRR set-up

(either large or small), indicates that fewer of these particles are needed to form and maintain the tribofilm on the specimen surface. This is consistent with their bigger ability to exfoliate under the combined efforts of normal pressure and shear reported in the literature [66] and schematized on **Figure 3.12**.

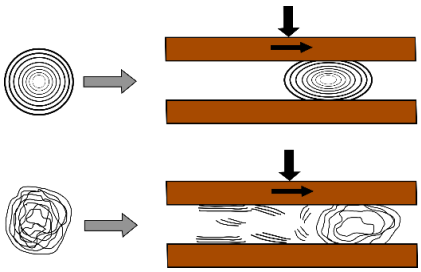

Figure 3.12. Facilitated exfoliation of poorly crystalline IF-MoS_2 under a given load and shear stress

In order to verify the hypothesis of a progressive nanoparticle starvation of the contact, another HFRR test was carried out on the LC sample (PAO + 1wt% LC) but with a higher frequency (20 Hz instead of the 10 Hz used before and reported in **Table 3.3**). The duration of the test was unchanged (4 hours), which lead to a greater number of cycles than previously (288 000 instead of 144 000). As the stroke remained the same, the average velocity of the ball on the disc was doubled, leading to milder contact conditions. Under these new conditions, the theoretical central film thickness h_c was 4.2 nm, leading to a film thickness ratio of approximately 0.07.

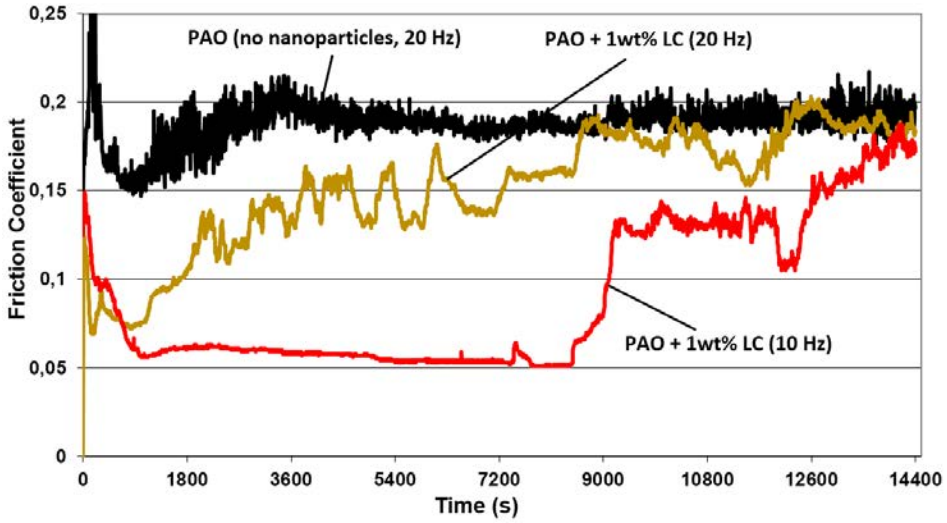

Figure 3.13. Tribological behavior of LC nanoparticles for 2 operating conditions (10 Hz and 20 Hz)

In these conditions, the base oil alone produced a coefficient of friction averaging 0.19, while the addition of 1wt% of LC permitted a minimum coefficient of friction of 0.07 (**Figure 3.13**).

This lower efficiency in terms of friction reduction was predictable as fullerene-like nanoparticles are known to be most efficient for more severe lubrication regimes, their exfoliation (and thus tribofilm formation) being then facilitated [64]. The maximum friction reduction did however not last long, as the coefficient of friction started increasing progressively after only 1100 seconds (22 000 cycles). This result confirms that the nature of the test tends to progressively starve the contact in nanoparticles, phenomenon occurring faster if the frequency of the reciprocating motion is increased. The reducing number of nanoparticles passing through the contact is thought to slow down tribofilm regeneration until it is either worn off or damaged, resulting in an increase in friction. In order to verify this hypothesis, this last HFRR test was repeated and interrupted after 17 minutes (1020 seconds), in order to compare the surface compositions during maximum friction reduction and at the end of the test (**Figure 3.14**).

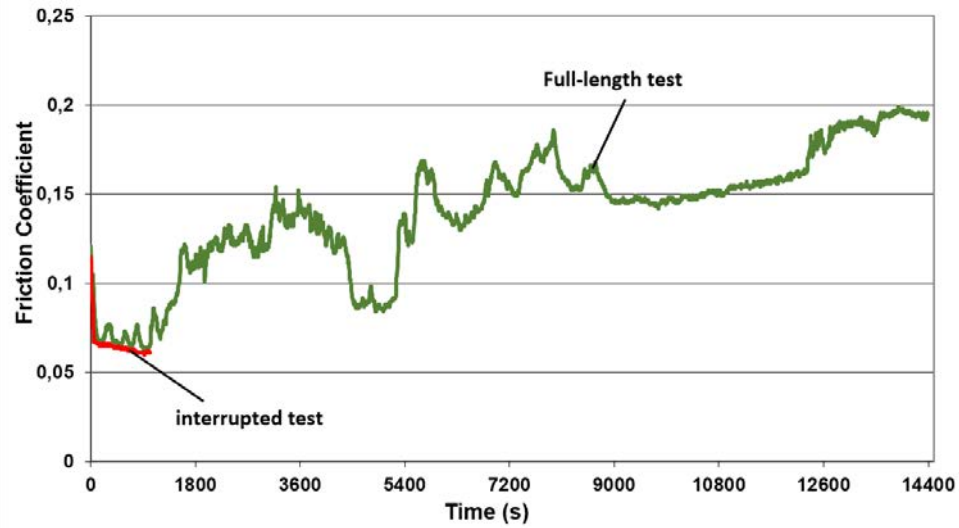

Figure 3.14. Full-length and interrupted test using 1wt% LC IF-MoS_2 in order to compare the surfaces during and after testing

The wear scars corresponding to these two tests are shown on **Figure 3.15**. Most of the wear took place during the second part of the test, which is consistent with the hypothesis of a progressive wearing off or damaging of the tribofilm. The worn volume at the end of the test was approximately three times larger than for the same test carried out at 10 Hz (660.10^3 μm^3 compared to the 211.10^3 μm^3 reported in **Table 3.4**), although the contact conditions were less severe due to a higher average surface velocity. This may be due to the higher number of cycles achieved during the 4 hours of the test but also to the reduced durability of the tribofilm, as the minimum friction coefficient was only maintained during 1 100 seconds at 20 Hz (20 400 cycles out of 288 000) instead of 8 500 seconds at 10 Hz (85 000 cycles out of 144 000).

XPS analyses were carried out on these worn surfaces to confirm that the increase in friction was due to a deterioration of the tribofilm, reinforcing the hypothesis of a progressive starving of the contact in nanoparticles during the test. The results for the molybdenum (Mo 3d) and sulfur (S 2p) energy peaks are shown on **Figure 3.16**. After 17 minutes of testing (top spectra), Mo $3d_{5/2}$ peaks corresponding to Mo – S species appear at 229.8 eV, which was also the energy peak of the MoS_2 found in the nanoparticles (see **Table 3.2**). The corresponding S $2p_{3/2}$ peak was found at 162.0 eV, confirming the presence of a MoS_2 tribofilm on the wear surface. The shifting of this

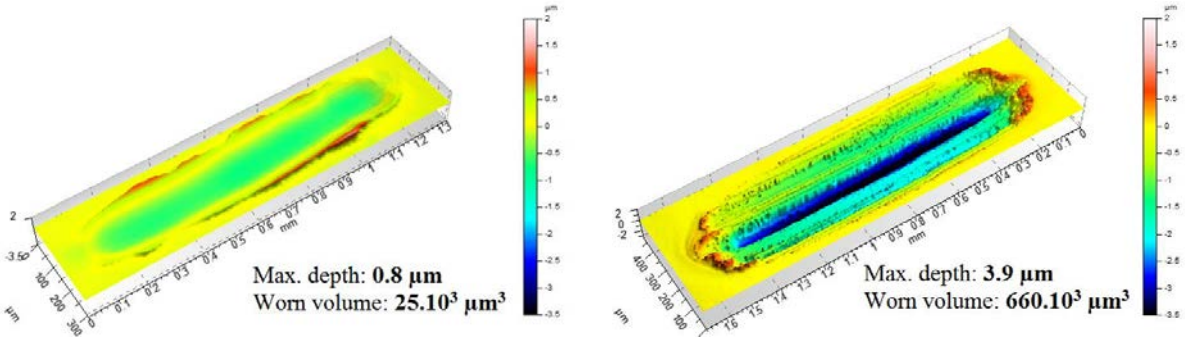

Figure 3.15. Wear scars corresponding to the 20 Hz HFRR test with 1wt% LC IF-MoS_2 after 17 minutes (left) and 4 hours (right)

peak towards the lower energies (from 162.7 eV for the LC IF-MoS_2 to 162.0) may indicate the presence of iron sulfides, and Mo – O species were also found at 232.2 eV. These S – Fe and Mo – O bonds are consistent with the presence of an MoS_2 tribofilm on an Fe substrate [65], as described later in this work (see ***3. 3. 3. Tribofilm analysis***). After the end of the four hour test, the very low intensities made it difficult to distinguish the Mo 3d and S 2p peaks (bottom spectra on **Figure 3.16**). The atomic concentrations of iron compared to molybdenum and sulfur (Fe/(Fe+Mo+S) ratio) increased from 26 at.% after 17 minutes of testing to 68 at.% at the end of test, confirming the deterioration of the MoS_2 tribofilm.

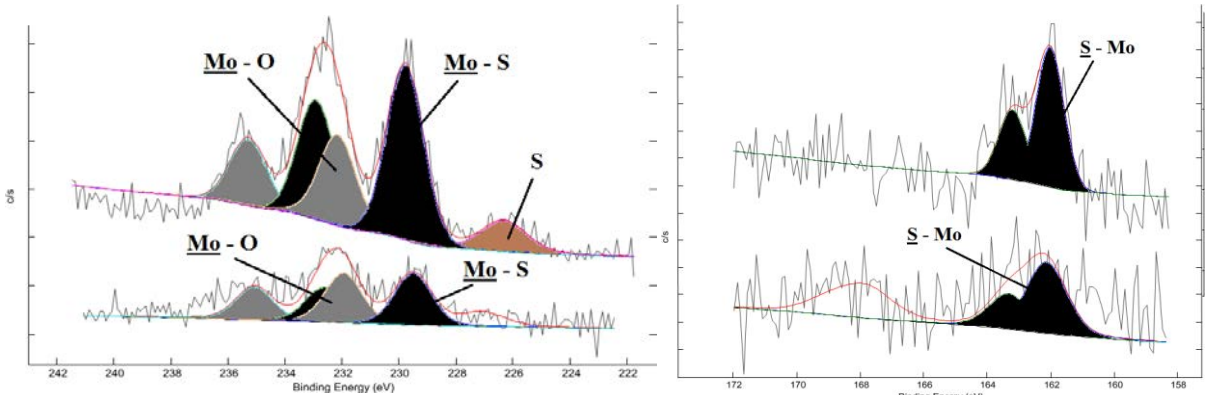

Figure 3.16. XPS analyses of the wear scars after 17 minutes (top spectra) and 4 hours (bottom spectra) of testing - Mo 3d (left) and S 2p (right) energy peaks

These analyses confirm the formation of an MoS_2 tribofilm from the IF-MoS_2 at the beginning of the tribological tests. Due to the reciprocating nature of the HFRR, a progressive starvation of the contact in nanoparticles occurs during the tests, until the tribofilm can no longer regenerate and is progressively damaged, resulting in an increase in friction. The benefit in using less crystalline nanoparticles was then confirmed, as fewer are needed to maintain an effective tribofilm on the friction surfaces.

These tests showed that the efficiency of IF-MoS_2-induced friction reduction depends partly on the nature of the nanoparticle, but also of the oil flow around the contact. An additional test was carried out in order to verify if the performance of the less efficient LC nanoparticles could be enhanced by creating an artificial oil recirculation. This was achieved by stirring manually the oil in the bottom specimen holder of the HFRR with a clean steel rod during the first and third hour of the test. The result is shown on **Figure 3.17**, where the friction coefficients are compared for the stirred and unstirred LC-doped base oil. The manual stirring of the oil affected the measurement of the friction force, but a reference test carried out in the same conditions on the base oil alone

showed that the average friction coefficient remained the same for the stirred and unstirred oil (**Figure 3.18**). During the first hour of the test, stirring the oil continuously stabilized the average friction coefficient to its lowest level, at 0.07. Recirculating the oil ensured a continuous feeding of the contact in nanoparticles, which is thought to have maintained a homogeneous tribofilm on the contact surfaces. When the stirring stopped after 72 000 cycles, the friction coefficient remained stable for approximately half an hour (36 000 cycles) before increasing drastically. This behavior is due to a wearing out of the tribofilm, due to a progressive starvation of the contact in nanoparticles. The maximum friction reduction achieved during this second hour of the test may have lasted longer than for the reference test with no stirring (36 000 cycles instead of approximately 20 000 cycles) because the contact was well fed in IF-MoS_2 for 72 000 cycles during the first hour, which most likely led to the formation of a thicker and more homogeneous tribofilm. The lubricant was stirred again during the third hour of the test, which led to an immediate and significant reduction of the friction coefficient back to its lowest value of 0.07. Friction then remained low throughout the test, including during the fourth hour (cycles 216 000 through 288 000). After 216 000 cycles, the combined two hours of stirring seemingly permitted the formation of a tribofilm thick and homogeneous enough to withstand 72 000 cycles, despite its partial degradation during the second hour of the test.

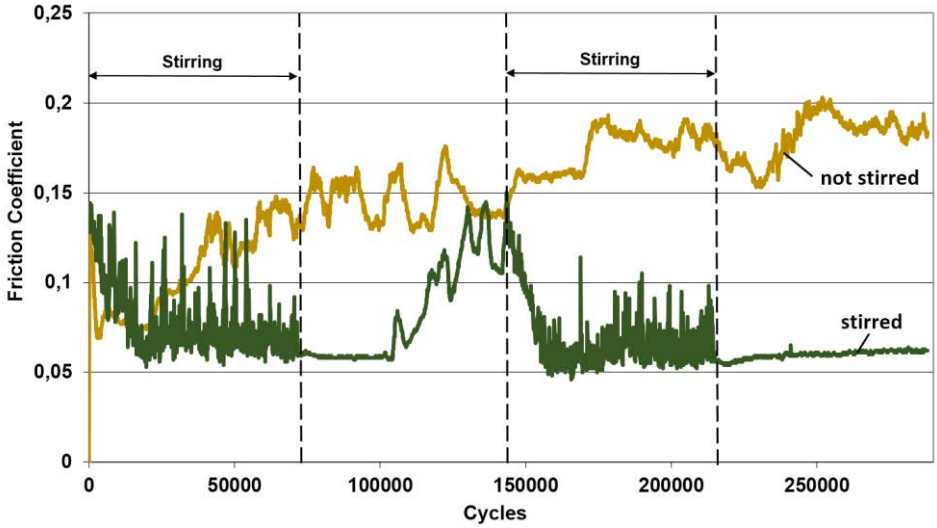

Figure 3.17. Performance of LC-type IF-MoS_2 enhanced by modifying the oil flow around the contact

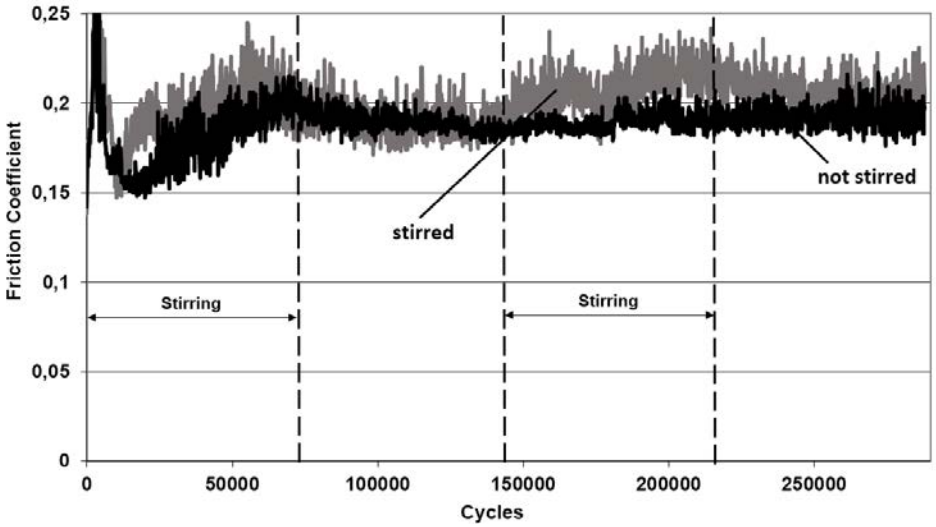

Figure 3.18. Effect of oil stirring on the measurement of the friction coefficient

For the range of MoS_2 nanoparticle studied, these tribological tests show that similar friction coefficients may be obtained regardless of size or crystallinity. In the case where a continuous feeding of the contact in nanoparticles is ensured, for instance through the stirring of the oil, the maximum friction reduction proved stable even for the larger and more crystalline nanoparticles. However IF-MoS_2 containing more structural defects (either large or small) are more efficient, as fewer are needed to create and maintain a friction-reducing tribofilm on the contact surfaces. These less crystalline nanoparticles will therefore prove more beneficial in applications where oil recirculation is not ensured such as alternating contacts in finite volumes of oil, or droplet lubrication prior to testing.

3. 3. 3. Tribofilm analysis

In order to attribute the differences in nanoparticle performance to their size and morphology alone, the wear surfaces were analyzed by XPS and the compositions of the observed tribofilms were compared to the chemical nature of the IF-MoS_2 recorded previously (**Figure 3.4** and **Figure 3.5**).

The molybdenum (Mo 3d) and sulfur (S 2p) spectra for the poorly crystalline nanoparticles are shown on **Figure 3.19** (small IF-MoS_2) and **Figure 3.20** (large IF-MoS_2). At the end of the HFRR tests (**Figure 3.8**), both the Mo $3d_{5/2}$ and the S $2p_{3/2}$ peaks corresponding to MoS_2 (229.8 eV and 162.3 eV for the SpC and 229.9 eV and 162.4 eV for the LpC) can be found on the wear scar, indicating the adhesion of a tribofilm on the wear surfaces. The slight shifting of the S $2p_{3/2}$ peaks towards the lower energies (from 162.7 eV to 162.3 eV) may be due to the presence of iron sulfides. Both surface analyses also revealed peaks corresponding to Mo(VI) and S(VI) species, at 232.7 eV and 169.0 eV in the case of the SpC and 232.5 eV and 168.6 eV for the LpC. These observations are consistent with those made in [65], where two hypotheses are made regarding the adhesion of an MoS_2 tribofilm on a steel substrate. After finding molybdenum and sulfur oxidized species and iron sulfide on a worn surface after IF-MoS_2 testing, the authors evoked the possibilities

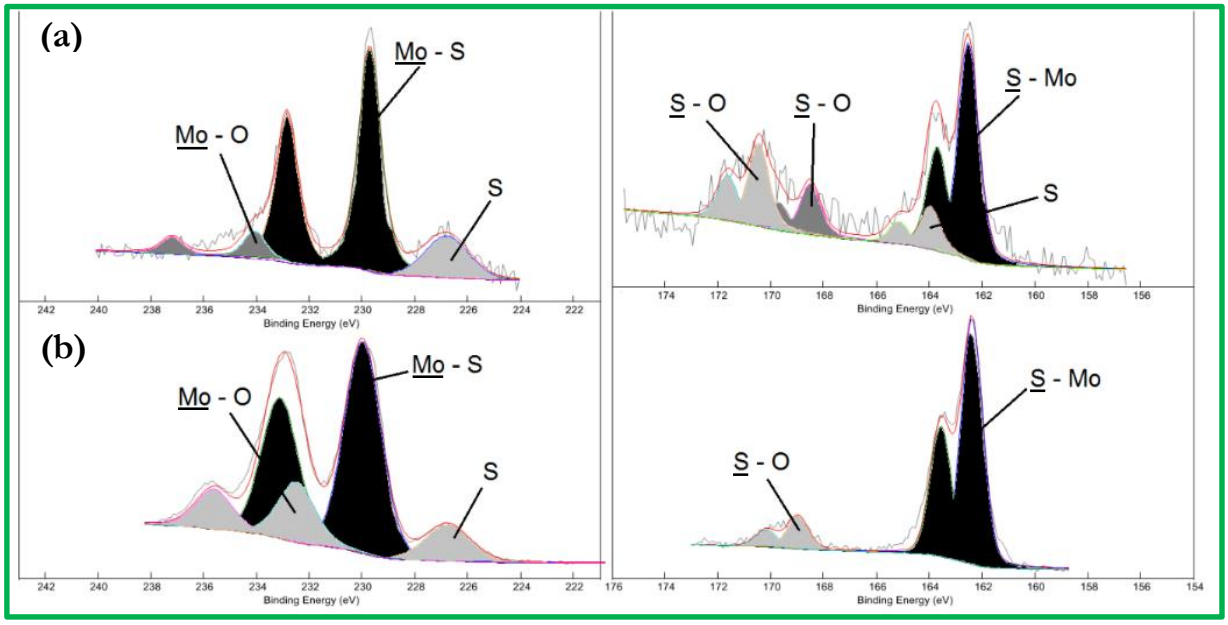

Figure 3.19. XPS spectra of molybdenum (left) and sulfur (right) for the SpC IF-MoS_2 (a) Powder and (b) Tribofilm after 144 000 cycles

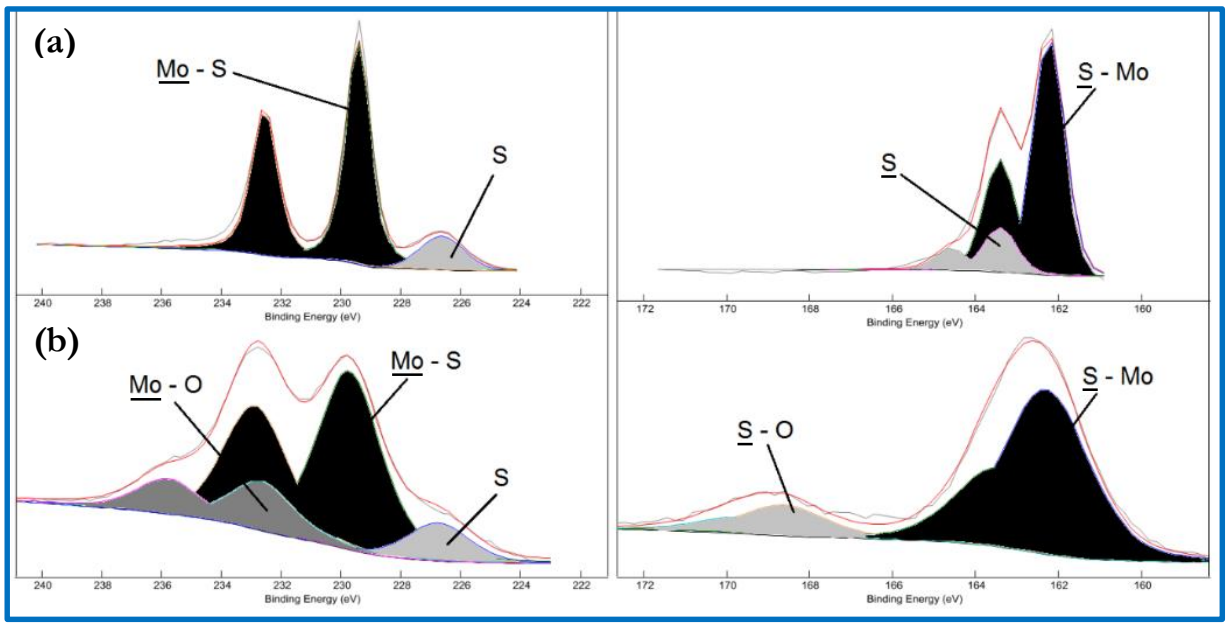

Figure 3.20. XPS spectra of molybdenum (left) and sulfur (right) for the LpC IF-MoS_2 (a) Powder and (b) Tribofilm after 144 000 cycles

of either (a) a tribofilm adhesion through the bonding of molybdenum and sulfur with the oxygen found in the native surface oxide layer of the steel, or (b) a quasi-immediate wearing off of the oxide layer at the beginning of the test, followed by S – Fe interactions and an oxidization of the tribofilm after its adhesion. A quantification of Fe, Mo and S on the surface revealed an atomic ratio (Fe) / (Fe + Mo + S) of 15% and 17% for the SpC and LpC nanoparticles respectively, confirming the possible presence of small amounts of iron sulfides in the tribofilm. In the case of the poorly crystalline LpC and SpC IF-MoS_2, the low friction at the end of the tribological tests suggests that the tribofilms found on the wear scar surfaces remain relatively thick and homogeneous, which is consistent with the high concentrations of molybdenum and sulfur (when compared to iron) found on the surface.

The molybdenum (Mo 3d) and sulfur (S 2p) spectra for the more crystalline SC and LC nanoparticles are shown on **Figure 3.21** and **Figure 3.22** respectively. The analysis carried out on the wear scars after HFRR testing revealed low intensities for the molybdenum and sulfur energy peaks. The atomic ratio (Fe) / (Fe + Mo + S) for these analyses were 44% (SC) and 35% (LC), which confirms that a smaller amount of MoS_2 was found on the worn surface. This is consistent with the results shown on **Figure 3.8**, where the friction coefficient for these more crystalline nanoparticles had increased drastically before the end of the test. The composition of the tribofilm was however similar to those formed when using the poorly crystalline nanoparticles, with the main Mo $3d_{5/2}$ and S $2p_{3/2}$ energy peaks corresponding to the Mo – S species found at 229.5 eV and 161.8 eV for the SC IF-MoS_2 (**Figure 3.21(b)**) and 229.5 eV and 162.1 eV for the LC IF-MoS_2 (**Figure 3.22(b)**). The Mo – O and S – O species observed previously were visible again, with energy peaks found at 232.1 eV and 166.8 eV (small IF-MoS_2, **Figure 3.21(b)**) on one hand, and 231.9 eV and 167.7 eV (large IF-MoS_2, **Figure 3.22(b)**) on the other.

A more important shifting of the main sulfur energy peaks towards the lower bonding energies (from 162.8 eV to 161.8 eV for the SC IF-MoS_2 and from 162.7 eV to 162.1 eV for the LC IF-MoS_2) was observed for these more crystalline nanoparticles. The higher concentration of iron found on these surfaces may therefore be due to higher quantities of iron sulfides in the tribofilm,

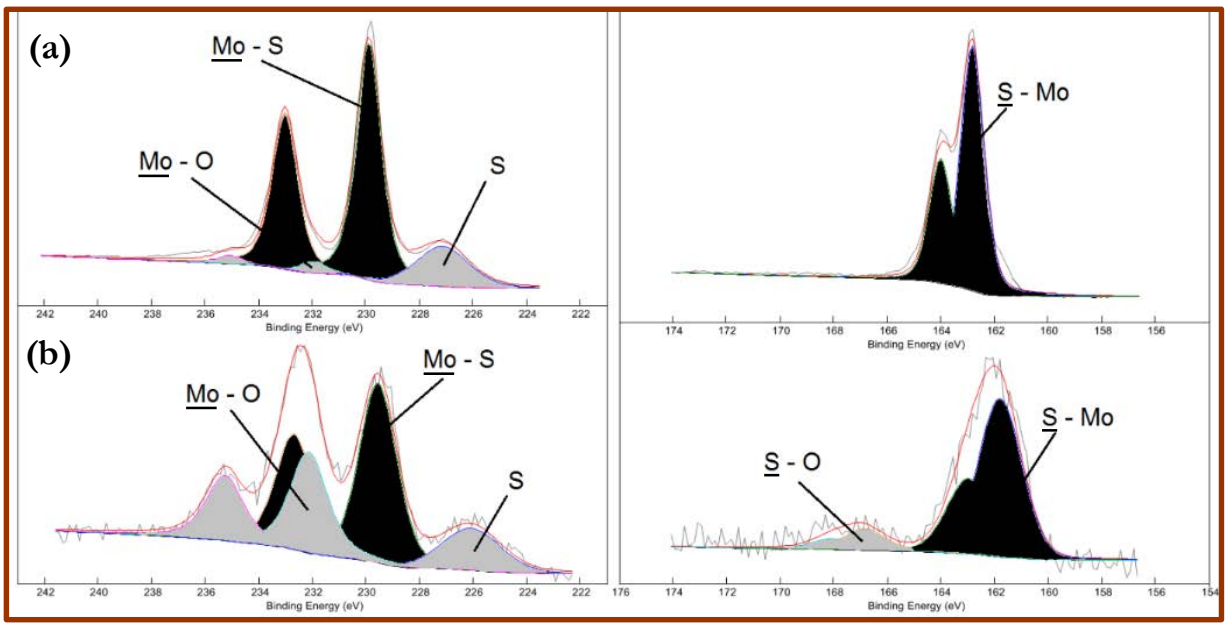

Figure 3.21. XPS spectra of molybdenum (left) and sulfur (right) for the SC IF-MoS_2
(a) Powder and (b) Tribofilm after 144 000 cycles

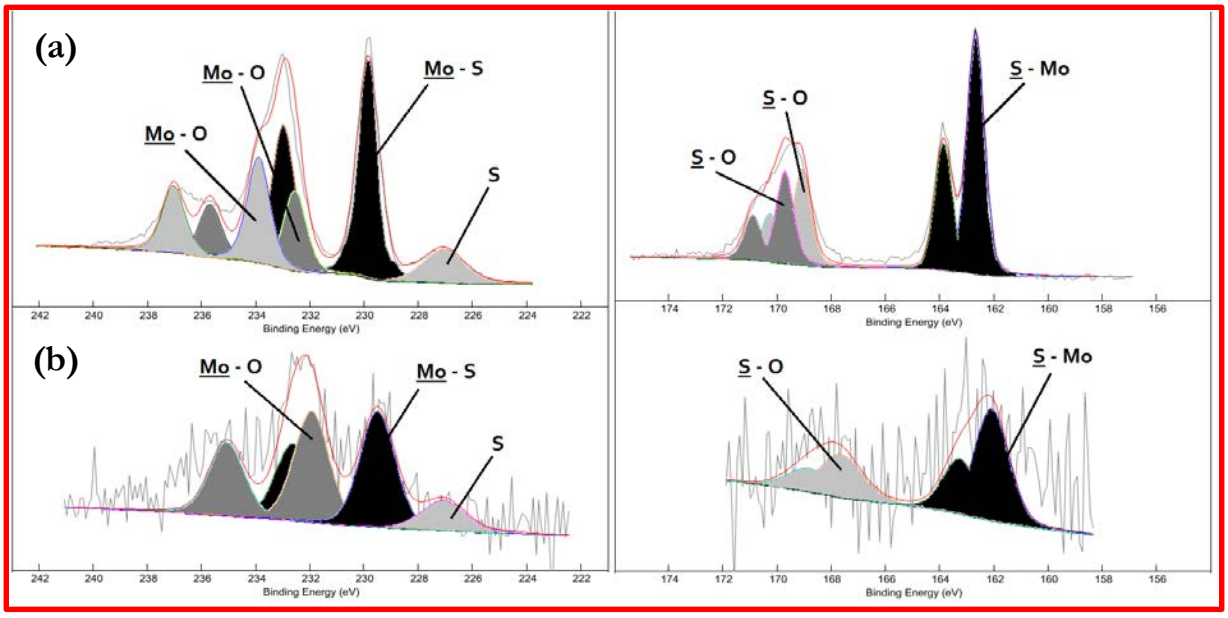

Figure 3.22. XPS spectra of molybdenum (left) and sulfur (right) for the LC IF-MoS_2
(a) Powder and (b) Tribofilm after 144 000 cycles

altering its lubricating properties. As more wear took place during the testing of the SC and LC IF-MoS_2, these Fe – S species may be due to the embedding of wear particles in the tribofilm [81], as schematized on **Figure 3.23(a)** (the tribofilm was only drawn on the flat surface for the sake of clarity, but is in reality present on both steel surfaces). These iron sulfides could also have been formed from the interactions between the sulfur contained in the exfoliated MoS_2 sheets and the Fe atoms of the substrate, enabling the adhesion of the tribofilm. A progressive wearing off of the tribofilm during the HFRR tests would explain why more iron sulfide can be observed for the SC and LC nanoparticles (**Figure 3.23(b)**). In this scenario, the fact that iron sulfide was only found at the surface when part of the tribofilm has been worn off would suggest that it may be – at least partly – responsible for the adhesion of the MoS_2 tribofilm on the steel substrate. It would then remain to be determined whether the Mo – O and S – O bonding by the oxidized species is essential

to the adhesion of the tribofilm, or if the oxidization of the MoS_2 tribofilm occurs after its adhesion to the surface. This adhesion does not seem to depend on the initial oxidation level of the IF-MoS_2 nanoparticles, as similar tribofilms were formed after using either small, oxidized, poorly crystalline IF-MoS_2; small, poorly oxidized, crystalline IF-MoS_2; large, poorly oxidized, poorly crystalline IF-MoS_2; or large, oxidized, crystalline IF-MoS_2.

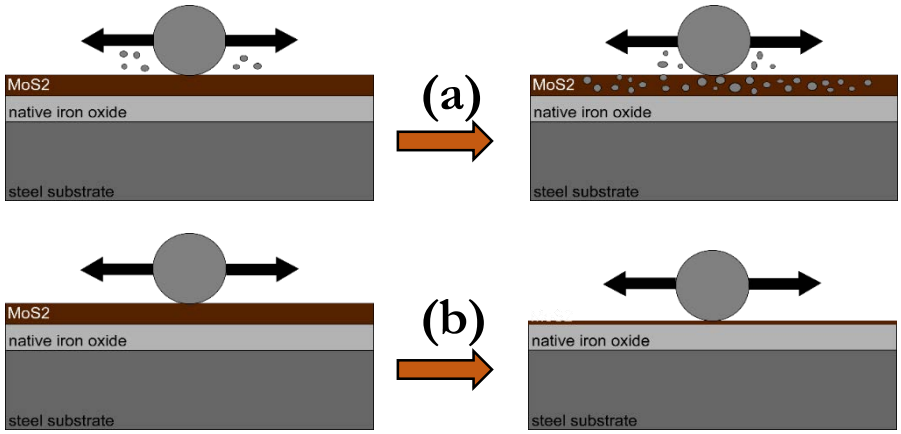

Figure 3.23. Possible scenarios for the loss of tribological performance of the more crystalline IF-MoS_2 and the presence of higher quantities of iron sulfides at the surface of the corresponding wear scars

In order to investigate the degradation of the tribofilm leading to the increase in friction observed at the end of the HFRR tests in the case of the more crystalline nanoparticles (see **Figure 3.8**), cross-sections were extracted from the wear scars (**Figure 3.9**) resulting from the testing of the SpC and LC IF-MoS_2. The cross-sections were taken from the center of the wear scars using the Focused Ion Beam (FIB) technique (**Figure 3.24**). The resulting lamellas showed a 10 µm wide area of the extreme surface of the scars.

TEM images of the cross-section of the wear scar obtained for the more efficient SpC nanoparticles are shown on **Figure 3.25**. The lamella was covered with a thin platinum layer and a thicker tungsten carbide layer to protect the surface (WC and Pt layers shown on **Figure 3.25**(a)). The tribofilm was found to cover the whole surface of the cross-section, with a thickness varying between 30 and 100 nm. The extreme surface of the tribofilm exhibited large layers of MoS_2 platelets, arranged parallel to the surface (**Figure 3.25**(d)). These layers were significantly larger than the MoS_2 platelets found in the nanoparticle structure (**Figure 3.3**(b)), implying that the MoS_2 liberated during the exfoliation of the nanoparticles was rearranged due to the shear in the contact

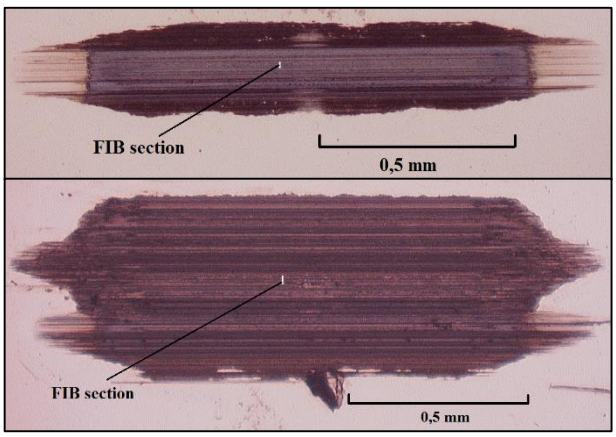

Figure 3.24. Positioning of the FIB cross-sections for the SpC (top) and LC (bottom) IF-MoS_2 wear scars (sections not to scale)

to form these parallel layers. This rearrangement explains the good friction reducing properties of the MoS_2 tribofilm, as the friction between the two original steel counterparts evolves into friction between parallel MoS_2 layers, which exhibit low resistance to shear [26]. Some layers of MoS_2 however seem to have been trapped in the tribofilm without having suffered modifications after their exfoliation from their nanoparticles, as pointed out on **Figure 3.25**(c). These unscathed layers were always found at some distance from the extreme surface. This observation implies that the shear occurring in the contact is responsible for orienting the layers parallel to the surface.

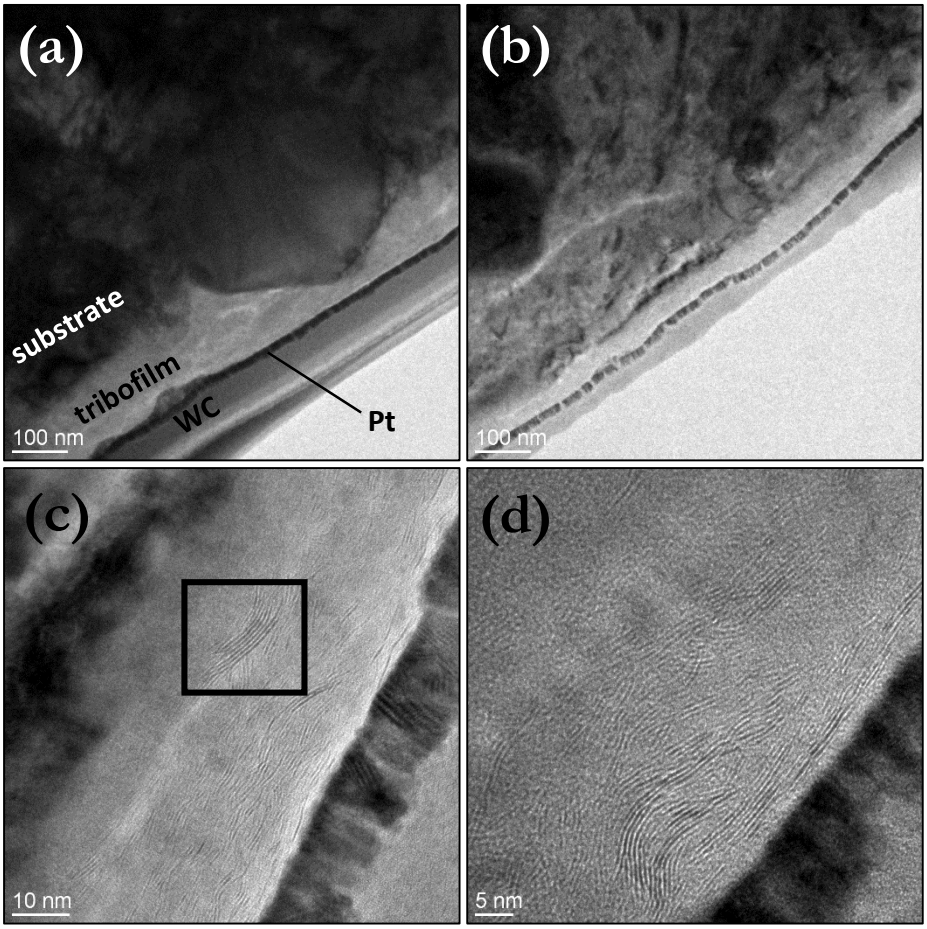

Figure 3.25. FIB cross-section of the wear scar at the end of the HFRR test for the PAO+1% SpC IF-MoS_2 blend

At high magnifications, the tribofilm was often found to be composed of two layers. The top layer, nearest to the surface, appeared close to white on the TEM images and consisted of what resembled parallel MoS_2 platelets. Between this top layer and the substrate was a darker intermediate layer, which did not contain any platelets. Energy-dispersive X-ray spectroscopy (EDX) was carried out on the FIB cross-section to obtain the elemental composition of the tribofilm. The numbers on **Figure 3.26**(a) and **Figure 3.26**(b) indicate the location of the different analyses, and the relative atomic concentrations of molybdenum, sulfur, oxygen and iron are reported on the adjacent graph for each analysis.

Locations 1 and 7 of **Figure 3.26**(a) as well as 1 and 2 of **Figure 3.26**(b) were chosen inside the top layer. The corresponding analyses revealed high contents of molybdenum, sulfur and oxygen and fairly low amounts of iron. This composition is consistent with the XPS analysis showed on **Figure 3.19**, and confirms that the top layer of the tribofilm consists of MoS_2 platelets as well as M – O and S – O species.

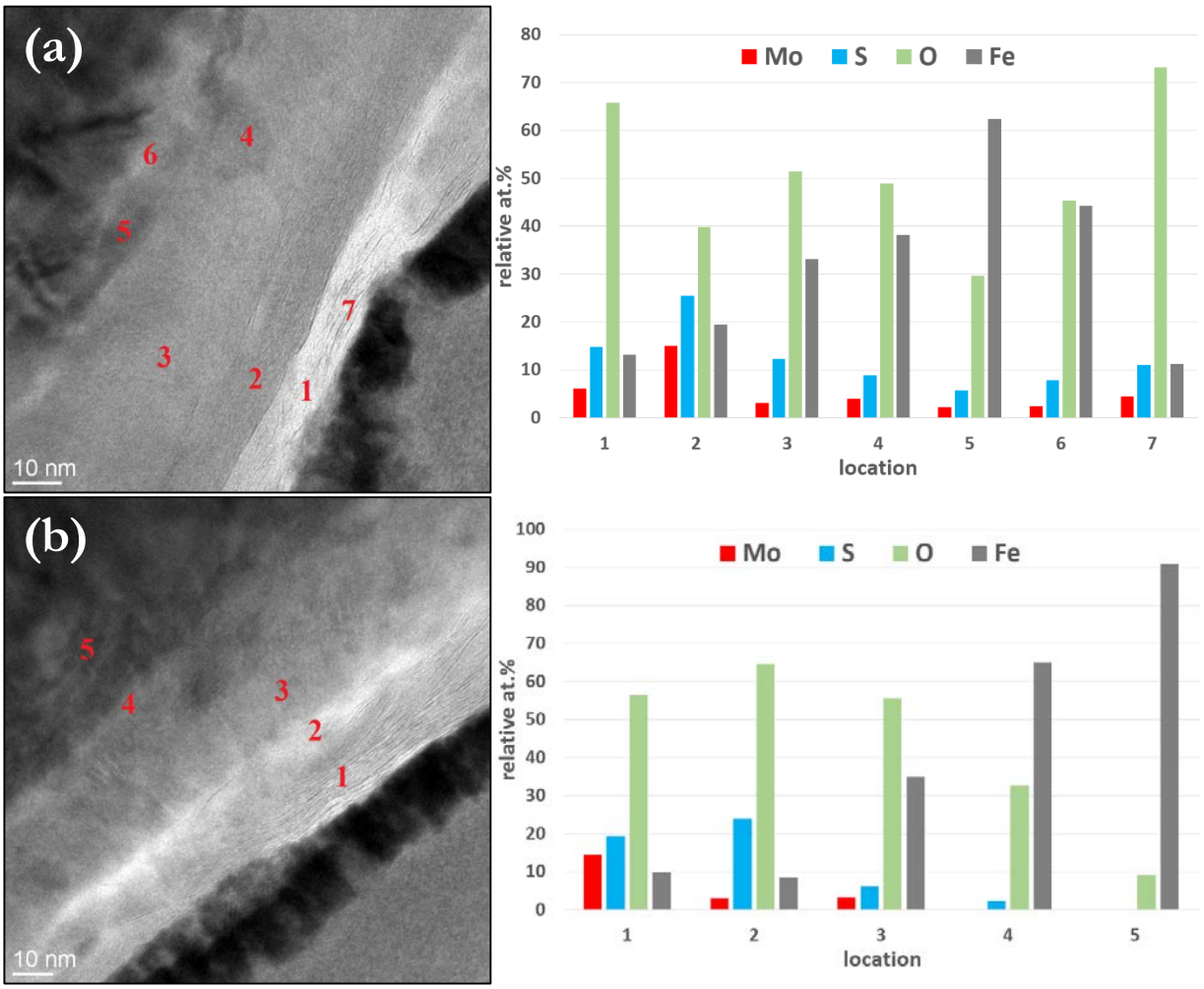

Figure 3.26. EDX analyses at different locations of the wear surface for the SpC IF-MoS_2

The intermediate layer described previously was also analyzed (locations 2 to 6 on **Figure 3.26**(a) and 3-4 on **Figure 3.26**(b)), and revealed much higher concentrations of iron, although molybdenum and sulfur were still found in small quantities. This layer may therefore still contain MoS_2, but is most likely composed of iron oxides and possibly iron sulfides. Its presence may result from the modification of the native iron oxide layer by the bonding of the MoS_2 (through S – Fe and Mo – O species, as suggested in [65]). The native iron oxide layer could also have been partly worn off during the first cycles of the friction test, and this intermediate layer could then result from a bonding of the sulfur found in the MoS_2 platelets with the iron of the substrate. The presence of large quantities of oxygen would then result from the oxidation of the tribofilm during its formation. The composition found at location 4 on **Figure 3.26**(b), which was in the intermediate layer but close to the steel substrate, could reinforce this hypothesis. Sulfur was indeed detected but not molybdenum, possibly indicating the presence of iron sulfides which could have enabled the adhesion of the tribofilm. The low amount of sulfur found could however also indicate that molybdenum was also present, but in quantities too low to be detected by the EDX analysis.

The FIB cross-section of the wear scar for the more crystalline LC nanoparticles revealed a totally different morphology of the surface. Images of the lamella are shown on **Figure 3.27**, on which the protective platinum layer was indicated to locate the extreme surface. Large portions of the cross-section were not at all covered by a tribofilm, leaving the bare substrate reach the surface. Other parts of the lamella, on the other hand, contained large areas resembling the intermediate

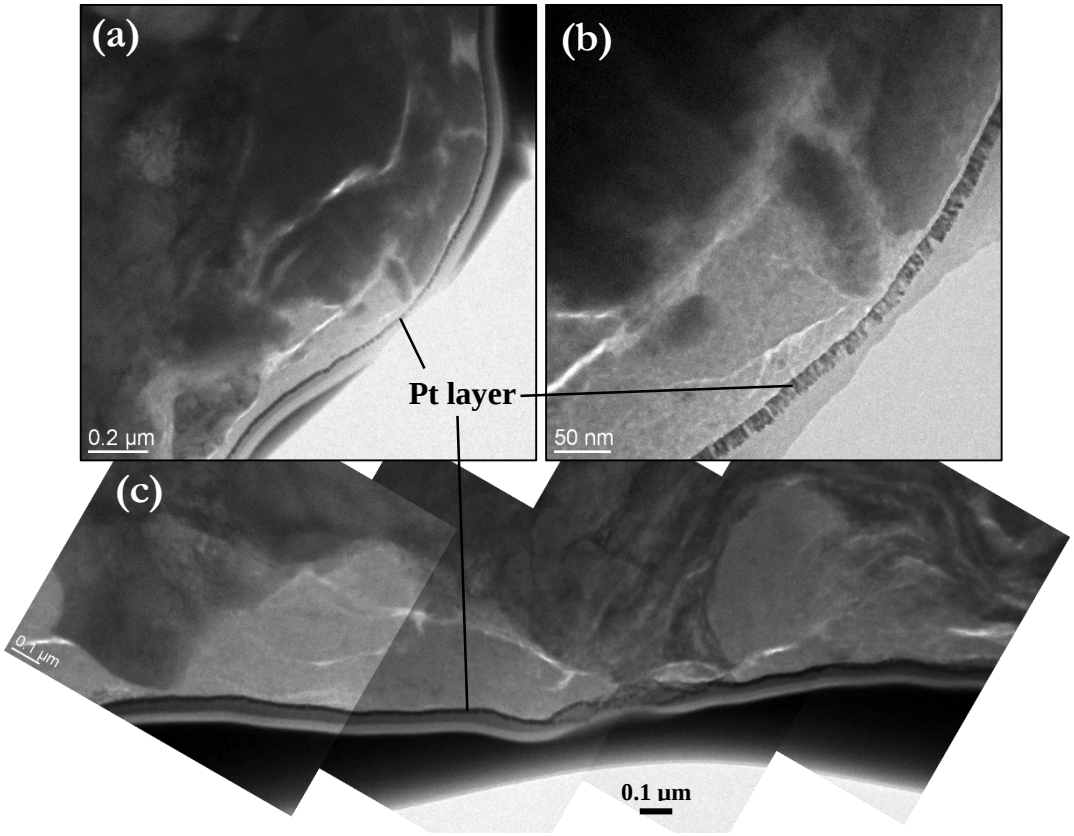

Figure 3.27. FIB cross-section of the wear scar at the end of the HFRR test for the PAO+1% LC IF-MoS2 blend

layer of the tribofilm observed previously (**Figure 3.26**). These areas were unevenly distributed and of different sizes. **Figure 3.27**(a) and (b) show a film with a thickness varying between 50 and 100 nm, whereas **Figure 3.27**(c) reveals seemingly identical areas reaching depths up to 1 µm. No MoS_2 platelets (such as the ones shown on **Figure 3.25**(d)) were found throughout the entire cross-section.

This film was furthermore sometimes found to be trapped inside the substrate, such as shown on **Figure 3.28**. Several EDX analyses were carried on this image in order to verify the composition of the different areas. The darker areas (locations 1, 3 and 5) consisted mostly of steel, with very high contents of iron. Traces of molybdenum (location 1) and sulfur (locations 1 and 3) were also

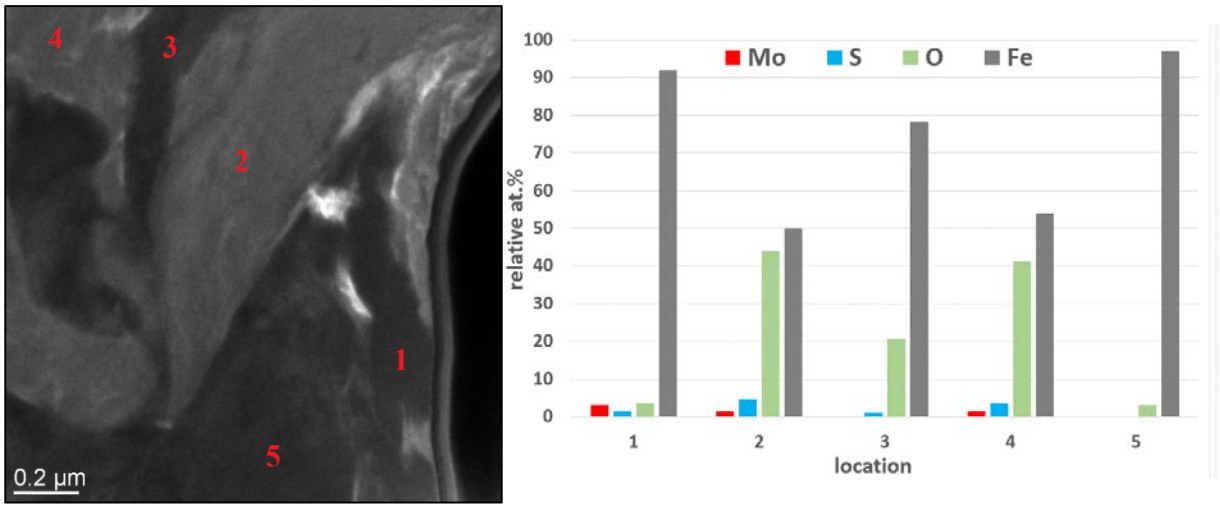

Figure 3.28. EDX analyses at different locations of the wear surface for the LC IF-MoS2

found, attesting of a reaction with the MoS_2 from the nanoparticles. Locations 2 and 4 were chosen inside the lighter areas, which appeared to be mostly iron oxides. Low contents of molybdenum and sulfur were also found, with a stoichiometry close to MoS_2. This composition was similar to the ones found on locations 5 and 6 on **Figure 3.26**(a), which were at the limit between the intermediate layer of the tribofilm and the substrate.

To confirm that molybdenum and sulfur were found below the surface of the wear scar, several EDX maps tracing Mo, S, Fe, Cr, O and Pt were carried out on the FIB cross-section (**Figure 3.29**). The edge of the sample is made visible by the platinum layer, whereas steel can be recognized by the high concentrations in iron and localized chromium. These images clearly reveal areas containing large amounts of molybdenum, sulfur and oxygen trapped inside the steel substrate.

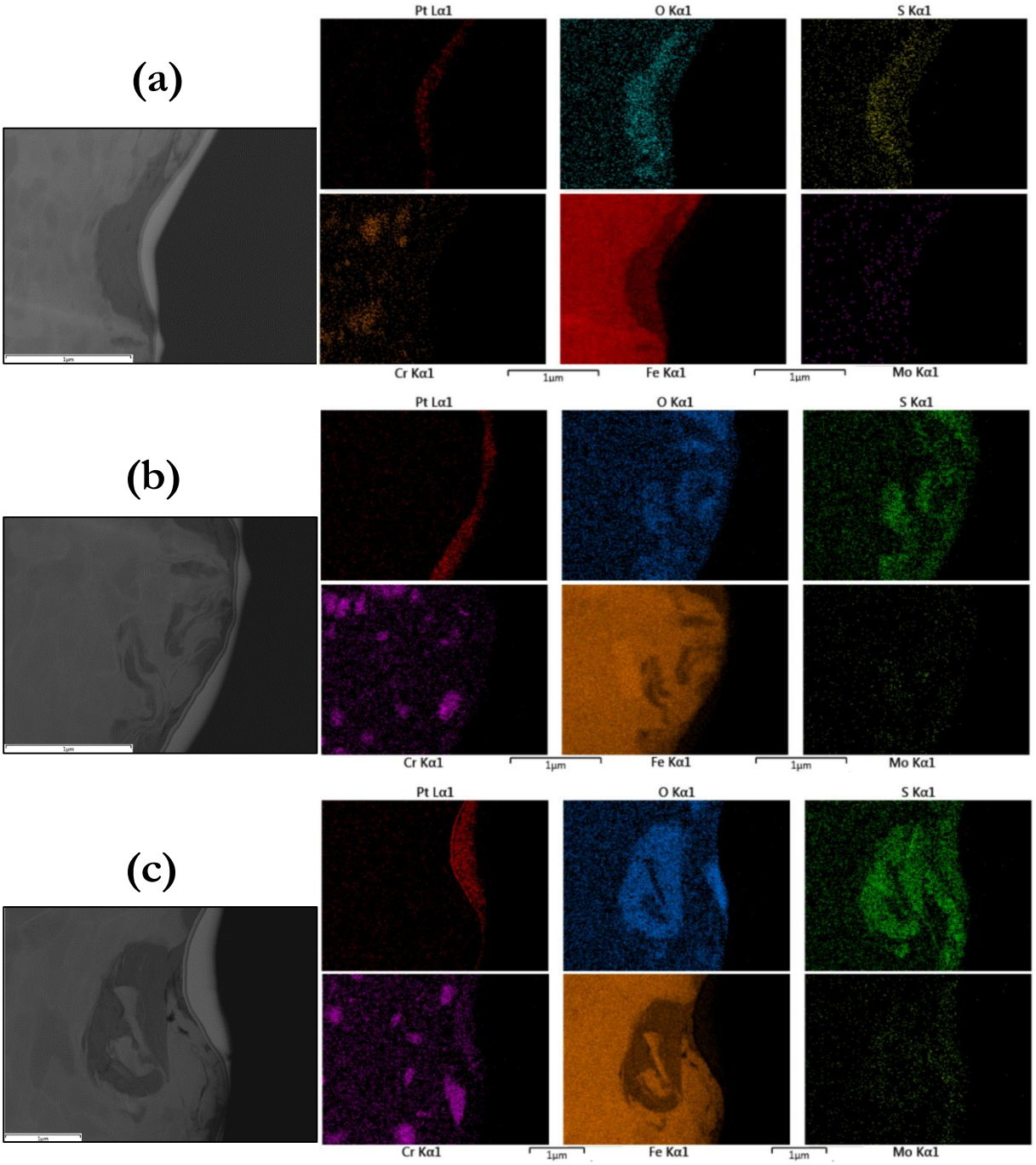

Figure 3.29. EDX maps of the main elements present on the FIB cross-section of the wear scar for the LC IF-MoS_2

The absence of a tribofilm on large portions of the extreme surface, as well as the change in composition of the tribofilm in the remaining areas (with the absence of MoS_2 platelets) explains the much higher friction coefficient recorded at the end of the HFRR test for the LC IF-MoS_2 compared to the SpC nanoparticles. These TEM observations also provide indications regarding the evolution of the tribofilm in the case of the more crystalline nanoparticles. The surface was indeed likely to resemble the one observed for the SpC IF-MoS_2 during the beginning of the test, when maximum friction reduction was achieved (cycles 10 000 to 90 000 on **Figure 3.8**). The sufficient amount of LC nanoparticles then entering the contact ensured the formation of an efficient MoS_2 tribofilm, with MoS_2 layers aligned parallel to the surface providing great friction and wear reduction. The progressive starvation of the contact in IF-MoS_2, combined to the lower exfoliating capacities of the more crystalline nanoparticles, then led to fewer MoS_2 platelets reaching the contact surfaces. As the regeneration of the tribofilm was slowed down, the continued rubbing of the surfaces most likely caused a progressive wear of the top layer of the tribofilm (locations 1 and 7 on **Figure 3.26**(a)), as previously proposed on **Figure 3.23**(b). As the tribofilm formed was not homogeneous and of equal initial thickness throughout the surface, this wearing off led to steel-steel contacts in some places while others were still covered by a tribofilm with a composition similar to that of the intermediate layer observed on **Figure 3.26**(a) (locations 2 – 6). The increasing number of steel-steel contacts would then lead to a progressive rise in friction and wear as adhesion (through localized micro-welding) would be likely to take place. This could in turn lead to the covering of the remaining tribofilm by steel through the smearing of the surface, which would explain why traces of sulfur and molybdenum were found as deep as 1 µm beneath the extreme surface at the end of the test with the LC nanoparticles.

3. 3. 4. Tribological properties of commercial h-MoS_2 microparticles

The results shown in this chapter so far indicate that the main parameter governing the efficiency of IF-MoS_2 nanoparticles is their crystallinity, regardless of size. The IF-MoS_2 generating the most friction reduction were the SpC and LpC nanoparticles, which did not have a "fullerene-like" aspect due to their many structural defects. In the light of these results, the use of perfectly engineered fullerene-like nanoparticles seems questionable. A recent study by Kogovsek et al [82]

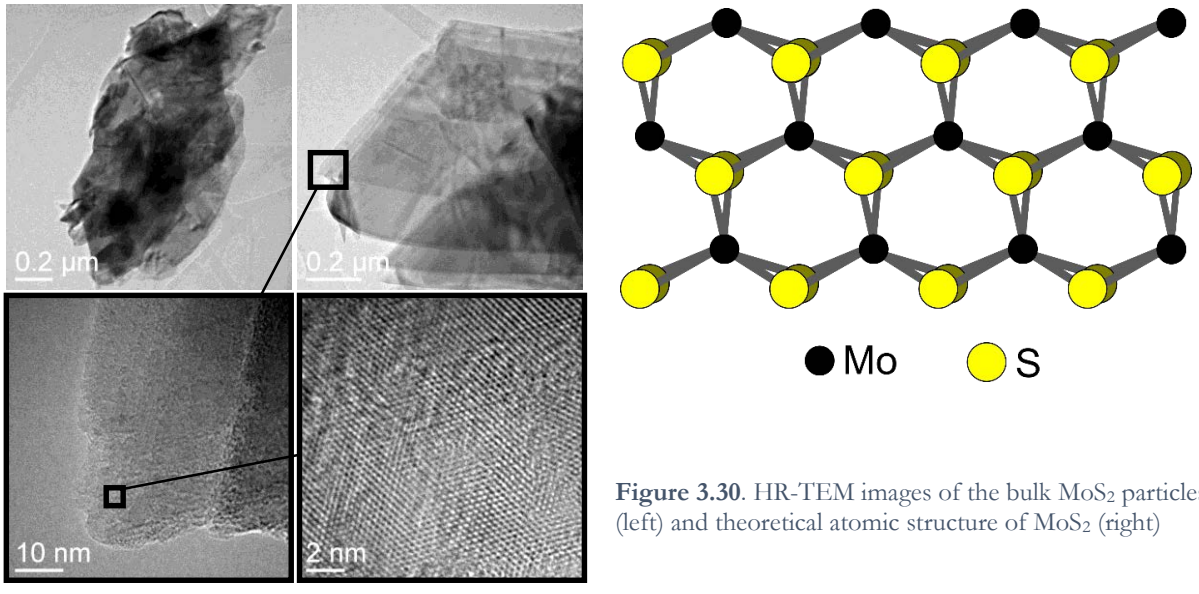

Figure 3.30. HR-TEM images of the bulk MoS_2 particles (left) and theoretical atomic structure of MoS_2 (right)

furthermore suggests that the chemical nature of the additives affects friction reduction much more significantly than their size or shape, as similar tribological test results were obtained for many different kinds of MoS_2 micro- and nanoparticles (nanotubes, 2µm platelets and 10µm platelets). To check these hypotheses, the tribological performances of bulk MoS_2 particles were compared to those of the poorly crystalline IF-MoS_2 tested before. These particles consisted in micrometric assemblies of MoS_2 platelets (**Figure 3.30**). XPS analysis was carried out on the MoS_2 powder (**Figure 3.31**), revealing their purity. The Mo $3d_{5/2}$ energy peak was found at 229.8 eV and the S $2p_{3/2}$ and S 2s peaks at 162.5 eV and 227.2 eV respectively, which attests of a composition similar to the IF-MoS_2 nanoparticles. The h-MoS_2 was added to the PAO base oil tested previously, with a weight concentration of 1%. The operating conditions used were the same as those described in **Table 3.3**.

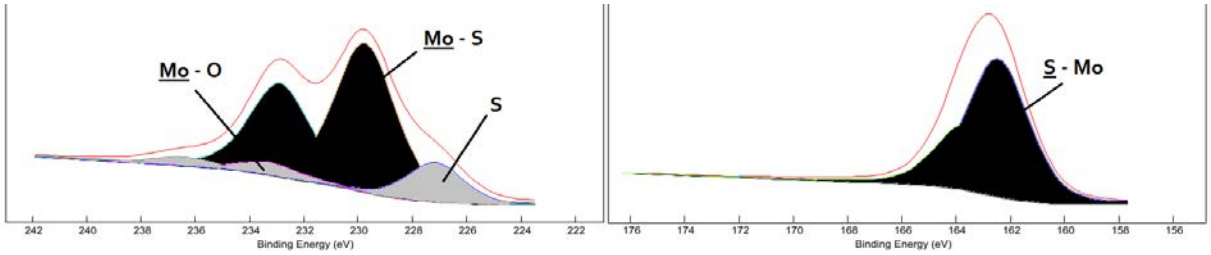

Figure 3.31. XPS spectra of molybdenum (right) and sulfur (left) of the bulk MoS2 particles

The h-MoS_2 proved much less effective than the IF-MoS_2 nanoparticles in boundary lubrication, with a minimum coefficient of friction achieved of 0.09 instead of 0.06 (**Figure 3.32**). These particles were also less efficient in time, as the maximum friction reduction only lasted for a few cycles before friction started increasing back to the value achieved with the base oil alone. The IF-MoS_2 were also more effective in reducing wear, as the corresponding wear scars were significantly smaller than the one obtained when using the h-MoS_2 (**Figure 3.33**).

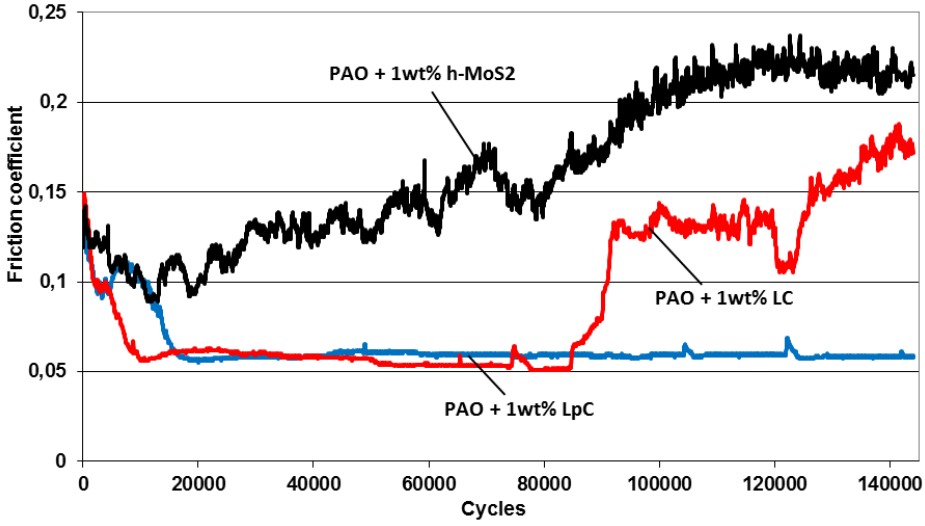

Figure 3.32. Comparison of the friction reducing properties of h-MoS_2 particles and IF-MoS_2 nanoparticles

In order to attribute this behavior to the size and structure of the MoS_2 particles alone, XPS analyses were carried out on the wear surfaces at the end of the test and at the moment of maximum friction reduction. To achieve this, the test with the PAO + 1wt.% h-MoS_2 blend was repeated and interrupted after 18 000 cycles (**Figure 3.34**).

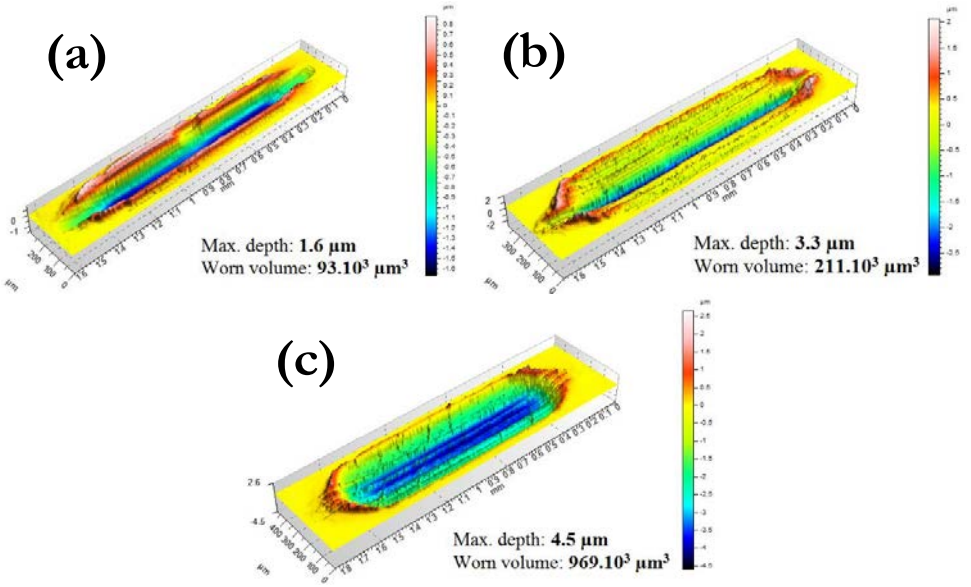

Figure 3.33. Wear scars after the HFRR testing of (a) LpC IF-MoS_2, (b) LC IF-MoS_2 and (c) h-MoS_2

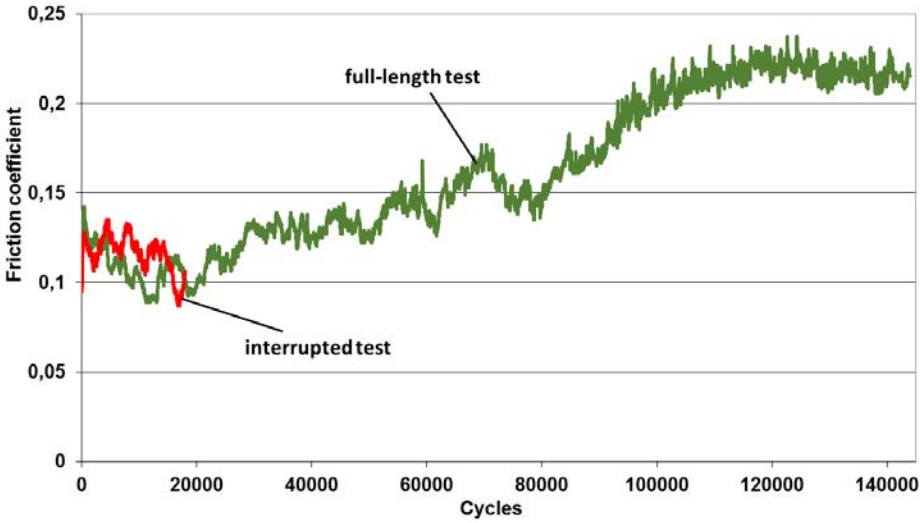

Figure 3.34. Full-length and interrupted test using 1wt% h-MoS_2 particles in order to compare the surfaces during and after testing

The analyses carried out on the wear scars at the end of both tests reported on the figure above are shown on **Figure 3.35**. An MoS_2 tribofilm was found on the surface after 18 000 cycles (top spectra), with Mo $3d_{5/2}$ and S $2p_{3/2}$ peaks corresponding to Mo - S found at respectively 229.7 eV and 161.9 eV. Mo – O species were also found, with another Mo $3d_{5/2}$ energy peak appearing at 232.8 eV. This surface composition is very similar to those obtained when using IF-MoS_2 nanoparticles (**Figure 3.19** to **Figure 3.22**). The shifting of the S $2p_{3/2}$ peak towards the lower energies (from 162.5 eV for the h-MoS_2 powder to 161.9 eV for the tribofilm) may indicate the presence of significant quantities of iron sulfides. The relative concentration of iron compared to molybdenum and sulfur (Fe/(Fe+Mo+S) ratio) was 45 at.%, which is much higher than the 16 at.% measured on average at the end of the tests carried out using the SpC and LpC IF-MoS_2. These two observations are consistent with the higher friction coefficient resulting from the use of h-MoS_2 particles, which do not appear to form a tribofilm as thick and/or homogeneous as the IF-MoS_2 in these conditions.

At the end of the 4h test (144 000 cycles achieved on **Figure 3.34**), the Mo $3d_{5/2}$ and S $2p_{3/2}$ peaks previously measured were barely – or not – distinguishable (bottom spectra on **Figure 3.35**). The relative concentration of iron compared to molybdenum and sulfur had then increased to 82 at.%, confirming that very low quantities of Mo and S remained on the surface.

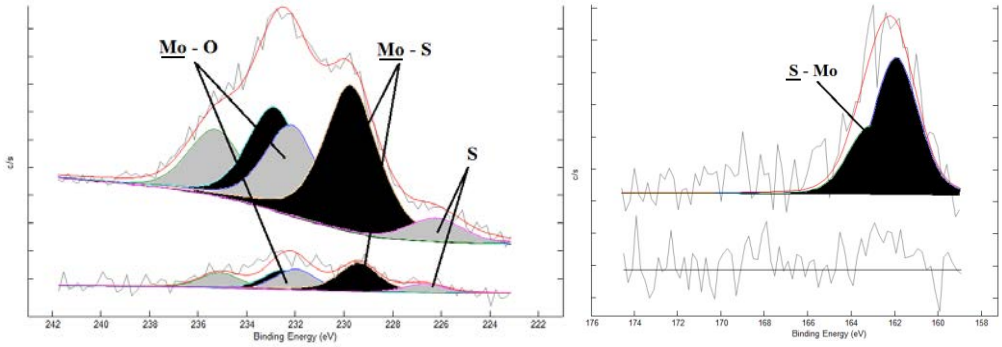

Figure 3.35. XPS analyses of the wear scars after 18 000 (top spectra) and 144 000 (bottom spectra) cycles of testing - Mo 3d (left) and S 2p (right) energy peaks

This final test on h-MoS_2 (micro-) particles confirmed the benefits in using nano-sized nanoparticles for reducing friction and wear in severe boundary lubrication regimes. For equal weight concentrations, the availability of these bigger micro-particles in and near the contact is thought to be too low to ensure permanent tribofilm regeneration. Nanoparticles may also pass through the contact more easily because of their reduced size. For similar contact conditions, this results in the formation of thinner and/or more heterogeneous tribofilms and therefore to higher friction and wear. These tribofilms are furthermore likely to be worn off the contact surfaces prematurely, leading to less durable performances. For real-life applications, the use of IF-MoS_2 nanoparticles over MoS_2 microparticles is thought to hold many more advantages: their low mass and small size should facilitate their dispersion in the oil media and reduce the risks related to clogging, and their spherical and closed structure are more likely to reduce chemical interactions with other additives or surfaces outside the contact area.

3. 4. Conclusions

Four types of IF-MoS_2 of different sizes and morphologies were tested in severe conditions under pure sliding (boundary lubrication regime, splash lubrication with 2 mL of oil and high number of cycles). All IF-MoS_2 proved very effective in reducing friction and wear, with the most efficient nanoparticles maintaining maximum friction reduction (from 0.20 to 0.06) for more than 140 000 cycles.

In the conditions studied, nanoparticle size and morphology did not impact the minimum friction coefficient reached. The presence of structural defects in the nanoparticles did however affect their effectiveness in time, as the poorly crystalline IF-MoS_2 (not "fullerene-like") maintained minimum friction over a significantly higher number of cycles, regardless of their size. The facilitated exfoliation of these nanoparticles under the combined actions of normal pressure and shear is thought to facilitate tribofilm formation and regeneration when a fewer number of nanoparticles is available in the contact.

The efficiency of the more crystalline fullerene-like nanoparticles in time was found to match

that of the less crystalline IF-MoS_2, as long as proper oil recirculation is ensured during the test. The deterioration of the tribofilm after a given number of cycles is thought to be due to a progressive starvation of the contact in nanoparticles, which can be avoided by maintaining a homogeneous dispersion of the IF-MoS_2 in the oil. This may be achieved by mixing the oil, or by using adequate dispersants.

XPS analyses were carried out on all the IF-MoS_2 powders and on the wear scars after tribological testing. Although some nanoparticles seemed more oxidized than others, this did not seem to affect the tribochemistry of the contact as all the tribofilms formed on the surfaces had similar chemical compositions. In the case of the more crystalline nanoparticles, the higher atomic concentration of iron relative to Mo and S and the bigger shifting of the sulfur peaks towards lower energies suggested higher quantities of iron sulfides on the wear surfaces. The observation of FIB cross-sections of the wear surfaces for both the poorly crystalline and the more crystalline nanoparticles revealed the evolution of the surface during the HFRR tests. A 50 – 100 nm tribofilm first forms on the surface, consisting of two main layers. The top, thinner layer is made of MoS_2 platelets arranged parallel to the surface, providing low friction in the contact. An intermediate layer, containing iron oxides and sulfides, links it to the substrate. In the case of the more crystalline IF-MoS_2, their difficulty to exfoliate combined to the starvation of the contact in nanoparticles leads to a progressive wearing off of the tribofilm and to the apparition of steel-steel contacts, increasing the friction and wear in the contact.

As size did not affect nanoparticle efficiency for a given morphology (for diameters ranging from 150 nm to 350 nm and in the test conditions used), the tribological performance of bulk MoS_2 microparticles was compared to those of the IF-MoS_2. This test confirmed the interest of using nano-sized particles, as the MoS_2 microparticles produced higher friction and wear than the IF-MoS_2. The poorer availability of these significantly bigger particles in and around the contact (for a given weight concentration) is thought to be responsible for their lower performances.

Chapter Four

Tribological behavior of IF-MoS_2 in the presence of dispersants

The objective of the previous chapter was to determine which parameters were influential in the synthesis of efficient MoS_2 nanoparticle additives. The second step in formulating an efficient nanoparticle-doped lubricant is to study the interactions between the IF-MoS_2 and the other additives present in the oil. In this chapter, the IF-MoS_2 were found to lose their friction-reducing properties in the presence of the succinimide-based dispersants commonly used in automotive lubricants. An experimental investigation was carried out to understand the reason of this lack of effectiveness by combining surface analyses, contact observations and nanoparticle observations.

4. 1. Introduction

The work presented in Chapter Three has confirmed the potential of IF-MoS_2 nanoparticle additives in severe boundary lubrication conditions, but a number of issues are still to be addressed before exploiting this new technology effectively in industrial applications. As of today, the main difficulty concerns the optimal dispersion of the nanoparticles in liquid media. This step is however crucial, as nanoparticle agglomeration may result in many flaws, such as obstructions and contact starvation [73]. The results presented previously (***3. 3. 2. Effects of the oil flow on nanoparticle starvation of the contact***) also highlight the importance of a proper dispersion of the nanoparticles, in order to guarantee additive availability throughout the media for large volumes of oil.

In automotive lubricants, the use of succinimide-based dispersants is widespread to avoid the agglomeration of particle contaminants (wear debris, soot particles, external contamination…) and the solubilization of non-miscible liquids. They are generally added in relatively large quantities in the lubricant formulation, so as to effectively disperse all future particles in the oil.

This introduction will first focus on the phenomena leading to particle sedimentation and agglomeration, before exposing the impact of succinimide-based dispersants on IF-MoS_2-doped lubricants. An experimental investigation is then carried out to understand the effects of the dispersants on the three main phases of the mechanism related to nanoparticle lubrication, namely (i) the passing of the nanoparticles inside the contact, (ii) the exfoliation of these nanoparticles and (iii) the formation of a friction-reducing tribofilm from the adhesion of the exfoliated MoS_2 platelets on the steel surfaces.

4. 1. 1. Nanoparticle sedimentation and colloidal interaction energies in nanoparticle suspensions

When added to a fluid medium, nanoparticles are submitted to different types of motions. First witnessed by Robert Brown and proven theoretically by Albert Einstein in 1905 [83], the Brownian movement is the random motion of the particles resulting from the numerous collisions with the surrounding fluid molecules. The nanoparticles are also prone to sedimentation, as schematized on **Figure 4.1**.

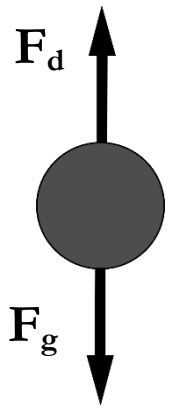

Figure 4.1. Forces acting on a particle sedimenting in a fluid medium

The drag force F_d exerted on a spherical particle in a viscous fluid was derived by Stokes in 1851 as:

$$F_d = 6\pi\eta r U_p \tag{10}$$

where η is the dynamic viscosity of the fluid ($Pa.s^{-1}$), r is the radius of the particle (m) and U_p is the particle velocity ($m.s^{-1}$).

This law is valid for individual, homogeneous particles with smooth surfaces in a laminar flow and very small Reynolds numbers ($Re < 1$, which is verified here given the very small size of the nanoparticles).

The force due to gravity is given by the difference of the weight of the particle and its buoyancy:

$$F_g = \frac{4}{3}\pi r^3(\rho_p - \rho_f)g \tag{11}$$

where ρ_p and ρ_f are the volumetric mass densities of the particle and the fluid respectively ($kg.m^{-3}$), and g is the gravitational acceleration (9,81 $m.s^{-2}$).

The steady-state settling velocity of the particles can then be determined from the force balance $F_d = F_g$, and is given by:

$$U_s = \frac{2(\rho_p - \rho_f)gr^2}{9\eta} \tag{12}$$

Assuming a volumetric mass of MoS_2 of 5000 $kg.m^3$ and the volumetric mass and dynamic viscosity of the PAO base oil at 25 °C, the settling velocity of the SpC IF-MoS_2 considered in this chapter would be:

$$U_s = \frac{2(5000-823)\times 9.81\times\left(75\times10^{-9}\right)^2}{9\times 0.087} = 0.59 \text{ nm/s}$$

In these conditions, the settling of all the nanoparticles contained in a 10cm-high flask (not taking wall effects into account) would take approximately $1.7x10^8$ seconds, equivalent to nearly 5.5 years. In reality, sedimentation occurs much faster because of the agglomeration of individual nanoparticles. As the settling velocity is dependent on r^2, the formation of large agglomerates will drastically reduce the sedimentation time.

While studying Al_2O_3 nanoparticle suspensions in 2007, K. Lu summarized the colloidal interaction energies leading to particle agglomeration [84]. The total interaction energy $E_T(h)$ for such suspensions was found to be:

$$E_T(h) = E_{vdw}(h) + E_{es}(h) + E_{ster}(h) + E_{dep}(h) \tag{13}$$

where h is the separation distance between the nanoparticles, $E_{vdw}(h)$ is the van der Waals interaction energy (attractive), $E_{es}(h)$ the electrostatic energy (repulsive), $E_{ster}(h)$ the steric energy (repulsive) and $E_{dep}(h)$ the depletion energy (attractive).

An electric double layer can be formed on the nanoparticles using electrolytes, creating a repulsive energy $E_{es}(h)$ between two close particles. The use of dispersants may also achieve this by forming an adsorbed polymer layer on the nanoparticle surface, source of a steric repulsion $E_{ster}(h)$. The presence of small particles in the oil may however cause attractive depletion forces between the larger nanoparticles.

In the case of IF-MoS_2 nanoparticles dispersed in a PAO base oil with no other additives, it can be assumed that the electrostatic, steric and depletion energies are negligible. The total interaction energy between two nanoparticles is then reduced to van des Waals interactions, derived by Gregory as being [85]:

$$E_{vdw}(h) = -\frac{Ar}{12h}\left[1 - \frac{5.32h}{100}\ln\left(1+\frac{100}{5.32h}\right)\right] \tag{14}$$

where A is the Hamaker constant.

A commonly used approximation for the Hamaker constant for van der Waals attractions between two solids 1 and 2 in a medium 3 [86] was proposed by Israelachvili in 1992:

$$A_{123} \approx \left(\sqrt{A_{11}} - \sqrt{A_{33}}\right)\left(\sqrt{A_{22}} - \sqrt{A_{33}}\right) \quad (15)$$

In the case of two IF-MoS_2 nanoparticles separated by PAO oil, this relation becomes:

$$A = \left(\sqrt{A_{MoS_2}} - \sqrt{A_{PAO}}\right)^2 \quad (16)$$

J. Polesel-Maris et al. estimated A_{MoS2} to be 2 eV (3.2×10^{-19} J) [87], while for typical hydrocarbon oils $A_{oil} \approx 5.5 \times 10^{-20}$ J. From equation (14), the Hamaker constant for the IF-MoS_2 in the base oil is then approximately 1.1×10^{-19} J. The van der Waals interaction energies can then be determined depending on nanoparticle size and separation distance (**Figure 4.2**).

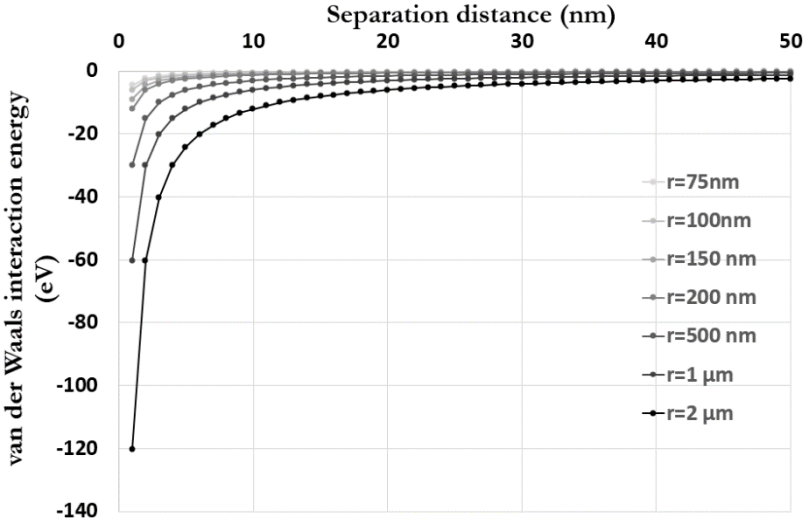

Figure 4.2. Van der Waals interaction energies for IF-MoS_2 of different sizes

Even though these calculations were made using a number of hypothesis, this result clearly shows that the attractive energies leading to particle agglomeration are significant only at close range, and become much greater for larger particles or agglomerates. Particle agglomeration and sedimentation are closely linked, as equation (10) shows that the settling velocity also depends greatly on particle/agglomerate size (the radius is squared). Larger agglomerates will therefore approach other agglomerates faster, leading to higher attractive energies between these agglomerates and to the formation of even larger agglomerates, which will in turn settle faster.

The use of dispersant additives to counterbalance the van der Waals attractive energies between individual nanoparticles is therefore vital to prevent agglomeration and slow down particle sedimentation.

4. 1. 2. Presence of dispersants on the oil and impact on IF-MoS_2-related friction reduction

The IF-MoS_2 nanoparticles tested in the previous chapter led to tremendous friction reduction in particularly severe contact conditions (boundary lubrication regime during a high number of cycles). To illustrate their extreme friction reducing capacities, the results obtained using the base oil alone (PAO) and the IF-MoS_2-doped base oil (PAO+1wt% SpC IF-MoS_2) were compared to the performance of a recent, fully-formulated gearbox oil in the same test conditions (given in

Table 3.3). The viscosities of both oils were comparable, with viscosities of 8.0 cSt at 100°C (51.1 cSt at 40°C) for the commercial lubricant and 9.3 cSt at 100°C (54.0 cSt at 40°C) for the PAO base oil.

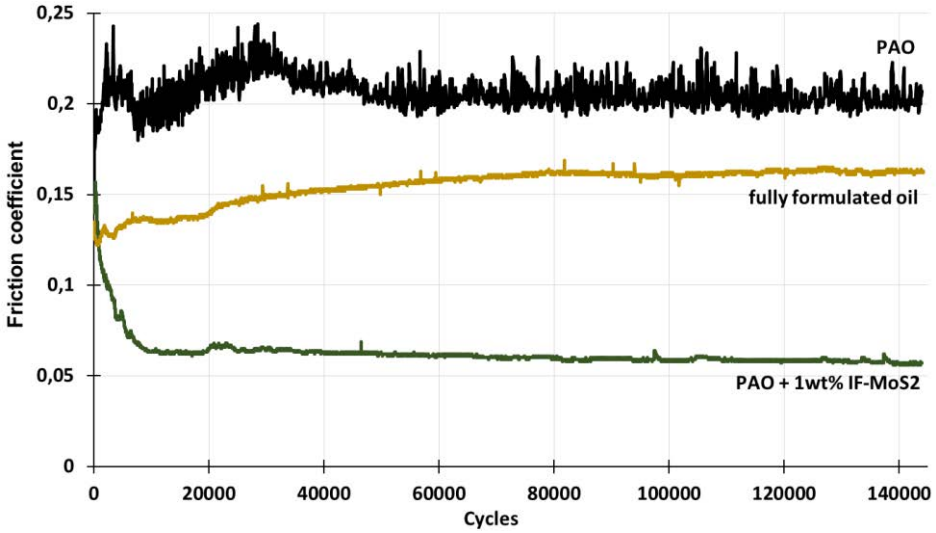

Figure 4.3. Compared performances of a PAO base oil with and without IF-MoS_2 and a fully formulated oil (test conditions given in **Table 3.3**)

Although this commercial lubricant exhibited a lower friction than the PAO oil throughout the test (**Figure 4.3**), the nanoparticle-doped base oil proved to be much more efficient, by reducing the coefficient of friction to 0.06 at the end of the test instead of 0.16 for the fully formulated oil. In an attempt to benefit from the additives in the commercial oil and achieve better friction reduction, this commercial lubricant was then doped with different concentrations (0.5wt%, 1wt% and 2wt%) of IF-MoS_2 and tested in the same conditions. Surprisingly, all tests revealed very similar results (**Figure 4.4**). Under the operating conditions used, the benefits due to the addition of IF-MoS_2 in the oil were totally lost when using a fully formulated lubricant instead of the PAO base oil used previously.

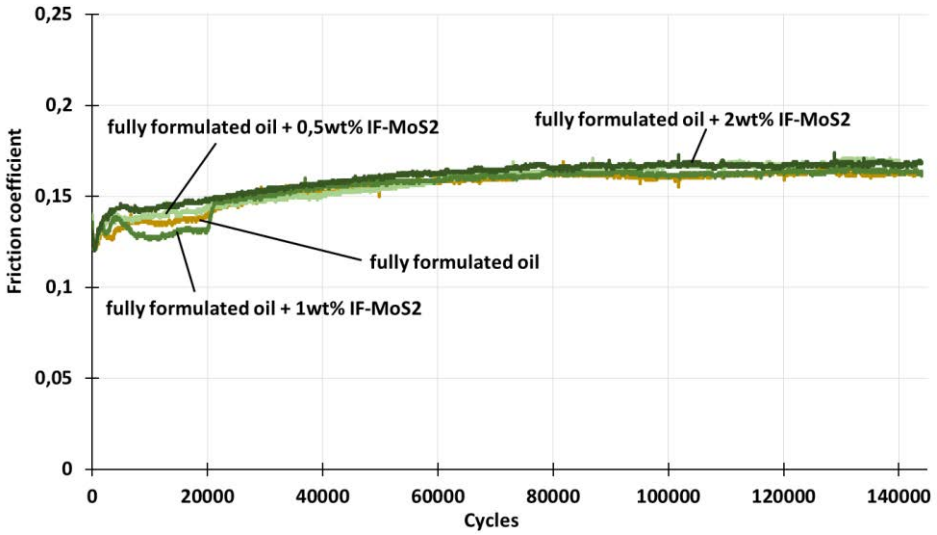

Figure 4.4. Tribological testing of a nanoparticle-doped fully formulated commercial lubricant

Since the IF-MoS_2 proved efficient in the absence of other additives in the oil, (at least) one of the additives contained in the commercial oil may prevent the lubrication mechanism associated to the IF-MoS_2 (exfoliation in the contact and formation of a lubricating tribofilm) from taking

place. Among the additives contained in a fully formulated oil, dispersants are likely to interact with the MoS_2 nanoparticles, as they are specifically designed - and used - to keep all particles contained in the lubricant (wear debris, soots, external contamination…) suspended and well dispersed.

In order to test the possible effects of dispersants on nanoparticle-doped lubricants, dispersant concentrations similar to those found in commercial automotive oils were added to the PAO base oil. The resulting dispersant/IF-MoS_2 ratios ranged from 0.5 to 10. The dispersant used was provided by a major additive company, and is similar to those currently used in common automotive lubricants. They are succinimide-based and consist in a polar, lipophilic molecular group connected to a longer, non-polar, oil-miscible molecular chain. The lipophilic groups of the dispersants will tend to cover the whole surface of the particles contained in the lubricant, while the oil-miscible chains will ensure the proper dispersion of the particles. The four formulations (dispersant/IF-MoS_2 ratios of 0.5, 1, 5 and 10) produced exactly the same friction coefficient throughout the tribological test (**Figure 4.5**). This result confirmed that the dispersants were (at least partly) responsible for the lack of improvement witnessed on **Figure 4.4** when adding IF-MoS_2 to the commercial oil.

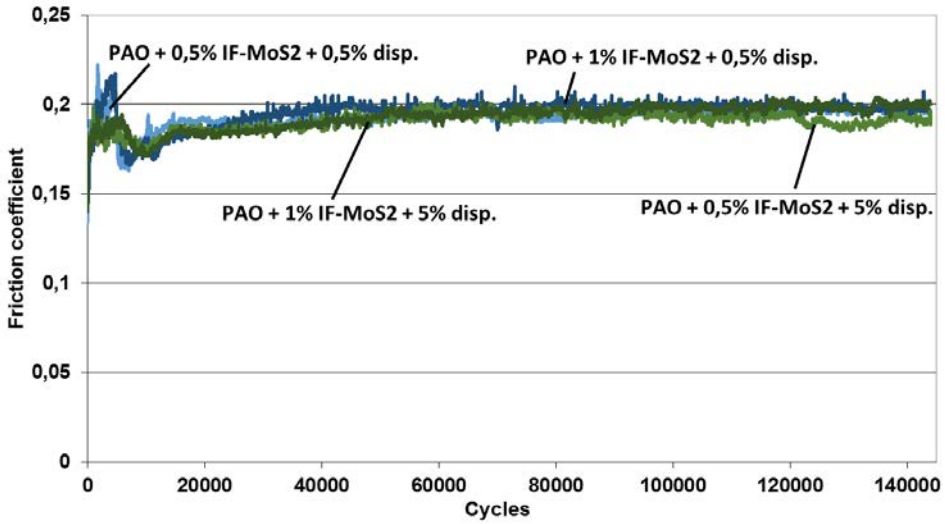

Figure 4.5. Tribological testing of a PAO base oil containing various concentrations of IF-MoS_2 and dispersants

The influence of the presence of dispersants on the lubrication mechanisms involved in nanoparticle lubrication will be investigated in this chapter.

4. 2. Understanding the effects of dispersants on nanoparticle lubrication

4. 2. 1. Tribological behavior and tribofilm formation

In order to better understand the effects of dispersants on nanoparticle lubrication, three oil formulations were considered: (a) the PAO base oil containing 1% nanoparticles and no dispersant, (b) the PAO base oil containing 5% dispersant and no nanoparticles, and (c) the PAO base oil containing both 1% IF-MoS_2 and 5% dispersant. The IF-MoS_2 used throughout this chapter are the SpC nanoparticles shown on **Figure 3.3**.

To test the quality of the dispersion obtained when adding dispersants to the oil, DLS measurements were carried out on the two PAO samples containing 1% IF-MoS_2 (with and without dispersant). When no dispersant was used, the average agglomerate size was 422 nm, with

agglomerates ranging from 200 nm to 1 µm (**Figure 4.6**). The addition of 5% dispersant resulted in a thinner size distribution and reduced the mean agglomerate size to 174 nm, which is close to the mean nanoparticle size. This result confirms that common dispersants are effective in dispersing IF-MoS_2 nanoparticles properly.

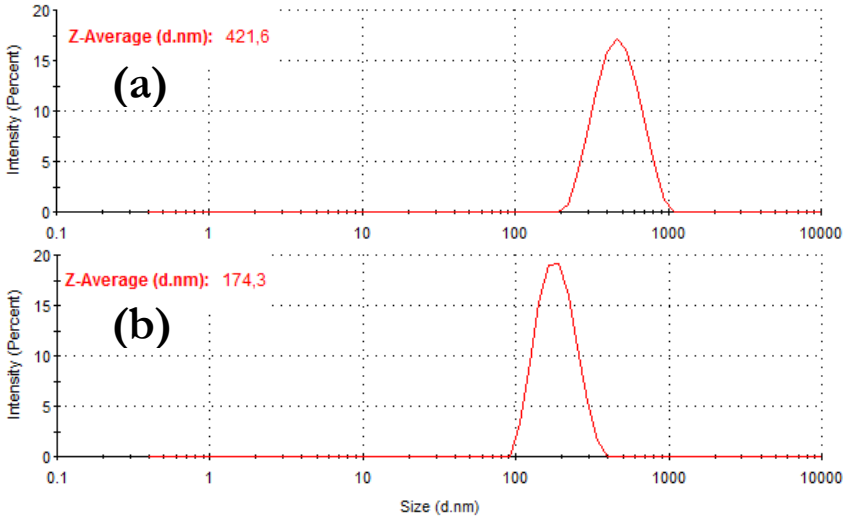

Figure 4.6. Nanoparticle agglomerate size distributions for the oils containing 1% IF-MoS_2 with (a) no dispersant and (b) with 5% dispersant

As mentioned previously (part ***3. 3. 1***), the presence of 1wt% of IF-MoS_2 in the PAO base oil did not modify its viscosity. The addition of dispersants, on the other hand, had an influence: the viscosities measured at 40°C and 100°C rose from 54.0 cSt (PAO alone) to 71.3 cSt (PAO + disp.) and from 9.3 cSt (PAO alone) to 11.7 cSt (PAO + disp.) respectively.

The PAO base oil containing 5% dispersant was submitted to the same tribological test than the PAO + 1% IF-MoS_2 (**Figure 4.3**) and the PAO + 1% IF-MoS_2 + 5% dispersant (**Figure 4.5**, test conditions given in **Table 3.3**). As expected from the testing of the different dispersant/IF-MoS_2 ratios (**Figure 4.5**), the presence of nanoparticles in the base oil did not have any effect on the friction coefficient when dispersants were used (**Figure 4.7**). This additional test also revealed that the slight decrease of the friction coefficient obtained with the different dispersant/IF-MoS_2 ratios (**Figure 4.5**) compared to the PAO base oil alone (**Figure 4.3**) was solely due to the dispersants. Although their presence may have various effects on the contact (adsorption on the rubbing surfaces, dispersion of the wear debris…), their influence on the oil viscosity is most likely to have reduced the friction coefficient. The presence of 5% dispersant in the PAO increased the viscosity from 14.8 cSt to 18.9 cSt at the test temperature (80°C), which may have contributed to a slightly better surface separation.

The wear scars obtained for these three tests are shown on **Figure 4.8**. The wear was comparable for both tests carried out in the presence of dispersants (with and without the IF-MoS_2 nanoparticles), and was greatly reduced when the IF-MoS_2 were used alone.

The main friction and wear reducing mechanism occurring during lubrication by fullerene-like nanoparticles is the formation of a tribofilm on the contacting surfaces, resulting from the exfoliation of the nanoparticles passing through the contact. The absence of any friction reduction and the higher wear when both IF-MoS_2 and dispersants are added to the base oil may then be due to the non-formation of a lubricating tribofilm on the rubbing counterparts. To verify this, XPS

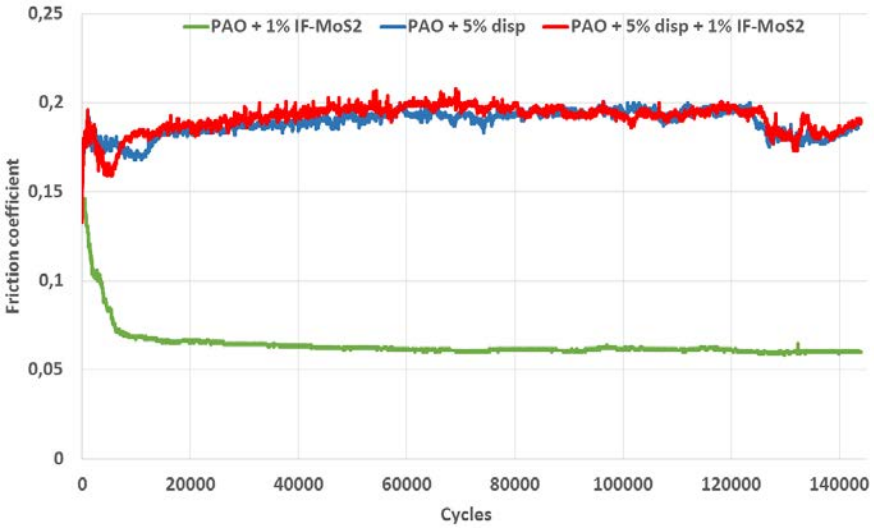

Figure 4.7. HFRR testing of the base oil containing IF-MoS_2 and/or dispersants

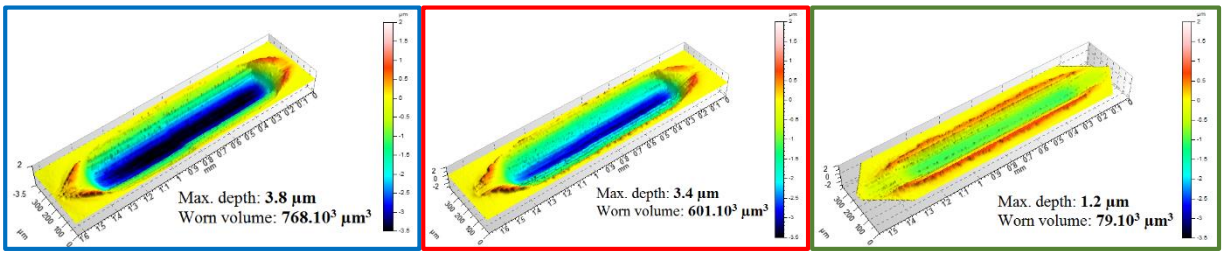

Figure 4.8. Wear scars for the HFRR tests showed on **Figure 4.7**: PAO + 5% disp. (left), PAO + 5% disp. + 1% IF-MoS_2 (center) and PAO + 1% IF-MoS_2 (right)

analyses were carried out on the wear scars at the end of these three tests, and the spectra obtained for molybdenum (Mo 3d), sulfur (S 2p), carbon (C 1s) and oxygen (O 1s) are shown on **Figure 4.9**.

For the oil containing no dispersants and providing significant friction reduction (PAO + 1% IF-MoS_2), the Mo $3d_{5/2}$ and the S $2p_{3/2}$ peaks corresponding to MoS_2 (229.8 eV and 162.3 eV respectively) can be found on the wear scar, indicating the adhesion of a tribofilm on the contacting surfaces. Mo(VI) and S(VI) species were also found at 232.7 eV and 169.0 eV respectively, which is consistent with the O – Mo species detected at 530.7 eV and the O – S species found at 531.9 eV.

The XPS spectra obtained when analyzing the wear scars corresponding to the two other oils (PAO + 5% dispersant and PAO + 1% IF-MoS_2 + 5% dispersant) showed many similarities, with little to no energy peaks detected in the Mo 3d and the S 2p regions and identical results for the C 1s and O1s spectra. O – C species were found at 531.4 eV, which was confirmed by the energy peaks corresponding to C – O and C = O species measured at 286.0 eV and 288.4 eV. For these two oils, O – Fe species were found at 529.8 eV in the O 1s region. These peaks indicate the presence of a layer of iron oxides at the extreme surface of the wear scars when dispersants were used, instead of the MoS_2 tribofilm previously found for the blend containing no dispersants. The absence of O – Fe and O – C species on the spectra corresponding to the PAO + 1wt% IF-MoS_2 blend moreover suggests that the absence of dispersants resulted in the formation of an MoS_2 tribofilm thick enough to conceal any native oxides possibly remaining at the surface of the substrate.

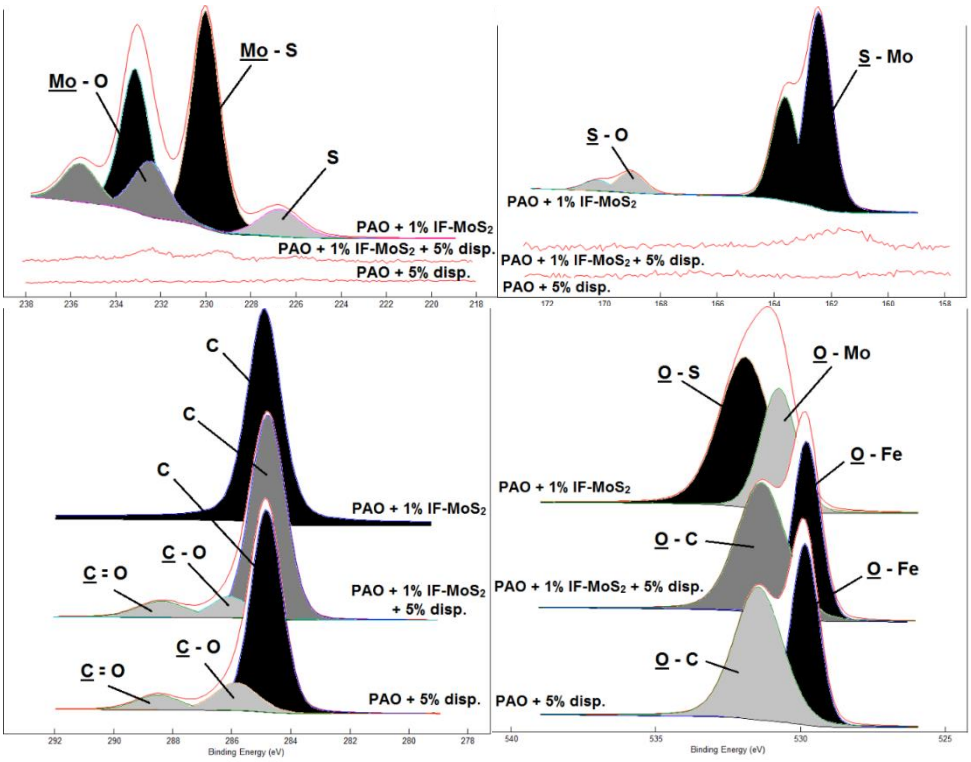

Figure 4.9. XPS spectra of Mo 3d, S 2p, C 1s and O 1s obtained on the wear scars shown on **Figure 4.8**

In the presence of dispersants, these analyses reveal identical extreme surface compositions whether or not the oil contained IF-MoS_2 nanoparticles, with no sign of an MoS_2 tribofilm formed at the surface. These results most likely indicate that tribofilm adhesion did not occur on the steel substrate during the test. As XPS analysis only covers the extreme surface (depth of a few nanometers), the similarities between the spectra recorded for both tests containing dispersants (with and without IF-MoS_2) could however also suggest that the molybdenum and/or sulfur did react with the substrate during the test, but that the resulting layer was then covered by dispersant molecules and/or wear debris. In order to eliminate this possibility, in-depth profiles were carried out by XPS using ion etching on the wear surfaces resulting from these three friction tests (**Figure 4.10**).

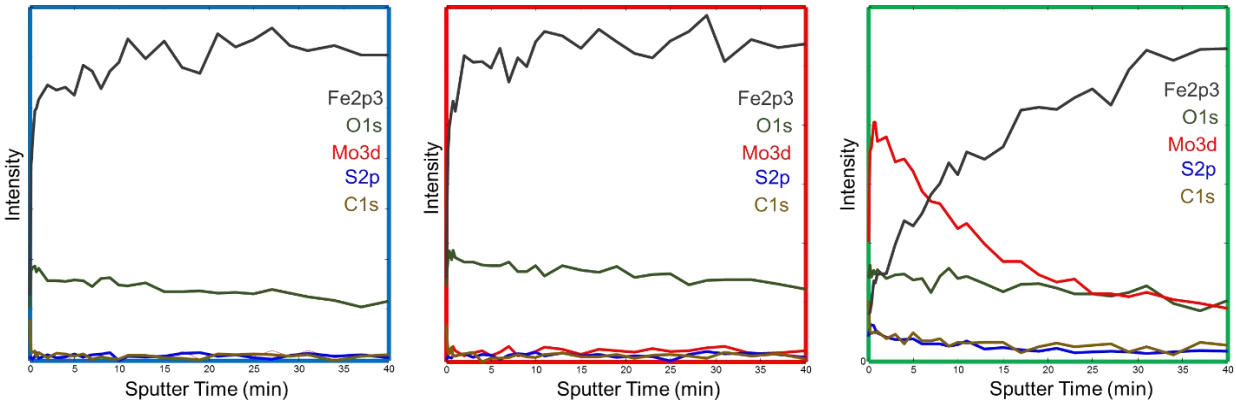

Figure 4.10. Ion etching profiles by XPS of the wear surfaces resulting from the test on **Figure 4.7**
PAO + dispersant (blue), PAO + dispersant + IF-MoS_2 (red), PAO + IF-MoS_2 (green)

The profile measured for the wear scar corresponding to the test with no dispersants clearly revealed the tribofilm, with decreasing intensities of the energy peaks corresponding to molybdenum and sulfur and a higher intensity of iron for increasing depths (depending on the

sputter time). The profiles corresponding to both tests containing dispersants (with and without the IF-MoS_2) were very similar, with no molybdenum nor sulfur detected and a high quantity of iron found at all analyzed depths. These profiles clearly indicate that no MoS_2 tribofilm adhesion takes place during the tribological tests when dispersants are added to the oil to disperse the IF-MoS_2 nanoparticles.

The formation of this tribofilm in the case of boundary lubrication using IF-MoS_2 is a three-step process: (i) the nanoparticles must enter and pass through the contact, (ii) when in the contact, the IF-MoS_2 should be submitted to the normal pressure and shear of the surfaces and exfoliate, creating free MoS_2 layers in the contact and (iii) these layers must react chemically with the steel surfaces to create the low friction tribofilm [65]. In the presence of dispersants, one or several of these three steps does not seem to take place.

In the case of an optimal dispersion of the nanoparticles, several phenomena could potentially reduce the quantity of particles passing through the contact. The absence of agglomerates could for example modify particle entrapment conditions. The flow of individual particles around and near the contact may also be modified, as their reduced mass (compared to agglomerates) will change their inertia in the oil.

If these well-dispersed nanoparticles do enter the contact, their exfoliation may not take place in the same way as for agglomerated particles. The ratio between their size and the surface separation will indeed be smaller, so that individual nanoparticles may not suffer the same amounts of compression and shear for mixed lubrication regimes (supposing some local gaps subsist between both surfaces in the contact).

Finally, if the IF-MoS_2 enter the contact and are exfoliated, the presence of succinimide-based dispersants in the oil may affect the tribochemistry of the contact. The dispersant molecules could indeed excessively adsorb on the steel surfaces, and/or encapsulate the MoS_2 platelets released during nanoparticle exfoliation. In these conditions, the chemical bonding that is thought to be responsible for the adhesion of MoS_2 tribofilms on the surface (between the molybdenum and sulfur of MoS_2 and the oxygen and iron found in the native iron oxide layer [65]) may not take place.

4. 2. 2. In-vivo contact visualization and nanoparticle observations

The three steps mentioned above must be investigated to understand why the IF-MoS_2 lose their effectiveness in the presence of dispersants. The previous section revealed that the adhesion of an MoS_2 tribofilm did not take place in these conditions. The two remaining questions will be answered in this section, namely: do the IF-MoS_2 enter the contact in the presence of dispersants? If so, are the well-dispersed IF-MoS_2 exfoliated in the contact?

Two NTR tests (refer to ***2. 2. 3.*** for details) were carried out to observe the contact lubricated by IF-MoS_2-doped lubricant with and without dispersants, in pure-sliding reciprocating conditions (test parameters summarized in **Table 4.1**). The image was focused on the surface of the ball in order to observe the interactions of the IF-MoS_2 with steel.

Figure 4.11 compiles 6 images for each test: the initial (before the beginning of the test) and final (at the end of the test) contact zones, as well as one image extracted from the video at regular

intervals (every 100 cycles of the test). In the absence of dispersants (column on the left), the nanoparticle agglomerates are clearly visible. They coalesce at the entry of the contact (on either side depending on the direction of motion), and can be seen passing through it. A film can be seen forming rapidly on the surface of the ball and progressively covering the whole contact zone. This is consistent with the tribological result obtained on **Figure 4.7** and the XPS measurements shown on **Figure 4.9**, where the presence of an MoS_2 tribofilm on the surface explained the spectacular friction reduction observed.

Load (N)	**5**
Maximum hertzian pressure (GPa)	**1.4**
Stroke length (mm)	**2**
Frequency (Hz)	**0.75**
Number of cycles (-)	**500**
Material (ball)	**AISI 52100 (100Cr6)**
Material (flat)	**sapphire**
Temperature (°C)	**ambiant**

Table 4.1. Test conditions used for the Nanovisu tests

The same test, but carried out with dispersants in the oil, is shown on the column on the right of **Figure 4.11**. The nanoparticles, in a seemingly less agglomerated state, can also be seen passing through the contact. Their adhesion to the steel surface of the ball however appears to be altered: the layer is not formed as fast and does not appear to be as thick as for the oil not containing any dispersants. The XPS analysis carried out after the HFRR test in the presence of dispersants furthermore suggests that this layer was totally removed while cleaning the sample (n-heptane rinse followed by a ten-minute ultrasonic bath in n-heptane), implying that no chemical bonding took place. This was not the case for the blend without dispersants, as an MoS_2 tribofilm was found on the surface after the HFRR sample had been submitted to the same cleaning procedure before the XPS analysis.

These test results confirm that the presence of dispersants in the oil does not prevent the nanoparticles from entering the contact, but does not bring an answer to whether these nanoparticles exfoliate in the contact or not.

To pursue this investigation further, nanoparticles were collected from the wear scar at the end of the HFRR test with the oil containing dispersants, and the samples were observed using High-Resolution Transmission Electron Microscopy (HR-TEM). **Figure 4.12** shows what appears to be an intact nanoparticle (on the right) alongside a damaged nanoparticle, which has clearly passed through the contact and suffered partial exfoliation (**Figure 4.12**(b)). One whole part of the particle was ripped away from its core (**Figure 4.12**(a)), and MoS_2 platelets can be seen near the nanoparticle (**Figure 4.12**(c)). These loose MoS_2 platelets seem to remain enclosed in a coating surrounding both nanoparticles, which may consist of remaining dispersant. More evidence of damaged nanoparticles were found on the grid (highlighted on **Figure 4.13**), confirming that the nanoparticles were effectively exfoliated when passing through the contact, even when in a well-dispersed state.

These two experiments show that well-dispersed nanoparticles enter the contact and exfoliate, forming the MoS_2 platelets needed for the formation of a tribofilm on the contact surfaces. The

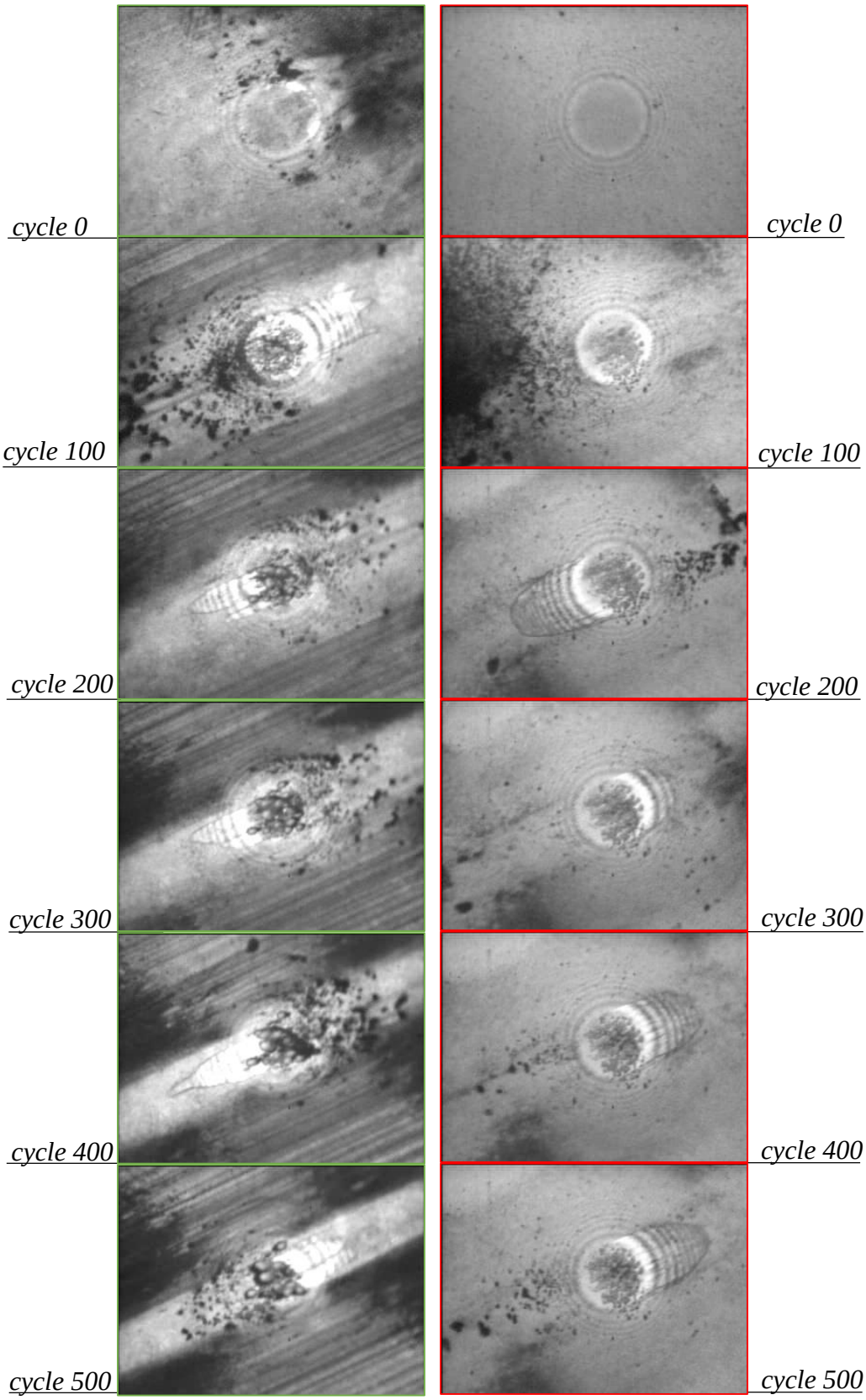

Figure 4.11. Nanovisu tests for the nanoparticle-doped base oil (1 wt%) with (right) and without (left) dispersants (5%)

chemical bonding needed to secure the adhesion of this tribofilm does however not seem to happen. This could be caused by an excessive adsorption of the dispersants on the steel surfaces, and/or by a complete coating of the exfoliated platelets in dispersants, preventing Mo – O, S – O

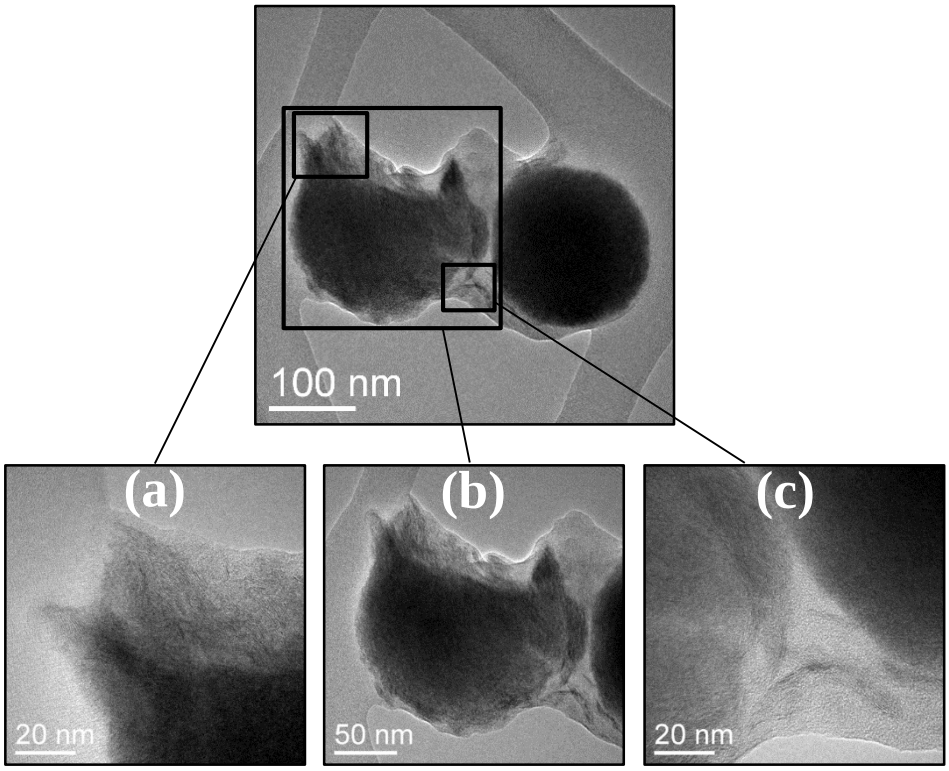

Figure 4.12. Nanoparticles collected after tribological testing in the presence of dispersants – damaged (left) and intact (right) IF-MoS_2

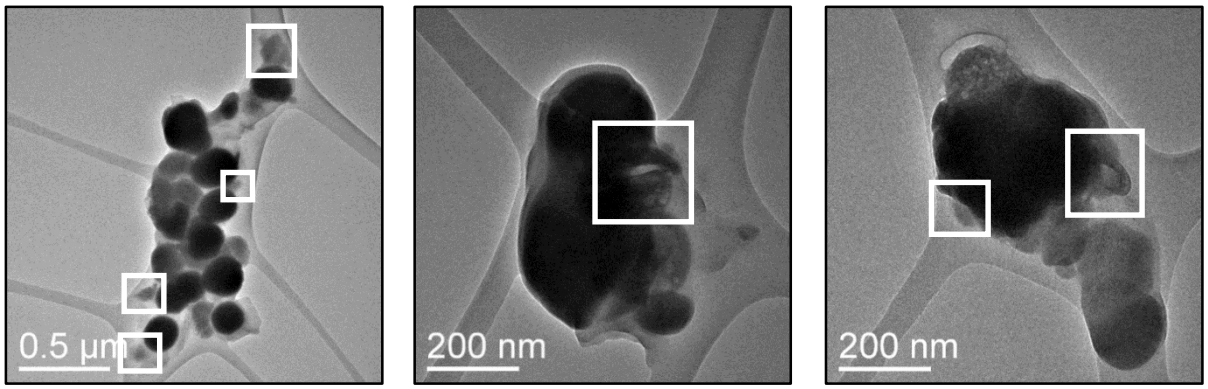

Figure 4.13. Damaged nanoparticles collected on the wear scar after HFRR testing in the presence of dispersants

and S – Fe bonding to occur between the MoS_2 and the iron oxide of the surfaces.

As of today, most studies concerning nanoparticle-doped lubricants did not consider dispersants. The great friction-reducing properties of these additives were therefore most likely obtained for agglomerated nanoparticles, modifying their flow in the oil and their entrapment conditions at contact entry. The results shown in this chapter indicate that the dispersion of the nanoparticles in itself is not responsible for their lack of effectiveness in the presence of dispersants. This observation raises interesting prospects, as the use of different dispersant additives or dispersing methods such as particle polarization could disperse the IF-MoS_2 while maintaining their tribological properties.

The need for dispersants in automotive lubricants is however vital in order to disperse any particle contaminants in the oil. As succinimide-based dispersants continue to be widely used for this purpose, their compatibility with IF-MoS_2 nanoparticles remains of great interest.

4. 3. Finding the balance between nanoparticle dispersion and performance

4. 3. 1. Estimation of the quantity of dispersants needed

The role of dispersants in commercial engine and gearbox oils is to prevent all particle contaminants (wear debris, soot, external particles…) from agglomerating. As these contaminants will appear gradually in the oil, dispersants must initially be added in excess to the lubricant. In the case of nanoparticle lubrication, the test results presented in this work suggest that this excessive quantity of dispersants may be detrimental. A quick estimation of the quantity of dispersant needed to fully disperse 1wt% of IF-MoS_2 was made, by using the following hypotheses (**Figure 4.14**):

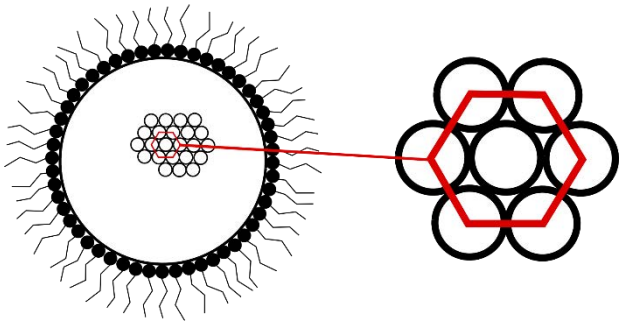

Figure 4.14. Schematic top view of a nanoparticle covered in dispersant molecules (hexagonal packing)

a. The IF-MoS_2 are all perfectly spherical and have the same size;

b. The hydrophobic groups of the dispersant molecules are all identical and perfectly spherical;

c. The surface of each nanoparticle is covered at 90.7% by these hydrophobic groups, which are then arranged in a hexagonal lattice around the nanoparticle (densest arrangement possible, with a density of $\frac{\pi}{2\sqrt{3}}$);

d. $\Phi_{IF\text{-}MoS2}$=150 nm; $\Phi_{succ.}$=1 nm; ϱ_{PAO}= 0.83 g/cm^3; $\varrho_{IF\text{-}MoS2}$= 5 g/cm^3; $\varrho_{succ.}$= 1.4 g/cm^3.

By using these simple hypotheses, the number of IF-MoS_2 contained in one liter of oil is:

$$N_{IF-MoS_2} = \frac{M_{IF-MoS_2}}{m_{IF-MoS_2}} = \frac{\%_{IF-MoS_2} \times M_{PAO}}{v_{IF-MoS_2} \times \rho_{IF-MoS_2}} = \frac{\%_{IF-MoS_2} \times M_{PAO}}{\frac{4}{3}\pi r_{IF-MoS_2}^{\ 3} \times \rho_{IF-MoS_2}} \quad (17)$$

$$N_{IF-MoS_2} = \frac{3 \times 0.01 \times 830}{4\pi\left(75 \times 10^{-9}\right)^3 \times 5 \times 10^6} \approx 9.39 \times 10^{14}$$

where $N_{IF\text{-}MoS2}$ and $M_{IF\text{-}MoS2}$ are the number and total mass of IF-MoS_2 in one liter of PAO, $m_{IF\text{-}MoS2}$, $v_{IF\text{-}MoS2}$ and $r_{IF\text{-}MoS2}$ are the mass, volume and radius of an individual IF-MoS_2, and $\%_{IF\text{-}MoS2}$ and $\varrho_{IF\text{-}MoS2}$ are the weight concentration and volumetric mass of the IF-MoS_2.

The number of dispersant molecules needed to completely recover these IF-MoS_2 nanoparticles is then:

$$N_{disp.} = \frac{S_{IF-MoS_2} \times d_a}{s_{disp.}} = \frac{N_{IF-MoS_2} \times s_{IF-MoS_2} \times d_a}{s_{disp.}} = \frac{N_{IF-MoS_2} \times 4\pi r_{IF-MoS_2}^{\ 2} \times d_a}{\pi r_{disp.}^{\ 2}} \quad (18)$$

$$N_{disp.} = \frac{9.39\times10^{14}\times4\pi\times\left(75\times10^{-9}\right)^2\times0.907}{\pi\left(0.5\times10^{-9}\right)^2} \approx 7.67\times10^{19}$$

where N_{disp} is the number of dispersant molecules needed, $S_{IF\text{-}MoS2}$ is the total surface of IF-MoS_2 to cover, d_a is the density of the hexagonal arrangement (90,7%), $s_{disp.}$ is the surface covered by a single molecule of dispersant, $s_{IF\text{-}MoS2}$ is the surface of a single IF-MoS_2 and $r_{disp.}$ is the radius of the hydrophobic groups of the dispersant molecules.

The final dispersant weight concentration required to exactly (completely but with no excess) cover all the nanoparticles in the oil would then be:

$$\%_{disp.} = \frac{M_{disp.}}{M_{PAO}} = \frac{N_{disp.}\times m_{disp.}}{M_{PAO}} = \frac{N_{disp.}\times v_{disp.}\times \rho_{disp.}}{M_{PAO}} \quad (19)$$

$$\%_{disp.} = \frac{7.67\times10^{19}\times4\pi\times\left(0.5\times10^{-9}\right)^3\times1.4\times10^{6}}{3\times830} = 0.0067\text{wt}\%$$

This rapid calculation was made using very simple hypotheses, and is only shown here to give an estimation of the order of magnitude sought. The result found is much lower than the concentrations usually used in automotive lubricants.

4. 3. 2. Tribological effect and XPS profiles

As the order of magnitude of the quantity of dispersants needed was found to be much lower than currently used, a new oil formulation was made containing the same PAO base oil as used previously as well as 1wt% IF-MoS_2 and 0.05wt% of succinimide-base dispersant.

DLS measurements were carried out on this new lubricant, to confirm that the low quantity of dispersant used was sufficient to prevent the formation of agglomerates in the oil (**Figure 4.15**). This measurement was very similar to the one obtained when using 5wt% dispersant, with a thin size distribution and an average agglomerate size of 180.2 nm. This result confirms that a dispersant concentration of 0.05wt% was sufficient to efficiently disperse 1wt% of the IF-MoS_2 used in this study.

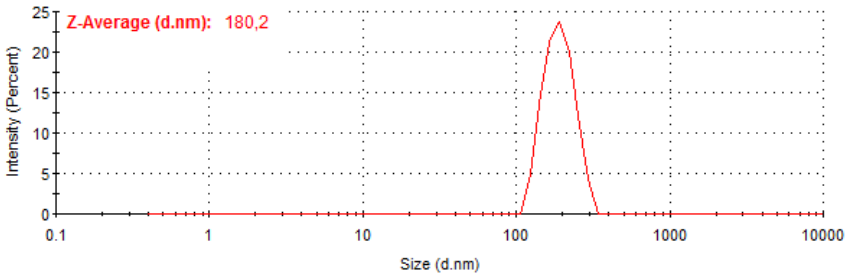

Figure 4.15. Nanoparticle agglomerate size distribution for the lubricant containing 0.05wt% of dispersants

This new oil was then tested in the same tribological conditions as the ones used previously, and the results were compared to the reference tests with only the base oil, and the base oil containing 1wt% IF-MoS_2 (with no dispersants, **Figure 4.16**). During the first 90 000 cycles of the test, the friction reduction compared to the base oil alone was only half of the reduction obtained

for the nanoparticle-doped oil with no dispersant, with a friction coefficient averaging 0.13. After 90 000 cycles, the friction coefficient suddenly dropped and stabilized to approximately 0.06, which is close to the maximum friction reduction obtained in the absence of dispersants. Additional testing showed that this behavior was repeatable, although the number of cycles achieved until the drop in friction may vary.

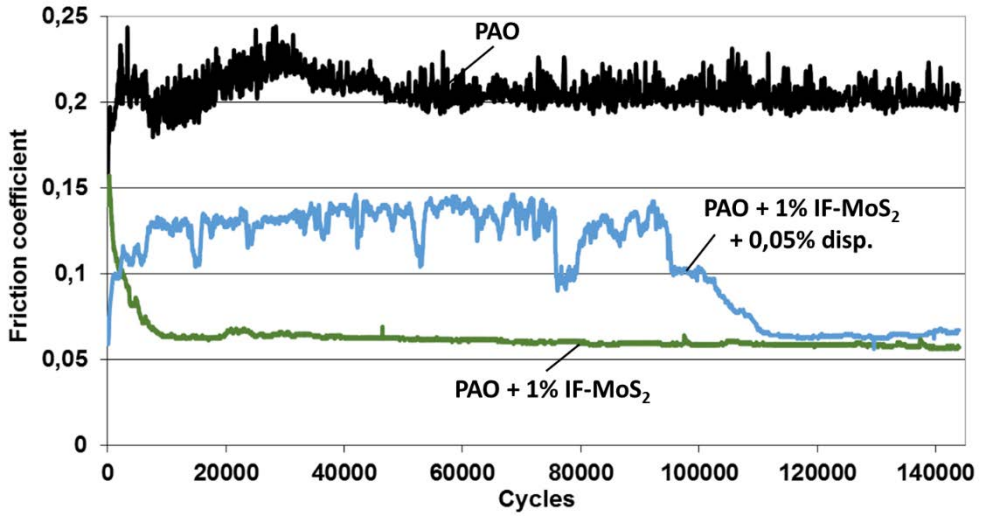

Figure 4.16. Tribological performance of the IF-MoS_2-doped base oil containing 0.05 wt% of dispersants

The NTR was used to visualize the contact when lubricated with this oil, in the same conditions as used previously (**Table 4.1**). After the first 500 cycles (column on the left), the results were similar to those obtained in the presence of 5% dispersant: the particles were seen passing through the contact, but did not seem to form a thick film on the steel surface of the ball (**Figure 4.17**). The test was then continued for an extra 1500 cycles (column on the right).

Substantial film adhesion then started taking place between 750 and 1000 cycles, and the ball surface then resembled the one obtained during the test without dispersants, with a seemingly thick film progressively covering most of the contact area. This behavior is consistent with the one observed for the HFRR friction test (**Figure 4.16**): the presence of the dispersant in the oil, even in low concentrations, appears to prevent the adhesion of the MoS_2 film on the surface during a given number of cycles. A sudden change then occurs, and the MoS_2 platelets released by the IF-MoS_2 are suddenly able to form an efficient friction-reducing tribofilm on the contacting surfaces. This behavior may be due to a small excess in dispersants remaining in this new oil formulation, which could prevent tribofilm formation at the beginning of the test by adsorbing on the steel surface and/or by enveloping the MoS_2 platelets released from the nanoparticles. These residual dispersant molecules may have been consumed after a consequent number of cycles, by the wear of the surfaces and/or after having dispersed the many wear debris and MoS_2 platelets released in the contact. From this moment onwards, the absence of free dispersant molecules in the oil seems to permit tribofilm formation, even though - in this scenario - the nanoparticles entering the contact would still be likely to be covered in dispersant molecules.

To verify the proper dispersion of the IF-MoS_2 nanoparticles when this maximum friction was achieved in the presence of dispersants, a final DLS measurement was carried out on an oil sample containing 1wt% IF-MoS_2 and 0.05wt% dispersant, collected at the end of the HFRR test shown on **Figure 4.16**. The results were very similar to those obtained before the test, with an average

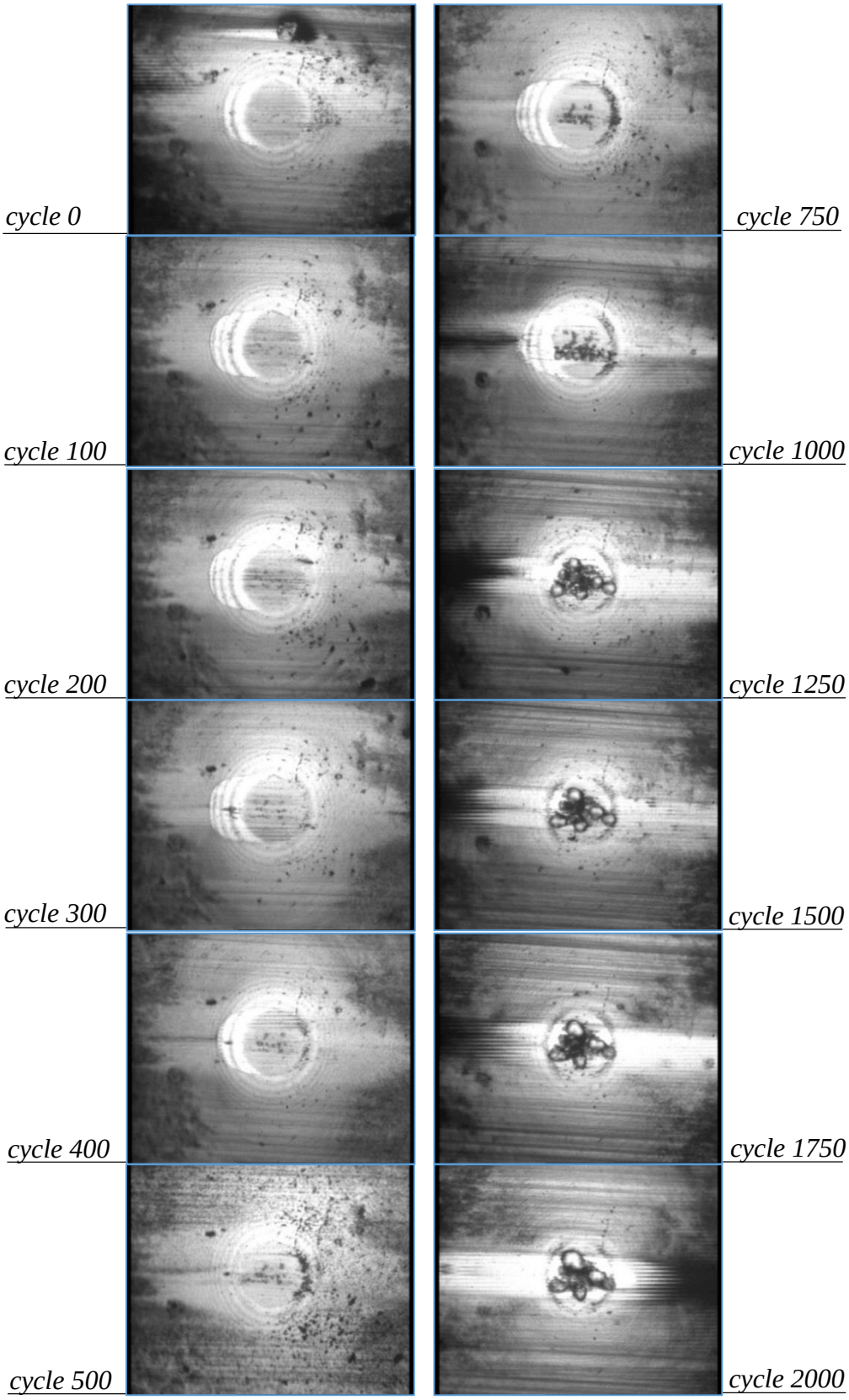

Figure 4.17. Nanovisu test for the PAO base oil containing 1wt% IF-MoS_2 and 0.05wt% dispersants

size of 181.5 nm (**Figure 4.18**). This measurement confirms that a balance between friction reduction and presence of dispersants was found, although it could only be achieved after a "running-in" period which may have consumed all the excess dispersant found in the oil.

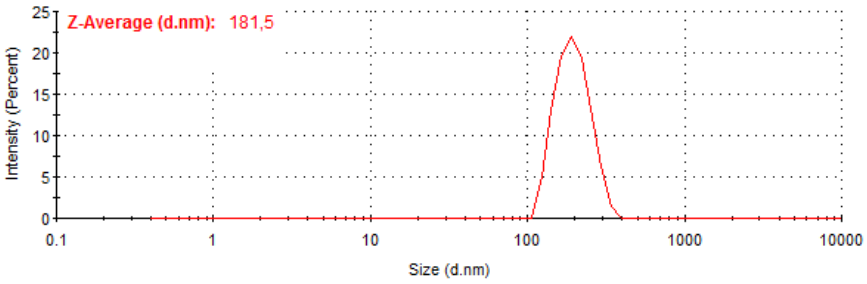

Figure 4.18. Nanoparticle agglomerate size distribution at the end of the tribological test (PAO base oil containing 1wt% IF-MoS_2 and 5wt% dispersants)

4. 4. Conclusions

In this chapter, Inorganic Fullerene-like (IF-)MoS_2 nanoparticles were added to a fully formulated commercial lubricant in an attempt to reduce friction in severe boundary lubrication regimes. This addition had no effect on the behavior of the oil, even though the nanoparticles used exhibited outstanding friction and wear reduction capacities when used with a PAO base oil alone. The excess in dispersants used in the commercial oil to prevent the agglomeration of particle contaminants was found to be - at least partly - responsible for the lack of effectiveness of the IF-MoS_2.

When dispersants are present in the oil, XPS analysis revealed identical extreme surface compositions whether or not nanoparticles were added to the oil, implying that the lubrication mechanism leading to the formation of a low-friction tribofilm on the surfaces did not take place. This lubrication mechanism is a three-step process, all of which may be affected by the presence of dispersants in the nanoparticle-doped oil:

Step 1. The nanoparticles enter the contact;

Step 2. The nanoparticles exfoliate under the combined pressure and shear of the opposing surfaces;

Step 3. The newly formed MoS_2 platelets react with the surface to form a low-friction and wear-reducing tribofilm.

Real-time observations of the contact revealed the passing of nanoparticles in the contact, confirming that the reduced size and inertia of the particle agglomerates did not prevent them from reaching the contact entry nor from being entrapped by the surfaces. HR-TEM observations of nanoparticles collected on the wear scar at the end of friction tests showed many damaged and exfoliated nanoparticles, as well as released MoS_2 platelets, which seemed to be trapped in a coating possibly made of dispersant molecules. From these results, the presence of dispersants in the oil was found not to affect the steps 1 & 2 mentioned above, implying that well-dispersed nanoparticles could also provide important friction reduction. The presence of succinimide-based dispersants rather seemed to prevent the tribo-chemical reactions between the nanoparticles and the surfaces from taking place, leading to the absence of tribofilm adhesion. This may be due to an excessive adsorption of the dispersant on the contact surfaces, and/or to the full covering of the liberated MoS_2 in dispersant molecules.

A much lower concentration of dispersants than currently used in common commercial lubricants was found to correctly disperse the nanoparticles in the oil, while also permitting

significant friction reduction after the completion of the first 90 000 cycles. Contact observations confirmed that the MoS_2 only started adhering to the surface after a running-in period. The potential excess in dispersants present in the oil at the beginning of the test may have been consumed during the first part of the test, by encapsulating the wear debris and the numerous platelets of MoS_2 liberated by the exfoliation of the nanoparticles, and/or by the progressive wearing off of the steel surface on which they adsorb.

These results are promising in terms of finding the right balance between nanoparticle dispersion and optimal friction reduction, but seem to imply that a very precise dosing of the dispersant molecules is necessary in order to fully disperse the nanoparticles while leaving no excess in dispersants in the oil.

Chapter Five

Aiming for automotive applications

Part of the difficulty in creating a fully-formulated lubricant containing nanoparticle additives has been shown in the previous section. Achieving this goal will however be vain if the performance of such lubricants does not meet expectations in complex mechanical systems. This chapter focuses on particular aspects linked to the use of IF-MoS_2 in real-life applications: their behavior under a variety of conditions was studied, such as ambient temperatures and different lubrication regimes. Component-orientated benefits were also investigated, by testing their friction and wear reducing potential for rough surfaces and their influence on Rolling Contact Fatigue.

5. 1. Introduction

The ultimate objective in the development of nanoparticle-doped lubricants is to be able to use them efficiently in real-life applications, such as automotive engines and/or gearboxes. The exceptional tribological properties of IF-MoS_2 nanoparticles when added to different base oils were detailed in the literature, as synthesized in **Chapter One**. The work presented in **Chapter Three** confirmed this potential and showed that nanoparticle size and agglomeration were not necessarily an issue if proper oil recirculation was ensured, as friction and wear reduction were maintained for a significant number of cycles.

In order to industrialize the use of nanoparticles, many challenges remain to be faced. The results presented in **Chapter Four** highlight the incompatibility of IF-MoS_2 with excessive amounts of succinimide-based dispersants, although the dispersion of the nanoparticles in itself does not seem to be the cause of their lack of effectiveness in oils containing dispersants. The main difficulty in formulating commercial lubricants containing nanoparticles may therefore reside in finding dispersing agents capable of dispersing both the nanoparticles and particle contaminants, while not interfering with tribofilm formation.

This step will however be of limited interest if nanoparticle-doped lubricants are finally found to be inefficient – or even detrimental – in complex mechanical systems. The aim of this chapter is to provide an insight on the potential of IF-MoS_2 nanoparticles in various scenarios met in automotive engines and/or gearboxes. The lubrication regimes encountered for different components will first of all be explored so as to establish the behavior of IF-MoS_2 nanoparticles for contact conditions less severe than boundary lubrication. The effects of nanoparticle-doped lubricants on rough contacts will then be studied, given the rarity of perfectly smooth surfaces in mass-produced vehicles. A final series of tests will then be carried out to investigate the possible influence of IF-MoS_2 on crack initiation and propagation, which is of particular interest in the case of high-cycle components prone to fatigue such as gears.

5. 2. Exploring the different lubrication regimes

5. 2. 1. Boundary lubrication: Influence of temperature

All tribological tests presented in this work so far were carried out at 80°C, which is a typical operating temperature for automotive contacts. Additives must however be active for a wide range of temperatures in order to ensure the effectiveness of the lubricant at all times. The first few miles of every trip are for example particularly critical for motorized vehicles, as the oil requires some time to reach its optimal temperature. The adhesion and composition of tribofilms formed by many current boundary additives indeed depend on temperature, and are generally less efficient under ambient temperature.

Because of their lubricating mechanism, Inorganic Fullerene-like nanoparticles are thought to be equally active regardless of temperature. The formation of protective and low-shear strength tribofilms depends solely on the exfoliation of the nanoparticles, which is a mechanical process induced by the combined effects of shear and normal pressure of the contacting surfaces. To verify this, the HFRR tests carried out in section ***3. 3. (Tribological testing of the IF-MoS2***

nanoparticles) on the LC and SpC IF-MoS_2 (**Table 3.1**, p.54) were repeated under a temperature of 30°C (complete test conditions given in **Table 3.3**, p.58).

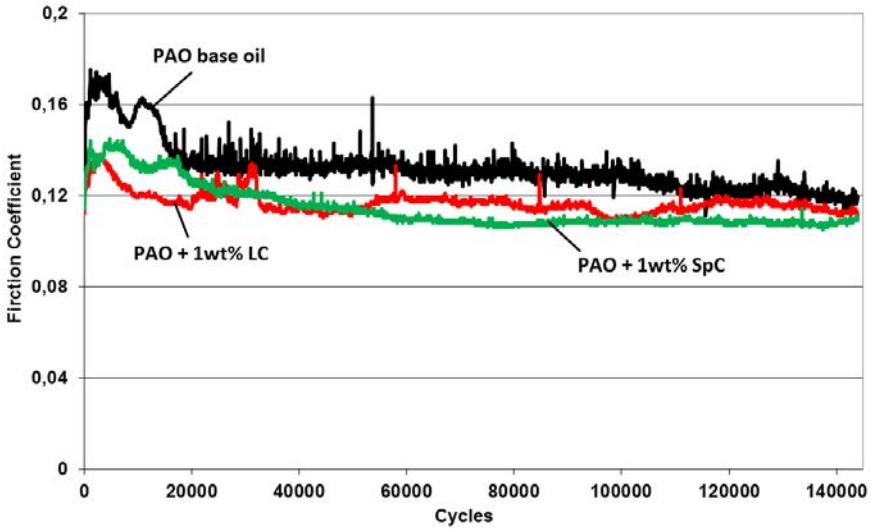

Figure 5.1. HFRR testing of the LC and SpC IF-MoS_2 under ambient temperature

The friction coefficients obtained during the four hour tests (144 000 cycles) are showed on **Figure 5.1**. For both types of nanoparticles, the addition of 1 wt% of IF-MoS_2 in the PAO base oil only provided a slight decrease in friction during the test. The change in viscosity induced by this lower temperature (from 14.8 cSt at 80°C to 83.3 cSt at 30°C) however reduced the severity of the test by creating better surface separation, as attested by the lower friction coefficient obtained with the PAO base oil alone (from 0.20 at 80°C to 0.13 at 30°C on average). The reduced effectiveness of the nanoparticles under ambient temperature may therefore simply be due to the milder contact conditions (as in ***3. 3. 2***, where the velocity of the ball was increased) rather than to their inability to form a tribofilm on the surfaces. This assumption was partly confirmed by the significant reduction of the wear occurring when IF-MoS_2 were added to the PAO (**Figure 5.2**).

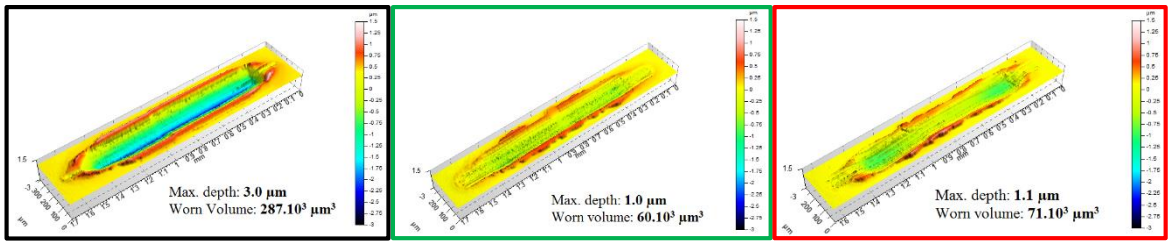

Figure 5.2. Comparison of the wear scars obtained for the PAO base oil alone (left), the PAO+1wt% SpC IF-MoS_2 (center) and the PAO+1wt% LC IF-MoS_2 (right)

XPS analyses were carried out on the wear surfaces in order to verify the capacity of the IF-MoS_2 to form tribofilms on the surfaces at ambient temperature (**Figure 5.3**). Main Mo $3d_{5/2}$ and S $2p_{3/2}$ energy peaks corresponding to Mo – S species were found at 229.3 eV and 161.1 eV respectively, revealing the presence of an MoS_2 tribofilm on the surface. The composition of the surface of this tribofilm was however somewhat different than after the tests carried out at 80°C (***3. 3. 3. Tribofilm analysis***, p.67), with more intense energy peaks found for the Mo – O and S – O species (Mo $3d_{5/2}$ at 232.6 eV and S $2p_{3/2}$ at 168.8 eV respectively). This could imply that either the test temperature or the milder contact conditions were sufficient to form a protective intermediate tribofilm layer (such as the one visible on the FIB cross-sections on p.72), but not

severe enough to induce an effective adhesion of parallel MoS_2 nano-sheets (providing low friction) on top of this intermediate layer.

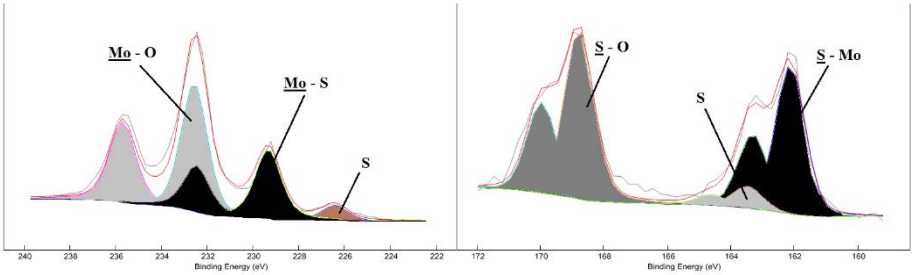

Figure 5.3. Mo 3d (left) and S 2p (right) energy peaks found after XPS analysis on the wear scar after HFRR testing for the PAO+1wt% SpC IF-MoS_2 blend at ambient temperature

This was confirmed by comparing the XPS profiles carried out on the wear scar for the PAO + 1wt% SpC IF-MoS_2 tested at 80°C (**Figure 4.10**, p. 90) with profiles acquired on the wear scar for the same blend tested at 30°C (**Figure 5.4**).

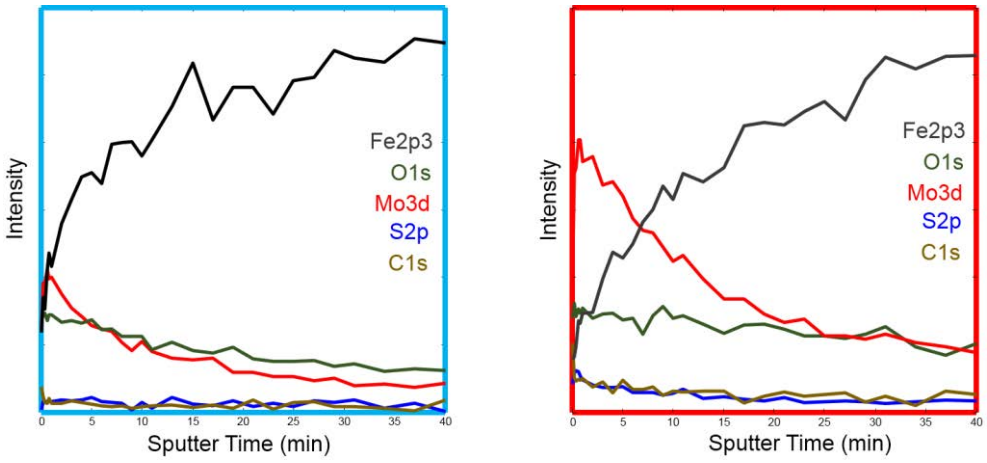

Figure 5.4. Ion etching profiles by XPS of the wear surfaces resulting from the testing of the PAO + 1wt% SpC IF-MoS2 at 30°C (left) and 80°C (right)

The intensity of the Mo 3d profile was found to be much closer to that of the O 1s profile in the early stages of the sputtering, indicating a more oxidized tribofilm. Although the precise thicknesses of the tribofilms are difficult to estimate from these analyses given their thinness and the approximate precision of the sputter rate, the tribofilm formed at 30°C seemed thinner due to a more rapid decrease of the intensity of the Mo 3d profile relative to Fe 2p3 in the same etching conditions. Sulfur, which presented a low profile intensity even in the case of a thick, homogeneous tribofilm at 80°C was not detected during the measurement of the profiles for the test carried out at 30°C.

These results indicate that the tribofilm formed under ambient temperature (all other test conditions being identical) was thinner than the one formed at 80°C, and contained more oxide species. This is in accordance with the tribofilm formation of MoDTC, as reported in the literature [17].

To verify the influence of temperature on the tribofilm-forming capacity of IF-MoS_2 nanoparticles regardless of viscosity, extra HFRR tests were carried out with two different PAO base oils. The first one was the PAO 4 and PAO 40 blend used in this study so far (9.3 cSt at 100°C and 54.0 cSt at 40°C), and the other was a PAO 2 (theoretical viscosity of 1.7 cSt at 100°C and 5.1

cSt at 40°C). Both base oils were then tested on the HFRR in the same conditions as previously except for the temperature (117°C and 30°C for the PAO 4/40 and PAO 2 respectively), leading to an identical theoretical viscosity of 6.7 cSt for both oils. Given this very low viscosity, both base oils produced very high friction coefficient when tested alone. The addition of 1 wt% SpC IF-MoS_2 produced significant friction reduction in both cases, with friction coefficients dropping from approximately 0.355 (base oil alone) to 0.075 (with the IF-MoS_2) at the end of the test (**Figure 5.5**). Wear reduction was also substantial in both cases, confirming the potential of IF-MoS_2 nanoparticles at ambient temperature for severe boundary lubrication regimes (**Figure 5.6**).

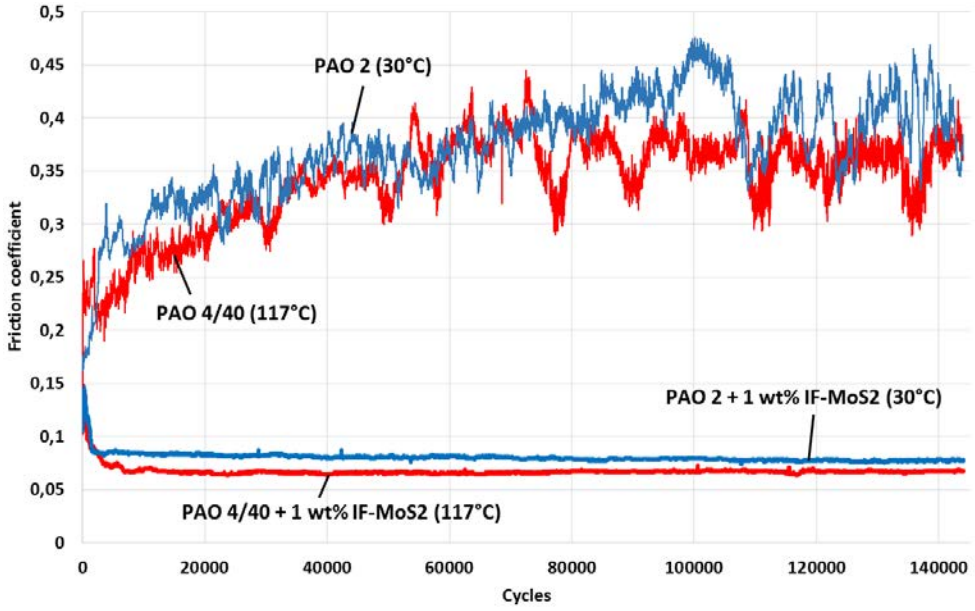

Figure 5.5. HFRR testing of PAO 2 at 30°C (blue) and PAO 4/40 at 117°C (red) with and without 1 wt% SpC IF-MoS_2

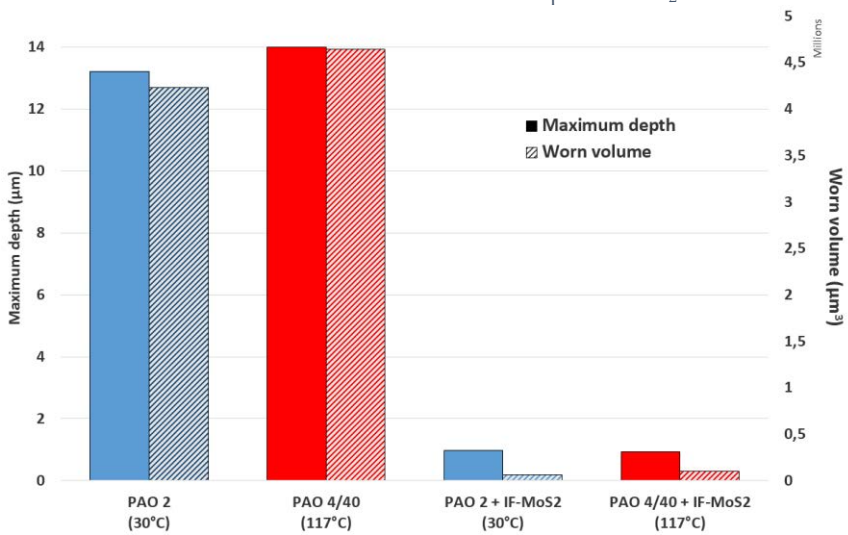

Figure 5.6. Maximum depth and worn volume of the wear scars after the HFRR tests shown on **Figure 5.5**

Although the friction coefficients for both base oils containing 1 wt% IF-MoS_2 were fairly similar at the end of each test, the friction reduction was slightly greater for the PAO4/40 tested at 117°C throughout the test (0.07 instead of 0.085 on average). This could be due to a slight difference in viscosity between both oils at the chosen temperatures or to thermal effects unrelated to the use of the nanoparticles, as the PAO 2 also produced a slightly higher friction coefficient than the PAO 4/40 throughout the test when tested alone. A precise measurement of the

viscosities of these base oils at 30°C (for the PAO 2) and 117°C (for the PAO 4/40) would be needed to confirm this hypothesis. The test temperature may also have had an influence on the composition of the tribofilm, modifying its tribological properties. To verify this, XPS analyses were carried out on the two wear scars resulting from the testing of the PAO 2 and the PAO 4/40 with 1 wt% IF-MoS_2. The main Mo 3d and S 2p spectra for both measurements are shown on **Figure 5.7**. Both tribofilms showed similar compositions, with high-intensity Mo – S energy peaks revealing MoS_2 tribofilms similar to those formed at 80°C with the PAO 4/40 base oil used throughout this work (showed in ***3. 3. 3***).

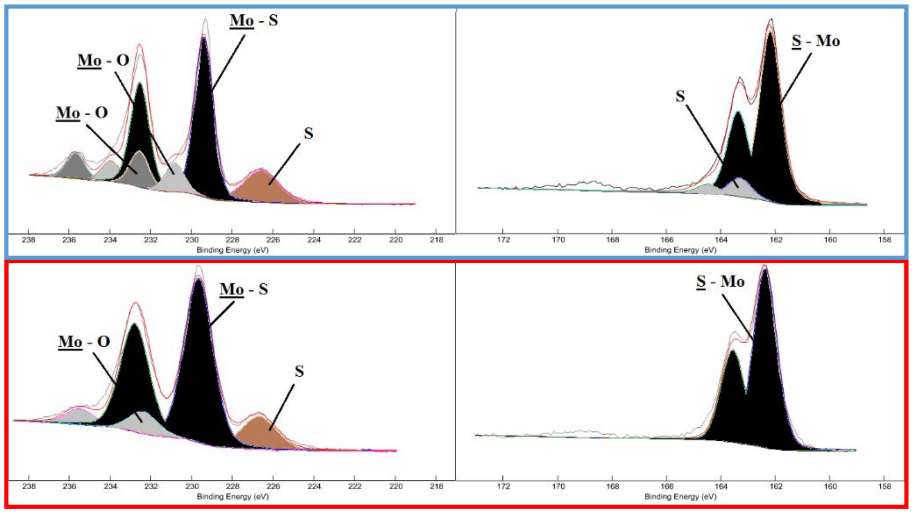

Figure 5.7. Mo 3d (left) and S 2p (right) spectra measured on the wear scars of the PAO2+IF-MoS_2 test carried out at 30°C (top) and the PAO4/40+IF-MoS_2 test carried out at 117°C (bottom)

These analyses show that IF-MoS_2 are effective in forming friction-reducing MoS_2 tribofilms regardless of temperature, as long as the contact undergoes severe boundary lubrication. This characteristic is a significant advantage over most friction-reducing additives, which require thermal activation to be fully effective. The test carried out at 30°C with the PAO 4/40 base oil however revealed that tribofilm formation is altered when surface separation is increased, reducing the tribological potential of IF-MoS_2-doped base oils. The objective of the next section is to estimate whether or not these additives can be beneficial under milder contact conditions.

5. 2. 2. Mixed lubrication: behavior in rolling-sliding conditions

All the tribological tests presented in this study so far were carried out in pure-sliding conditions with a high contact pressure, leading to severe boundary lubrication. If the friction and wear reducing properties of IF-MoS_2 nanoparticles were already known in these conditions, their behavior in milder contact conditions and when partial rolling takes place in the contact is vital prior to their use in automotive lubricants.

In order to cover a wide range of operating conditions, a series of Stribeck curves were plotted for different Slide-to-Roll Ratios (SRRs) on the Mini-Traction Machine (MTM). The lubricant consisted of the same PAO4/40 base oil as for the rest of this work, with and without 1 wt% of LC IF-MoS_2 (**Table 3.1**, p.54). Both specimens used (ball and disc) were smooth, with measured Rq roughness parameters between 1 and 4 nm on the disc.

For the testing of the PAO base oil alone, two Stribeck curves (rolling velocity decreasing from 2 $m.s^{-1}$ to 0.02 $m.s^{-1}$ to delay surface alteration at low velocities) were plotted. A running-in period of 30 minutes was carried out between the two Stribeck curves, at minimum rolling velocity (0.02 $m.s^{-1}$) and with the same SRR than for the rest of the test. When in the presence of IF-MoS_2 nanoparticles, the first step (initial Stribeck curve) was skipped in order to avoid centrifugation of the IF-MoS_2 at high velocities which would modify the feeding of the contact in IF-MoS_2 for the rest of the test. The final Stribeck curve was plotted for increasing velocities from 0.02 $m.s^{-1}$ to 2 $m.s^{-1}$ for the same reason.

A temperature of 80°C and a contact pressure of 1.4 GPa (load of 45 N) were chosen for all the tests, as these conditions are representative of automotive applications and similar to those used for the HFRR tests reported throughout this work. The theoretical central film thickness (see **Appendix B**) is identical for all SRRs and varies from approximately 0.12 μm to 5 nm for rolling velocities ranging from 2 $m.s^{-1}$ to 0.02 $m.s^{-1}$. Considering the initial surface roughness, these conditions lead to film thickness ratios varying from λ=28 to λ=1. A transition between the full-film and mixed lubrication regime should therefore take place during these tests.

Step	Description	Temperature (°C)	Contact Pressure (GPa)	Rolling Velocity ($m.s^{-1}$)	SRR (%)	Duration (min)
1 *	*Stribeck curve*	**80**	**1.4**	**$2 > V_R > 0.02$**	***x*** **	-
2	*Running-in*			**0.02**	***x*** **	**30**
3	*Stribeck curve*			**$2 > V_R > 0.02$**	***x*** **	-
** this step was skipped for the testing of the PAO containing the IF-MoS_2*						
*** these steps were repeated for SRRs of 10, 20, 30, 40 and 50%*						

Table 5.1. MTM test procedure for the evaluation of the potential of IF-MoS_2 nanoparticles in mixed lubrication

The five Stribeck curves obtained for the different SRRs (ranging from 10 to 50%) can be plotted as a surface, representing the friction coefficient as a function of the rolling velocity and the SRR. The resulting maps are shown on **Figure 5.8**.

Typical surface topographies and surface profiles obtained at the end of the tests for low (10%) and high (50%) SRRs are furthermore shown on **Figure 5.9** to account for the wear suffered by the discs during these tests. The Rq roughness parameter was determined for these profiles, taking into account only the width of the wear scar.

At the beginning of the test, the PAO produced very typical Stribeck curves (**Figure 5.8**(a)): the friction coefficient decreased steadily for rolling velocities ranging from 2.0 $m.s^{-1}$ to approximately 0.3 $m.s^{-1}$ (full-film lubrication), before rising abruptly for lower velocities (mixed lubrication). The transition between these two regimes appeared at slightly higher velocities for higher SRRs, most probably due to film thinning caused by local thermal effects and/or to an increased deterioration of the surface roughness. The friction coefficient was higher for the higher SRRs over the whole range of velocities covered, due to the increased shearing of the oil film in the HD regime and of the surfaces in mixed lubrication.

After the running period with the base oil alone (**Figure 5.8**(b)), the friction coefficients were very similar to the initial measurements in the full-film lubrication regime. The wear of the surfaces (**Figure 5.9** (A1) and (A2)) may indeed have induced slight changes in the contact pressure, but the contact conditions were otherwise identical. The friction coefficients recorded in the mixed lubrication regime were however somewhat larger than before running-in for the higher SRRs. This

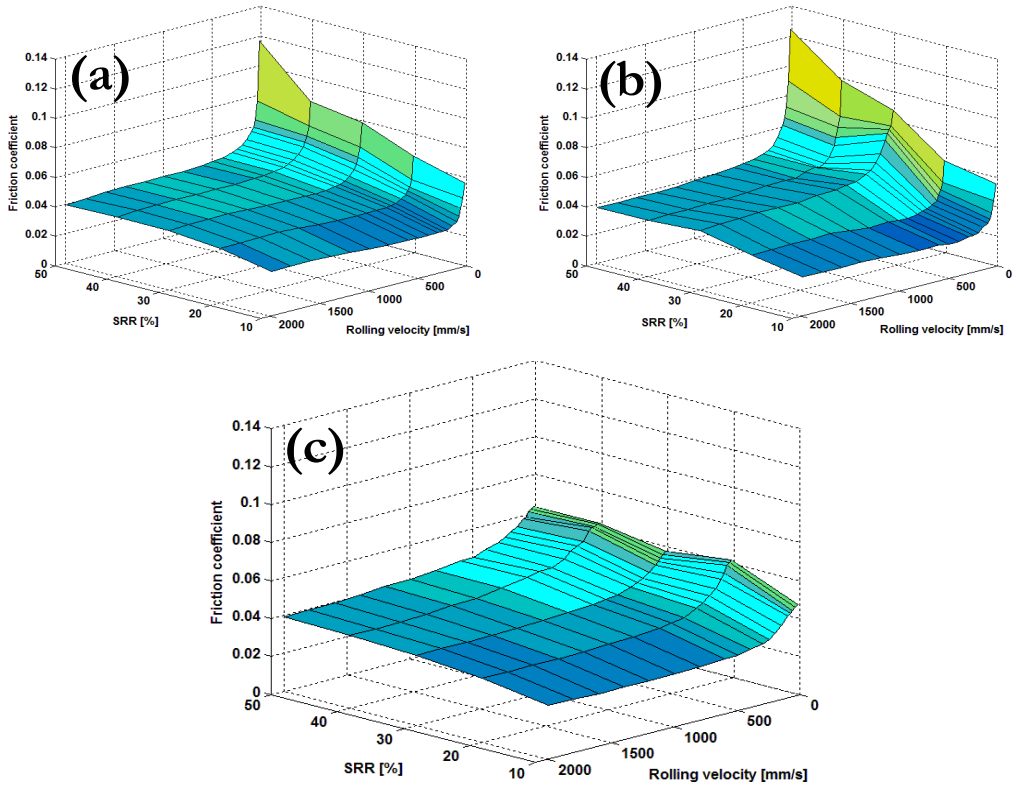

Figure 5.8. Mapping of the Stribeck curves depicting the influence of IF-MoS_2 on friction in mixed lubrication
(a) PAO alone before running-in;
(b) PAO alone after running-in;
(c) PAO + IF-MoS_2 after running-in

can be explained by a larger damaging of the wear surfaces under high slip, revealed by the deeper and, more importantly, rougher grooves than for low SRRs. At 50% SRR for instance, the roughness (Rq parameter) of the surface was indeed increased by ten, with a final roughness of the wear scar of approximately 50 nm.

In the presence of 1 wt% of IF-MoS_2 nanoparticles, the final Stribeck curves revealed a behavior identical to the initial curve for the PAO in the full-film lubrication regime. Friction coefficients were however greatly reduced in the mixed lubrication regime, with final values comprised between 0.045 and 0.065 for all SRRs. This result implies that the IF-MoS_2 were successful in forming an effective tribofilm on the surfaces, even under milder contact conditions with as little as 10% SRR. Once formed, this tribofilm provided greater friction reduction for the higher Slide-to-Roll Ratios. For the minimum rolling velocity tested (0.02 $m.s^{-1}$), the reduction was of 16% (from 0.057 to 0.048) at 10% SRR and 46% (from 0.117 to 0.063) at 50% SRR compared to the initial set of Stribeck curves (measured before running-in). This is furthermore consistent with the results obtained on the HFRR with an identical mean velocity but pure sliding (200 % SRR), where the order of magnitude of the friction reduction approached 70% (from 0.2 to 0.06). The maximum friction coefficients obtained for the higher SRRs (40% and 50%) were nearly identical, with values of 0.064 and 0.063 respectively. This friction coefficient is very close to the one obtained for pure sliding on the HFRR, which would suggest that MoS_2 tribofilms resulting from the use of IF-MoS_2 nanoparticles provide a limit to the friction coefficient achievable for a given set of operating conditions, regardless of the amount of shear in the contact. This limit seems

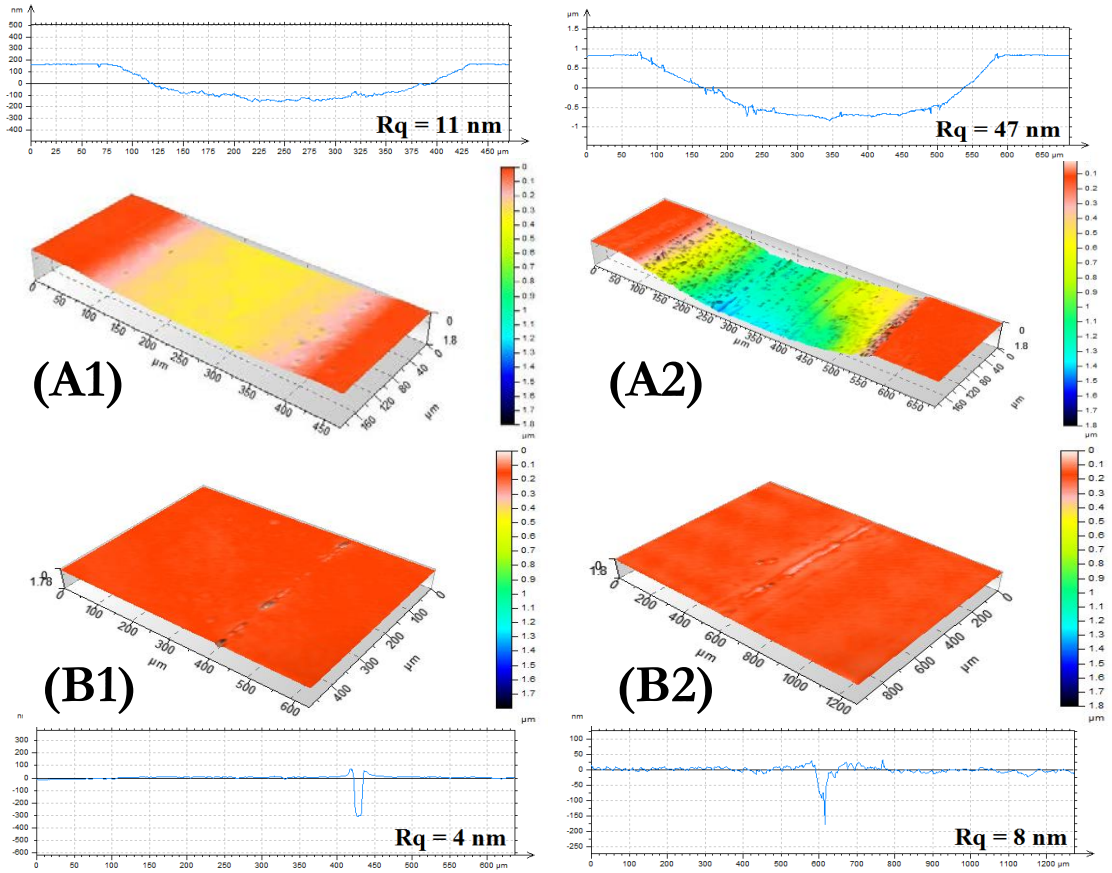

Figure 5.9. Typical surface topographies and profiles obtained at 10% (1) and 50% (2) SRR for the PAO alone (A) and the PAO + IF-MoS_2 (B). Rq values were determined taking into account only the wear scar.

to be obtained for SRRs as low as 40%, over which friction remains constant as long as the tribofilm is unharmed.

The presence of IF-MoS_2 nanoparticles also provided great wear reduction, as the surfaces were mostly undamaged at the end of the tests for all SRRs tested. The wear scars exhibited a single, shallow groove to the most (the images shown on **Figure 5.9**(B1) and (B2) picture the most damaged zones of their respective wear scars). The average surface roughness Rq was furthermore only slightly altered for the higher SRRs (8 nm for 50% SRR, measured outside the groove) and unscathed for lower Slide-to-Roll ratios.

For the operating conditions tested in this section, the use of IF-MoS_2 proved beneficial in the mixed lubrication regime and did not affect the behavior of the oil in full-film lubrication. There is however a true risk of contact starvation, and therefore of a drastic increase in friction and wear, linked to the presence of particles in the oil (see part ***1. 2. 4***, p. 33). Extra tests covering a wider range of contact conditions were carried out in the next section in order to further investigate this risk.

5. 2. 3. Full-film lubrication and associated risks

The presence of particles (soot, wear debris, external contaminants…) in engine or gearbox lubricant may lead to contact starvation and premature wear, as described in ***1. 2. 4. Particle contamination of lubricants and associated risks***. Although the nanoparticles studied in this

work are significantly smaller than most particle contaminants found in lubricants, their relatively high concentration in the oil and their tendency to agglomerate (when used without dispersants) constitutes a real risk for the surfaces. Despite providing great friction and wear reduction in boundary lubrication regimes, they would not be viable additives if they were to generate wear and power losses in milder contact conditions.

In order to investigate the risks linked to the use of nanoparticle in full-film lubrication regimes, a series of MTM tests were carried out for a variety of operating conditions. All tests were carried out with the PAO base oil alone, and repeated for the PAO + 1 wt% IF-MoS_2 (LC type, averaging 350 nm in diameter). The specimens had smooth surfaces during all tests.

Traction (varying SRR) and Stribeck (varying rolling velocity) curves were plotted for different temperatures (30°C and 80°C), contact pressures (0.73, 1.01 and 1.53 GPa), rolling velocities (traction curves measured at 0.2 and 1 $m.s^{-1}$) and Slide-to-Roll Ratios (Stribeck curves measured at 10% and 20% SRR). All traction curves had an SRR varying from 0% to 30%, while the rolling velocity ranged from 0.2 $m.s^{1}$ to 2 $m.s^{-1}$ for the Stribeck curves. These operating conditions led to a wide spectrum of film thicknesses, as reported in **Table 5.2**. The smallest theoretical central film thickness during these tests was 25 nm (for 1.53 GPa, 0.2 $m.s^{-1}$ and 80°C), resulting in a film thickness ratio λ of 3.5 (assuming a surface roughness Rq=5 nm) and a surface separation approximately 14 times smaller than the diameter of the nanoparticles. The largest central film thickness was 550 nm (0.73 GPa, 2 $m.s^{-1}$ and 30°C), which is larger than individual nanoparticles and ensures a λ ratio over 75.

Temperature	**30°C**		**80°C**	
Rolling velocity **Contact pressure**	**0.2 $m.s^{-1}$**	**2 $m.s^{-1}$**	**0.2 $m.s^{-1}$**	**2 $m.s^{-1}$**
0.73 GPa	118 nm	550 nm	29 nm	136 nm
1.01 GPa	110 nm	515 nm	27 nm	127 nm
1.53 GPa	101 nm	474 nm	25 nm	117 nm

Table 5.2. Theoretical central film thicknesses (Dowson-Higginson) for the different operating conditions used

In the absence of IF-MoS_2 nanoparticles (dotted lines on **Figure 5.10**), the traction curves exhibited a very typical behavior. Increasing contact pressures lead to higher friction coefficients for all conditions tested. The reduction of the oil viscosity due to a higher lubricant temperature led to a drop in friction, as the viscous friction of the thinner oil film decreased. At 30°C, an increase of the rolling velocity from 0.2 $m.s^{-1}$ to 1 $m.s^{-1}$ led to a slight increase in friction as the oil film was thicker. At 80°C, however, the lower friction obtained at 1 $m.s^{-1}$ suggested that mixed lubrication was reached for a rolling velocity of 0.2 $m.s^{-1}$. This was confirmed by the Stribeck curves plotted in these conditions (**Figure 5.11**). At high temperature, a rise in friction was indeed observed under approximately 1 $m.s^{-1}$ for both contact pressures and SRRs tested, attesting of the transition from the full-film to the mixed lubrication regime. All Stribeck curves plotted for the PAO base oil alone also showed a very foreseeable behavior, with higher friction coefficients measured for higher SRRs and for the thicker oil films induced by lower temperatures or higher rolling velocities.

The presence of 1 wt% IF-MoS_2 in the base oil had little to no effect on the friction coefficient, as plotted in full lines on **Figure 5.10** and **Figure 5.11**. Identical traction and Stribeck curves were obtained under all contact conditions under 30°C and for most measurements points under 80°C. A slight increase in friction was noticed for the higher SRRs under thin film conditions (rolling

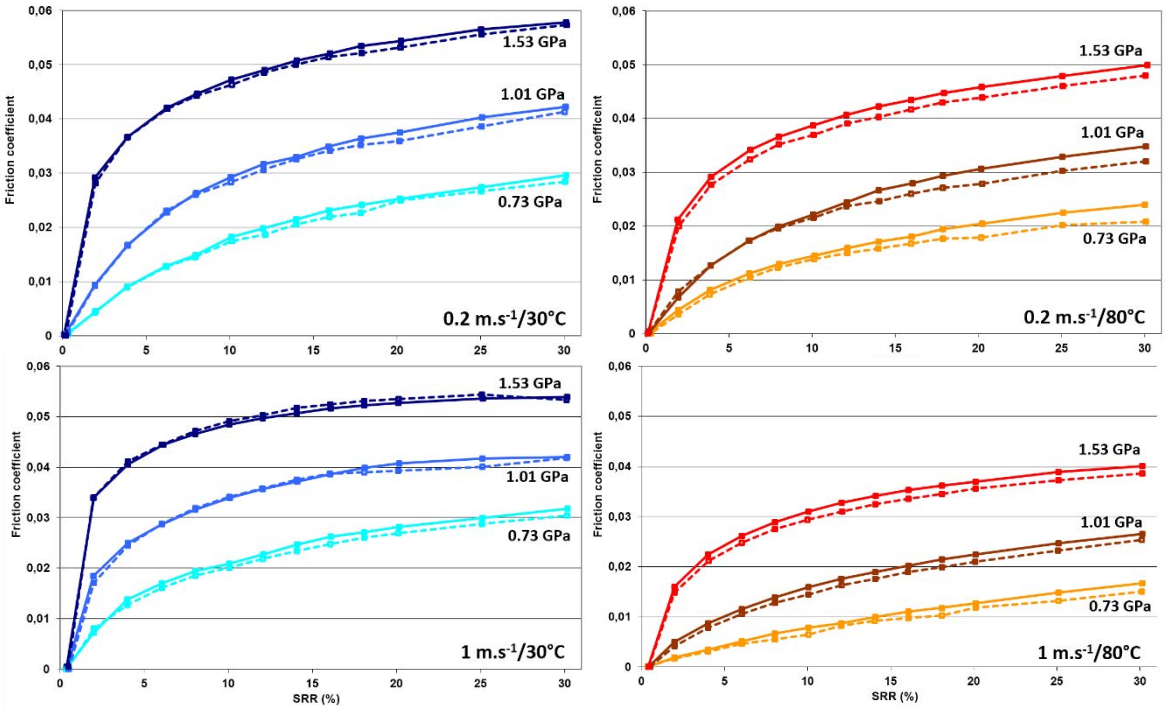

Figure 5.10. Traction curves in full-film lubrication conditions: PAO base oil (dotted lines) and PAO + IF-MoS_2 (full lines), tests at 30°C (blue, left) and 80°C (yellow/red, right), 0.2 m.s^{-1} (top) and 2 m.s^{-1} (bottom)

velocity of 0.2 m.s^{-1}). No wear was recorded on the discs after the testing of both blends, although the surface roughness was slightly altered by the transition in the mixed lubrication regime (Rq averaging 10 nm in the wear scar).

From these tests, IF-MoS_2 appear to be harmless in full-film lubrication regimes. Further testing for broader contact conditions and/or numerical simulations would be needed to extend this claim. Specific attention should furthermore be given to the case of very thin films with high

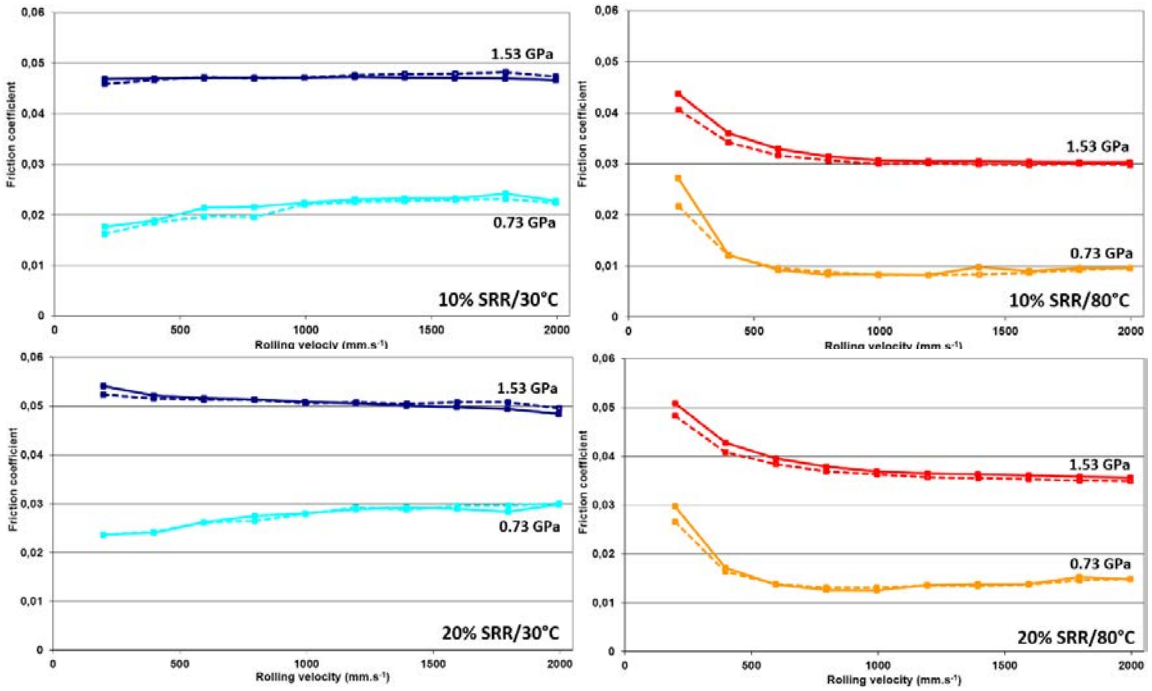

Figure 5.11. Stribeck curves in full-film lubrication conditions: PAO base oil (dotted lines) and PAO + IF-MoS2 (full lines), tests at 30°C (blue, left) and 80°C (yellow/red, right), 10% SRR (top) and 20% SRR (bottom)

Slide-to-Roll ratios, as it appeared to be more at risk with a slight raise in friction during these tests. Endurance tests could for example be performed, by maintaining stable conditions for an extended duration to verify that nanoparticle agglomeration at contact entry does not appear in time. This type of test could however prove difficult to perform on an MTM as the rotation of the disc may induce centrifugal effects on the IF-MoS_2 and their potential agglomerates, leading them away from the contact.

While particle agglomeration at contact entry leads to oil starvation in the case of contaminants such as soot and wear debris, the resulting effect might not be as detrimental in the case of IF-MoS_2. The results showed in the previous section (***5. 2. 2. Mixed lubrication: behavior in rolling-sliding conditions***) indeed show that tribofilm formation can also occur in the case of severe rolling/sliding conditions. Oil starvation due to the agglomeration of IF-MoS_2 at contact entry in full-film lubrication regimes may therefore lead to nanoparticle entrapment and exfoliation. In the case where the use of nanoparticles would be found to induce oil starvation in a number of engine or gearbox contacts, their use might therefore not be abandoned altogether.

5. 3. Real-life applications

5. 3. 1. Rough surfaces

Surfaces as smooth as those studied in this work so far are rare in real-life applications. Although they may be found in specific components such as bearings, many surfaces operating in severe lubrication regimes (where the use of IF-MoS_2 might hold an interest) have a non-negligible roughness. In order to investigate the performance of nanoparticle-doped lubricants in these conditions, a series of tests was carried out on the MTM with rough discs using the same operating conditions as presented in part ***5. 2. 2*** (**Table 5.1**, p. 107). The initial surface roughness of the discs is showed on **Figure 5.12**. All discs had an Rq roughness parameter between 0.11 and 0.15 µm, with an average of 0.13. Considering a surface roughness of Rq = 5 nm for the (smooth) ball, the chosen operating conditions lead to a maximum lambda ratio of 1, which was its lowest value in the presence of smooth surfaces (part ***5. 2. 2***). The initial surface roughness should therefore lead

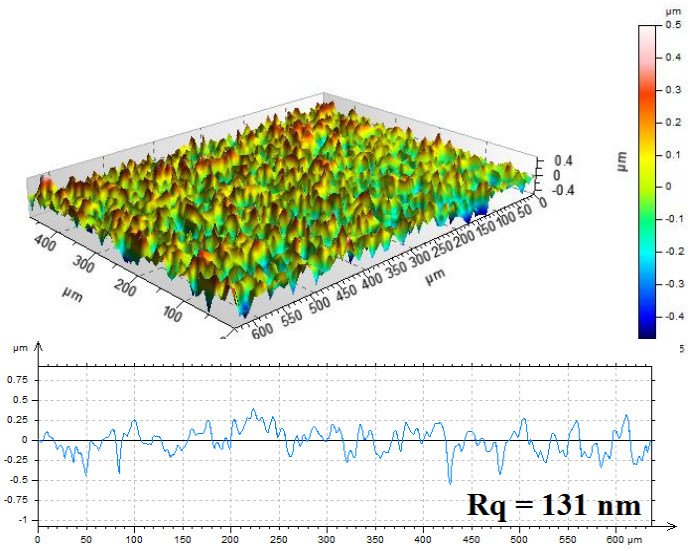

Figure 5.12. Surface topography and profile for rough MTM discs

to mixed/boundary lubrication during the measurements of the first Stribeck curves (before running-in).

This was confirmed during the testing of the PAO base oil alone, as reported on **Figure 5.13**(a). The friction coefficient measured for all SRRs at the beginning of the test was much higher than for smooth surfaces (**Figure 5.8**(a)) for all the conditions tested, and barely reached values smaller than 0.1 for the highest velocities. At low SRR, the friction coefficient increased progressively as the lubrication regime became more severe for lower rolling velocities. The friction coefficient did not change noticeably for decreasing velocities until approximately 0.5 $m.s^{-1}$ for the higher SRRs (40% and 50%), which may be due to a progressive decrease in surface roughness due to wear during the first stages of the test. Under 0.5 $m.s^{-1}$, the thinning of the oil film led to drastic increases in friction for all SRRs. The highest friction coefficients were obtained at the lowest velocity for all tests (0.02 $m.s^{-1}$) and had similar values (0.15 - 0.16) for SRRs ranging from 20% to 50%. A higher value (0.18) was however recorded for the test carried out at 10%. This could confirm that more wear took place at higher SRR, resulting in lower film thickness ratios (due to a reduced surface roughness) and therefore milder contact conditions.

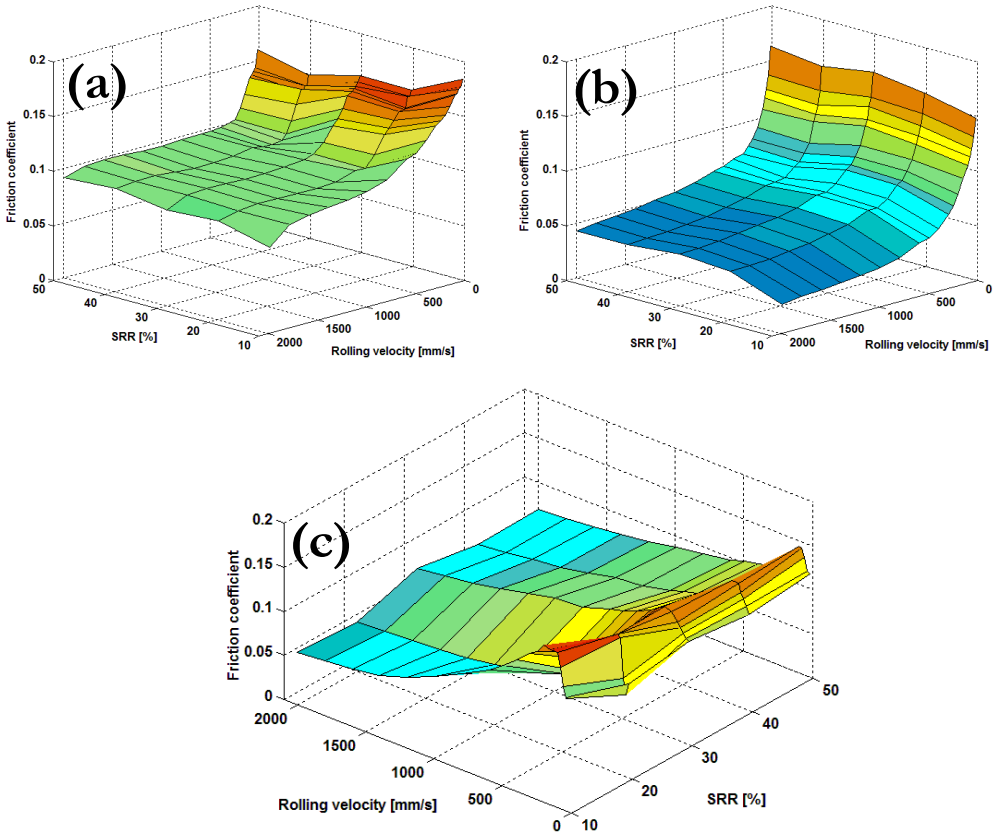

Figure 5.13. Mapping of the Stribeck curves depicting the influence of IF-MoS_2 in the presence of rough surfaces (a) PAO alone before running-in; (b) PAO alone after running-in; (c) PAO + IF-MoS_2 after running-in

After the running-in period, the friction coefficients for the PAO base alone at high velocities (over 1.5 $m.s^{-1}$) were very similar to the measurements carried out for the same test but with smooth surfaces. Their values were indeed under 0.05, attesting of full-film lubrication. The transition to mixed lubrication then took place for velocities under 1.5 $m.s^{-1}$ on average, and the friction coefficients then increased significantly until reaching their maximum values for the lowest rolling velocities. These maximum friction coefficients were similar before and after running-in for SRRs

ranging from 20 to 50%, which suggests that most of the wear took place during the measurement of the initial Stribeck curve (before running-in). The final maximum friction coefficient at 10% SRR, on the other hand, was significantly lower than before running-in, implying that the surface roughness was mostly modified during the running-in period.

The topographies and surface profiles of the final wear scars for the testing of the PAO base oil alone at 10% and 50% SRR are shown on **Figure 5.14**(A1) and (A2). A large amount of wear was observed in both cases, with a much deeper wear track at high SRR. This resulted in the reduction of the surface roughness inside the track with Rq values of 23 nm and 42 nm for 10% and 50% SRR respectively. These smoother surfaces are consistent with the final Stribeck curves (after running-in), which displayed a delayed transition from the full-film to the mixed lubrication regimes.

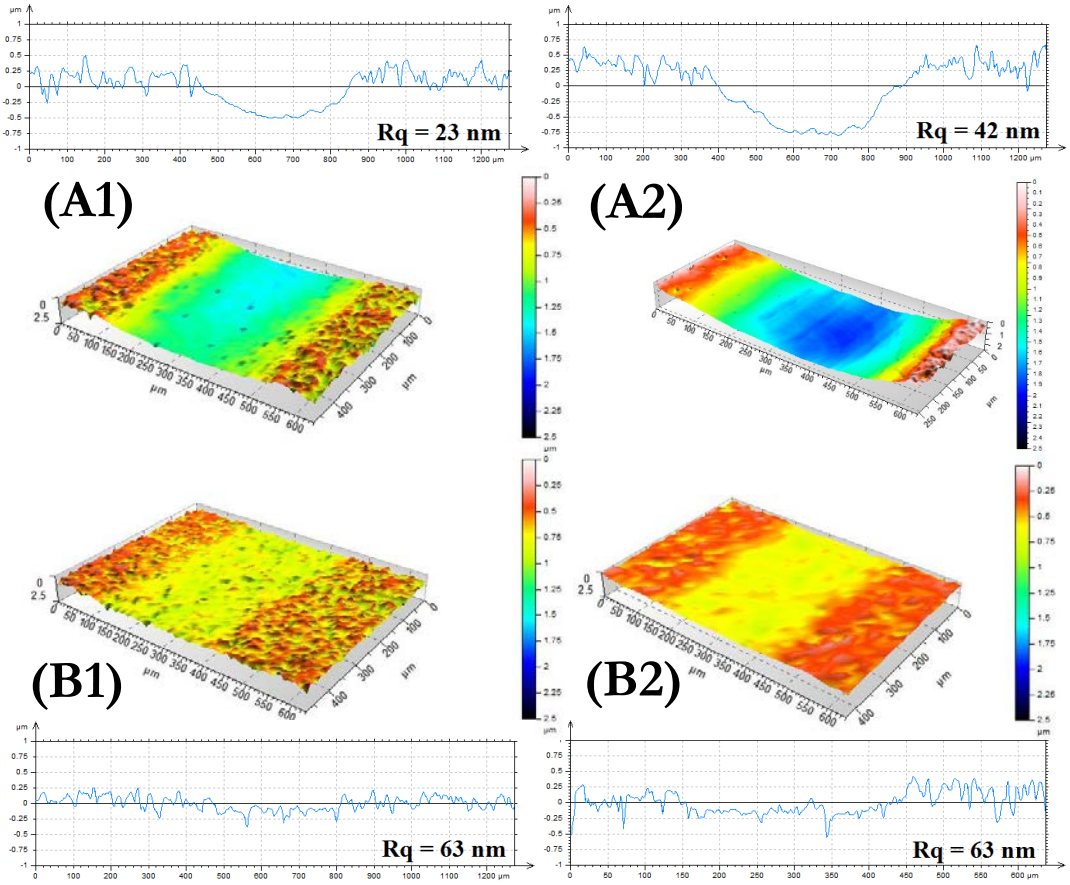

Figure 5.14. Typical surface topographies and profiles obtained at 10% (1) and 50% (2) SRR for the PAO alone (A) and the PAO + IF-MoS_2 (B). Rq values were determined taking into account only the wear scar.

After the running-in period, the oil containing 1 wt% IF-MoS_2 produced friction coefficients comparable to the PAO alone at 2 $m.s^{-1}$. The transition from full-film lubrication to mixed lubrication however seemed to occur for higher velocities, with friction coefficients increasing for velocities under 2 $m.s^{-1}$. This behavior indicates that the surface roughness was reduced during the running-in, but not as much as for the PAO base oil alone. This was confirmed by the observations of the wear scars at 10% and 50% SRR (**Figure 5.14**(B1) and (B2)), which showed barely distinguishable grooves and Rq parameters of 63 nm inside the contact area.

All Stribeck curves plotted for the PAO+IF-MoS_2 had similar trends, with a maximum friction coefficient measured between 0.08 and 0.2 $m.s^{-1}$ depending on the SRR. Friction then decreased

drastically for lower speeds as severe boundary lubrication was reached. Compared to the initial set of Stribeck curves plotted for the PAO base oil alone, the friction coefficient measured for the PAO + IF-MoS_2 was lower for all the velocities tested except for a small range located on average between 0.2 and 0.5 $m.s^{-1}$. As mentioned previously, this may however be due to a premature wearing of the surface in the case of the base oil alone, leading to milder contact conditions.

Overall, tribofilm formation seemed to have taken place during the running-in period in the presence of IF-MoS_2, as the surfaces were only slightly altered at the end of test compared to the PAO base alone. Although this tribofilm proved effective in the most severe contact conditions tested, friction remained high in the early (least severe) stages of the mixed lubrication regime.

A sketch of the average Stribeck curves obtained for the four series of tests carried out on the MTM (PAO with and without IF-MoS_2 for smooth and rough surfaces) is shown on **Figure 5.15**. The behaviors of the initial curves (before running-in) of the tests with the base oil alone are drawn along with those of the final curves (after running-in) of the tests with the PAO + IF-MoS_2, in order to compare the influence of the MoS_2 tribofilm on friction for rough surfaces, as the wear polished the contact surface during the running-in with the PAO base oil alone. The respective positions of the red and blue curves (for rough surfaces) are given for a different surface roughness, as the surface was altered in the case of the PAO + IF-MoS_2 (most likely before tribofilm formation).

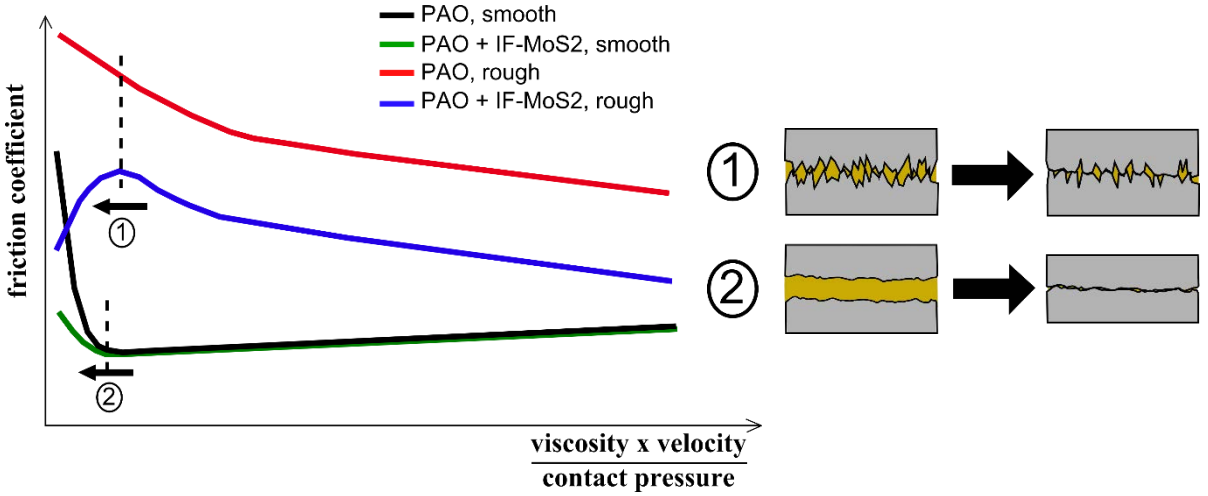

Figure 5.15. Representative Stribeck curves measured during the four series of tests on the MTM (left) and transitions between the different lubrication regimes (right)

Although all the operating conditions and surface roughnesses tested led to tribofilm formation during the running-in period, the IF-MoS_2 proved inefficient in terms of friction reduction for rough surfaces in the milder mixed lubrication regimes. A sudden change in behavior occurred for the lower velocities, when they became increasingly effective for the more severe contact conditions. This threshold may occur at the transition between the mixed and boundary lubrication regimes, when the thinning of the oil films allows for larger asperity deformation and more continuous metal-metal contacts (transition 1 on **Figure 5.15**). In the case of smooth surfaces, this transition is likely to occur faster for a given set of operating conditions as smaller asperity deformation is needed, which would explain why immediate friction reduction was obtained after the transition (2 on **Figure 5.15**) from the full-film lubrication regime.

For rough surfaces, the IF-MoS_2 did not provide friction reduction as important as for the

smooth surfaces tested previously. This should however be put on the account of excellent anti-wear properties, which helped to maintain significant surface roughness through a severe running-in period. Friction reduction was furthermore achieved in the most severe lubrication regime, which is consistent with the results obtained by Kalin et al [34] in the case of MoS_2 nanotubes. Contrarily to the IF-MoS_2, these nanotubes however also provided significant friction reduction in the mixed lubrication regime. The authors add that MoS_2 nanotubes were observed on the surfaces after testing, which could imply that their geometry favors their retention in the valleys of the surface roughness. This phenomenon would then be likely to accelerate the transition from the full-film to the boundary lubrication regime, explaining the different behaviors witnessed for the IF-MoS_2 and the MoS_2 nanotubes. Additional testing would however be needed to ascertain this hypothesis.

5. 3. 2. Potential for components subject to fatigue

Rolling Contact Fatigue (RCF) is a common failure mode for repeatedly loaded components under high contact pressures, such as roller bearings or gears. Surface deterioration due to RCF is a three-step process: the cyclic loading first leads to crack initiation, which then propagates until it reaches the surface. A wear debris is then formed and ejected, forming a crater on the surface. These craters are alternatively referred to as "*spalls", "pits", "micropits"* or even *"flakes"* in the literature, as their definition has not been standardized. The nomenclature used in this work is (arguably) the most common, and has been proposed among others by Olver [88]:

- **spalling** refers to subsurface-initiated RCF;
- **pitting** refers to surface-initiated RCF;
- **micropitting** refers to the formation of shallow pits.

Subsurface-initiated cracking, leading to the formation of spalls, generally occurs in the maximum shear stress region. Cracks initiate at material heterogeneities such as porosity or small non-metallic inclusions (alumina, carbides…) [89]. Spalling is however becoming less of an issue nowadays, given the continuous improvement of steel cleanliness. Spalls are more commonly found in bearings, as they are loaded heavily and have relatively smooth surfaces.

The combined effects of surface roughness, repeated loading, and high Slide-to-Roll Ratios, on the other hand, favor the initiation of cracks at (or near) the surface in the case of gears. If the propagation of these cracks depends in part on the material properties [90], the lubricant has been shown to penetrate surface-related cracks [91] and impact their evolution [77]. The typical inclination of these cracks (20° - 30° depending on the SRR) usually leads to the apparition of shallow micropits, which may then precipitate the formation of larger and deeper pits [89].

In order to investigate the influence of nanoparticle-doped lubricants on RCF, comparative tests were carried out for the PAO 4/40 base oil alone and for a blend of the same PAO containing 1 wt% of SpC IF-MoS_2. The small IF-MoS_2 (average diameter of 150 nm) were chosen to test the possible influence of nanoparticle penetration inside the cracks. The tests were carried out by PowerTrib (test described in ***2. 2. 4***, p.46). They were set to run for 20 hours or to stop before completion in the case of large pit formation, detected through sudden variations in the acceleration signal. Although the PAO base oil provided a low friction coefficient (under 0.06) during the test,

the friction reduction when using IF-MoS_2 nanoparticles was significant enough to attest of tribofilm formation (**Figure 5.16**).

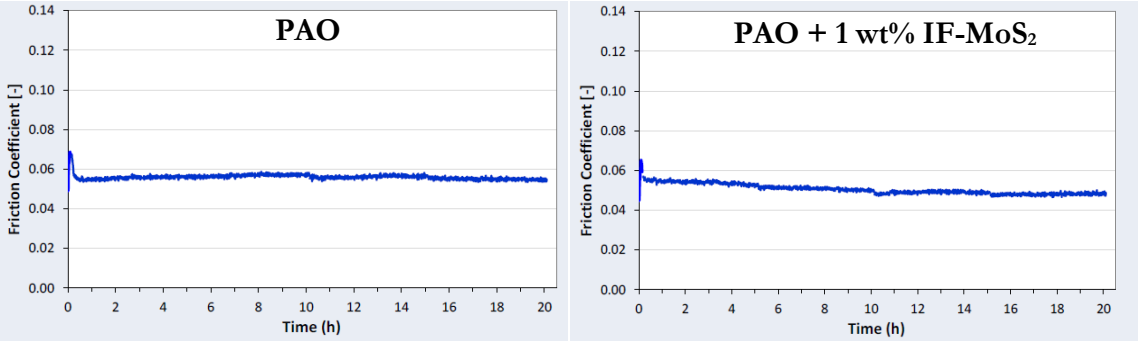

Figure 5.16. Evolution of the friction coefficients during the MPR testing of the PAO base oil alone (left) and the PAO containing 1 wt% IF-MoS_2 (right)

A typical image of the roller surfaces obtained for the PAO base oil alone (left) and the PAO + IF-MoS_2 (right) is shown on **Figure 5.18** for each monitoring step of the tests (2.5h, 5h, 10h, 15h and 20h). During the testing of the PAO alone, crack initiation sites were spotted after the 2.5 first hours and then progressively propagated during the test to finally form large micropits after 20 hours. Other initiation sites appeared throughout the test, and the final surface of the disc exhibited many micropits around its circumference.

The beginning of the test for the PAO + IF-MoS_2 was very similar, with a few crack initiation sites visible after 2.5 hours. The following monitoring steps however showed no visible evolution of the surface whatsoever, with no extra initiation sites nor propagation of the existing crack sites. Although such a site was purposely shown on **Figure 5.18**, few other sites were visible around the wear track.

3D images and surface profiles of the final surfaces for each lubricant are shown on **Figure 5.17**. The evolution of the cracking into a characteristic V-shaped micropit is clearly visible for the PAO alone, with a depth of approximately 10 µm. The micropit was confirmed to be at a much earlier stage in the case of the PAO + IF-MoS_2, with a reduced area and a maximum depth of 2 µm. The formation of an MoS_2 tribofilm on the surface in the early stages of the fatigue test may have prevented the apparition of new crack initiation sites after the first monitoring steps. A slight

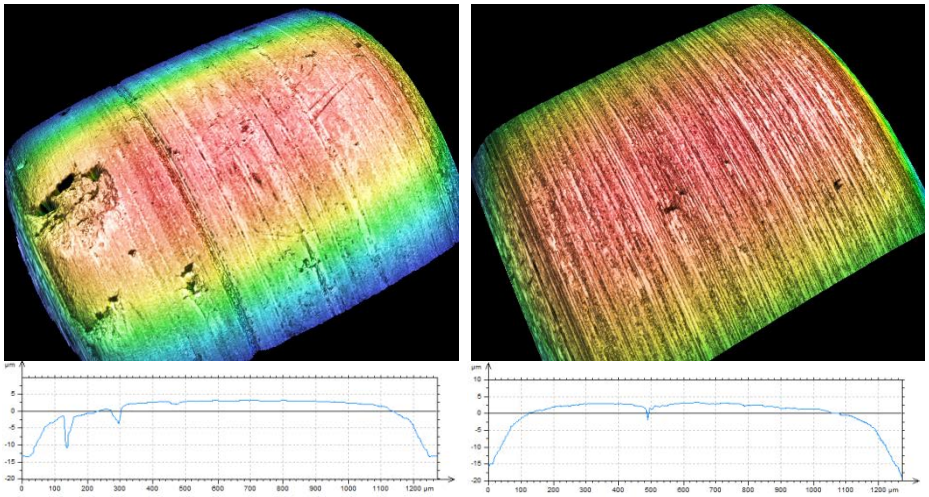

Figure 5.17. 3D topographies and profiles of the surfaces resulting from the MPR testing of the PAO (left) and PAO + 1 wt% IF-MoS_2 (right)

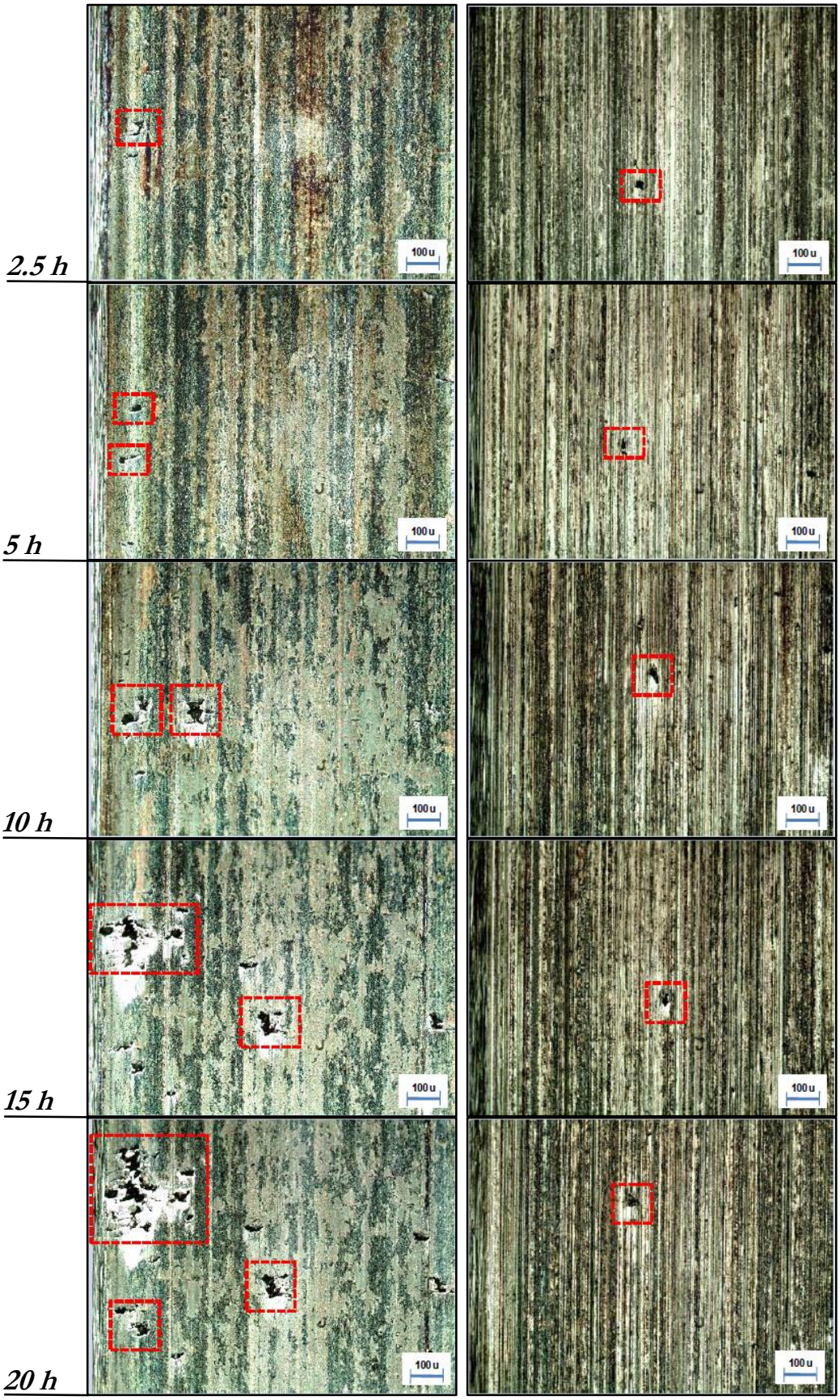

Figure 5.18. Typical images observed at each monitoring step of the MPR tests for the PAO base oil alone (left) and the nanoparticle-doped PAO (right)

but sudden decrease in friction was observed at the end of the first 3 hours of the test, which may correspond to the formation of this tribofilm.

The different stages of the test for the two lubricants were sketched on **Figure 5.19** according to this scenario. For the PAO base oil alone, the cyclic loading led to crack initiation and propagation, resulting in the formation of the large micropits observed previously. In the presence of IF-MoS_2, the tribofilm is thought to have formed after the initiation of the first few cracks at (or near) the surface. This tribofilm then seems to have prevented further crack initiation, by reducing the friction (and therefore shear stresses) between asperities and/or by being less brittle than steel. The tribofilm could therefore have remained undamaged where cracks would have initiated through the steel in the same conditions. The formation of this tribofilm over the existing initiation sites is furthermore likely to have prevented (or at least limited) lubricant seepage inside the cracks, which is thought to apply high hydraulic pressure on the crack lips and therefore to be responsible for the mode I propagation of surface-related cracks [77].

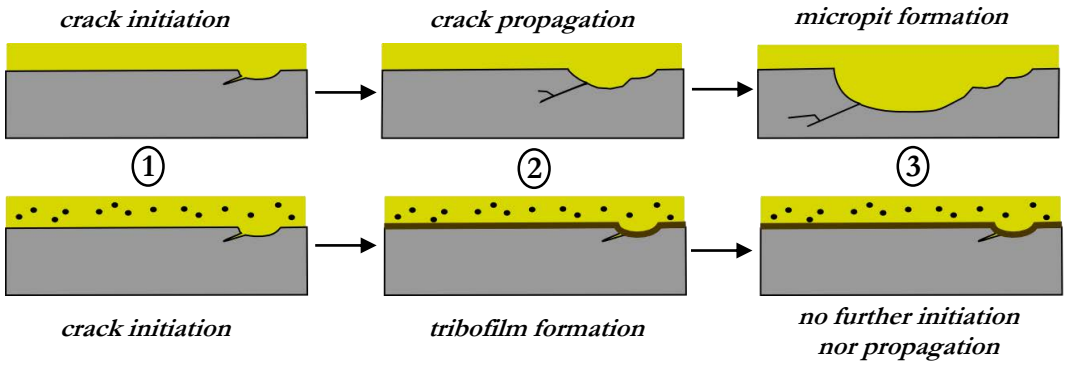

Figure 5.19. Possible stages of crack initiation and propagation for the PAO alone (top) and for the nanoparticle-doped PAO (bottom)

Cross-sections of both rollers were extracted with a cutoff wheel and observed by Scanning Electron Microscopy (SEM). For the specimen lubricated with the PAO alone, the many micropits found showed extensive crack propagation and branching (**Figure 5.21**). Cracks as long as 30 µm were found under the surface, suggesting that propagation was an ongoing process at the end of the experiment. Prolonged testing could therefore have led to the formation of larger and deeper pits.

Cross-sections of the roller lubricated with the nanoparticle-doped PAO exhibited very little cracking, and damaged sites proved difficult to find. A micropit very similar to the ones shown previously (**Figure 5.17** and **Figure 5.18**) is pictured on **Figure 5.20**. It is approximately 2 µm deep, and shows no sign of crack propagation. No other cracks were noticed on the roller, confirming that the presence of the IF-MoS_2 in the oil was effective in preventing crack initiation and propagation, increasing the resistance of the roller to RCF. The formation of the MoS_2 tribofilm at the surface is thought to be the main reason for this beneficial effect. Further experiments would be needed to fully understand the interactions of IF-MoS_2 with crack formation and propagation, such as closer observations of the cracks to determine if a tribofilm is formed inside the micropits or if the nanoparticles penetrate inside the freshly initiated cracks.

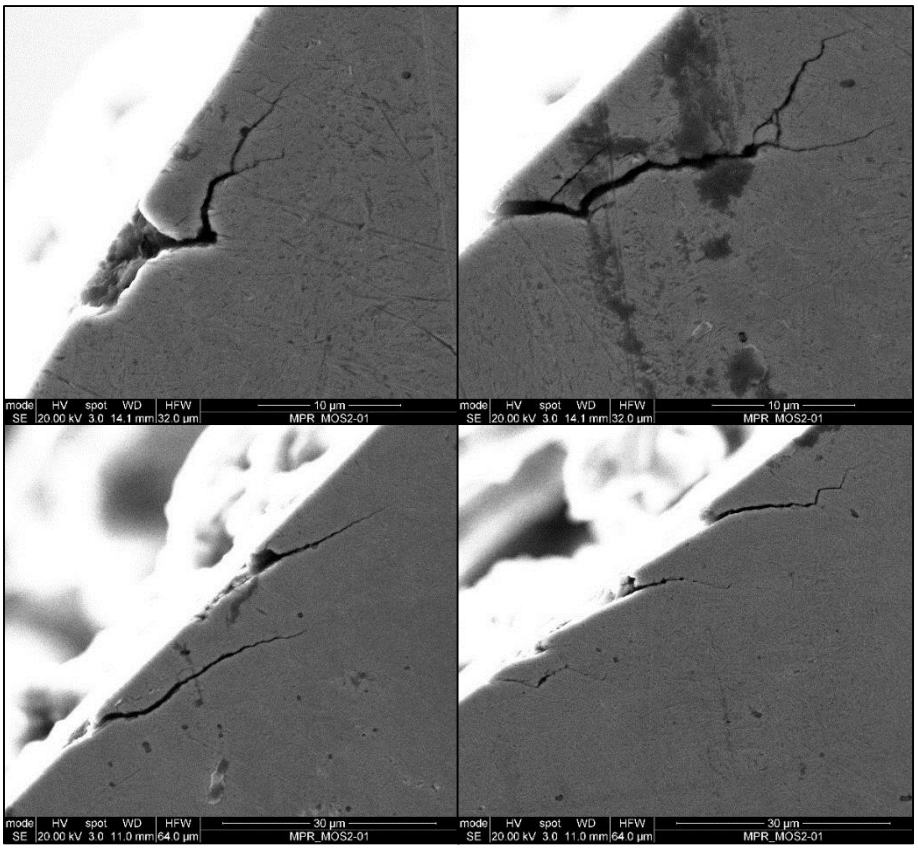

Figure 5.21. Cross-sections of the roller tested with the PAO base oil

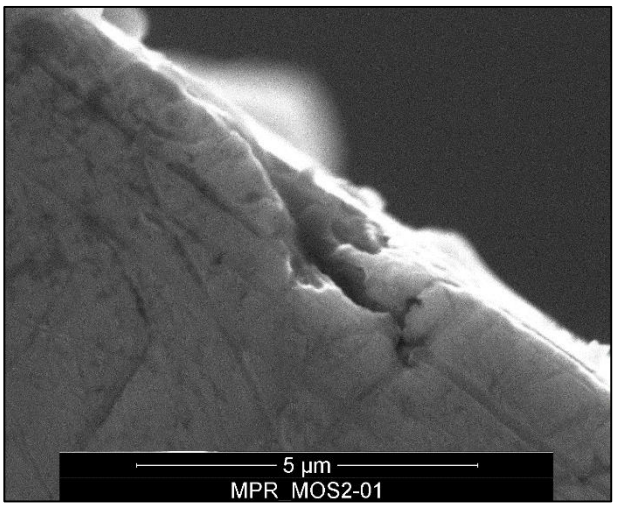

Figure 5.20. Cross-section of the roller tested with the PAO + 1 wt% IF-MoS_2

5. 4. Conclusions

After the investigations on nanoparticle morphology and interactions with dispersants presented in the two previous chapters, the aim of this final section was to provide the reader with some insight regarding the potential of IF-MoS_2 additives for automotive applications.

The IF-MoS_2 nanoparticle were first of all shown to be capable of forming efficient MoS_2 tribofilms on steel surfaces at ambient temperatures, as long as the contact still undergoes severe boundary lubrication despite the increase in oil viscosity. This proves to be a significant advantage over all current additives requiring thermal activation to be fully active.

The behavior of the IF-MoS_2 was then investigated in milder rolling/sliding conditions than the pure sliding used so far in this work. Tribofilm was shown to adhere to the surfaces and provide significant friction and wear reduction even for Slide-to-Roll Ratios as small as 10%. For a given mean surface velocity (0.02 $m.s^{-1}$), identical friction coefficients were furthermore measured at 40% SRR, 50% SRR and 200% SRR (on the HFRR). This suggests that IF-MoS_2 nanoparticles provide a maximum friction coefficient regardless of slip (for a given set of operating conditions), and that this threshold may be reached for SRRs as low as 40%.

The risks of contact starvation associated to the incorporation of nanoparticles in the oil in the full-film regime were furthermore evaluated by a series of tests covering a wide range of film thicknesses. The IF-MoS_2 appeared to be harmless in the conditions tested, although further testing and/or numerical simulations would be needed to generalize this claim.

The potential of IF-MoS_2 nanoparticles when confronted to rough surfaces was then studied. Great wear reduction was observed during the tests, again for SRRs as low as 10%. The preservation of the surface roughness however lead to more severe contact conditions after running-in (compared to the base oil alone), which was not beneficial in terms of friction in the mixed lubrication regime. For surfaces with comparable surface roughnesses, the IF-MoS_2 only provided significant friction reduction in the most severe conditions tested. This reduction in friction is thought to occur only in the boundary lubrication regime, when the deformation of the asperities is large enough to ensure continuous tribofilm-tribofilm contact between the surfaces.

The influence of IF-MoS_2 on the resistance of the surfaces to RCF was finally investigated. The addition of nanoparticles in the lubricant formulation greatly improved the fatigue life of the specimens. Only a few crack initiation sites were formed at the beginning of the test, and no subsequent crack initiation nor propagation were then noticed for further cycling. The formation of the MoS_2 tribofilm after the beginning of the test is thought to have prevented crack initiation altogether, and stopped the propagation of the existing cracks.

The results presented in this chapter show the extent of the potential of IF-MoS_2 for real-life applications, such as automotive engines or gearboxes. Their presence in future lubricants could improve vehicle efficiency and component lifespan, by reducing friction and wear in a number of contacts operating in various lubrication regimes.

Conclusions

The potential of Inorganic Fullerene-like molybdenum disulfide nanoparticles for automotive applications has been investigated throughout this work. Although many issues remain to be addressed, progress has been made regarding the understanding of these nanoscale additives and how they may significantly reduce friction and wear in different types of contacts.

A state of the art on nanoparticle lubrication was first of all exposed in **Chapter One**, depicting the various types of nanoparticles and their characteristics. Although nanoparticles of different nature have shown interesting tribological properties, Inorganic Fullerene-like metal dichalcogenides, and molybdenum disulfide in particular, stand out by their outstanding friction and wear reducing capacities in the most severe lubrication regimes. These nanoparticles have been shown to exfoliate when submitted to a sufficient amount of combined normal pressure and shear, liberating MoS_2 nanosheets inside the contact. These nanosheets are then thought to react chemically with the substrate, forming low-friction protective tribofilms on the rubbing surfaces. Despite the understanding of the main lubrication mechanism associated to nanoparticle lubrication, many uncertainties were found to remain before considering the incorporation of IF-MoS_2 in future automobile lubricants.

Chapter Two was dedicated to the presentation of the many experimental techniques and methodologies used during this study, with vital information for a full understanding of the results presented in chapters three to five. These chapters are each dedicated to one of the successive steps needed to formulate an efficient nanoparticle-doped lubricant for automotive applications, namely: the identification of the parameters governing the efficiency of the nanoparticles, the dispersion of these nanoparticles in the oil, and the resulting tribological potential for real-life applications.

The main objective of **Chapter Three** was to differentiate the respective influences of the size and structure of the fullerene-like nanoparticles on their tribological performance. To achieve this, four different types of IF-MoS_2 were synthesized and tested in severe boundary lubrication conditions. All the nanoparticles produced an identical maximum friction reduction, regardless of size or crystallinity. The less crystalline nanoparticles, both large and small, were however found to be more efficient as fewer are needed inside the contact to maintain a homogeneous and effective tribofilm. Observations and analyses of the formed tribofilms furthermore revealed two layers. The top, friction-reducing layer was found to contain high contents of molybdenum disulfide, with MoS_2 sheets oriented in the direction of sliding at the extreme surface. The intermediate layer, found between this top layer and the substrate, contained higher amounts of oxygen and possibly iron sulfides. This layer may therefore result from the presence of a native iron oxide layer on the sample, which may play an important role in the adhesion of the MoS_2 tribofilm on steel surfaces. The less efficient, more crystalline IF-MoS_2 were then found to match the performances of the less crystalline nanoparticles when proper oil recirculation was imposed, ensuring a permanent feeding of the contact in nanoparticles. This result may be of importance for industrial applications, as nanoparticle-doped lubricants could prove efficient in systems with sufficient oil recirculation even without achieving an ideal dispersion of the additives. For applications with minimal oil stirring, an optimal dispersion of the nanoparticles seems needed to ensure durable friction and wear

reduction. In both cases (sufficient oil recirculation or ideal dispersion of the nanoparticles), the size and structure of the IF-MoS_2 should have little to no effect on their tribological performance (in the ranges studied here). Succeeding in the synthesis of very small nanoparticles (under 50 nm in diameter) with perfectly engineered fullerene-like structures does therefore not seem of primary interest for industrial use. For identical mass concentrations, the benefits of using nanoscale particles over significantly larger microparticles was however shown.

Having witnessed the high tribological potential of the IF-MoS_2 when added to a base oil alone, their addition to a fully-formulated lubricant was tested in **Chapter Four**. This new formulation exhibited similar performances than the non-doped oil, and the lack of effectiveness of the IF-MoS_2 was shown to be – at least partly – due to the presence of dispersants in the lubricant. An experimental investigation was then carried out in order to understand how these additives prevented the nanoparticles from reducing friction and wear. The newly dispersed IF-MoS_2 were found to enter the contact and exfoliate, but failed in forming a tribofilm on the steel surfaces. This behavior was attributed to the adsorption of the dispersants on the exfoliated nanosheets and/or the friction surfaces, preventing a chemical bonding of the MoS_2 onto the substrate. A balance between nanoparticle dispersion and good tribological performance was finally found, but for dispersant concentrations much lower than commonly used in commercial lubricants. Once the nanoparticles dispersed, the lack of remaining dispersant molecules in the oil enables tribofilm adhesion. The lubricant is however then thought to lose its dispersing properties, which remains an issue for industrial applications. These results are nevertheless encouraging, as the dispersion of the nanoparticles was shown not to be responsible for their lack of efficiency. In other words, alternative dispersing agents or processes should succeed in dispersing the IF-MoS_2 while guaranteeing their efficiency, as optimally-dispersed nanoparticles are able to enter the contact and exfoliate.

The final chapter of this work, **Chapter Five**, was dedicated to exploring the potential of IF-MoS_2 nanoparticles in a wide range of scenarios related to automotive lubrication. These additives first of all formed highly efficient tribofilms on steel surfaces at ambient temperatures. The IF-MoS_2 were then shown to provide significant friction and wear reduction in relatively mild rolling-sliding conditions, even for Slide-to-Roll Ratios (SRRs) as low as 10%. For a given contact pressure, mean surface velocity and temperature, the nanoparticles moreover provided similar friction coefficients at 40%, 50% and 200% SRR. The friction resulting from MoS_2 tribofilms may therefore become independent of the amount of sliding occurring in the contact above a given threshold (40% SRR here). In similar test conditions, the nanoparticles greatly reduced wear in the case of rough surfaces. The preservation of the surface roughness was however detrimental in terms of friction in the milder conditions tested, as the transition from the full-film to the mixed lubrication regime occurred at higher velocities. Friction reduction was however observed for the lower velocities, when the boundary lubrication regime was thought to ensure a sufficiently continuous contact between the surfaces for the tribofilm to be efficient. The risks of contact starvation related to the presence of nanoparticles in the oil was furthermore investigated in the case of full-film lubrication, and no detrimental effect was found for the wide range of conditions considered. The high potential of IF-MoS_2 in increasing the resistance of components to Rolling Contact Fatigue (RCF) was finally shown. The fatigue life of the specimens was greatly improved when lubricated with nanoparticle-doped oil, which was attributed to the absence of crack initiation and propagation once the tribofilm had been formed on the surfaces.

This work shows the extent of the potential of IF-MoS_2 nanoparticles for automotive engines and gearboxes. Their presence in future lubricants is likely to increase vehicle efficiency and component lifespan, by reducing friction and wear in a large number of contacts. Several issues however remain to be addressed before considering the formulation of a commercial IF-MoS_2-doped oil.

The biggest challenge in order to maximize the efficiency of the IF-MoS_2 in various environments is, arguably, to ensure an optimal dispersion of the nanoparticles in the fluid while maintaining their efficiency. As shown previously, this can be achieved by using low amounts of dispersants to fully disperse the additives while leaving little to no excess dispersant molecules in the oil. The resulting formulation is however not exploitable for industrial applications, having lost its ability to disperse particle contaminants (wear debris, soots…).

Aside from their increasing lubrication capacities in the more severe lubrication regimes, the use of IF-MoS_2 instead of more common Friction Modifiers (FM) is thought to be beneficial in terms of additive durability. These nanoparticles are indeed theoretically chemically inert and are consumed only when needed inside severe contacts. This aspect could be investigated further by comparing the friction reducing capacities of a given concentration of IF-MoS_2 and MoDTC, for example, during high-cycle tribological tests. Although theoretically stable, the durability of the IF-MoS_2 nanoparticles in time could also be studied using various ageing techniques.

The results presented in this work minimize the risks associated to the presence of nanoparticles in the oil in the case of full-film contacts. The tests were however carried out in a wide but limited range of operating conditions, which is not sufficient to eliminate the possibility of contact starvation altogether. Numerical simulations or more extensive testing, including film thickness measurements and/or contact visualizations, could bring a better understanding to the flow of nanoparticles near and inside fully-lubricated contacts.

A glimpse of the potential of IF-MoS_2 nanoparticles in protecting steel surfaces from RCF was shown in this work, but additional testing and surface characterizations are needed to fully understand how they prevent surface-initiated pitting. The test results shown here seem to indicate that the initiation of cracks at the surface stops occurring as soon as a tribofilm is formed on the substrate, which would need confirmation. The IF-MoS_2 also seemed to prevent the propagation of existing surface-initiated cracks, which could imply either that the additives interact with the crack lips or that a tribofilm was formed inside the micropits.

Component-oriented testing would finally be necessary in order to estimate the true potential of nanoparticle-doped lubricants at the scale of a whole vehicle. Meshing tests could for example be considered to simulate the lubrication of a gearbox, while considerable friction and wear reduction might also be observed in the valve train. These tests are however quite difficult to achieve, given the large volumes of oil (and therefore quantity of nanoparticles) needed.

Other, less technical aspects may also have to be considered before commercializing the very first nanoparticle-doped oil. The sanitary risks related to the use of nanoparticles, even dispersed in oil, will for example have to be totally and undoubtedly excluded. From a marketing viewpoint, the black aspect of nanoparticle-doped oils may also refrain customers from buying such lubricants… unless they can be convinced to choose a darker oil for a brighter future.

Appendix A - *Theory of Hertz*

Considering perfectly rigid and smooth counter parts, the static loading of a surface onto another will often result in a point or line contact. In reality however, the surfaces will deform elastically to form a contact surface, generating a contact pressure at the interface. Heinrich Hertz was the first to propose a solution for these types of contact, which are now commonly referred to as "hertzian contacts" [92].

In the case of a point contact between non-conformal bodies 1 and 2, the area, contact pressure and elastic deformation of the contact can be estimated if the geometry (local curvature radii of the surfaces) and the material properties (Young's modulus E and Poisson's ratio ν) of both surfaces are known.

The maximum contact pressure P_h and the deformation δ for an elliptical contact of major semi-axis *a* and minor semi-axis *b* can be approximated by the following equations [93] :

$$\begin{cases} \dfrac{a}{b} \approx \left(\dfrac{R'}{R''}\right)^{2/3} & P_h = \dfrac{3w}{2\pi ab} \approx \left(\dfrac{6wE^{*2}}{\pi^3 R_e^{\,2}}\right)^{1/3} \\ \sqrt{ab} \approx \left(\dfrac{3wR_e}{4E^*}\right) & \delta \approx \left(\dfrac{9w^2}{16R_e E^{*2}}\right)^{1/3} \end{cases}$$

where R' *and* R" *are the major and minor relative radii of curvature, respectively* ($\frac{1}{R'} = \frac{1}{R_1'} + \frac{1}{R_2'}$ *and* $\frac{1}{R''} = \frac{1}{R_1''} + \frac{1}{R_2''}$),

R_i' *and* R_i" *are the maximum and minimum radius of curvature of surface i at the contact,*

R_e *is the equivalent radius of curvature given by* $R_e = \sqrt{R'R''}$,

w *is the load (given in N),*

and E^* *is the equivalent Young's modulus given by* $\frac{1}{E^*} = \frac{1-\nu_1^{\,2}}{E_1} + \frac{1-\nu_2^{\,2}}{E_2}$.

In the case of a contact between a sphere of radius R_1=R and a flat counter-surface (R_2=∞), the contact surface is circular of radius a (**Figure A. 1.**) and these equations are reduced to:

$$a = \left(\frac{3wR}{4E^*}\right)^{1/3} \qquad P_h = \frac{3w}{2\pi a^2} = \left(\frac{6wE^{*2}}{\pi^3 R^2}\right)^{1/3} \qquad \delta = \frac{a^2}{R} = \left(\frac{9w^2}{16RE^{*2}}\right)^{1/3}$$

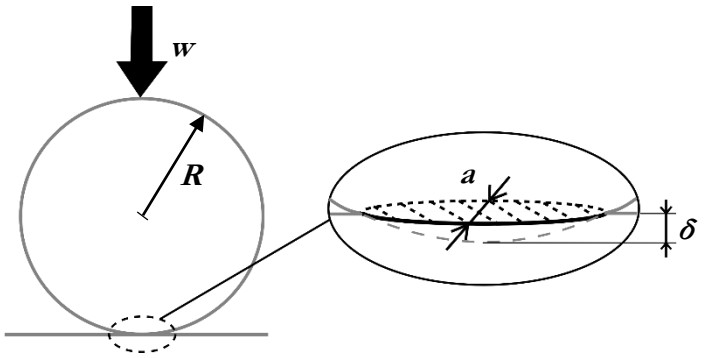

Figure A.1. Hertzian contact between a sphere and a flat surface

Appendix B - *Elastohydrodynamic lubrication*

Elastohydrodynamic lubrication (EHL) is a full-film lubrication regime occurring for highly loaded contacts, resulting in very thin oil films. The high pressures generated in the oil film greatly increase the viscosity of the lubricant, resulting in large elastic deformations. Any EHL contact can be made equivalent to either a cylinder-on-flat, ellipse-on-flat or sphere-on-flat configuration using the equivalent radii of curvature described in **Appendix A**. The cross-section of such a contact along the entraining direction is schematized in **Figure B. 1**.

The geometry of the surfaces creates a pressure build-up in the fluid at contact entry, enabling surface separation. In the central zone of the contact, the high viscosity of the oil results in a near-constant film thickness h_c and a pressure distribution close to the Hertzian case [94]. The sudden drop in pressure met by the oil at contact exit causes the formation of a geometrical constriction of the surfaces to ensure a constant mass flow. This restriction creates a minimum film thickness h_m and a characteristic spike in the pressure field.

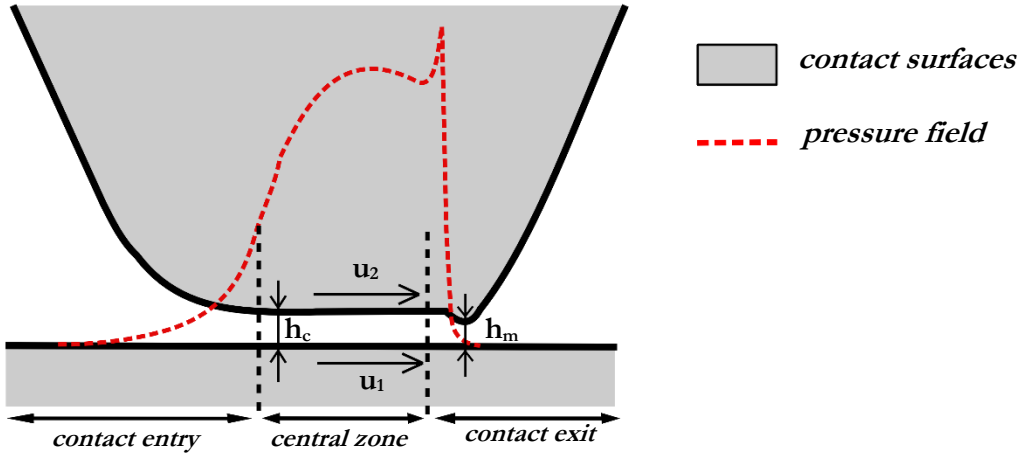

Figure B. 1. Typical EHL contact and corresponding pressure field

In the case of a point contact, Hamrock and Dowson proposed expressions of the minimum and central film thickness in which the ellipticity ratio was considered [95–97]. These formulae were shown to provide good approximations for a wide range of contacts, and are widely used today. The film thickness depends on the velocity of the surfaces, the material properties as well as the load applied to the contact. The following dimensionless parameters were defined to take these into account:

$$U = \frac{\eta_0 u}{E' R} \qquad G = \alpha E' \qquad W = \frac{w}{E' R^2}$$

where η_0 is the dynamic viscosity at ambient pressure (in Pa.s^{-1}), u is the rolling velocity ($u_1+u_2/2$, in m.s^{-1}), E' is the reduced Young's modulus given by $\frac{2}{E'} = \frac{1-\nu_1^2}{E_1} + \frac{1-\nu_2^2}{E_2}$ *(in Pa), R is the reduced radius of curvature in the rolling direction (in m), a is the piezoviscous coefficient (in Pa^{-1}) and w is the load (in N).*

The following dimensionless central and minimum film thicknesses can then be derived from these parameters:

$$H_c = 2.69U^{0.67}G^{0.53}W^{-0.067}(1-0.61e^{-0.73k})$$
$$H_m = 3.63U^{0.68}G^{0.49}W^{-0.073}(1-e^{-0.68k})$$

where k is the ellipticity ratio (k=a/b with a>b).

The absolute minimum and central film thicknesses can finally be deduced from the reduced radius of curvature as follows:

$$H_c = \frac{h_c}{R} \qquad H_m = \frac{h_m}{R}$$

Appendix C - *Repeatability of the test results*

C. 1. Repeatability of the HFRR tests

The simple ball-on-flat configuration of the HFRR set-up provides the test results with great repeatability for short tests. For high-cycle and/or severe testing conditions, the higher wear and therefore amount of debris may slightly alter the repeatability of the results.

To illustrate this, the results for identical tests carried out on the PAO base oil alone in the conditions described in **Table 3.3** (p. 58) but at a frequency of 20 Hz are shown on **Figure C. 1**. At 30°C, all the tests showed perfect repeatability during the 4 hours. For more severe conditions, the friction curves however drifted slightly apart after approximately 5000 seconds (100 000 cycles). The severity of the test conditions also affected the stability of the friction coefficient, most likely due to a high amount of wear debris passing through the contact.

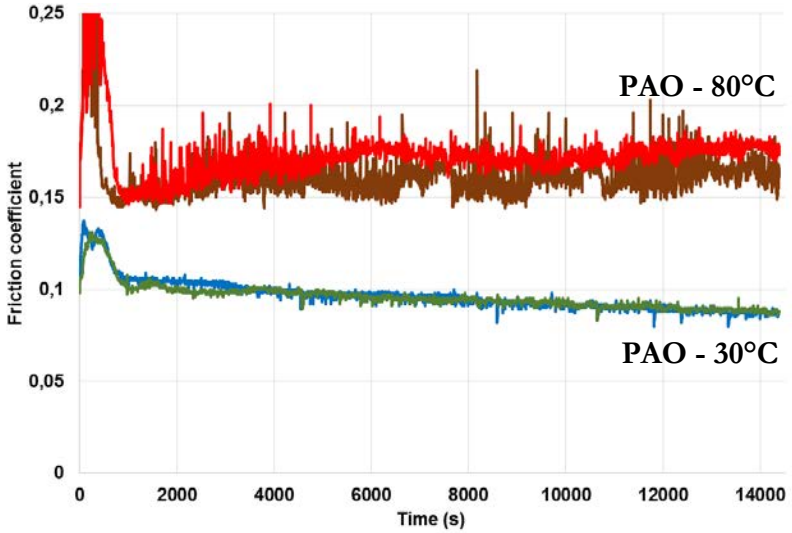

Figure C. 1. Repeatability of the test results for the PAO base alone tested at 30°C and 80°C

When testing nanoparticle-doped lubricants, the repeatability of the tests is affected by the dispersion of the nanoparticles and/or nanoparticle agglomerates in the oil. For high-cycle testing, the availability of the nanoparticle additives near the contact may indeed differ from a test to the

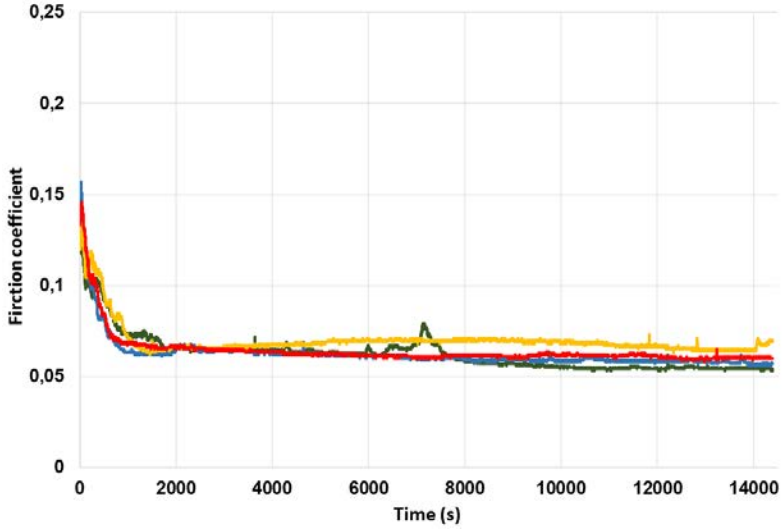

Figure C. 2. Repeatability of the test results for the PAO + 1wt% SpC IF-MoS_2

other. This did not affect the results significantly for the most efficient (poorly crystalline) nanoparticles, as lower quantities of IF-MoS_2 were shown to maintain effective tribofilms on the contact surfaces. Four identical tests for the PAO + 1 wt% SpC IF-MoS_2 (conditions given in **Table 3.3**) are for example illustrated on **Figure C. 2**. The measured friction was identical during the first 4000 seconds, before showing slight variations throughout the rest of the test.

The reduced durability of the performances of the more crystalline IF-MoS_2 during the HFRR tests was showed to come from the progressive starvation of the contact in nanoparticles. The moment of the test when this occurs may vary from a test to the other, as illustrated on **Figure C. 3**. Four identical tests (conditions given in **Table 3.3**) for the PAO + 1 wt% LC IF-MoS_2 are shown. Similar minimum friction coefficients are achieved at the beginning of all tests, before rising abruptly between 4000 and 9000 seconds. The general trend of the results is however similar for all tests, with a maximum friction reduction achieved and stabilized in the early stages of the tests before suddenly rising significantly before completion.

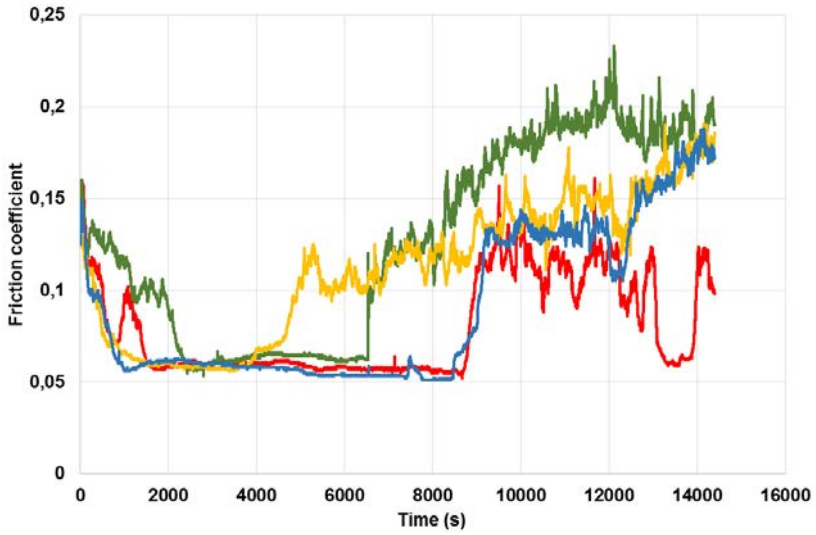

Figure C. 3. Repeatability of the test results for the PAO + 1wt% LC IF-MoS2

All the HFRR tests presented in this work were repeated, and the results shown are the most representative of all the results for the sake of clarity.

C. 2. Repeatability of the MTM tests

The results obtained on the MTM are also made very repeatable by the simple nature of the test. In full-film lubrication regimes, the absence of wear provides the rig with a near-perfect repeatability. Four identical tests carried out with the PAO base oil are for instance shown on **Figure C. 4**, with traction and Stribeck curves plotted at 80°C for different loads. The results show only a very slight variation from one test to the other. As the presence of IF-MoS_2 in the base oil had little to no effect on the tribological results (see part **5. 2. 3**), their testing also proved very repeatable.

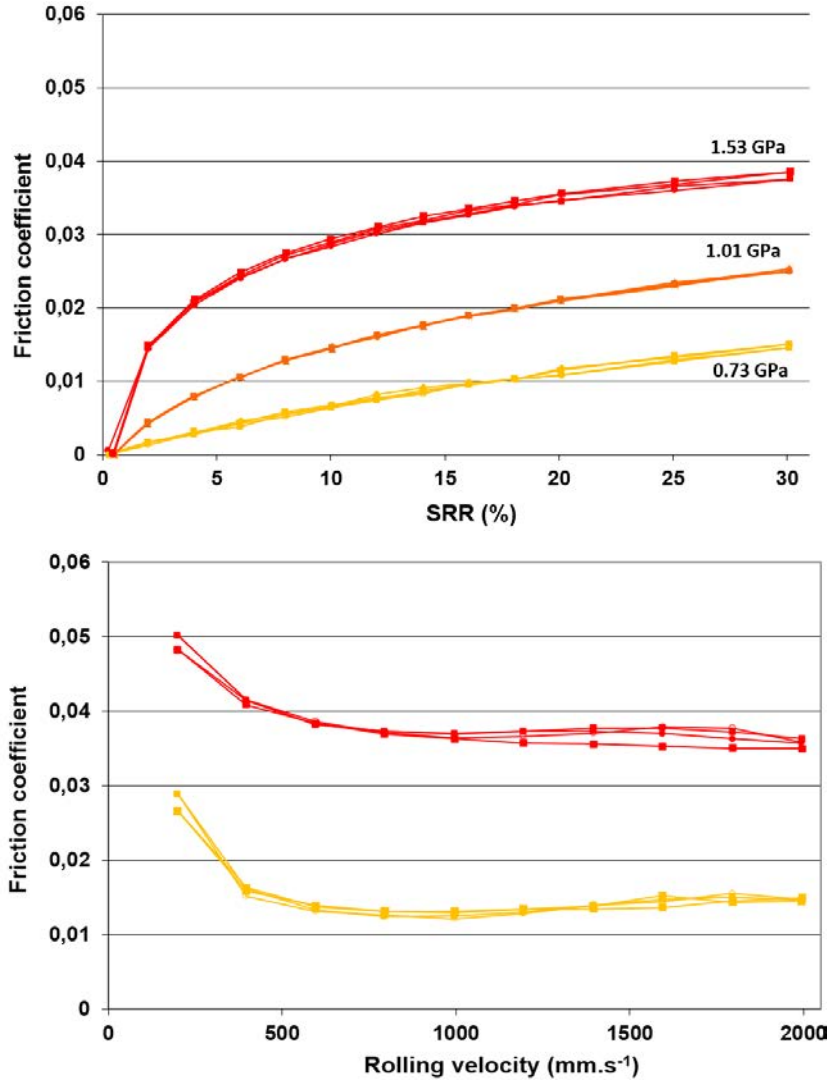

Figure C. 4. Repeatability of the MTM results for the PAO base oil alone

C. 3. Repeatability of the MPR tests

The repeatability of fatigue test results is always difficult to achieve, given the number of parameters influencing crack initiation and propagation. The MPR rig was designed to minimize these deviations, with a simple test configuration and the preparation of very similar test samples (discs and barrels). The test method used by PowerTrib for the tests presented in this work was furthermore specifically designed for an optimal repeatability of the results.

Given the relatively large volume of lubricant needed to carry out each test (150 mL), the tests showed in part **5. 3. 2** were only carried out twice. The results were however very repeatable, and the difference observed between the behaviors of both oils was significant enough to be presented in this work. The friction coefficient measured during all four tests are showed on **Figure C. 5**. The results are strictly identical for the testing of the PAO alone, and vary slightly at the end of the testing of the PAO + 1wt% IF-MoS_2. This variation may be due to changes in nanoparticle availability throughout the oil during the test, as observed on the HFRR (**Figure C. 2.**). The main objective of these tests was to evaluate the potential effects of the presence of IF-MoS_2 in the oil on crack initiation and propagation, and the influence discussed in this work was also very

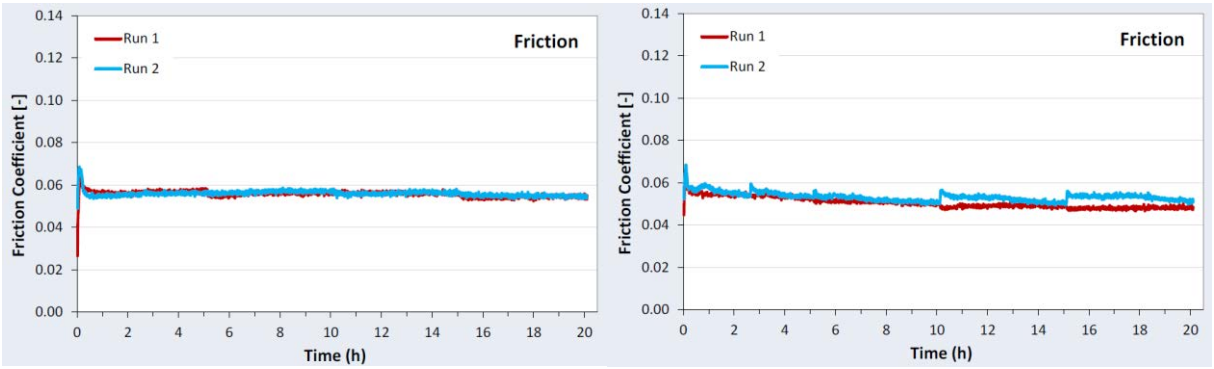

Figure C. 5. Repeatability of the friction measurements during the MPR tests for the PAO alone (left) and the PAO + 1wt% IF-MoS_2 (right)

repeatable. The evolution of a typical section of the barrel for the base oil alone and for the PAO + 1 wt% IF-MoS_2 during both runs are shown on **Figure C. 6** and **Figure C. 7** respectively.

For the PAO base oil alone, the apparition of crack initiation zones and their evolution into micropits occurred at the same rate throughout the test. The density and size of the micropits around the wear track were furthermore similar at the end of both tests. When 1 wt% IF-MoS_2 were added to the base oil, rare crack initiation sites were spotted in the early stages of both tests, but showed no signs of evolution throughout the tests.

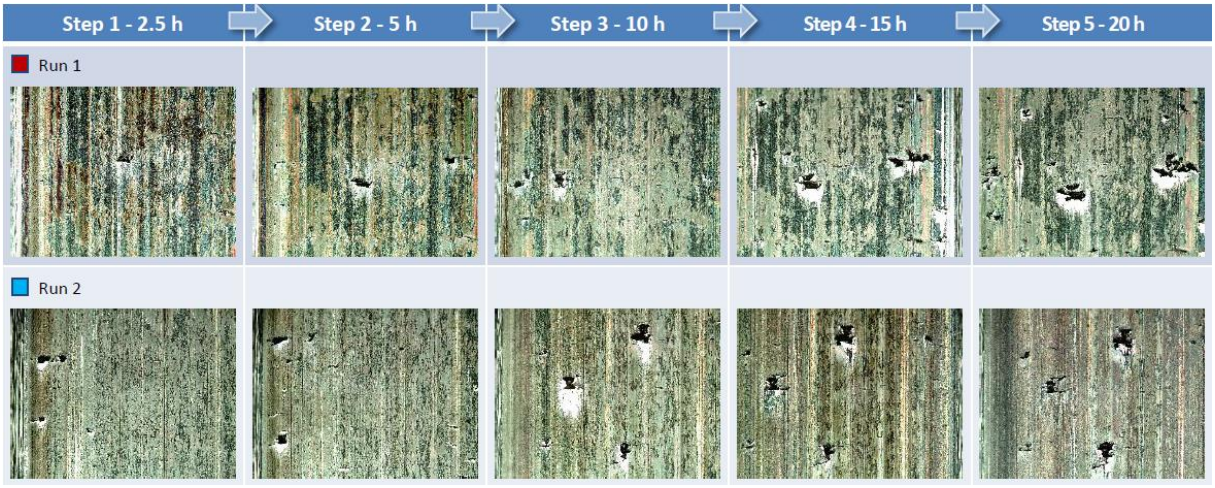

Figure C. 6. Evolution of the contact surface during both MPR runs on the PAO base oil alone

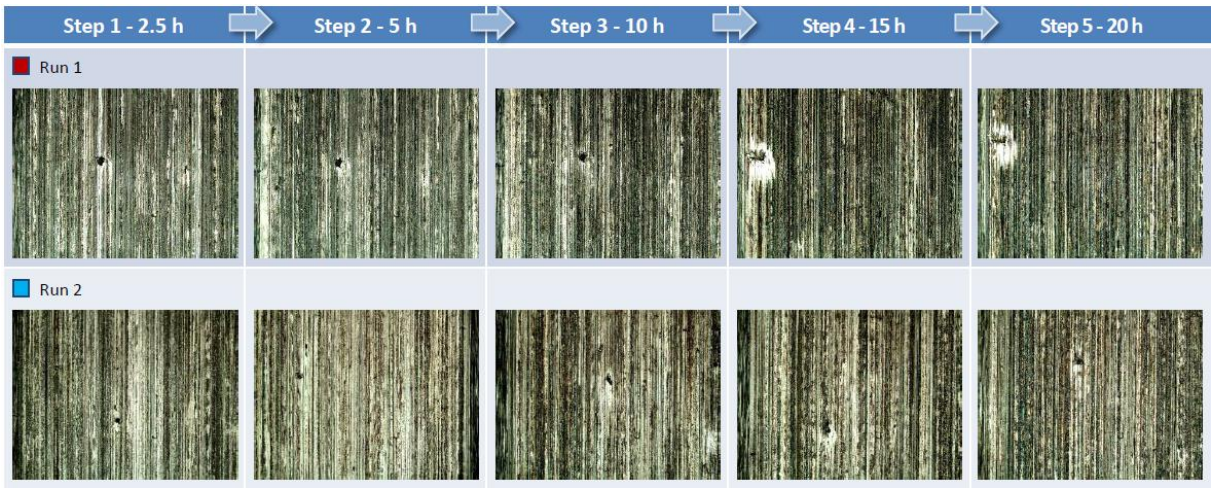

Figure C. 7. Evolution of the contact surface during both MPR runs on the PAO + 1wt% IF-MoS_2

Appendix D - *Résumé étendu*

Ce manuscrit de thèse ayant été rédigé en langue anglaise, un résumé étendu des travaux et des principaux résultats est proposé en français dans cette annexe finale.

D. 1. Introduction

De nos jours, l'automobile reste largement considérée comme le mode de transport offrant le meilleur compromis entre facilité, rapidité, confort et autonomie de déplacement. Les contraintes environnementales actuelles, ainsi que la hausse perpétuelle du prix des énergies fossiles, incitent les constructeurs automobiles à améliorer sans cesse le rendement de leurs véhicules. De nombreuses pistes sont explorées pour réduire la consommation des voitures actuelles, allant du développement de technologies hybrides à l'amélioration de l'aérodynamique des véhicules en passant par l'optimisation des chambres de combustion des moteurs. La composition et le comportement des lubrifiants utilisés dans les moteurs et les boîtes de vitesses ont un rôle déterminant dans cette recherche d'efficacité, puisqu'ils influent directement sur le frottement généré au sein de chaque contact lubrifié.

L'objectif de ce travail de thèse, fruit d'une collaboration entre le LaMCoS, le LTDS et PSA Peugeot Citroën, est d'évaluer le potentiel de lubrifiants dopés aux nanoparticules dans le cadre d'une application automobile. Les nanoparticules Inorganiques de type Fullerène (IF-) présentent en effet un fort potentiel tribologique, à la fois en tant que réducteur de frottement que d'usure. Après un état de l'art portant sur les fondamentaux de la lubrification automobile et sur l'historique des lubrifiants dopés aux nanoparticules, ce manuscrit aborde les trois étapes fondamentales permettant d'entrevoir une formulation de lubrifiants dopés aux nanoparticules, à savoir : (a) la synthèse de nanoparticules performantes ; (b) leur incorporation dans une huile totalement formulée et (c) le potentiel des huiles dopées dans des conditions se rapprochant d'une application automobile.

D. 2. Etat de l'art

Bien qu'il subsiste des débats au sujet des facteurs influents sur le réchauffement climatique, l'utilisation d'énergies fossiles par l'Homme contribue de manière importante à l'émission de gaz à effets de serre. En 2004, le secteur des transports représentait à lui seul 13.1% des émissions globales de la planète. Depuis le début des années 1990, de nombreuses mesures internationales ont été prises pour limiter les émissions polluantes. Les normes dites « Euro », notamment, fixent les seuils maximaux autorisés pour l'émission de différents composés (CO, HC, NO_x et micro-particules) pour chaque type de véhicule commercialisé. Au-delà de ces contraintes légales, la réduction de la consommation des véhicules (qui est intimement liée à la quantité d'émissions polluantes) est désormais devenue un véritable argument de vente face à la perpétuelle hausse du prix des carburants. Alors que de nombreuses actions sont prises par les constructeurs pour optimiser le rendement de leurs véhicules (évolution des pneumatiques, aérodynamique, allègement…), le frottement au sein du GMP (Groupe Moto-Propulseur, consitué du moteur et de la boîte de vitesses) demeure une source de perte de puissance considérable (voir **Figure D. 2. 1**).

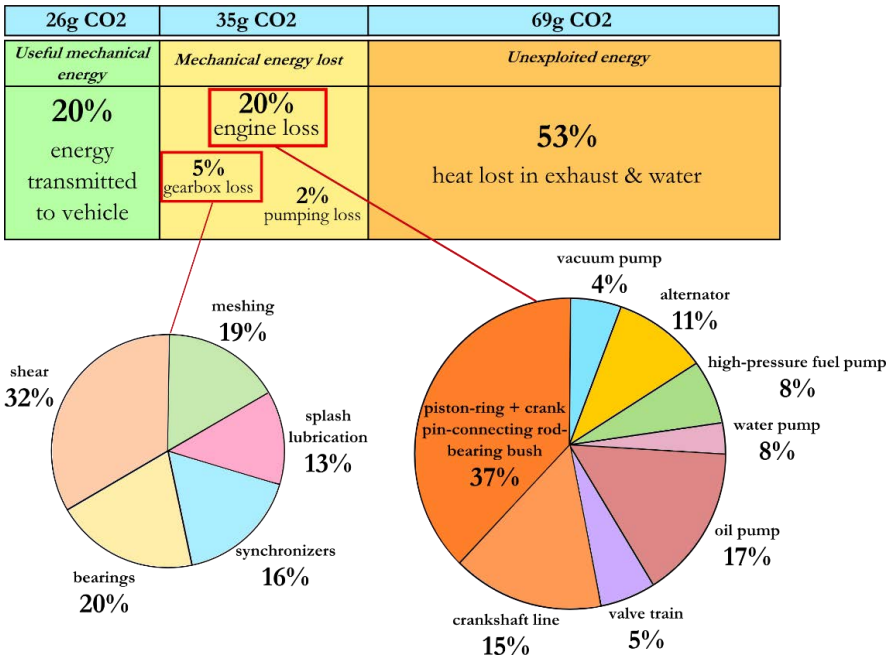

Figure D. 2. 1. Estimation des principales sources de pertes d'énergie et émissions de CO_2 correspondantes pour un moteur Diesel 1.6L classique et sa boîte de vitesses (valeurs extraites de données PSA Peugeot Citroën)

Bien que ce problème puisse être abordé de différentes manières (géométries et matériaux des composants, revêtements ou traitements de surface…), les lubrifiants utilisés jouent un rôle déterminant dans le rendement global du GMP et sa résistance aux phénomènes d'usure. Ils agissent en effet sur un grand nombre de contacts, et contribuent au refroidissement et au nettoyage (via l'élimination des contaminants particulaires tels que les débris d'usure et les suies de combustion par exemple) des contaminants de l'ensemble du système.

Etant donné la variété des éléments lubrifiés, la formulation finale de l'huile doit être performante pour une large étendue de conditions de contact. Les différents régimes de lubrification potentiellement rencontrés peuvent être décrits par la courbe de Stribeck, comme illustré sur la **Figure D. 2. 2**. Le lubrifiant doit alors être capable de limiter les pertes par frottement ainsi que l'usure dans tous les scénarii rencontrés, allant d'un régime de lubrification limite (aucune séparation des surfaces) à une lubrification en film complet (absence de contact direct entre les surfaces antagonistes).

Afin de répondre à ces critères et de couvrir une étendue de conditions de fonctionnement de plus en plus large, les lubrifiants actuels ont une formulation complexe. L'huile de base, pouvant être soit végétale, minérale et/ou synthétique, est ainsi enrichie d'additifs anti-rouille, anti-corrosion, anti-oxidants, anti-mousse, détergents, dispersants, modificateurs de viscosité, émulsifiants, etc. Les additifs anti-usure, réducteurs de frottement et extrême-pression ont quant à eux pour objectif de protéger les surfaces et de diminuer les pertes par frottement dans les contacts se trouvant en régime de lubrification mixte/limite. Ils forment généralement des films protecteurs à faible résistance au cisaillement, appelés tribofilms, sur les substrats par adsorption ou par réaction chimique avec la surface.

Les récentes découvertes en termes de synthèse de nanoparticules ont considérablement élargi les possibilités d'additivation de lubrifiants, notamment en ce qui concerne les additifs réducteurs de frottement et anti-usure. Certaines nanoparticules présentent en effet de nombreux avantages

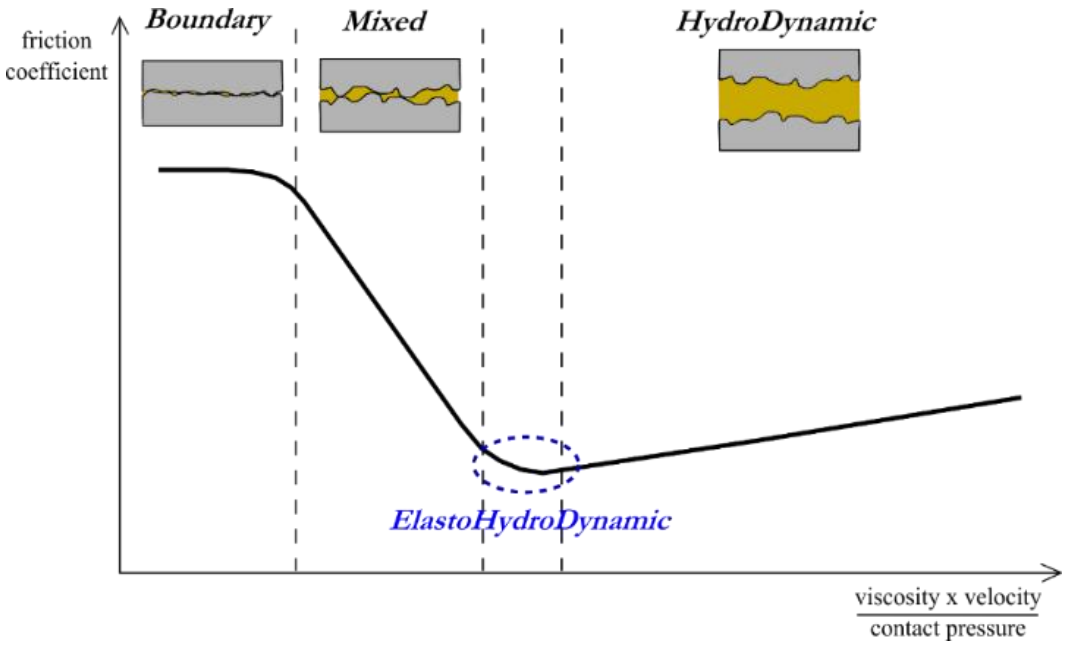

Figure D. 2. 2. Courbe de Stribeck et régimes de lubrification associés

par rapport aux additifs conventionnels, de par leur caractère chimiquement inerte et leur mécanisme de lubrification impliquant la libération de composés actifs directement et exclusivement au sein du contact.

Il existe aujourd'hui de nombreux types de nanoparticules, de différentes compositions, formes, structures et tailles (**Figure D. 2. 3**). Les principales géométries de nanoparticules sont sphérique et tubulaire (ces dernières étant communément appelées « nanofibres » ou « nanotubes »), toutes deux ayant montré des propriétés intéressantes lorsqu'incorporées dans un lubrifiant ou déposées sur une surface. La possibilité de synthétiser des nanoparticules de carbone sphériques de très petite taille (environnant 10 nm de diamètre pour les « onions de carbone ») et des nanotubes

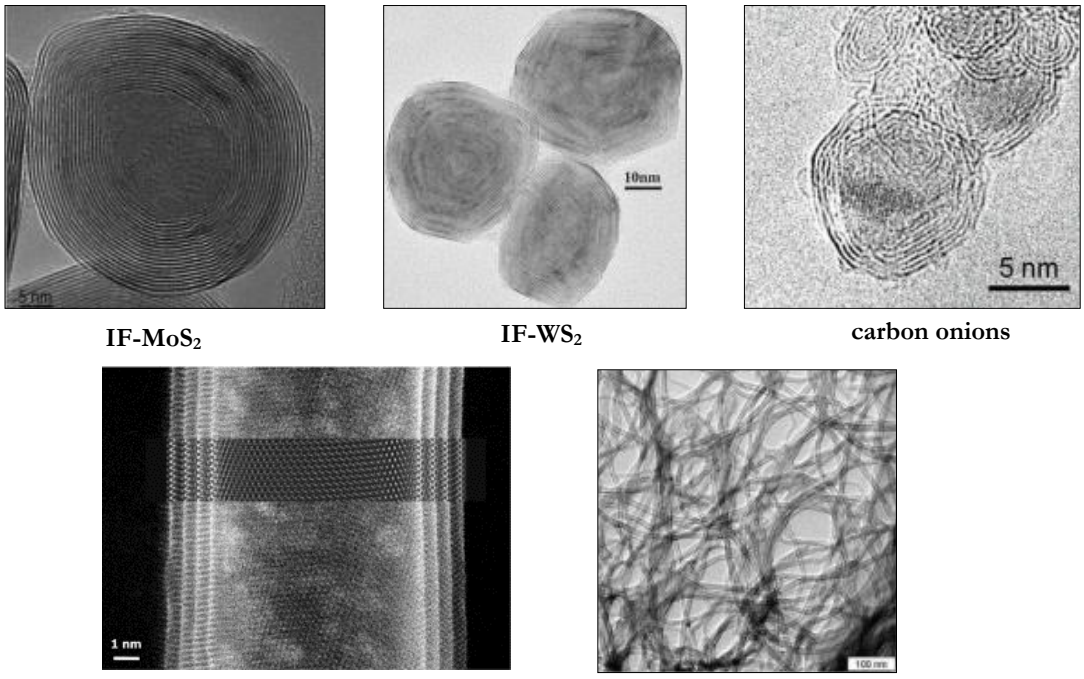

IF-MoS_2 **IF-WS_2** **carbon onions**

WS_2 and C nanotubes (nanofibers)

Figure D. 2. 3. Exemples des différents types de nanoparticules existants [10,23,51,56,64]

de carbone au nombre de parois contrôlé (allant de une à plus d'une dizaine) a en effet permis d'obtenir des réductions de frottement parfois spectaculaires. Les nanoparticules ayant laissé entrevoir le plus gros potentiel tribologique semblent cependant être celles appartenant à la famille des dichalcogénures métalliques (composés MX_2 avec M-Mo, W, Nb, Ta, Ti, Zr, Hf, Re… et X=S, Se, Te…), notamment dans le cas des disulfures de molybdène (MoS_2) et de tungstène (WS_2).

En 1992, Pr. Tenne parvint à synthétiser pour la première fois des nanoparticules inorganiques de type fullerène, avec une structure particulière rappelant celle du fullerène C60. Les couches de WS_2 ou de MoS_2, selon le cas, sont alors concentriques et parallèles entre elles, procurant aux nanoparticules des propriétés spécifiques. Ces nanoparticules (IF-MoS_2 et IF-WS_2) ont par la suite exhibé des performances tribologiques remarquables pour les conditions de contact les plus sévères. Il a depuis été montré que ces nanoparticules s'exfoliaient sous les sollicitations combinées de la pression et du cisaillement, libérant des feuillets de MoS_2 ou de WS_2 au sein du contact. Ces feuillets réagissent alors avec les surfaces pour former des tribofilms protecteurs et à bas coefficient de frottement (**Figure D. 2. 4**).

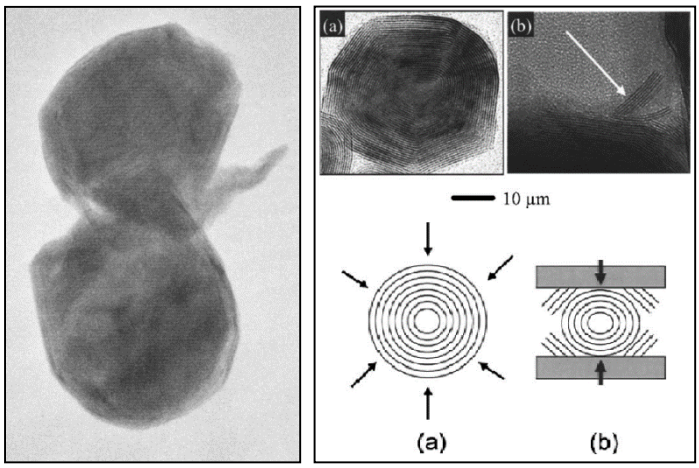

Figure D. 2. 4. Exfoliation d'IF-WS_2 telle qu'observée par Leshchinsky et al (gauche) et Joly-Pottuz et al (en haut à droite), et comportement schématique de nanoparticules de type fullerène sous pression hydrostatique (a) et uni-axiale (b)

Depuis leur découverte, les nanoparticules inorganiques de type fullerène ont fait l'objet de nombreuses études, permettant par exemple de mieux comprendre l'influence de leur concentration dans l'huile ou de la pression de contact exercée. Le nombre de défauts structurels présents au sein des nanoparticules, parfois plus simplement désigné comme leur « cristallinité », semble par ailleurs avoir une influence sur leurs performances tribologique puisqu'il est susceptible de modifier leur capacité à être exfoliées (**Figure D. 2. 5**). Les procédés de synthèse utilisés dans

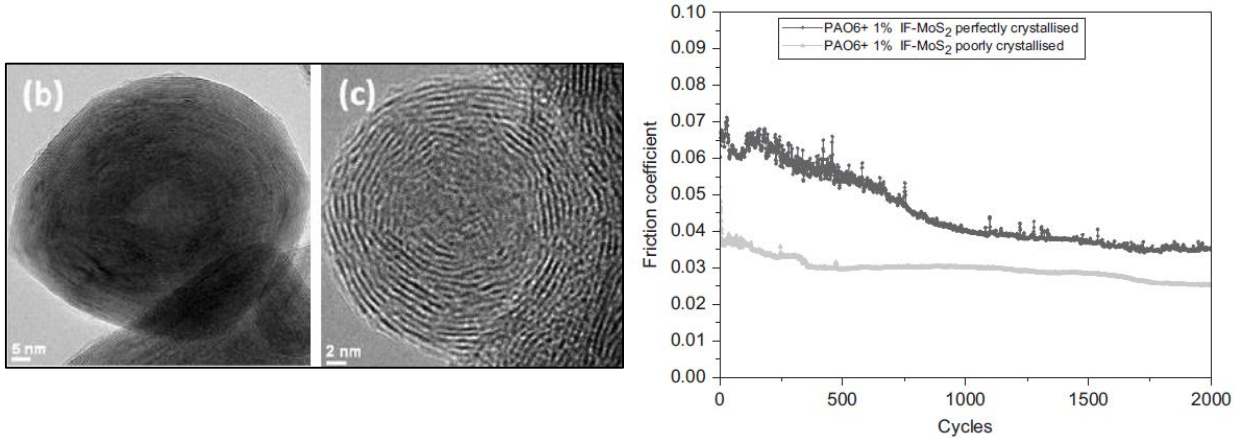

Figure D. 2. 5. IF-MoS_2 cristalline (gauche) et peu cristalline (centre), et performance tribologique associée (droite)

cette étude n'avait cependant pas permis d'obtenir des nanoparticules de tailles identiques, rendant impossible la différentiation des influences respectives de la taille et de la cristallinité des nanoparticules sur leurs performances.

Si une additivation des lubrifiants par des nanoparticules inorganiques de type fullerène parait très prometteuse pour les contacts les plus sévères, la présence de corps solides dans les huiles peut également avoir des effets indésirables. Le rôle des dispersants est justement d'éviter l'agglomération des contaminants particulaires (débris d'usure, suies de combustion, contaminants extérieurs…) afin de pouvoir les éliminer via les filtres prévus à cet effet. Outre les risques évidents d'indentation des surfaces, l'accumulation de particules à l'entrée des contacts habituellement lubrifiés en film complet peut en effet provoquer leur sous-alimentation, entraînant une forte hausse du frottement et des risques d'usure accrus (**Figure D. 2. 6**).

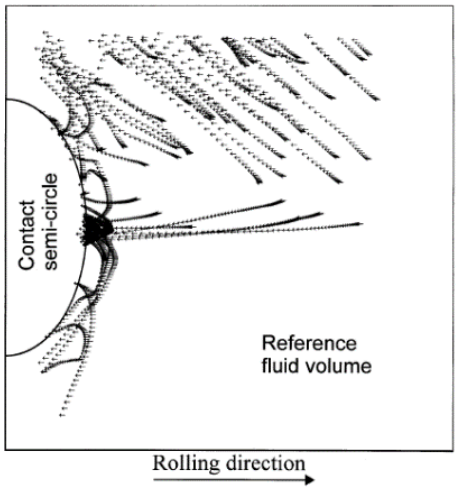

Figure D. 2. 6. Prédiction de la trajectoire d'une particule de 20 μm lorsqu'elle est placée aléatoirement en amont d'un contact EHD (h_c=0.3 μm)

Afin de pouvoir envisager une éventuelle utilisation de nanoparticules pour une application automobile, il est ainsi primordial de s'assurer que ces additifs ne présenteront pas de risques pour certains composants du moteur et/ou de la boîte de vitesses.

D. 3. Influence de la taille et de la structure des nanoparticules IF-MoS_2

La première étape à accomplir avant d'envisager une formulation de lubrifiants dopés aux IF-MoS_2 consiste à comprendre l'influence des propriétés intrinsèques aux nanoparticules sur leur comportement tribologique. S'il a déjà été démontré que la présence de nombreux défauts structurels au sein des nanoparticules favorise la formation de tribofilms en facilitant leur exfoliation, il est généralement admis qu'une réduction de leur taille sera également bénéfique puisqu'elle favorisera le passage des nanoparticules dans le contact. Aucune étude n'a cependant permis de différentier les influences respectives de la cristallinité et de la taille des nanoparticules.

Quatre types de nanoparticules, variant de par leur taille et leur cristallinité, ont été synthétisés dans cette étude (**voir Figure D. 3. 1**) : larges et cristallines (LC), larges et peu cristallines (LpC), petites et cristallines (SC) et petites et peu cristallines (SpC). Pour une concentration massique donnée, la différence de taille entre les petites IF-MoS_2 (150 nm de diamètre) et les plus larges (350 nm) résulte en une quantité de petites nanoparticules (SC et SpC) environ 13 fois plus importante dans l'huile que pour les plus larges. Une analyse des IF-MoS_2 par XPS a révélé des compositions

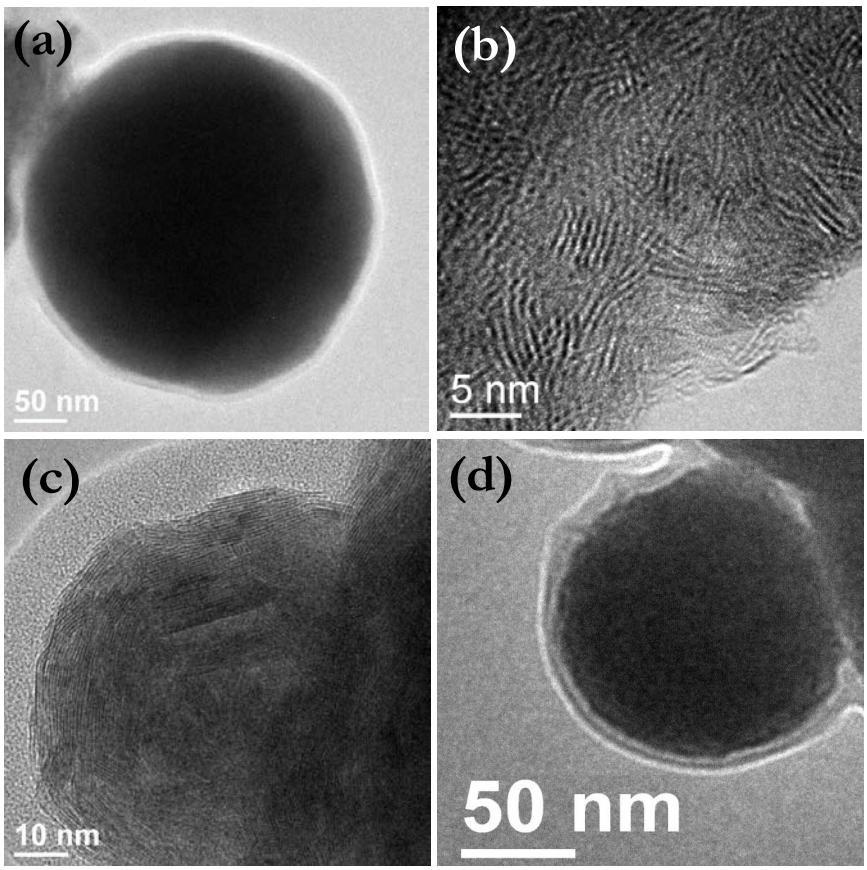

Figure D. 3. 1. Images HR-TEM des nanoparticules IF-MoS_2 de type LC (a), LpC (b), SC (c) et SpC (d)

chimiques très similaires, confirmant que la méthode de synthèse utilisée permet de ne varier que la taille et la structure des nanoparticules.

Le comportement tribologique de ces quatre types de nanoparticules lorsqu'incorporées dans une huile de base synthétique (PAO) a ensuite été comparé sur HFRR (High Frequency Reciprocating Rig), dans des conditions de contact sévères (régime de lubrification limite et nombre de cycles élevé). Toutes les IF-MoS_2 testées ont permis d'obtenir une réduction spectaculaire de l'usure et du coefficient de frottement par rapport à l'huile de base seule, de 0.2 à 0.06 environ (voir

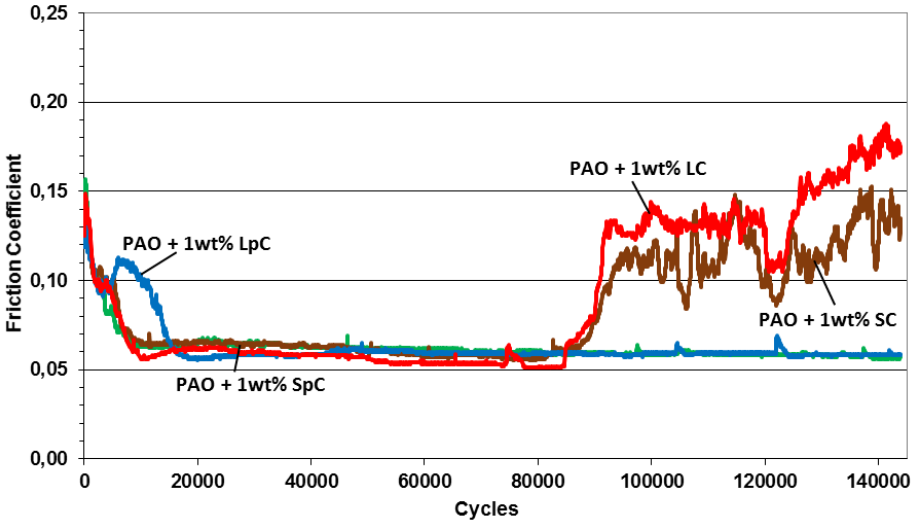

Figure D. 3. 2. Comparaison des coefficients de frottement obtenus pour les quatre types de nanoparticules testées

Figure D. 3. 2).

Ces résultats mettent clairement en évidence l'influence de la cristallinité des nanoparticules testées, indépendamment de leur taille. Les IF-MoS_2 peu cristallines, à la fois petites et larges (SpC et LpC) ont en effet permis de maintenir un frottement faible durant la totalité des essais, tandis que les deux types d'IF-MoS_2 plus cristallines (SC et LC) semblent perdre de leur efficacité en cours d'essai. Des essais supplémentaires, couplés à des analyses de surface par XPS, ont permis de constater que des tribofilms de même nature étaient formés sur les surfaces en début d'essai pour les quatre types de nanoparticules. La nature alternative de l'essai provoque ensuite une sous-alimentation progressive du contact en cours d'essai. Dans le cas des nanoparticules plus cristallines, la réduction du nombre d'IF-MoS_2 pénétrant dans le contact ne suffit alors plus à maintenir un tribofilm homogène et performant. L'efficacité accrue des nanoparticules peu cristallines est alors mis en évidence, puisque leur facilité d'exfoliation permet de maintenir un coefficient de frottement et une usure faible malgré un nombre réduit d'IF-MoS_2 dans le contact (et ce indépendamment de la taille des nanoparticules). Etant donné les bonnes performances en frottement obtenues avec les IF-MoS_2 les plus larges et cristallines en début d'essai, l'alimentation du contact en nanoparticules parait être le facteur le plus influent sur leurs performances. Cette hypothèse a été confirmée par des essais lors desquels une recirculation d'huile était imposée par agitation de l'huile (**Figure D. 3. 3**). Il est alors possible de maintenir un tribofilm homogène sur les surfaces et de garantir de bonnes performances tribologiques, quelle que soit la taille et la cristallinité des nanoparticules utilisées.

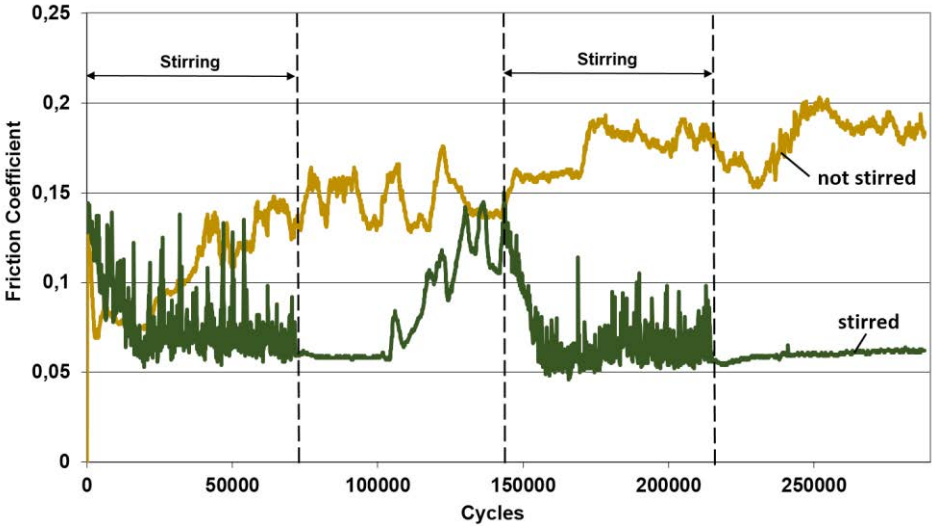

Figure D. 3. 3. Performance accrue des IF-MoS_2 de type LC lors de la modification du flux d'huile aux alentours du contact

L'ensemble des tribofilms formés en surface par les quatre types de nanoparticules a été analysé par XPS et comparé aux analyses faites sur les IF-MoS_2 seules afin de garantir que les différences de comportement observées ne soient pas d'ordre chimique. Tous les tribofilms attestent de compositions similaires, avec toutefois des quantités réduites de molybdène et de soufre sur les surfaces en fin d'essai pour les particules les plus cristallines. Les spectres des IF-MoS_2 de type LC et SC laissent par ailleurs entrevoir la possibilité d'une présence de sulfates de fer à l'extrême surface des traces d'usure, confirmant la dégradation des tribofilms en fin d'essai. Des coupes FIB (Focused Ion Beam) ont alors été effectuées sur les échantillons correspondants aux particules LC (cristallines) et SpC (peu cristallines) afin d'observer la morphologie des surfaces

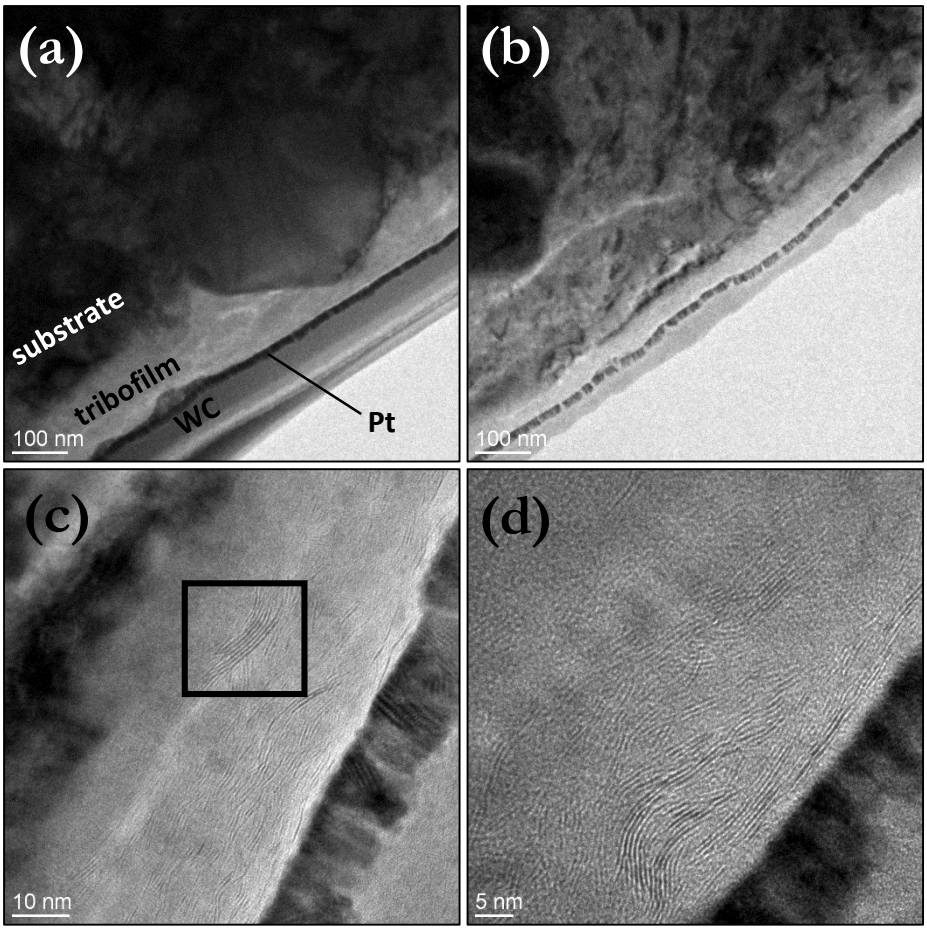

Figure D. 3. 4. Coupe FIB de la trace d'usure résultante de l'essai HFRR du mélange PAO+1% IF-MoS_2 SpC

correspondantes en fin d'essai.

Dans le cas des nanoparticules SpC, ayant produit un faible coefficient de frottement durant toute la longueur de l'essai, les observations réalisées par MET (Microscope Electronique à Transmission) montrent un tribofilm homogène d'une épaisseur comprise entre 30 et 100 nm (**Figure D. 3. 4**). Il est par ailleurs possible de distinguer les feuillets de MoS_2 dans la partie supérieure du tribofilm, orientés de façon parallèle à la surface et procurant le faible frottement en cours d'essai. Pour les IF-MoS_2 de type LC, en revanche, ces observations ont révélé une surface

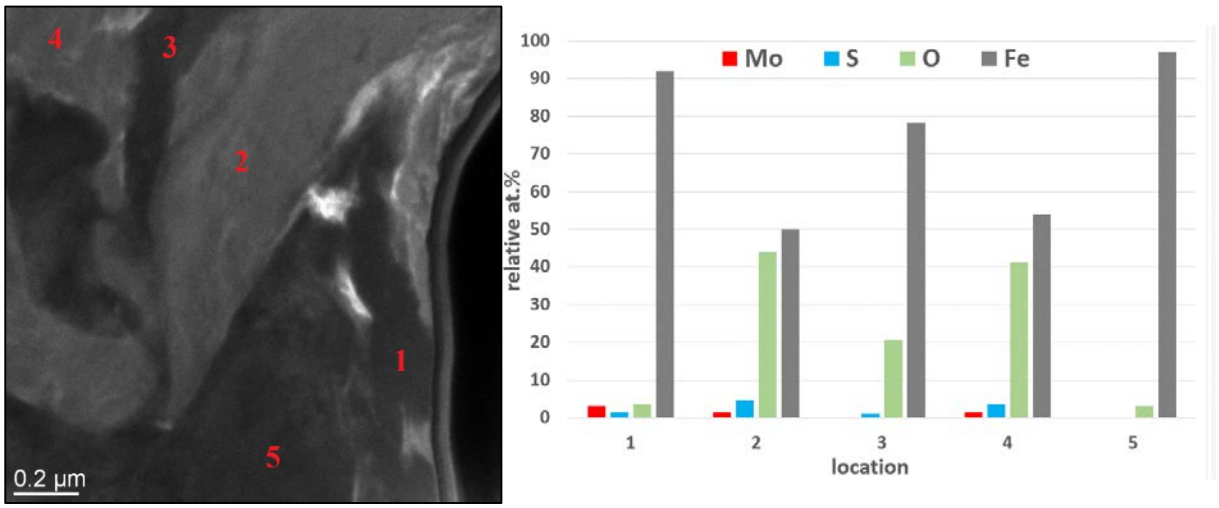

Figure D. 3. 5. Analyses EDX réalisées en différents points de la coupe FIB de la trace d'usure correspondant à l'essai des IF-MoS_2 de type LC

très hétérogène, où des zones ayant pu appartenir au tribofilm se retrouvent piégées à l'intérieur du substrat suite à une usure importante (**Figure D. 3. 5**). Ces observations, couplées à des analyses chimiques de type XPS et EDX, ont permis de reconstituer l'évolution des tribofilms en cours d'essai pour les IF-MoS_2 de différentes cristallinités ; allant de leur formation à leur dégradation en passant par les mécanismes d'adhésion possibles.

L'ensemble des résultats présentés dans cette section met en avant l'absence d'une quelconque influence de la taille des nanoparticules sur leur comportement tribologique, pour les conditions de contact et la gamme de tailles considérées et en l'absence de dispersants dans l'huile (provoquant une agglomération inévitable des IF-MoS_2). Leurs performances ont donc été comparées à celles d'une même concentration massique de micro-particules h-MoS_2 de composition chimique identique, dans les mêmes conditions de contact (**Figure D. 3. 6**). Malgré la formation d'un tribofilm de composition chimique identique que pour les IF-MoS_2, ces additifs présentent des performances nettement inférieures avec une réduction de frottement moindre et une usure accrue. Ces résultats sont mis sur le compte d'une éventuelle plus grande difficulté à pénétrer au sein du contact, et surtout à leur moins grande disponibilité dans l'huile. La taille des particules ne semble ainsi pas influer sur leurs performances tant que celle-ci demeure assez faible (de l'ordre de la centaine de nanomètres).

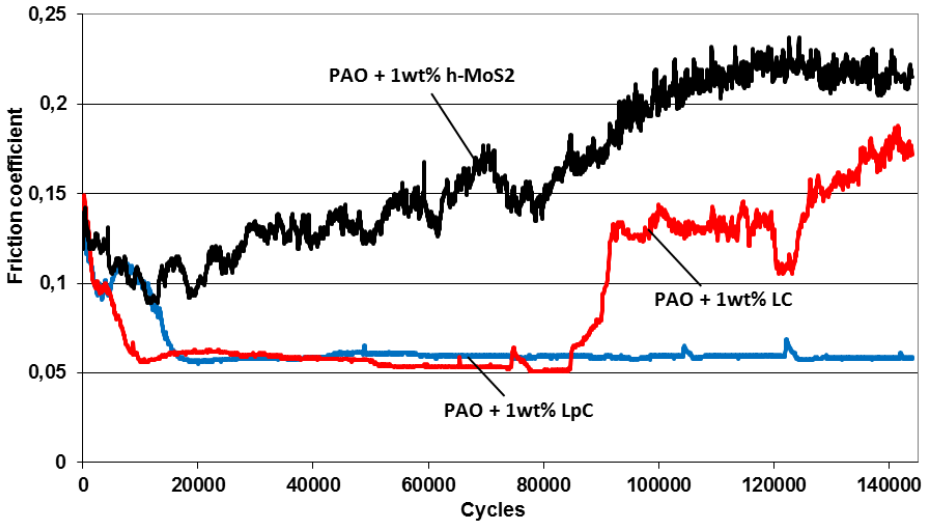

Figure D. 3. 6. Comparaison des propriétés tribologiques de particules h-MoS_2 et de nanoparticules IF-MoS_2

D. 4. Comportement tribologique des IF-MoS_2 en présence de dispersants

Le chapitre précédent constitue une première étape en vue d'une formulation de lubrifiant dopé aux nanoparticules, puisqu'il apporte des informations sur les paramètres intrinsèques aux IF-MoS_2 ayant une influence sur leur potentiel tribologique. Il faut par la suite incorporer ces nanoparticules dans des formulations d'huiles complètes, et déterminer comment elles se comportent en présence d'autres additifs. Les premiers essais tribologiques effectués en ce sens dans le Chapitre IV montrent que la présence de nanoparticules dans une huile totalement formulée n'apporte aucune diminution du coefficient de frottement. Parmi les additifs présents dans ce lubrifiant, les dispersants sont par nature les plus à même d'interagir avec les IF-MoS_2, puisque leur rôle est d'éviter toute agglomération de particules présentes dans l'huile. Des essais supplémentaires ont donc été réalisés en incorporant seulement des IF-MoS_2 et des dispersants (de type succinimide,

largement utilisés dans le secteur automobile) dans l'huile de base utilisée dans le chapitre précédent. La présence de nanoparticules dans l'huile n'a alors encore une fois eu aucun impact sur le frottement en cours d'essai, et ce pour tous les ratios IF-MoS_2/dispersants testés.

Afin de comprendre l'influence de ces dispersants de type succinimide sur l'action tribologique des IF-MoS_2, trois formulations de référence ont été considérées (**Figure D. 4. 1**) : huile de base avec dispersants (sans IF-MoS_2, en bleu) ; huile de base avec IF-MoS_2 (sans dispersants, en vert) et huile de base avec IF-MoS_2 et dispersants (en rouge).

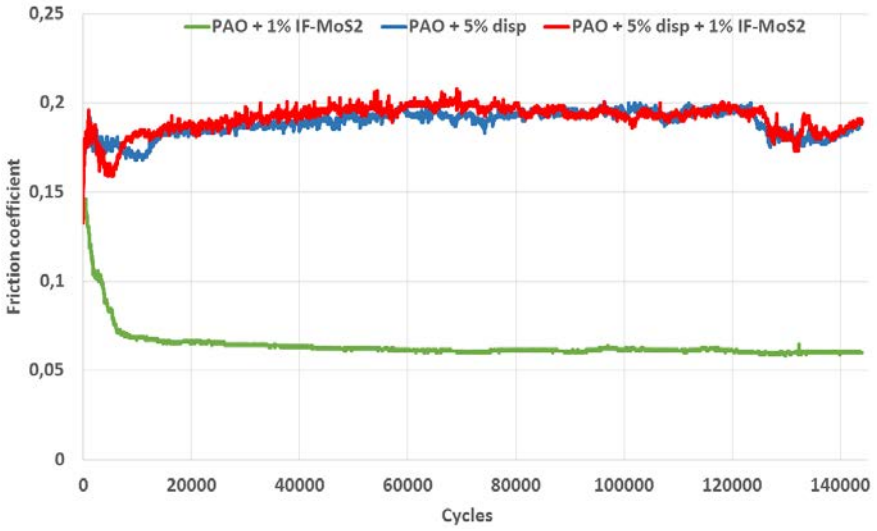

Figure D. 4. 1. Essais HFRR de l'huile de base contenant des IF-MoS_2 et/ou des dispersants

La capacité des dispersants à empêcher l'agglomération des nanoparticules a tout d'abord été vérifiée par DLS (Dynamic Light Scattering, voir **Figure D. 4. 2**). Lorsque les IF-MoS_2 sont incorporées dans l'huile de base sans dispersants, des agglomérats pouvant atteindre 1 µm se forment, avec une taille moyenne estimée à environ 420 nm. La présence de dispersants réduit considérablement la taille de ces agglomérats qui sont alors compris entre 100 et 400 nm avec une moyenne à 174 nm, soit une taille très proche des nanoparticules individuelles (aux alentours de 150 nm de diamètre).

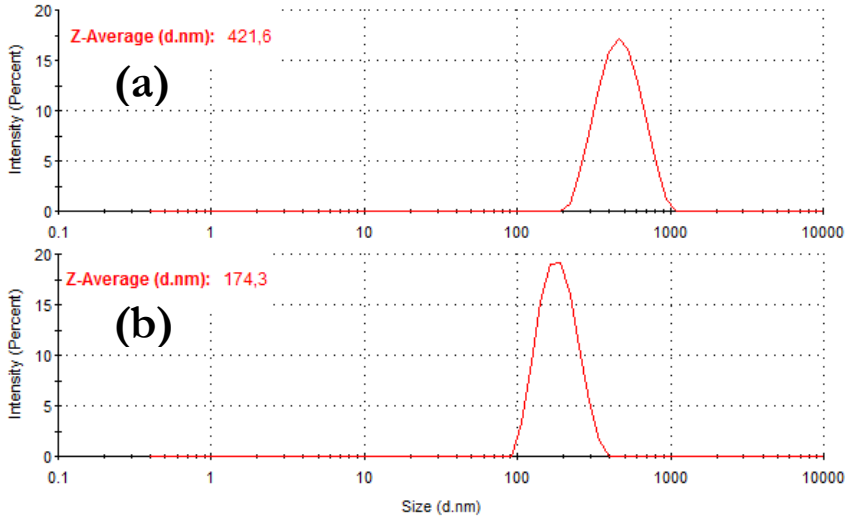

Figure D. 4. 2. Distribution des tailles d'agglomérats de nanoparticules SpC pour les huiles contenant 1% IF-MoS_2 sans dispersant (a) et avec 5% de dispersant (b)

Afin de tenter de comprendre l'absence de gain en frottement obtenu par les nanoparticules en présence de dispersants, des analyses de surface comparatives ont été menées par XPS sur les traces d'usure des trois essais de référence montrés précédemment. Tandis que les spectres révèlent la présence d'un tribofilm MoS_2 dans le cas de la formulation ne comportant pas de dispersants (conformément aux résultats décrits dans le chapitre précédent), les deux analyses restantes (huiles contenant des dispersants, avec et sans IF-MoS_2) exhibent des compositions de surface identiques. Afin de vérifier que ces mesures ne correspondent pas à une éventuelle adsorption excessive des dispersants sur le substrat, pouvant potentiellement masquer des traces d'une réaction du MoS_2 avec la surface, des profils ont été réalisés par abrasion ionique pour déterminer la composition élémentaire des quelques premières dizaines de nanomètres de la surface (**Figure D. 4. 3)**.

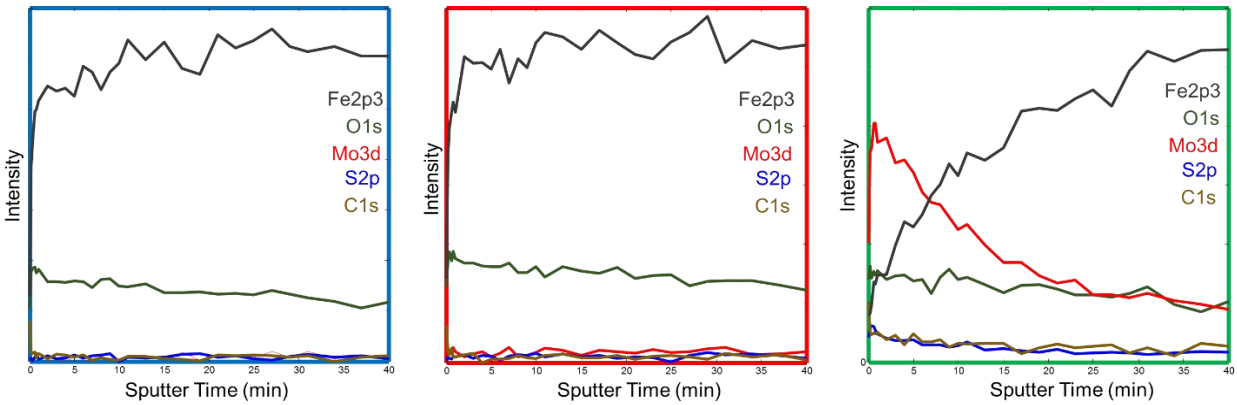

Figure D. 4. 3. Profils XPS réalisés par abrasion ionique sur les traces d'usure correspondants aux essais montrés sur la **Figure D. 4. 1** : PAO + dispersant (bleu), PAO + dispersant + IF-MoS_2 (rouge), PAO + IF-MoS_2 (vert)

Ces résultats montrent clairement que le MoS_2 provenant des nanoparticules n'a pas réagi avec le substrat pour former un tribofilm lorsque l'huile contenait des dispersants de type succinimide. Etant donné le mécanisme de lubrification associé aux nanoparticules, trois hypothèses ont été émises pour expliquer cette absence de tribofilm :

(a) la dispersion des IF-MoS_2 ne leur permet pas de pénétrer au sein du contact (modification du flux des nanoparticules aux alentours du contact et/ou des conditions de piégeage des IF-MoS_2 par les surfaces antagonistes) ;

(b) les IF-MoS_2 non-agglomérées pénètrent au sein du contact mais ne parviennent pas à être exfoliées ;

(c) les nanoparticules pénètrent dans le contact et sont exfoliées, mais la présence de dispersants modifie la tribochimie du contact et empêche l'adhésion du tribofilm.

Afin de répondre à ces interrogations, plusieurs techniques expérimentales ont été employées. Le passage des nanoparticules dispersées au sein du contact a tout d'abord été confirmé en observant le contact en cours d'essai à l'aide d'un disque en saphir (**Figure D. 4. 4**). Ces images ont de plus révélé une différence d'aspect de la surface de la bille (en acier), laissant entrevoir une influence des dispersants sur l'adhésion du tribofilm MoS_2.

Des nanoparticules ont également été prélevées sur la trace d'usure à la fin de l'essai HFRR correspondant à l'huile contenant à la fois des dispersants et des nanoparticules (courbe rouge sur la **Figure D. 4. 1**). Des observations au MET ont révélé des nanoparticules ayant subi une exfoliation partielle dans le contact, libérant des feuillets de MoS_2 (**Figure D. 4. 5**). A l'issue de

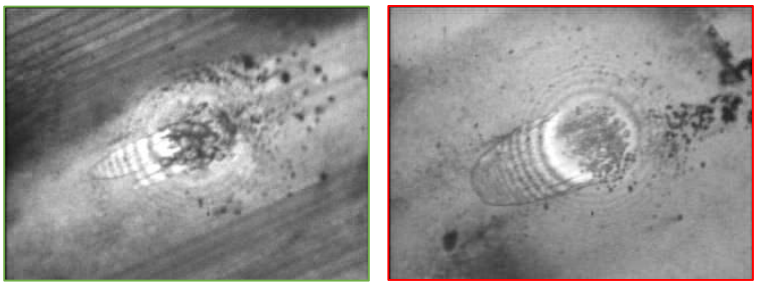

Figure D. 4. 4. Essais Nanovisu de l'huile de base dopée aux nanoparticules (1 wt%) avec (doite) et sans (gauche) dispersants (5%)

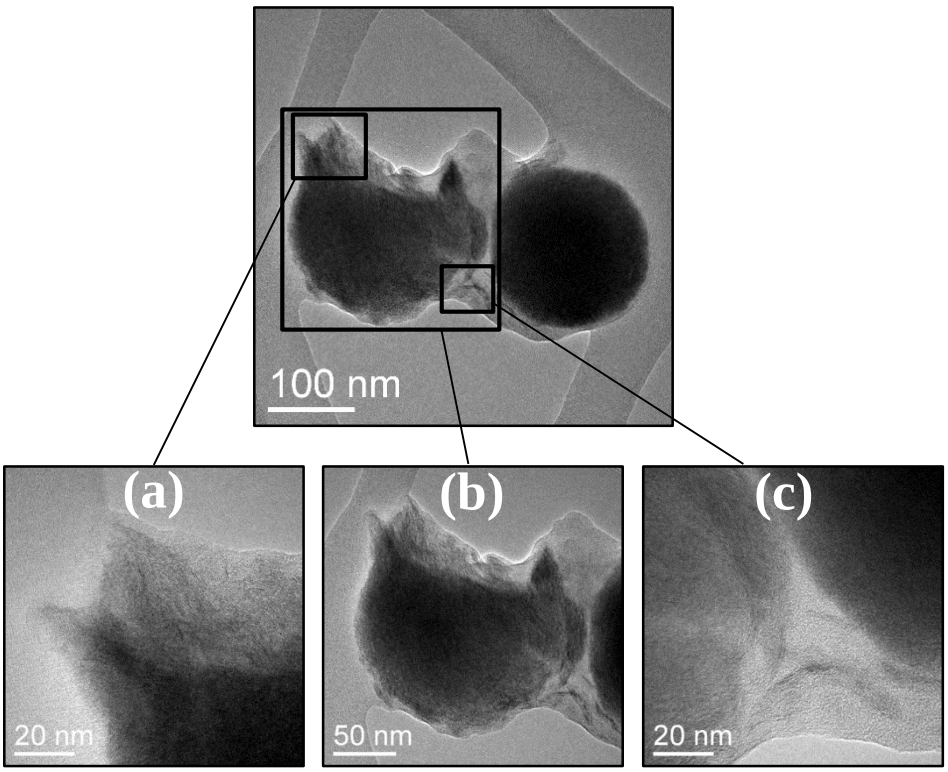

Figure D. 4. 5. Nanoparticules prélevées après essai tribologique en présence de dispersants – IF-MoS_2 endommagée (gauche) et intacte (droite)

l'essai HFRR, les nanoparticules ainsi que les feuillets libérés semblent par ailleurs être pris dans ce qui pourrait être du dispersant.

Ces résultats montrent que les nanoparticules, même correctement dispersées, parviennent à pénétrer au sein du contact et à être exfoliées par les surfaces antagonistes. La libération de feuillets de MoS_2 au sein du contact a donc bien lieu, ce qui permet l'adhésion d'un tribofilm lorsque l'huile ne contient pas de dispersants. La cause de la non-formation de ce tribofilm semble donc être de nature tribo-chimique, une adsorption excessive des dispersants sur les surfaces de contact et/ou sur les feuillets libérés lors de l'exfoliation des nanoparticules pouvant empêcher les réactions chimiques permettant l'adhésion du tribofilm (Mo – O et S – Fe notamment).

Dans les huiles automobiles, les dispersants sont initialement présents en excès dans la formulation, afin de pouvoir disperser par la suite l'ensemble des contaminants pénétrant dans le lubrifiant. Dans la suite de ce chapitre, il a été montré qu'une concentration de dispersants

beaucoup plus faible (0,05%) que celles habituellement employées (3 – 5%) permettait de disperser efficacement le pourcent massique d'IF-MoS_2 incorporées dans l'huile de base.

L'essai de cette nouvelle formulation d'huile (PAO + 0,05% dispersants + 1% IF-MoS_2) permet d'obtenir des gains en frottement comparables à ceux obtenus en l'absence de dispersants, à l'issue des premières dizaines de milliers de cycles lors desquels la faible quantité de dispersants en excès dans l'huile pourrait être monopolisée par la libération progressive de feuillets de MoS_2 et par l'apparition de débris d'usure (**Figure D. 4. 6**). Il semble dès lors possible d'obtenir un compromis entre dispersion des nanoparticules et performance tribologique, en incorporant dans l'huile la quantité exacte de dispersants nécessaires à la dispersion des nanoparticules (sans excès). La formulation résultante perdrait alors cependant ses capacités dispersives, ce qui demeure problématique pour le secteur automobile.

Les résultats obtenus dans ce chapitre montent cependant que la dispersion des nanoparticules n'est en soi pas un obstacle à la formation de tribofilm, puisque les nanoparticules dispersées parviennent à pénétrer au sein du contact et à y être exfoliées. Il est cependant nécessaire de poursuivre la recherche d'un dispersant adéquat, n'empêchant pas les feuillets de MoS_2 de réagir chimiquement avec le substrat.

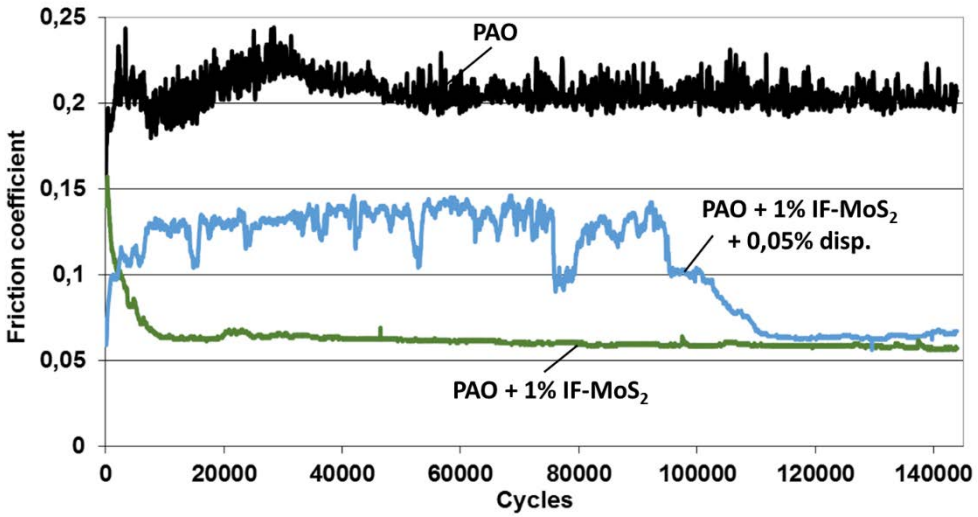

Figure D. 4. 6. Performance tribologique de l'huile de base dopée aux IF-MoS_2 et contenant 0,05 wt% de dispersants

D. 5. En prévision d'une application sur véhicule

Les résultats exposés dans les deux chapitres précédents ont permis de déterminer quels types de nanoparticules IF-MoS_2 avaient le plus grand potentiel tribologique, et de mesurer les difficultés liées à leur incorporation dans des lubrifiants totalement formulés. Afin que ces travaux ne demeurent pas vains, il est toutefois nécessaire de s'assurer que la présence de nanoparticules dans les huiles détient un véritable potentiel sur véhicule, dans un environnement parfois très différent de ceux rencontrés sur les tribomètres de laboratoire. Ce chapitre a pour but d'explorer ce potentiel dans une vaste gamme de conditions, pour des températures, des états de surface et des régimes de lubrification différents de ceux testés jusqu'à présent.

L'influence de la température de l'huile sur la capacité des IF-MoS_2 à réduire le frottement et

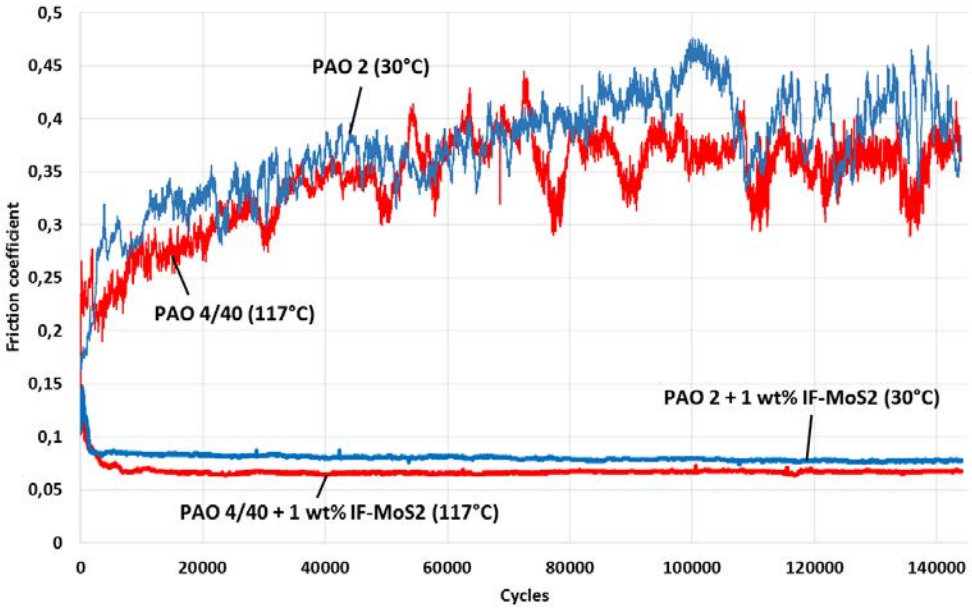

Figure D. 5. 1. Essai HFRR d'une PAO 2 à 30°C (bleu) et de la PAO 4/40 à 117°C (rouge) avec et sans 1 wt% IF-MoS_2 SpC

l'usure a d'abord été évaluée. Pour des conditions d'essai identiques, les performances des nanoparticules sont réduites à température ambiante, malgré la formation de tribofilm sur les surfaces antagonistes. Ce résultat peut cependant être expliqué par la viscosité accrue de l'huile, réduisant la sévérité de l'essai. Des huiles de base de différentes viscosités ont par la suite été utilisées afin de réaliser des essais HFRR à des températures différentes, tout en conservant des

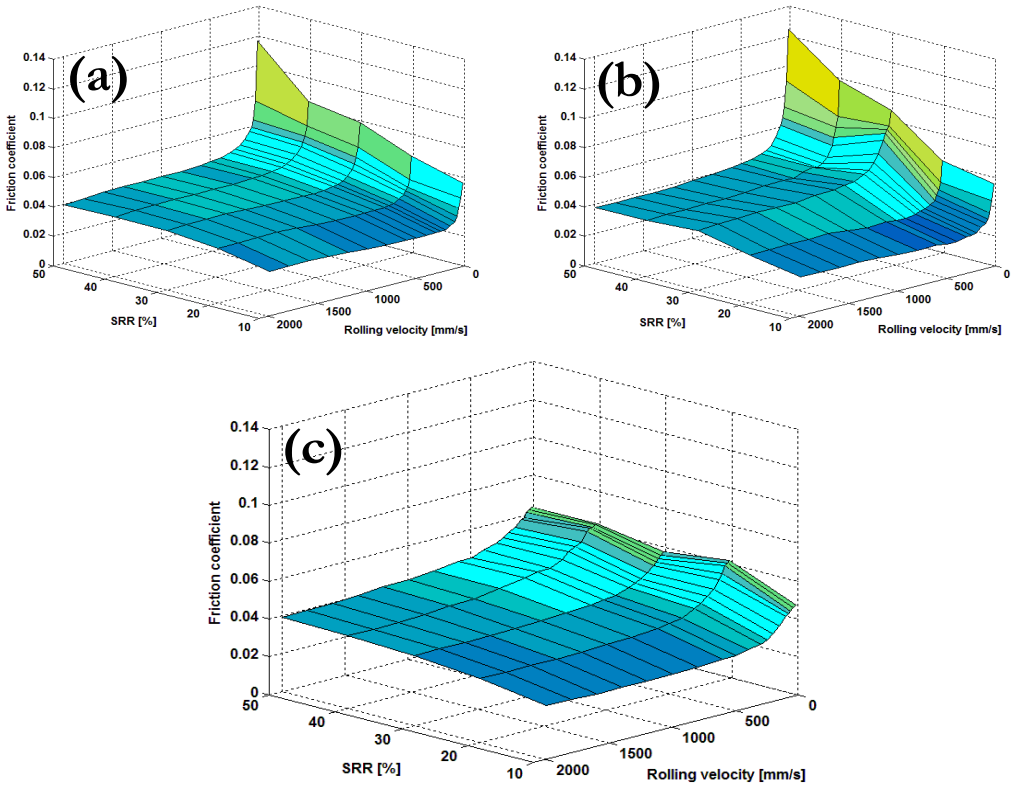

Figure D. 5. 2. Représentation surfacique des courbes de Stribeck montrant l'influence des IF-MoS_2 sur le frottement en régime de lubrification mixte
(a) PAO seule avant rodage;
(b) PAO seule après rodage;
(c) PAO + IF-MoS_2 après rodage.

viscosités comparables (**Figure D. 5. 1**). Des gains en frottement similaires ainsi que des tribofilms de même composition ont alors été obtenus à température ambiante et à 117°C, confirmant le fort potentiel lubrifiant des nanoparticules à température ambiante tant que les conditions de contact demeurent sévères.

Si la capacité des IF-MoS_2 à réduire le frottement et l'usure est exacerbée dans les régimes de lubrification les plus sévères, leur comportement n'a jusqu'à présent pas été étudié dans des conditions plus représentatives de la multitude de contacts rencontrés sur véhicule. Des essais MTM (Mini-Traction Machine) ont permis d'évaluer leur potentiel dans différentes conditions de roulement-glissement et pour une large étendue d'épaisseurs de films d'huile, allant du régime de lubrification mixte à une lubrification en film complet (**Figure D. 5. 2**). La capacité des IF-MoS_2 à former des tribofilms pour des SRR (Slide-to-Roll Ratio) aussi faibles que 10% a été constatée, permettant des gains en frottement conséquents en régime de lubrification mixte et une réduction drastique de l'usure des surfaces. A vitesse égale, les coefficients de frottement obtenus à 40%, 50% et 200% (sur HFRR) de SRR étaient par ailleurs identiques, laissant présager d'un plafond de frottement maximal obtenu (une fois le tribofilm de MoS_2 formé) à partir de 40% de glissement (SRR). Le comportement des lubrifiants non dopé (huile de base seule) et dopé (contenant des nanoparticules) était de plus similaire en film complet, permettant d'écarter en partie le risque d'une éventuelle sous-alimentation due à l'agglomération de nanoparticules en entrée de contact.

Afin d'évaluer ce risque plus précisément, de nombreuses courbes de traction (mesure du coefficient de frottement en fonction du glissement) et de Stribeck (mesure du coefficient de frottement en fonction de la vitesse de roulement) ont par la suite été tracées en comparant les résultats obtenus avec et sans nanoparticules dans l'huile de base. Ces essais ont permis de couvrir une large gamme de conditions en régime de lubrification hydrodynamique, en variant la température, la pression de contact, la vitesse de roulement et le taux de glissement. La présence de nanoparticules dans l'huile n'a eu aucune influence néfaste pour l'ensemble des conditions

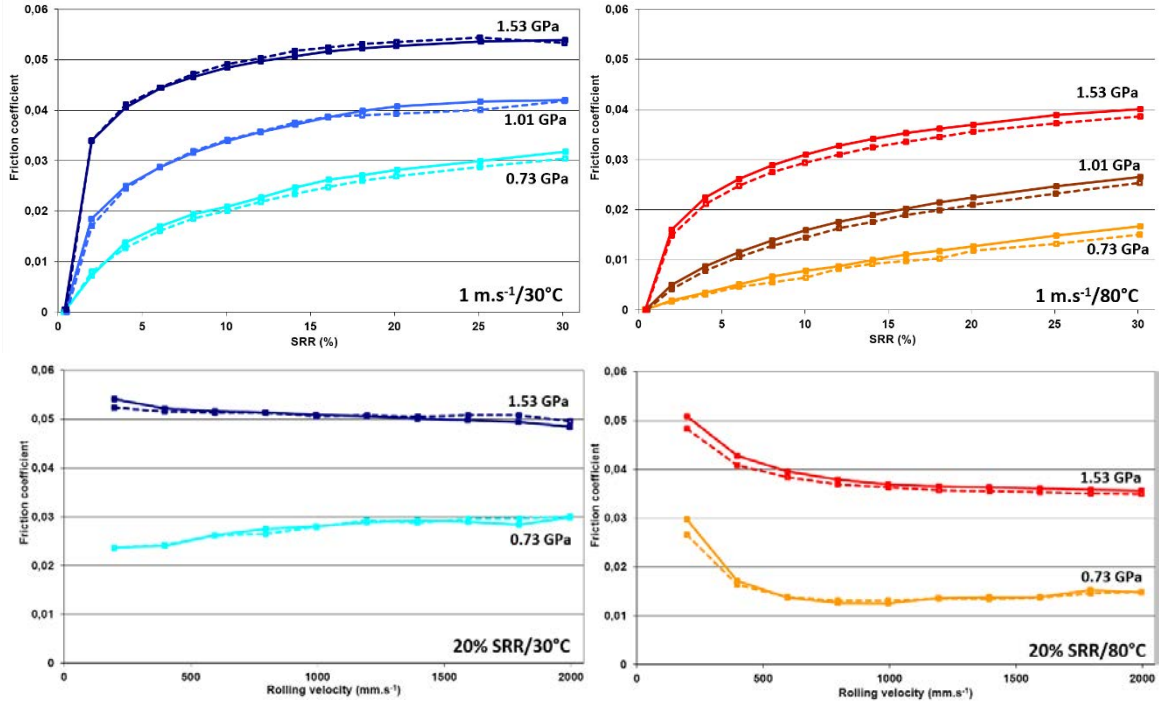

Figure D. 5. 3. Courbes de traction (haut) et de Stribeck (bas) dans des conditions de lubrification en film complet : PAO seule (pointillés) et PAO + IF-MoS_2 (lignes continues), essais à 30°C (bleu) et à 80°C (jaune/rouge)

testées (exemples de résultats illustrés sur la **Figure D. 5. 3**).

Les performances tribologiques des nanoparticules ont ensuite été évaluées en présence de surfaces rugueuses, en suivant le même protocole d'essai qu'utilisé lors des essais précédents (résultats présentés sur la **Figure D. 5. 2**). En présence d'IF-MoS_2, l'huile permet une réduction considérable de l'usure pour l'ensemble des conditions testées (**Figure D. 5. 4**). La faible réduction de frottement obtenue lors de ces essais est à mettre sur le compte d'une conservation remarquable de la rugosité des surfaces, au contraire du rodage important prenant place en présence de l'huile de base seule.

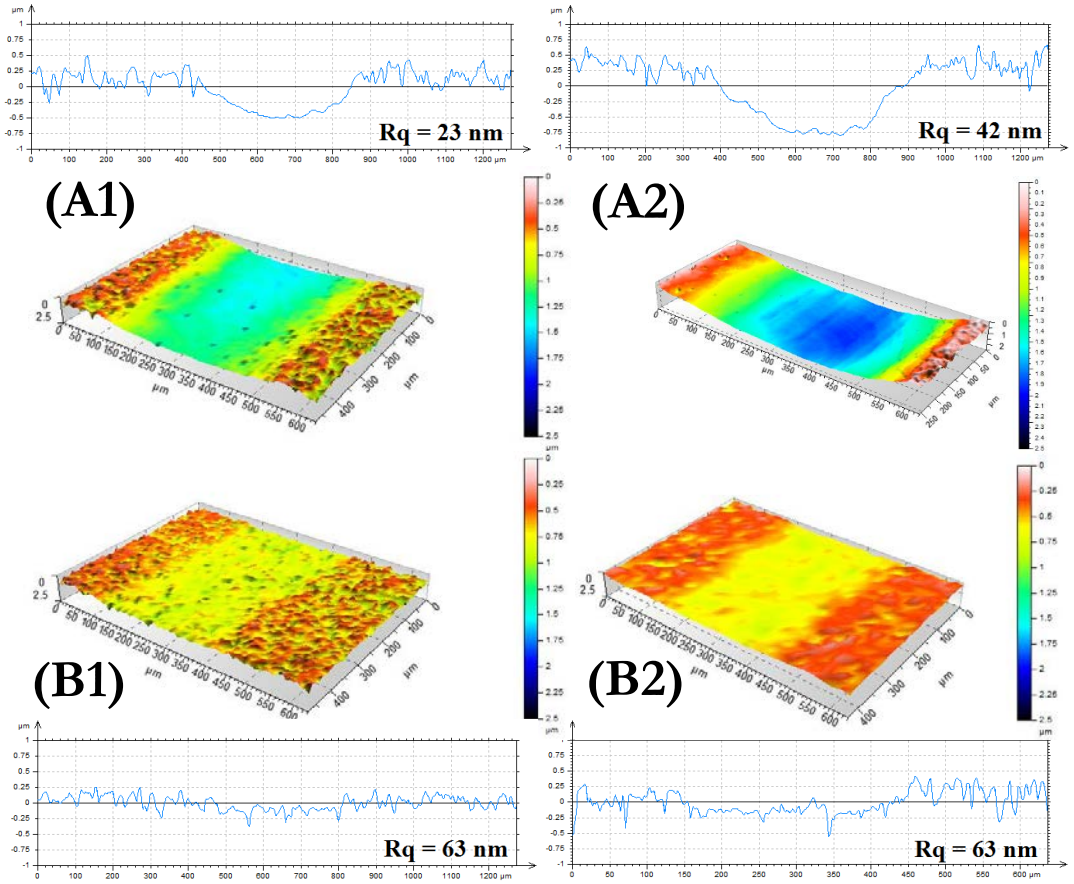

Figure D. 5. 4. Topographies et profils de surface mesurés à l'issue des essais réalisés à 10% (1) et 50% (2) de SRR pour la PAO seule (A) et la PAO + IF-MoS_2 (B). Les valeurs de Rq sont déterminées en ne prenant en compte que la trace d'usure.

La présence de nanoparticules dans les lubrifiants parait avoir des bienfaits considérables en termes de frottement et d'usure dans l'ensemble des conditions de contact testées jusqu'à présent, sans sembler présenter de risques pour les composants lubrifiés en film complet. La dernière série d'essais réalisée dans le cadre de cette étude a pour but d'évaluer le comportement de ces additifs face aux phénomènes de fatigue de contact, notamment rencontrés dans les engrenages de boîte de vitesses. Pour ce faire, des essais MPR (Micro-Pitting Rig) comparatifs ont été effectués sur l'huile de base seule et contenant des nanoparticules. La présence de nanoparticules dans l'huile a considérablement amélioré la résistance des galets à la fatigue de contact (**Figure D. 5. 5**). Le suivi de l'évolution des surfaces en cours d'essai a par ailleurs permis de constater que le comportement des surfaces en présence des deux formulations était comparable lors des premiers cycles, jusqu'à la formation de tribofilm dans le cas de l'huile dopée aux nanoparticules. L'initiation de fissures de fatigue en surface n'a alors plus lieu, et aucune propagation des fissures existantes n'est à déplorer

pendant le reste de l'essai. Des coupes longitudinales des pistes d'usure ont permis de distinguer les micro-écailles obtenues en fin d'essai, celles correspondant à l'huile de base seule présentant des signes de propagation au contraire de celles obtenues en présence de nanoparticules (**Figure D. 5. 6**).

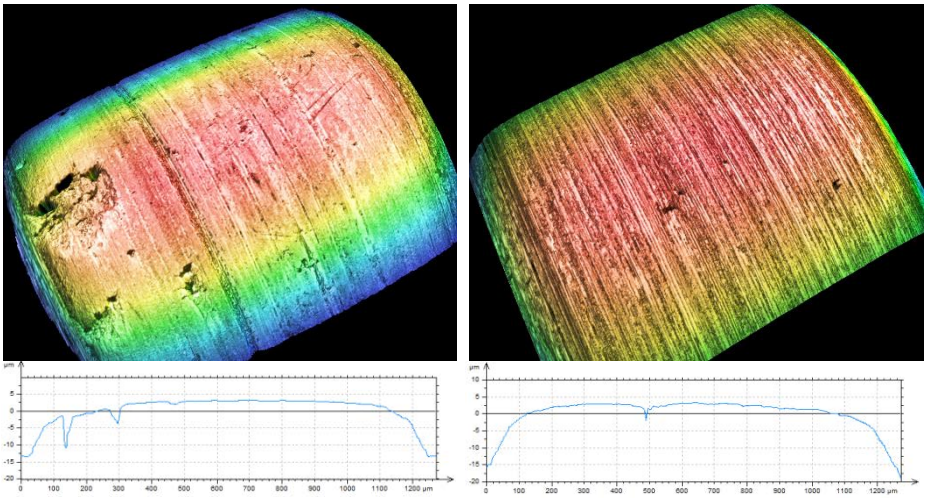

Figure D. 5. 5. Topographies 3D et profils des surfaces résultantes des essais MPR pour la PAO seule (gauche) et la PAO + 1 wt% IF-MoS_2 (droite)

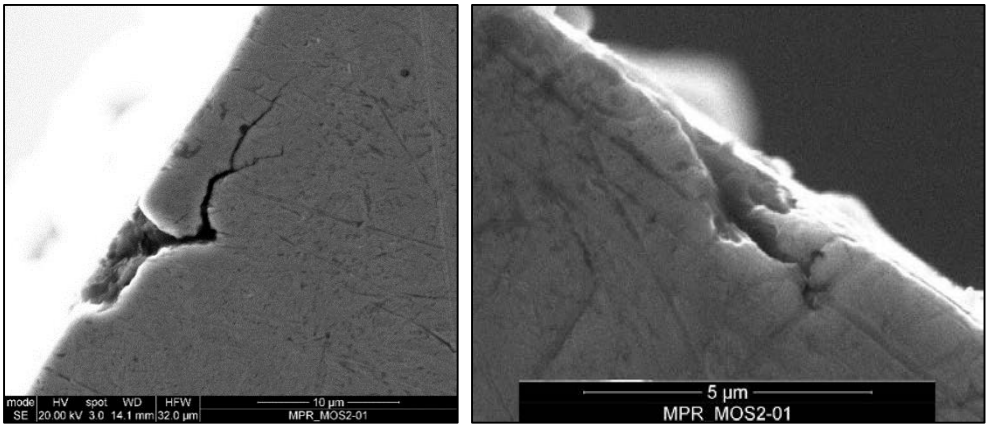

Figure D. 5. 6. Coupe du galet testé en présence de PAO seule (gauche) et de PAO + 1 wt% IF-MoS_2 (droite)

L'ensemble des résultats présentés dans ce chapitre montrent le fort potentiel des lubrifiants dopés aux IF-MoS_2 pour des applications automobiles, avec des performances tribologiques importantes dans une variété de conditions susceptibles d'être rencontrées dans un moteur ou une boîte de vitesses. Il sera désormais nécessaire d'effectuer des essais sur des bancs orientés composants, reproduisant fidèlement les contacts, afin d'estimer les véritables gains qu'il sera possible d'obtenir sur véhicule.

D. 6. Conclusions

Ce travail a permis de confirmer le fort potentiel des nanoparticules inorganiques de type fullerène pour des applications automobiles. Après un état des lieux retraçant l'histoire de l'utilisation des nanoparticules en tribologie, l'influence de leur taille et de leur cristallinité sur leur capacité de formation de tribofilms a été étudiée. Si le diamètre des nanoparticules n'a pas eu d'impact sur leurs performances (pour la gamme de taille considérée), la présence de défauts

structurels au sein des nanoparticules en augmente l'efficacité en permettant la formation et le maintien d'un tribofilm performant sur les surfaces malgré une alimentation moindre du contact en nanoparticules. Lorsqu'une recirculation de l'huile est assurée, en revanche, les nanoparticules de toutes les tailles et cristallinités testées ont atteint des performances équivalentes.

Le chapitre suivant explore le comportement des nanoparticules lorsqu'incorporées dans des huiles totalement formulées, et apporte des éléments de compréhension quant à l'absence de gains en frottement constatée en présence de dispersants de type succinimides. Une fois dispersées, les nanoparticules parviennent à pénétrer au sein du contact et à être exfoliées, conditions nécessaires à la formation du tribofilm. Une adsorption excessive des dispersants sur les feuillets de MoS_2 ainsi libérés et/ou sur le substrat semble cependant empêcher les réactions tribo-chimiques nécessaires à l'adhésion du tribofilm. Un équilibre entre dispersion des nanoparticules et performance tribologique a finalement été trouvé, mais pour des concentrations de dispersants très faibles. La formulation résultante perd alors ses propriétés dispersives, ce qui demeure problématique pour une application automobile.

Le dernier chapitre de ce manuscrit explore le comportement des nanoparticules dans différentes conditions de contact se rapprochant d'une application sur véhicule. Les nanoparticules apportent des gains en frottement et en usure pour une large variété de contacts, notamment à température ambiante, pour des taux de glissement relativement faibles et en présence de surfaces rugueuses. Les risques liés à la présence de corps solides dans le lubrifiant pour les contacts lubrifiés en film complet ont par ailleurs été partiellement levés, aucune hausse du coefficient de frottement n'ayant été relevée pour la large étendue de conditions de contact testées. Le potentiel des nanoparticules pour améliorer la résistance des composants à la fatigue de contact a enfin été entrevu.

Si ce travail permet d'envisager le dopage de lubrifiants avec des nanoparticules dans un futur proche, des interrogations subsistent pour en assurer une efficacité maximale. Différents dispersants ou détergents devront être testés afin de trouver celui offrant le meilleur compromis entre dispersion des nanoparticules et performance tribologique. La durabilité des nanoparticules (dans le temps et pour un nombre de cycles élevé) pourra également être étudiée et comparée à celle des additifs classiques, de type MoDTC. Le comportement des IF-MoS_2 dans les contacts lubrifiés en film complet devra également être étudié plus en détail, à l'aide de simulations numériques par exemple, pour écarter tout risque de sous-alimentation de contact sur véhicule. L'étude des mécanismes d'action des IF-MoS_2 face aux phénomènes de fatigue pourrait par ailleurs être approfondie, et des essais sur des bancs orientés composants donneront enfin une estimation réaliste des gains en frottement et en usure qu'il sera possible d'envisager sur véhicule.

Bibliography

[1] Risi, A. De, Donateo, T., and Laforgia, D., 2003, "Optimization of the Combustion Chamber of Direct Injection Diesel Engines," SAE Tech. Pap. 2003-01-1064.

[2] Torres, A. H. P., 2011, "Methods of optimizing combustion in a combustion chamber," United States Patent Application Publication n°US2011/0114059 A1.

[3] Rajamani, V. K., Schoenfeld, S., and Dhongde, A., 2012, "Parametric Analysis of Piston Bowl Geometry and Injection Nozzle Configuration using 3D CFD and DoE," SAE Tech. Pap. 2012-01-0700.

[4] Kapoor, A., Tung, S. C., Schwartz, S. E., Priest, M., and Dwyer-Joyce, R. S., 2001, "Automotive Tribology," Modern Tribology Handbook (vol. II, ch. 32), B. Bhushan, ed., CRC Press.

[5] Hamrock, B. J., Schmid, S. R., and Jacobson, B. O., 2004, Fundamentals of Fluid Film Lubrication, Marcel Dekker, Inc.

[6] Dowson, D., 1995, "Elastohydrodynamic and micro-elastohydrodynamic lubrication," Wear, **190**, pp. 125–138.

[7] Olver, A. V, 2002, "Gear lubrication - a review," Proc. Inst. Mech. Eng. Part J-Journal Eng. Tribol., **216**, pp. 255–267.

[8] Ayel, J., 1997, "Lubrifiants - Constitution," Techniques de l'Ingénieur, pp. 1–17.

[9] Born, M., and Ayel, J., 1998, Lubrifiants et fluides pour l'automobile, Technip.

[10] Chauveau, V., 2010, "Le pouvoir lubrifiant des nanotubes de carbone," PhD Thesis, Ecole Centrale de Lyon.

[11] Ayel, J., 1998, "Lubrifiants pour moteurs thermiques - Normes générales," Techniques de l'Ingénieur, pp. 1–16.

[12] Booser, E. R., ed., 1988, Handbook of Lubrication (Theory and Practice of Tribology), CRC Press.

[13] Ayel, J., 1996, "Lubrifiants - Propriétés et caractéristiques," Techniques de l'Ingénieur, pp. 1–17.

[14] Taylor, C. M., 1993, "Engine Tribology," Tribol. Ser., **26**.

[15] Ayel, J., 2002, "Lubrifiants - Additifs à action physique ou physiologique," Techniques de l'Ingénieur, pp. 1–18.

[16] Ayel, J., 2001, "Lubrifiants - Additifs à action chimique," Techniques de l'Ingénieur, pp. 1–18.

[17] Morina, A., Neville, A., Priest, M., and Green, J. H., 2006, "ZDDP and MoDTC interactions in boundary lubrication - The effect of temperature and ZDDP/MoDTC ratio," Tribol. Int., **39**(12), pp. 1545–1557.

[18] Joly-Pottuz, L., Dassenoy, F., Martin, J. M., Vrbanic, D., Mrzel, a., Mihailovic, D., Vogel, W., and Montagnac, G., 2005, "Tribological properties of Mo-S-I nanowires as additive in oil," Tribol. Lett., **18**(3), pp. 385–393.

[19] Dassenoy, F., Joly-Pottuz, L., Martin, J. M., Vrbanic, D., Mrzel, a., Mihailovic, D., Vogel, W., and Montagnac, G., 2007, "Tribological performances of $Mo_6S_3I_6$ nanowires," J. Eur. Ceram. Soc., **27**(2-3), pp. 915–919.

[20] Joly-Pottuz, L., Dassenoy, F., Vacher, B., Martin, J. M., and Mieno, T., 2004, "Ultralow friction and wear behaviour of Ni/Y-based single wall carbon nanotubes (SWNTs)," Tribol. Int., **37**(11-12), pp. 1013–1018.

[21] Chauveau, V., Mazuyer, D., Dassenoy, F., and Cayer-Barrioz, J., 2012, "In situ film-forming and friction-reduction mechanisms for carbon-nanotube dispersions in lubrication," Tribol. Lett., **47**(3), pp. 467–480.

[22] Joly-Pottuz, L., Vacher, B., Ohmae, N., Martin, J. M., and Epicier, T., 2008, "Anti-wear and Friction Reducing Mechanisms of Carbon Nano-onions as Lubricant Additives," Tribol. Lett., **30**(1), pp. 69–80.

[23] Joly-Pottuz, L., Matsumoto, N., Kinoshita, H., Vacher, B., Belin, M., Montagnac, G., Martin, J. M., and Ohmae, N., 2008, "Diamond-derived carbon onions as lubricant additives," Tribol. Int., **41**(2), pp. 69–78.

[24] Wu, Y. Y., Tsui, W. C., and Liu, T. C., 2007, "Experimental analysis of tribological properties of lubricating oils with nanoparticle additives," Wear, **262**(7-8), pp. 819–825.

[25] Padgurskas, J., Rukuiza, R., Prosyčevas, I., and Kreivaitis, R., 2013, "Tribological properties of lubricant additives of Fe, Cu and Co nanoparticles," Tribol. Int., **60**, pp. 224–232.

[26] Martin, J.-M., Donnet, C., and Le Mogne, T., 2000, "Superlubricity of molybdenum disulphide," Tribol. Int., **33**(2), pp. 148–149.

[27] Tenne, R., Margulis, L., Genut, M., and Hodes, G., 1992, "Polyhedral and cylindrical structures of tungsten disulphide," Nature, **360**, pp. 444–446.

[28] Margulis, L., Salitra, G., Tenne, R., and Talianker, L., 1993, "Nested fullerene-like structures," Nature, **365**, pp. 113–114.

[29] Afanasiev, P., Xia, G.-F., Berhault, G., Jouguet, B., and Lacroix, M., 1999, "Surfactant-Assisted Synthesis of Highly Dispersed Molybdenum Sulfide," Chem. Mater., **11**(11), pp. 3216–3219.

[30] Afanasiev, P., Geantet, C., Thomazeau, C., and Jouget, B., 2000, "Molybdenum polysulfide hollow microtubules grown at room temperature from solution," Chem. Commun., (12), pp. 1001–1002.

[31] Afanasiev, P., and Bezverkhy, I., 2002, "Synthesis of MoS_x ($5 > x > 6$) amorphous sulfides and their use for preparation of MoS_2 monodispersed microspheres," Chem. Mater., **14**(6), pp. 2826–2830.

[32] Nath, M., Mukhopadhyay, K., and Rao, C. N. R., 2002, "$Mo_{1-x}W_xS_2$ nanotubes and related structures," Chem. Phys. Lett., **352**, pp. 163–168.

[33] Kalin, M., Kogovšek, J., and Remškar, M., 2012, "Mechanisms and improvements in the friction and wear behavior using MoS_2 nanotubes as potential oil additives," Wear, **280-281**, pp. 36–45.

[34] Kogovšek, J., Remškar, M., Mrzel, a., and Kalin, M., 2013, "Influence of surface roughness and running-in on the lubrication of steel surfaces with oil containing MoS_2 nanotubes in all lubrication regimes," Tribol. Int., **61**, pp. 40–47.

[35] Rapoport, L., Feldman, Y., Homyonfer, M., Cohen, H., Sloan, J., Hutchison, J. ., and Tenne, R., 1999, "Inorganic fullerene-like material as additives to lubricants: structure–function relationship," Wear, **225-229**, pp. 975–982.

[36] Feldman, Y., Zak, a., Popovitz-Biro, R., and Tenne, R., 2000, "New reactor for production of tungsten disulfide hollow onion-like (inorganic fullerene-like) nanoparticles," Solid State Sci., **2**(6), pp. 663–672.

[37] Margolin, A., Popovitz-Biro, R., Albu-Yaron, A., Rapoport, L., and Tenne, R., 2005, "Inorganic fullerene-like nanoparticles of TiS_2," Chem. Phys. Lett., **411**(1-3), pp. 162–166.

[38] Yang, H., Liu, S., Li, J., Li, M., Peng, G., and Zou, G., 2006, "Synthesis of inorganic fullerene-like WS_2 nanoparticles and their lubricating performance," Nanotechnology, **17**(5), pp. 1512–1519.

[39] Rapoport, L., Lvovsky, M., Lapsker, I., Leshinsky, V., Volovik, Y., Feldman, Y., Zak, A., and Tenne, R., 2001, "Slow Release of Fullerene-Like WS_2 Nanoparticles as a Superior Solid Lubrication Mechanism in Composite Matrices," Adv. Eng. Mater., **3**(1-2), pp. 71–75.

[40] Rapoport, L., Lvovsky, M., Lapsker, I., Leshchinsky, W., Volovik, Y., Feldman, Y., and Tenne, R., 2001, "Friction and wear of bronze powder composites including fullerene-like WS_2 nanoparticles," Wear, **249**(1-2), pp. 149–156.

[41] Rapoport, L., Leshchinsky, V., Lvovsky, M., Nepomnyashchy, O., Volovik, Y., and Tenne, R., 2002, "Friction and wear of powdered composites impregnated with WS_2 inorganic fullerene-like nanoparticles," Wear, **252**(5-6), pp. 518–527.

[42] Rapoport, L., Leshchinky, V., Volovik, Y., Lvovsky, M., Nepomnyashchy, O., Feldman, Y., Popovitz-Biro, R., and Tenne, R., 2003, "Modification of contact surfaces by fullerene-like solid lubricant nanoparticles," Surf. Coatings Technol., **163-164**, pp. 405–412.

[43] Rapoport, L., Leshchinsky, V., Lapsker, I., Volovik, Y., Nepomnyashchy, O., Lvovsky, M., Popovitz-Biro, R., Feldman, Y., and Tenne, R., 2003, "Tribological properties of WS_2 nanoparticles under mixed lubrication," Wear, **255**(7-12), pp. 785–793.

[44] Rapoport, L., Nepomnyashchy, O., Lapsker, I., Verdyan, a., Soifer, Y., Popovitz-Biro, R., and Tenne, R., 2005, "Friction and wear of fullerene-like WS_2 under severe contact conditions: friction of ceramic materials," Tribol. Lett., **19**(2), pp. 143–149.

[45] Rapoport, L., Nepomnyashchy, O., Lapsker, I., Verdyan, a., Moshkovich, a., Feldman, Y., and Tenne, R., 2005, "Behavior of fullerene-like WS_2 nanoparticles under severe contact conditions," Wear, **259**(1-6), pp. 703–707.

[46] Joly-Pottuz, L., Dassenoy, F., Belin, M., Vacher, B., Martin, J. M., and Fleischer, N., 2005, "Ultralow-friction and wear properties of IF-WS_2 under boundary lubrication," Tribol. Lett., **18**(4), pp. 477–485.

[47] Leshchinsky, V., Popovitz-Biro, R., Gartsman, K., Rosentsveig, R., Rosenberg, Y., Tenne, R., and Rapoport, L., 2004, "Behavior of solid lubricant nanoparticles under compression," J. Mater. Sci., **39**(13), pp. 4119–4129.

[48] Joly-Pottuz, L., Martin, J. M., Dassenoy, F., Belin, M., Montagnac, G., Reynard, B., and Fleischer, N., 2006, "Pressure-induced exfoliation of inorganic fullerene-like WS_2 particles in a Hertzian contact," J. Appl. Phys., **99**(2), p. 023524.

[49] Tevet, O., Goldbart, O., Cohen, S. R., Rosentsveig, R., Popovitz-Biro, R., Wagner, H. D., and Tenne, R., 2010, "Nanocompression of individual multilayered polyhedral nanoparticles.," Nanotechnology, **21**(36), p. 365705.

[50] Tevet, O., Von-Huth, P., Popovitz-Biro, R., Rosentsveig, R., Wagner, H. D., and Tenne, R., 2011, "Friction mechanism of individual multilayered nanoparticles," Proc. Natl. Acad. Sci., **108**(50), pp. 19901–19906.

[51] Joly-Pottuz, L., Martin, J. M., Belin, M., Dassenoy, F., Montagnac, G., and Reynard, B., 2007, "Study of inorganic fullerenes and carbon nanotubes by in situ Raman tribometry," Appl. Phys. Lett., **91**(15), p. 153107.

[52] Perfiliev, V., Moshkovith, A., Verdyan, A., Tenne, R., and Rapoport, L., 2006, "A new way to feed nanoparticles to friction interfaces," Tribol. Lett., **21**(2), pp. 89–93.

[53] Moshkovith, A., Perfiliev, V., Verdyan, A., Lapsker, I., Popovitz-Biro, R., Tenne, R., and Rapoport, L., 2007, "Sedimentation of IF-WS_2 aggregates and a reproducibility of the tribological data," Tribol. Int., **40**(1), pp. 117–124.

[54] Tannous, J., Dassenoy, F., Bruhács, A., and Tremel, W., 2009, "Synthesis and Tribological Performance of Novel $Mo_xW_{1-x}S_2$ ($0 \leq x \leq 1$) Inorganic Fullerenes," Tribol. Lett., **37**(1), pp. 83–92.

[55] Schuffenhauer, C., Wildermuth, G., Felsche, J., and Tenne, R., 2004, "How stable are inorganic fullerene-like particles ? Thermal analysis (STA) of inorganic fullerene-like NbS_2, MoS_2, and WS_2 in oxidizing and inert atmospheres in comparison with bulk material," Phys. Chem. Chem. Phys., **6**, pp. 3991–4002.

[56] Bar Sadan, M., Heidelmann, M., Houben, L., and Tenne, R., 2009, "Inorganic WS_2 nanotubes revealed atom by atom using ultra-high-resolution transmission electron microscopy," Appl. Phys. A, **96**(2), pp. 343–348.

[57] Yadgarov, L., Rosentsveig, R., Leitus, G., Albu-Yaron, A., Moshkovich, A., Perfilyev, V., Vasic, R., Frenkel, A. I., Enyashin, A. N., Seifert, G., Rapoport, L., and Tenne, R., 2011, "Controlled Doping of MS_2 (M=W, Mo) Nanotubes and Fullerene-like Nanoparticles.," Angew. Chem. Int. Ed. Engl., **51**(1148), pp. 1148–1151.

[58] Tenne, R., 2003, "Advances in the synthesis of inorganic nanotubes and fullerene-like nanoparticles.," Angew. Chem. Int. Ed. Engl., **42**(42), pp. 5124–5132.

[59] Bar-Sadan, M., Kaplan-Ashiri, I., and Tenne, R., 2007, "Inorganic fullerenes and nanotubes: Wealth of materials and morphologies," Eur. Phys. J. Spec. Top., **149**(1), pp. 71–101.

[60] Wahl, K. J., Belin, M., and Singer, I. L., 1998, "A triboscopic investigation of the wear and friction of MoS_2 in a reciprocating sliding contact," Wear, **214**(2), pp. 212–220.

[61] Chhowalla, M., and Amaratunga, G. A. J., 2000, "Thin films of fullerene-like MoS_2 nanoparticles with ultra-low friction and wear," Nature, **407**(September), pp. 164–167.

[62] Rosentsveig, R., Margolin, A., Gorodnev, A., Popovitz-Biro, R., Feldman, Y., Rapoport, L., Novema, Y., Naveh, G., and Tenne, R., 2009, "Synthesis of fullerene-like MoS_2 nanoparticles and their tribological behavior," J. Mater. Chem., **19**(25), pp. 4368–4374.

[63] Cizaire, L., Vacher, B., Le Mogne, T., Martin, J. M., Rapoport, L., Margolin, a., and Tenne, R., 2002, "Mechanisms of ultra-low friction by hollow inorganic fullerene-like MoS_2 nanoparticles," Surf. Coatings Technol., **160**(2-3), pp. 282–287.

[64] Rosentsveig, R., Gorodnev, A., Feuerstein, N., Friedman, H., Zak, A., Fleischer, N., Tannous, J., Dassenoy, F., and Tenne, R., 2009, "Fullerene-like MoS_2 Nanoparticles and Their Tribological Behavior," Tribol. Lett., **36**(2), pp. 175–182.

[65] Tannous, J., Dassenoy, F., Lahouij, I., Mogne, T., Vacher, B., Bruhács, A., and Tremel, W., 2011, "Understanding the Tribochemical Mechanisms of IF-MoS_2 Nanoparticles Under Boundary Lubrication," Tribol. Lett., **41**(1), pp. 55–64.

[66] Lahouij, I., Vacher, B., Martin, J.-M., and Dassenoy, F., 2012, "IF-MoS_2 based lubricants: Influence of size, shape and crystal structure," Wear, **296**(1-2), pp. 558–567.

[67] Rapoport, L., Moshkovich, a., Perfilyev, V., Laikhtman, a., Lapsker, I., Yadgarov, L., Rosentsveig, R., and Tenne, R., 2012, "High Lubricity of Re-Doped Fullerene-Like MoS_2 Nanoparticles," Tribol. Lett., **45**(2), pp. 257–264.

[68] Lahouij, I., Dassenoy, F., Vacher, B., and Martin, J.-M., 2012, "Real Time TEM Imaging of Compression and Shear of Single Fullerene-Like MoS_2 Nanoparticle," Tribol. Lett., **45**(1), pp. 131–141.

[69] Cusano, C., and Sliney, H. E., 1981, "Dynamics of solid dispersions in oil during the lubrication of point contacts, Part I - Graphite," ASLE Trans., **25**(2), pp. 183–189.

[70] Wan, G. T. Y., and Spikes, H. A., 1987, "The Behavior of Suspended Solid Particles in Rolling and Sliding EHD Contacts," STLE Trans., **31**(1), pp. 12–21.

[71] Dwyer-Joyce, R. S., and Heymer, J., 1996, "The Entrainment of Solid Particles into Rolling Elastohydrodynamic Contacts," Tribol. Ser., **31**, pp. 135–140.

[72] Cann, P. M. E., Hamer, J. C., Sayles, R. S., Spikes, H. A., and Ioannides, E., 1996, "Direct Observation of particle entry and deformation in a rolling EHD contact," Tribol. Ser., **31**, pp. 127–134.

[73] Nikas, G. K., Sayles, R. S., and Ioannides, E., 1998, "Effects of debris particles in sliding/rolling elastohydrodynamic contacts," Proc. Inst. Mech. Eng. Part J-Journal Eng. Tribol., **212**(J5), pp. 333–343.

[74] Nikas, G. K., 2006, "A mechanistic model of spherical particle entrapment in elliptical contacts," Proc. Inst. Mech. Eng. Part J J. Eng. Tribol., **220**(6), pp. 507–522.

[75] Nikas, G. K., 2007, "Effects of operating conditions and friction on the entrapment of spherical debris particles in elliptical contacts," Proc. Inst. Mech. Eng. Part J J. Eng. Tribol., **221**(6), pp. 727–741.

[76] Nikas, G. K., 2010, "A state-of-the-art review on the effects of particulate contamination and related topics in machine-element contacts," Proc. Inst. Mech. Eng. Part J J. Eng. Tribol., **224**(5), pp. 453–479.

[77] Kaneta, M., and Murakami, Y., 1987, "Effects of oil hydraulic pressure on surface crack growth in rolling / sliding contact," Tribol. Int., **20**(4), pp. 210–217.

[78] Seeton, C. J., 2006, "Viscosity–temperature correlation for liquids," Tribol. Lett., **22**(1), pp. 67–78.

[79] Moshkovith, A., Perfiliev, V., Lapsker, I., Fleischer, N., Tenne, R., and Rapoport, L., 2006, "Friction of fullerene-like WS_2 nanoparticles: effect of agglomeration," Tribol. Lett., **24**(3), pp. 225–228.

[80] Aralihalli, S., and Biswas, S. K., 2012, "Grafting of Dispersants on MoS_2 Nanoparticles in Base Oil Lubrication of Steel," Tribol. Lett., **49**(1), pp. 61–76.

[81] Njiwa, P., Hadj-Aïssa, A., Afanasiev, P., Geantet, C., Bosselet, F., Vacher, B., Belin, M., Le Mogne, T., and Dassenoy, F., 2014, "Tribological properties of new MoS_2 nanoparticles prepared by seed-assisted solution technique," Tribol. Lett., **55**, pp. 473-481.

[82] Kogovšek, J., and Kalin, M., 2014, "Various MoS_2-, WS_2- and C-Based Micro- and Nanoparticles in Boundary Lubrication," Tribol. Lett., **53**(3), pp. 585–597.

[83] Einstein, A., 1905, "On the movement of small particles suspended in stationary liquids required by the molecular-kinetic theory of heat," Ann. Phys., **17**, pp. 549–560.

[84] Lu, K., 2008, "Theoretical analysis of colloidal interaction energy in nanoparticle suspensions," Ceram. Int., **34**(6), pp. 1353–1360.

[85] Gregory, J., 1981, "Approximate expressions for retarded van der Waals interaction," J. Colloid Interface Sci., **83**(1), pp. 138–145.

[86] Lefèvre, G., and Jolivet, A., 2009, "Calculation of Hamaker constants applied to the deposition of metallic oxide particles at high temperature," Proc. Int. Conf. Heat Exch. Fouling an Clean. VIII, pp. 120–124.

[87] Polesel-Maris, J., Guo, H., Zambelli, T., and Gauthier, S., 2006, "Mapping van der Waals forces with frequency modulation dynamic force microscopy.," Nanotechnology, **17**(16), pp. 4204–11.

[88] Olver, A. V., 2005, "The Mechanism of Rolling Contact Fatigue: An Update," Proc. Inst. Mech. Eng. Part J J. Eng. Tribol., **219**(5), pp. 313–330.

[89] Santus, C., Beghini, M., Bartilotta, I., and Facchini, M., 2012, "Surface and subsurface rolling contact fatigue characteristic depths and proposal of stress indexes," Int. J. Fatigue, **45**, pp. 71–81.

[90] Rabaso, P., Gauthier, T., Diaby, M., and Ville, F., 2013, "Rolling Contact Fatigue: Experimental Study of the Influence of Sliding, Load, and Material Properties on the Resistance to Micropitting of Steel Discs," Tribol. Trans., **56**(2), pp. 203–214.

[91] Meheux, M., Minfray, C., Ville, F., Mogne, T. L., Lubrecht, a a, Martin, J. M., Lieurade, H. P., and Thoquenne, G., 2010, "Effect of lubricant additives in rolling contact fatigue," Proc. Inst. Mech. Eng. Part J-Journal Eng. Tribol., **224**(J9), pp. 947–955.

[92] Hertz, H., 1881, "Über die Berührung fester elastischer Körper," J. für die reine und Angew. Math., **92**, pp. 156–171.

[93] Johnson, K. L., 1985, Contact Mechanics, Cambridge University Press.

[94] Dowson, D., and Ehret, P., 1999, "Past, present and future studies in elastohydrodynamics," Proc. Inst. Mech. Eng. Part J J. Eng. Tribol., **213**(5), pp. 317–333.

[95] Hamrock, B. J., and Dowson, D., 1976, "Isothermal Elastohydrodynamic lubrication of point contacts. I - Theoretical Formulation," Trans. ASME F, J. Tribol., **98**(4), pp. 223–229.

[96] Hamrock, B. J., and Dowson, D., 1976, "Isothermal Elastohydrodynamic lubrication of point contacts. II - Ellipticity parameter results," Trans. ASME F, J. Tribol., **98**(3), pp. 375–383.

[97] Hamrock, B. J., and Dowson, D., 1977, "Isothermal Elastohydrodynamic lubrication of point contacts. III - Fully Flooded Results," Trans. ASME F, J. Tribol., **99**(2), pp. 264–276.

Scientific contributions

List of Articles

- Rabaso, P., Dassenoy, F., Ville, F., Diaby, M., Vacher, B., Le Mogne, T., Belin, M., Cavoret, J., 2014, "An investigation on the reduced ability of IF-MoS_2 nanoparticles to reduce friction and wear in the presence of dispersants", Tribol. Lett., **55**, pp. 503-516.
- Rabaso, P., Ville, F., Dassenoy, F., Diaby, M., Afanasiev, P., Cavoret, J., Vacher, B., Le Mogne, T., 2014, Boundary lubrication: influence of the size and structure of Inorganic Fullerene-like MoS_2 nanoparticles on friction and wear reduction, *Accepted for publication in Wear*.

List of Oral presentations

- Rabaso, P., Ville, F., Dassenoy, F., Diaby, M., Cavoret, J., Le Mogne, T., Vacher, B., "Nanoparticle-doped lubricants: synthesis of efficient nanoparticles and behaviour in various lubrication regimes", 41st Leeds-Lyon Symposium on Tribology, Leeds, UK, 2014.
- Rabaso, P., Ville, F., Dassenoy, F., Diaby, M., Afanasiev, P., Vacher, B., Le Mogne, T., Cavoret, J., "Synthesis of efficient nanoparticles for boundary lubrication: influence of size and structure of Inorganic Fullerene-like (IF-) MoS_2 nanoparticles", STLE 69th Annual Meeting & Exhibition, Lake Buena Vista, USA, 2014.
- Rabaso, P., Ville, F., Dassenoy, F., Diaby, M., "Reduced efficiency of nanoparticle-doped lubricants in the presence of dispersants: an investigation", 1st African Conference in Tribology (ACT), Marrakesh, Morocco, 2014. ** Winner of the award for best oral presentation by a young researcher **
- Rabaso, P., Ville, F., Dassenoy, F., Diaby, M., "Nanoparticle-doped lubricants: tribological behaviour in different lubrication regimes and synthesis of efficient nanoparticles", 1st Porto-Lyon Tribology Workshop, Porto, Portugal, 2013.
- Diaby, M., Rabaso, P., Bordes, J.-M., Laurent, F., "Les leviers de baisse des pertes mécaniques dans les groups motopropulseurs : synergies et antagonisms", 25èmes Journées Internationales Francophones de Tribologie (JIFT), Ecully, France, 2014.

List of Posters

- Rabaso, P., Ville, F., Dassenoy, F., Cavoret, J., Vacher, B., Le Mogne, T., Belin, M., Diaby, M., "Tribological behavior of Inorganic Fullerene-like (IF-) MoS_2 nanoparticles in the presence of dispersants", STLE 69th Annual Meeting & Exhibition, Lake Buena Vista, USA, 2014.
- Rabaso, P., Ville, F., Dassenoy, F., Diaby, M., "Friction and wear reduction in severe lubrication regimes: synthesis of efficient MoS_2 nanoparticles", 40th Leeds-Lyon Symposium on Tribology & Tribochemistry Forum 2013, Ecully, France, 2013.

FOLIO ADMINISTRATIF

THESE SOUTENUE DEVANT L'INSTITUT NATIONAL DES SCIENCES APPLIQUEES DE LYON

Nom : **RABASO** Date de Soutenance : **13 novembre 2014**

Prénom : **Pierre**

Titre : **Nanoparticle-doped lubricants: potential of Inorganic Fullerene-like (IF-) molybdenum disulfide for automotive applications**

Nature : **Doctorat** Numéro d'ordre : **2014 ISAL 2014**

Ecole doctorale : **MEGA** (Mécanique, Energétique, Génie Civil, Acoustique)

Spécialité : **Mécanique**

Résumé :

Les enjeux environnementaux actuels, ainsi que la hausse continue du prix du pétrole, ont incité les constructeurs automobiles du monde entier à améliorer le rendement de leurs véhicules. Les propriétés tribologiques des lubrifiants des moteurs et boites de vitesses ont une influence considérable sur le rendement global des véhicules. Ils réduisent en effet le frottement généré par un grand nombre de contacts, et permettent parfois la réduction de la taille de différents composants en leur conférant une meilleure résistance à l'usure. Les avancées récentes en termes de synthèse de nanoparticules ont ouvert de nouvelles perspectives en termes d'additivation de lubrifiants avec, par exemple, la découverte des excellentes propriétés tribologiques des nanoparticules inorganiques de type fullerène comme le disulfure de molybdène ou de tungstène. L'objectif de ce manuscrit est d'évaluer le potentiel tribologique des nanoparticules IF-MoS_2 dans l'optique d'une application automobile.

L'influence de la taille et de la structure des nanoparticules a d'abord été étudiée. Les nanoparticules peu cristallines se sont révélées être plus apte à maintenir un tribofilm performant sur des surfaces en acier dans des conditions de lubrification limite, indépendamment de leur taille. Toutes les nanoparticules testées ont cependant atteint des performances équivalentes lorsqu'une recirculation de l'huile était imposée, permettant de maintenir une alimentation continue du contact en nanoparticules.

Une fois incorporées dans une formulation d'huile complète, les nanoparticules IF-MoS_2 perdent leurs propriétés tribologiques. Les dispersants contenus dans l'huile, bien que permettant une bonne dispersion des IF-MoS_2, semblent responsables de leur inefficacité en empêchant la formation de tribofilms sur les surfaces antagonistes. Une fois correctement dispersées, les nanoparticules pénètrent toujours le contact et se retrouvent bien exfoliées. Une adsorption excessive des dispersants sur les feuillets de MoS_2 ainsi libérés et/ou sur les surfaces en acier semble nuire à l'adhésion du tribofilm. Un équilibre entre dispersion des nanoparticules et performance tribologique a ensuite été trouvé, en utilisant de très faibles concentrations de dispersants.

Le comportement des huiles dopées en nanoparticules dans des conditions plus proches d'une application automobile a finalement été exploré. Les IF-MoS_2 ont permis une réduction significative du frottement et de l'usure à température ambiante et en roulement/glissement, à la fois pour des surfaces lisses et rugueuse. Les risques associés à la présence de nanoparticules dans l'huile dans les régimes de lubrification en film complet ont été partiellement levés. Aucun impact significatif n'a en effet été constaté sur le coefficient de frottement pour l'ensemble des conditions d'essais retenues. Le potentiel des nanoparticules IF-MoS_2 pour la protection des surfaces soumises à la fatigue de contact a enfin été démontré.

Mots-Clés : **nanoparticules IF-MoS_2, additifs, lubrification limite, frottement, usure, dispersants, fatigue de contact.**

Laboratoire(s) de recherche : **La**boratoire de **M**écanique des **Co**ntacts et des **S**tructures (LaMCoS, INSA Lyon)
Laboratoire de **T**ribologie et **D**ynamique des **S**ystèmes (LTDS, Ecole Centrale Lyon)

Directeurs de these : **Fabrice DASSENOY** (LTDS)
Fabrice VILLE (LaMCoS)

Président de jury : **Michel FILLON**

Composition du jury : **Fabrice DASSENOY, Moussa DIABY, Rob DWYER-JOYCE, Michel FILLON, Christophe GEANTET, Mitjan KALIN, Fabrice VILLE**